

**DEVELOPMENT OF DRUGS FROM THERAPEUTIC TARGETS  
IN COBRA VENOM USING STRUCTURE BASED  
DRUG DESIGN AND VIRTUAL SCREENING**

**MALEERUK UTSINTONG**

**A THESIS SUBMITTED IN PARTIAL FULFILLMENT  
OF THE REQUIREMENTS FOR  
THE DEGREE OF DOCTOR OF PHILOSOPHY  
(PHARMACEUTICAL CHEMISTRY AND PHYTOCHEMISTRY)  
FACULTY OF GRADUATE STUDIES  
MAHIDOL UNIVERSITY  
2008**

**COPYRIGHT OF MAHIDOL UNIVERSITY**

Thesis  
Entitled

**DEVELOPMENT OF DRUGS FROM THERAPEUTIC TARGETS  
IN COBRA VENOM USING STRUCTURE BASED  
DRUG DESIGN AND VIRTUAL SCREENING**

.....  
Ms. Maleeruk Utsintong  
Candidate

.....  
Assoc. Prof. Opa Vajragupta, Ph.D.  
Major-Advisor

.....  
Assist. Prof. Wichet Leelamanit, Ph.D.  
Co-Advisor

.....  
Prof. Arthur J. Olson, Ph.D.  
Co-Advisor

.....  
Prof. Banchong Mahaisavariya,  
M.D.  
Dean  
Faculty of Graduate Studies

.....  
Assoc. Prof. Leena Suntornsuk,  
Ph.D. (Pharmaceutical Chemistry)  
Acting Chair  
Doctor of Philosophy Programme in  
Pharmaceutical Chemistry and  
Phytochemistry  
Faculty of Pharmacy

Thesis  
Entitled

**DEVELOPMENT OF DRUGS FROM THERAPEUTIC TARGETS  
IN COBRA VENOM USING STRUCTURE BASED  
DRUG DESIGN AND VIRTUAL SCREENING**

was submitted to the Faculty of Graduate Studies, Mahidol University  
for the degree of Doctor of Philosophy (Pharmaceutical Chemistry and Phytochemistry)  
on  
September 23, 2008

.....  
Assist. Prof. Pornchai Rojsitthisak, Ph.D.  
Member

.....  
Ms. Maleeruk Utsintong  
Candidate

.....  
Assist. Prof. Wichet Leelamanit, Ph.D.  
Member

.....  
Assoc. Prof. Leena Suntornsuk, Ph.D.  
Chair

.....  
Prof. Arthur J. Olson, Ph.D.  
Member

.....  
Assoc. Prof. Opa Vajragupta, Ph.D.  
Member

.....  
Prof. Banchong Mahaisavariya, M.D.  
Dean  
Faculty of Graduate Studies  
Mahidol University

.....  
Assoc. Prof. Chuthamane Suthisisang,  
Ph.D.  
Dean  
Faculty of Pharmacy  
Mahidol University

## ACKNOWLEDGEMENTS

I would like to express my deep appreciation to the many people that have made this work possible. First of all, I would like to thank my advisor, Assoc. Prof. Opa Vajragupta, for her encouragement and inspiration throughout my study. She always give me invaluable advice.

To Assist. Prof. Wichet Leelamanit, Assoc. Prof. Penchome Peungvicha and Assoc. Prof. Yuvadee Wongkrajang, I am very grateful to express my gratitude for their helpful advices and cooperation. I would like to thank Dr. Atchara Kaewnoi for providing the redioides. I wish to thank Assoc. Prof. Leena Suntornsuk and Assist. Prof. Pornchai Rojsitthisak for kindness in providing suggestion and who were examiner of the thesis defense.

I am deeply thank to Prof. Arthur J Olson and Prof. Palmer Taylor for their valuable advice and guidance in this research.

A big thanks goes to all staffs in Prof. Arthur J Olson's laboratory at The Scripps Research Institute and Prof. Palmer Taylor's laboratory at the University of California, San Diago, especially, Dr. Garrett Morris, Dr. Lindy Lindstrom, Dr. Ruth Huey, Dr. Alexandre Gillet, Dr. Rodney Harris, Mrs. Peggy Graber, Dr. Todd Talley and Ms. Joannie Ho for their helpful suggestion and kind help.

A special acknowledgement is extended to Department of Pharmaceutical Chemistry, Faculty of Pharmacy, Mahidol University, for providing research facilities, the Royal Golden Jubilee (RGJ) Project, Thailand Reseach fund, Thai Ministry of University Affairs, Commission on Higher Education, Mahidol University Research fund for providing the opportunity to study in Ph.D. program, supporting the research fund in USA and the presentation at Austria.

As well, my special appreciation to my friend and other persons who have not been mentioned here for their helpful, friendship and encouragement. Finally, I wish to express my deepest gratitude and infinite thankfulness to my family for their love, encouragement and support throughout my life.

Maleeruk Utsintong

**DEVELOPMENT OF DRUGS FROM THERAPEUTIC TARGETS IN COBRA VENOM USING STRUCTURE BASED DRUG DESIGN AND VIRTUAL SCREENING.**

MALEERUK UTSINTONG 4636358 PYPP/D

Ph.D. (PHARMACEUTICAL CHEMISTRY AND PHYTOCHEMISTRY)

THESIS ADVISORS: OPA VAJRAGUPTA, Ph.D., WICHET LEELAMANIT, Ph.D., ARTHUR J. OLSON, Ph.D.

**ABSTRACT**

Alpha-cobratoxin ( $\alpha$ -cbtx), the long chain neurotoxin from *Naja kaouthia* acts on the postsynaptic nicotinic acetylcholine receptors (nAChR) and causes paralysis by preventing acetylcholine binding to nAChR.  $\alpha$ -Cbtx has been proposed as a potential target for anticobratoxin drug design. Investigation of redioides (A & G) binding mode to reveal the molecular mechanism of its antivenom action was achieved by means of molecular docking. The  $\alpha$ -cbtx/ acetylcholine binding protein (AChBP) complex (1YI5) was selected to construct  $\alpha$ -cbtx active binding site for docking. The constructed  $\alpha$ -cbtx template was validated with the control peptide (Ser182 – Tyr192 of AChBP) and the RMSD was less than 1.2 Å. Redioides bind to the  $\alpha$ -cbtx in the same location that the  $\alpha$ -cbtx binds to AChBP at the Asp27, Phe29, Arg33, Gly34, Lys35 and Val37 residues. The binding energies were -14.17 and -14.14 kcal/mol, respectively. Thus,  $\alpha$ -cbtx cannot bind to AChBP because some of its binding sites are occupied with redioides. The template was also employed in the virtual screening of over 1990 compounds in NCI diversity set and 39 hits were identified. The potential hits are NCI42258, NCI121865 and NCI134754 which competitively displace the antagonist ( $^{125}$ I  $\alpha$ -bungarotoxin) and the agonist ( $^3$ H epibatidine) from their mutually exclusive binding sites on *Lymnaea stagnalis* (*Ls*), *Aplysia californica* (*Ac*) and *Bulinus truncatus* (*Bt*) AChBPs. In particular, NCI121865 had  $K_d$  of 16.26 nM against *Ac* and 111 nM and 415 nM against *Ls* and *Bt*, respectively. The results from SDS-PAGE found that redioides neutralized and diminished the  $\alpha$ -cbtx band intensity. NCI121865 bound the  $\alpha$ -cbtx in crude venom resulting in the increase of the  $\alpha$ -cbtx band intensity. NCI42258 and NCI134754 changed some characteristics of the  $\alpha$ -cbtx and broadened  $\alpha$ -cbtx band. In the presence of AChBP, it was apparent that three hits and redioides bound to both  $\alpha$ -cbtx and AChBP. *In vivo*, three hits (5 mg/kg, i.v.) and redioides (0.5 mg/kg, i.v.) can prolong the survival times of the mice when injected 30 minutes before injection of the  $\alpha$ -cbtx (3LD<sub>50</sub> dose). Only NCI121865 and NCI134754 demonstrated the antivenom action; they can prolong the survival time when injected immediately after injection of the  $\alpha$ -cbtx. In clinical applications, NCI121865 and NCI134754 would be a very useful potential lead for the treatment of snakebite victims.

**KEY WORDS : ALPHA-COBRATOXIN / ANTICOBRATOXIN / DOCKING / ACETYLCHOLINE / VIRTUAL SCREENING.**

170 pp.

การพัฒนาจากบริเวณที่ออกฤทธิ์ในพิษงูโดยใช้เทคนิคการออกแบบยาจากโครงสร้างของโมเลกุลเป้าหมายและเทคนิคการคัดกรองประสิทธิภาพสูง (DEVELOPMENT OF DRUGS FROM THERAPEUTIC TARGETS IN COBRA VENOM USING STRUCTURE BASED DRUG DESIGN AND VIRTUAL SCREENING)

มาสิริรักษ์ อัดต์สินทอง 4636358 PYPP/D

ปร.ด. (เภสัชเคมีและพิษวิทยาเคมี)

คณะกรรมการควบคุมวิทยานิพนธ์: โสภา วัชรคุปต์, Ph.D., วิเศษฐ์ ลีลามานิตย์, Ph.D., Arthur J. Olson, Ph.D.

### บทคัดย่อ

แอลฟาโคบราที่ออกซินจากงูเห่าไทยเป็นนิวโรทอกซินชนิดสายโซ่ยาว ออกฤทธิ์โดยการจับที่โพสซิงแนบตึกของอะซิติลโคลีนรีเซปเตอร์ทำให้อะซิติลโคลีนไม่สามารถจับกับรีเซปเตอร์ได้ เป็นสาเหตุของการเกิดอัมพาต การวิจัยนี้เป็นการออกแบบสารต้านพิษงูโดยใช้แอลฟาโคบราที่ออกซินเป็นโมเลกุลเป้าหมายและศึกษากลไกการต้านพิษงูของสารเรดิโอไฮด์เอและบีจากสมุนไพรวัดตะนงโดยใช้เทคนิคโมเลกุลาร์ดีคอกกิง เริ่มจากการเตรียมแม่แบบของแอลฟาโคบราที่ออกซินโดยใช้ข้อมูลจากการเอ็กซ์เรย์ผลึกแอลฟาโคบราที่ออกซินที่จับกับอะซิติลโคลีนบายดิงโปรตีน (PDB: 1Y15) และใช้เปปไทด์ตำแหน่งที่ 182-192 ของอะซิติลโคลีนบายดิงโปรตีนในการตรวจสอบความถูกต้องของแม่แบบซึ่งผลการตรวจสอบให้ค่า RMSD น้อยกว่า 1.2 อังสตรอม กลไกการออกฤทธิ์ของสารเรดิโอไฮด์เอและบีคือ จับกับแอลฟาโคบราที่ออกซินที่ตำแหน่ง แอสพาราจิน27 ฟีนิลอะลานีน29 อาร์จินีน33 ไกลซีน34 ไลซีน35 และวาลีน37 ซึ่งเป็นบริเวณเดียวกันกับที่แอลฟาโคบราที่ออกซินจับกับบายดิงโปรตีนพลังงานในการจับต่ำสุดมีค่า -14.17 และ -14.14 กิโลแคลอรีต่อโมลตามลำดับ ดังนั้นแอลฟาโคบราที่ออกซินจึงไม่สามารถจับกับอะซิติลโคลีนบายดิงโปรตีนเนื่องจากกระดุมมีโนบางตัวของแอลฟาโคบราที่ออกซินถูกเรดิโอไฮด์เอจับอยู่ นอกจากนี้ยังใช้แม่แบบแอลฟาโคบราที่ออกซินมาคัดกรองสารจำนวน 1990 สารจากสถาบันมะเร็งแห่งชาติได้โครงสร้างสารที่มีศักยภาพจำนวน 39 สาร และเมื่อนำสารทั้ง 39 สารมาทดสอบในหลอดทดลองได้สารต้นแบบ 3 สารที่มีความสามารถในการแข่งขันกับแอลฟาบังกาโลที่ออกซินและสารอีพิบาดีนินที่ติดฉลากกัมมันตรังสีโดยแย่งจับกับอะซิติลโคลีนบายดิงโปรตีนทั้ง 3 ชนิด สาร NCI121865 มีฤทธิ์สูงสุดสามารถจับกับบายดิงโปรตีนจาก *Aplysia Lymnaea* และ *Bolinus* ที่ 16.26 111 และ 415 นาโนโมลาร์ ตามลำดับ ผลการศึกษาโดยใช้เจลอิเล็กโตรโฟรีซิสพบว่า เรดิโอไฮด์เอและบีสามารถลดความเข้มข้นของแอลฟาโคบราที่ออกซิน NCI121865 เพิ่มความเข้มข้นของแอลฟาโคบราที่ออกซิน NCI42258 และ NCI134754 เปลี่ยนคุณสมบัติแอลฟาโคบราที่ออกซิน ในกรณีที่มีทั้งบายดิงโปรตีนและพิษงูพบว่า สารต้นแบบทั้งสามสารและเรดิโอไฮด์เอจับได้ทั้งแอลฟาโคบราที่ออกซินและบายดิงโปรตีนเมื่อศึกษาต่อในหนูถีบจักรพบว่า สารต้นแบบและเรดิโอไฮด์เอสามารถยืดระยะเวลาการตายของหนูเมื่อนิดแอลฟาโคบราที่ออกซินหลังจากฉีดสาร 30 นาที แต่มีสารต้นแบบสองสารคือ NCI121865 และ NCI134754 เท่านั้นที่มีฤทธิ์ต้านพิษงู โดยสามารถยืดระยะเวลาการตายของหนูเมื่อนิดสารหลังจากแอลฟาโคบราที่ออกซินทันที ในทางคลินิก NCI121865 และ NCI134754 จะมีประโยชน์ในการพัฒนาเป็นสารต้านพิษงูในการรักษาผู้ถูกงูกัด

## CONTENTS

	<b>Page</b>
ACKNOWLEDGEMENTS	iii
ABSTRACT	iv
LIST OF TABLES	viii
LIST OF FIGURES	x
LIST OF SCHEMES	xiii
LIST OF ABBREVIATIONS	xiv
CHAPTER	
I. INTRODUCTION	1
II. LITERATURE REVIEW	4
Part I. Snake	4
Part II. Medicinal Plant against Snake Venom	24
Part III. Nicotinic Acetylcholine Receptor	27
Part IV. Automated Docking	33
Part V. Virtual Screening	36
III. EXPERIMENTAL	38
A. Molecular Modeling ( <i>In Silico</i> ) Experiment	38
1. Material	38
2. Method	38
B. <i>In Vitro</i> Binding Assay	42
1. Materials	42
2. Methods	43
C. <i>In Vitro</i> Experiment	49
1. Materials	49
2. Methods	49
IV. RESULTS AND DISCUSSION	53
A. Molecular Modeling ( <i>In Silico</i> ) Experiment	54
B. <i>In Vitro</i> Experiment	68
C. <i>In Vivo</i> Experiment	87
D. Summary	92

**CONTENTS (Cont.)**

	<b>Page</b>
V. CONCLUSION	94
REFERENCES	97
APPENDIX	107
Appendix A	108
Appendix B	115
Appendix C	119
Appendix D	121
BIOGRAPHY	170

## LIST OF TABLES

Tables	Page
1. Systematics of venomous snakes	6
2. Enzymes found in snake venoms	10
3. Main clinical features of snakebite	21
4. Medicinal plants in Thailand	25
5. 17 nAChR subunits	31
6. Notable variations of nAChR	32
7. The composition of separating gel and stacking gel	47
8. Critical values of Q	52
9. Amino acid residues of $\alpha$ -cobratoxin interacted with the control peptide and the AChBP in the crystal pose (1YI5)	59
10. Cluster analysis from docking $\alpha$ -cobratoxin with rediocides A and G	63
11. Amino acid residues of $\alpha$ -cobratoxin forming hydrogen bonds to rediocides	64
12. The top 175 compounds for each $\alpha$ -cobratoxin templates	66
13. Selected hits from virtual screening	67
14. Percent amino acid identity of AChBPs	68
15. NCI diversity set identified from virtual screening	76
16. $K_d$ of 4 hits on AChBPs	77
17. Amino acid residues of $\alpha$ -cobratoxin interacted with 3 hits	79
18. Toxicity test of rediocides and 3 hits (n=6)	88

**LIST OF TABLES (Cont.)**

<b>Tables</b>	<b>Page</b>
19. Protective effect of rediocides (A & G) and 3 hits against $\alpha$ -cobratoxin	90
20. Anti-cobratoxin of rediocides against $\alpha$ -cobratoxin	91
21. Anti-cobratoxin of 3 hits against $\alpha$ -cobratoxin	92
B1. The top 175 compounds for each $\alpha$ -cobratoxin	115
C1. The screening test data from radioligand competition assay	119

## LIST OF FIGURES

Figures	Page
1. Structures of rediocide A and G	2
2. The morphology of a venomous snake	5
3. Three species of cobras living in Thailand	8
4. The structure of $\alpha$ -cobratoxin	15
5. Pathways of complement activation	16
6. The diagram of the alternative pathway of CVF	17
7. Schematic drawing of the degradation products of human C3	18
8. The amino acid sequence of pro-CVF	20
9. The major components of <i>Lotthanong</i>	26
10. Acetylcholine receptor (nicotinic) from electric torpedo rays	28
11. Acetylcholine receptor blocked by cobra venom (PDB code: 1YI5)	28
12. The 1YI5 bound crystal between $\alpha$ -cobratoxin (chain F-J) and AChBP (chain A-E); (PDB: 1YI5)	55
13. The control peptide for the $\alpha$ -cobratoxin template validation	56
14. The clusters of docked control peptide in the same 3D structure (RMSD of 2 Å), docking energy is in kcal/mol	57
15. Superposition of crystallographic Ser182 – Tyr 192 of chain C from 1YI5 and docked orientation of control peptide (A-C)	58
16. Structures of rediocides A and G	60
17. Clusters of docked rediocides in the same 3D structure (RMSD < 2Å), (A) rediocide A and (B) rediocide G, docking energy is in kcal/mol	61

## LIST OF FIGURES (Cont.)

<b>Figures</b>	<b>Page</b>
18. The bound conformations of redioides in the active site of $\alpha$ -cobratoxin	62
19. The bound conformations of redioides in the active site of $\alpha$ -cobratoxin (A and B)	65
20. The amino acid sequences of AChBPs ( <i>Ac</i> , <i>Ls</i> and <i>Bt</i> ) and human nAChR ( $\alpha 7$ and $\alpha 1$ )	69
21. AChBPs bound to the bead by using the monoclonal anti-FLAG M2 antibody from mouse	70
22. Radioactive [ $^3\text{H}$ ] epibatidine or [ $^{125}\text{I}$ ] bungarotoxin bound to the binding protein and emitted the light	71
23. Screening test for the ability to displace the binding of [ $^3\text{H}$ ] epibatidine on AChBP from <i>Lymnaea stagnalis</i> ( <i>Ls</i> ), <i>Aplysia californica</i> ( <i>Ac</i> ) and <i>Bulinus truncatus</i> ( <i>Bt</i> )	72
24. The ability to displace the binding of [ $^3\text{H}$ ] epibatidine on AChBPs (~500 pM binding site) from <i>Lymnaea stagnalis</i> (A), <i>Aplysia californica</i> (B) and <i>Bulinus truncatus</i> (C)	73
25. The ability to displace the binding of [ $^{125}\text{I}$ ] $\alpha$ -bungarotoxin on AChBPs from <i>Lymnaea stagnalis</i> (A) and <i>Aplysia californica</i> (B)	74
26. The dock orientations of NCI42258 (indigo blue), NCI121865 (light green) and NCI134754 (purple) (A)	78
27. The amino acid residues of $\alpha$ -cobratoxin interacted with NCI42258 (A), NCI121865 (B) and NCI134754 (C) with distance < 4 Å	79
28. SDS-PAGE of the mixtures between crude venom and redioides (A & G)	81

**LIST OF FIGURES (Cont.)**

<b>Figures</b>	<b>Page</b>
29. SDS-PAGE of AChBP from <i>Aplysia stagnalis</i> in the presence of $\alpha$ -cobratoxin and rediocides (A & G)	82
30. SDS-PAGE of the mixtures between crude venom and 3 hits	84
31. SDS-PAGE of $\alpha$ -cobratoxin and AChBP from <i>Aplysia stagnalis</i> in the presence of 3 hits	86
32. LD <sub>50</sub> of $\alpha$ -cobratoxin (n=6)	87
33. Toxicity of rediocides (A & G). The mouse was injected with rediocides (A) and NCI134754 (B)	89

## **LIST OF SCHEMES**

<b>Schemes</b>	<b>Page</b>
A1. Virtual screening map	108
A2. Virtual screening data	109
A3. The virtual screening data to prepare the dpf files	112

## LIST OF ABBREVIATIONS

$\alpha$ -cbtx	alpha-cobratoxin
Å	angstrom
AChBP	acetylcholine binding protein
°C	degree celcius
g	gram
h	hour
IC <sub>50</sub>	50% inhibitory concentration
i.m.	intramuscular
i.v.	intravenous
l	liter
LD <sub>50</sub>	mean lethal dose
M	mole/liter, molar
mg	milligram
min	minute
ml	milliliter
mM	millimole/liter, millimolar
mmol	millimole
MW	molecular weight
nAChR	nicotinic acetylcholine receptor
NCI	National Cancer Institute
nM	nanomole/liter, nanomolar
NMR	nuclear magnetic resonance
PDB	Protein Data Bank
RMSD	root mean square deviation
rpm	round per minute
SD	standard deviation
µg	microgram

**LIST OF ABBREVIATIONS (Cont.)**

$\mu\text{l}$	microliter
v/v	volume by volume
w/v	weight by volume

## CHAPTER I

### INTRODUCTION

Snake bites are an occupational hazard, especially among tropical forest workers, farmers and agriculturists. In many cases, survivors are left with chronic functional disability from the necrotic effects of the venom, resulting in chronic ulceration, chronic renal failure and neurological sequelae from intracranial hemorrhages and thromboses or even amputation (1-4). Snake venoms contain complex mixtures that consist of several toxic proteins with diverse biological activities. Venom from the Thai cobra *Naja kaouthia* contains paralytic “neurotoxin” activity, which acts on nicotinic acetylcholine receptors (nAChR), cytolytic “cardiotoxin” activity, which acts on cell membranes, as well as phospholipase, and *D*-amino acid oxidase activities (5-7). Alpha-cobratoxin or neurotoxin 3 is the main component in cobra venom which accounts for 20-30% of the venom, dried weight. Antivenoms against many snake venoms have been produced and are being used for specific treatment of snake envenomations. Although polyvalent antivenom is an effective treatment, the recovery of the victim is slow and larger doses are needed. Furthermore, severe allergic reactions and serum sickness resulting from antivenom therapy are serious side effects. In Thailand, the only remedy for cobra bite is a monospecific antivenom produced by Queen Saovabha Memorial Institute, The Thai Red Cross Society. The horse antivenom against *Naja kaouthia* is very difficult to produce, expensive and in short supply. Only 20% of the horses immunized with Thai cobra venom produce adequate neutralizing activity for antivenom production. Furthermore, the neutralizing activity considered adequate is in fact quite low.

$\alpha$ -Cobratoxin (Cbtx), a member of the long  $\alpha$ -neurotoxin family, is obtained from the venom of *Naja kaouthia* (previously called *Naja naja siamensis*). Cbtx has 71 amino acid residues and 5 disulfide bridges (8). It consists of three finger-like loops: loop I, II and III. It blocks nerve transmission by binding to the nAChR on the

postsynaptic membranes of skeletal muscle and/or neurons, causing paralysis by preventing acetylcholine binding to the nicotinic acetylcholine receptor (9). nAChR mediates excitatory transmission at the neuromuscular junction and in the central and peripheral nervous systems. The soluble acetylcholine-binding protein (AChBP) from the freshwater snail *Lymnaea stagnalis* (*Ls*) is a structural homologue of the extracellular ligand-binding domain of muscle-type and neuronal nAChRs (10-11). Recently, the NMR and crystal structure of a Cbtx-AChBP complex (1YI5) was discovered (12-14). Since this initial discovery, AChBP have been identified in the molluskan species, *Bolinus truncatus* (*Bt*), and the marines-species, *Aplysia californica* (*Ac*) (15-16).

Application of medicinal plants with anti-snake venom activities might be useful as first aid treatment for victims of snake bite. There are about forty plants in Thailand reported to be effective in treating snake bites (17). One of the potential plants among these Thai plants was *Trigonostemon rediocides* (Kurz) Craib, which is known as *Lotthanong* in Thai belongs to the Euphorbiaceae family. The herb is particularly effective in treating snake bites especially against snake neurotoxins. According to the preliminary testing, it was found that the crude extract from Lotthanong's root can extend the survival time of the crude Thai cobra venom treated mice. In previous investigations of *T. rediocides*, the daphnanediterpenoids (rediocides A and G) (Figure 1) have been found to be the main components in the roots of this plant (18-21).

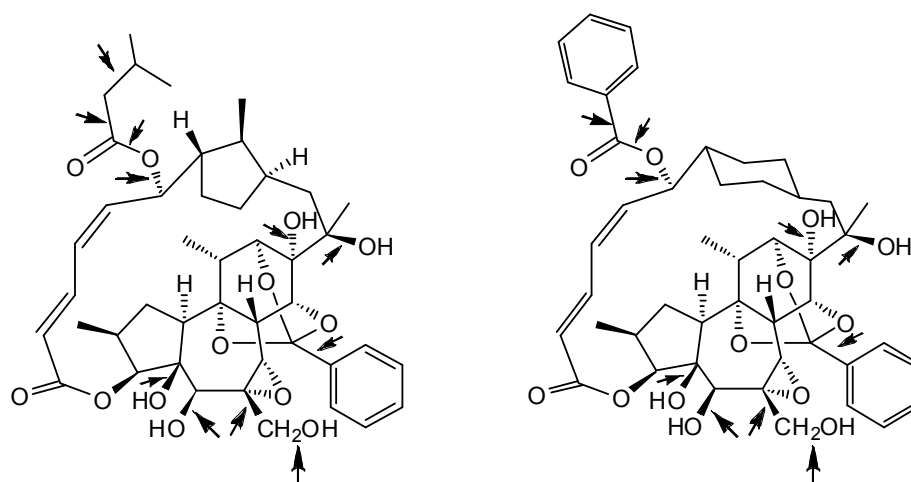


**Figure 1.** Structures of rediocide A (left) and G (right).

In search of an antidote of cobra venom by preventing the  $\alpha$ -cobratoxin from binding to the nAChR, the molecular docking was carried out to investigate the binding mode of redioides to  $\alpha$ -cobratoxin. This study aimed to find the mechanism of redioides against cobra venom at the molecular level to promote the utilization of medicinal plant in clinical use. In addition to the investigation of the molecular mechanism of redioides, virtual screening was accomplished by using  $\alpha$ -cobratoxin as template and docked with 1990 compounds in National Cancer Institute diversity set. The objective of virtual screening is to discover the structure of new lead for drug design (22). The *in vitro* SDS-PAGE and binding assay as well as *in vivo* anti-toxin tests were performed to support the *in silico* results. The findings will be useful for patients who are bitten by snakes and will be useful for medical and pharmaceutical treatment in Thailand.

## **CHAPTER II**

### **LITERATURE REVIEW**

#### **Part I. Snake**

##### **1. Snake and venomous snakes**

Snake are cold-blooded vertebrates of class Reptilia, subclass Synaptosuaria, order Squamata, suborder Serpentes, which related to turtles, crocodiles and lizards. Anatomically, snakes have a long tube shape with narrow tail and they have heat reception pits as a heat-detecting organ. Their skins cover with scales, which are also used in classification (23). Although, they are deaf to air-borne sounds and have very poor vision, they have keen sense of smell, and are highly sensitive to ground conducted vibrations. Since snakes lack internal means of regulating body temperature, diurnal and seasonal temperature variations influence their degree of activity (24).

One of the anatomical characters of dangerous venomous snakes that distinguish them from harmless ones is “venom apparatus”. The venom apparatus consists of venom glands, venom ducts that connect to venom fangs. The venom fangs are hollow and their function is like that of a hypodermic syringe (25). The morphology of a venomous snake is shown in Figure 2 (26). Generally, the function of the venom apparatus is to secure food and to aid in digestion of prey (27-29). Young snakes of poisonous families are considered venomous at birth (24).

Mostly, snakes eat small vertebrates and some eat prey, such as rodents, which are capable of inflicting serious injury. Rapid dispatch of the prey through the injection of venom; therefore, greatly reduce the hazard to the snakes. It is a safe rule that venomous snakes do not attack people; they bite defensively when threatened and sometimes only after warning signal has fail to deter. Indeed, many poisonous snakes have warning signals, the effectiveness of which would seem to depend upon the

surviving large animals learning to avoid the snakes concerned. Biting of venomous snakes to large animals such as man is secondary defensive in nature (30).

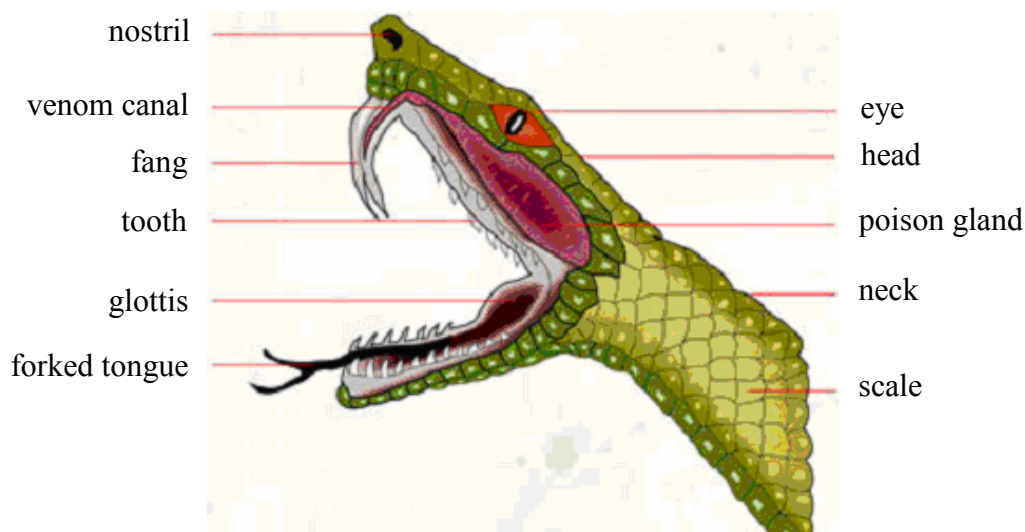


**Figure 2.** The morphology of a venomous snake.

There are numerous species of venomous snake reorted worldwide. Based on the morphological characteristics, three major families are classified as shown in Table 1 (30). Thailand locates in the tropical area where appropriate for inhabitant of many species of venomous snakes. There are 19 kinds of deadly venomous snake, 11 kinds of venomous snake, 28 kinds of mildly venemous snake and 24 kinds of venomous sea snake (31). Among these, the most medically important terrestrial venomous snakes of Thailand are 6 species, which belong to the Elapidae and Viperidae families. The elapids include *Naja kaouthia*, also known as *Naja naja siamensis* (Thai cobra), *Ophiophagus hannach* (King cobra) and *Bungarus fasciatus* (banded krait). While the vipers include *Daboia russelli siamensis* (Russell's viper), *Calloselasma rhodostoma* (Malaya pit viper) and *Trimeresurus albolabris* (green pit viper) (32-34). The monocellate Thai cobra, *Naja kaouthia*, is a major cause of snakebite mortality and morbidity throughout Thailand. There is a high incidence of cobra bite amongst the fisherman and rice farmer in rural part of Thailand (35).

**Table 1.** Systematics of venomous snakes (30)

<b>Family</b>	<b>Subfamily</b>	<b>Genera</b>
Colubridae	Pseudoboinae	3 genera
	Aparallactinae	16 genera
	Atractaspindra	Atractaspis
	Boiginae	27 genera
	Homalopsinae	10 genera
	Xenodontinae	11 opisthoglyphous genera
	Natricinae	1 opisthoglyphous genera
	Colubrinae	Dispholidus, Thelotornis plus 9 other opisthoglyphous genera
Viperidae	Azemiopinae	Azemiops
	Viperinae	Adenorpinus, Atheris, Bitis, Causus, Cerastes, Echis, Eristicophis, Pseudocerastes, Vipera
	Crotarinae	Agkistrodon, Bothrops, Crotalus, Lachesis, Sistrurus, Trimeresurus
Elapidae	Elapidae	Acanthophis, Aspidelaps, Aspidomorphus, Austrelaps, Boulengerina, Bungarus, Cacaphis, Calliophis, Cryptophis, Demansia, Dendroaspis, Denisonia, Drysdali, Echiopsis, Elapognathus, Elapsoidea, Furina, Glyphodon, Hemachatus, Hemiaspis, Homoroselaps, Hoplocephalus, Leptomicrurus, Loveridgelaps, Maticora, Micropechis, Micruroides, Micrurus, Naja, Notechis, Ogmodon, Ophiophagus, Oxyuranus, Parademansia, Paranaja, Parapistocalamus, Pseudechis, Pseudonaja, Rhinhoplocephalus, Simoselaps, Solomonelaps, Suta, Toxicocalamus, Tropidechis, Vermicella, Walterinnesia
	Laticaudinae	Laticauda
	Hydrophiinae	
	Ephalophiini	Aipysurus, Emydocephalus, Ehpalohpis, Hydrelaps, Parahydrophis
	Hydrophiini	Acalyptophis, Enhydrina, Hydrophis, Kerilia, Kolpophis, Pelamis, Thalassophis

## 2. Cobra

“Cobras” belong to family Elapidae, genus *Naja*. There are at least eight full species, which found throughout India and Southeast Asia (34). Cobras are easily distinguishable from other snakes by their neck can extend to be hood when there are in an erect position. Like all members of the Elapidae family, they have a pair of short, fixed fangs without covered sheath, which known as the Proteroglypha fangs, in front of the mouth (23-25).

There are three species of cobra presented in Thailand and are quite confusing in the identification. The first one is the monocellate non-spitting cobra or Thai cobra, (*Naja Kaouthia*). *Naja kaouthia* also known as *Naja naja siamensis* is the most dangerous cobra in Thailand. This specie is identified by an *O*-shaped marking on the back of the neck as shown in Figure 3a. Thai cobra is found in most parts of Thailand but mostly on central plain. Its length is around 755 mm (281-1680 mm). There are varies widely in its color and its hood-marking pattern. It is usually found in termite mounds, near habitation, forests and foothills up to 900 meters. It is also found in Myanmar, Laos, Vietnam and Malaysia. The other two species are spitting cobras, *Naja siamensis* and *Naja sumatrana*. These two species can spit venom to their enemies such as men and dogs to defense themselves, while this behavior is not found in *Naja kaouthia*. This could be due to the difference in physical characteristic of their fangs. *Naja siamensis* is found throughout the country except in the peninsular. In some area of Thailand, this specie variously known as Isan spitting cobra, the black spitting cobra and black and white spitting cobra. This form is also referred to as *N. atra* or *N. sputatrix* by some investigations. The *V*-shaped marking, *U*-shaped marking or *H*-shaped marking on the hood is used for define snakes in this species as shown in Figure 3b. The last one, *Naja sumatrana* (Golden spitting cobra) is occasionally found in southern part of Thailand particularly Surat Thani, Nakhon Sri Thamarat and Pattalung provinces. However, it is also found in Malaysia and Indonesia. This is the form referred to as *N. naja sputatrix* by some investigators (25, 28). Usually, there are not found any markig on the hood of snakes in this species as shown in Figure 3c (acellate) (23, 36-38).



The venoms of snakes are usually composed of a complex mixture of organic and inorganic components. Insoluble tissue debris is also often noted in the venom from milk snakes. The inorganic constituents of the venoms include: Ca, Cu, Fe, K, Mg, Mn, Na, P, Co and Zn. Not all of these metals are found in every type of venom, and amount of each metal varies with the species of snake. The biological role of each of the metals is not clear; however, it is likely that some of them, such as Ca, Mg, and Mn, are quite important for the stabilization of certain venom proteins. While others, in particular, Zn, Cu, Fe and Co, may be actual participants in the catalytic mechanisms of certain venom enzyme components, such as the metalloproteinases. Although, it is convenient to divide the organic compounds of the venom into proteinaceous and non-proteinaceous material; the majority of the crude venom is composed of proteinaceous components. The other compounds include carbohydrates, nucleosides, bioactive amines, amino acids and lipids. Carbohydrates are mainly present in the form of glycoprotein (41).

Proteinaceous material, proteins and peptides, comprise approximately 90-95% of the dry weight of the venom (42). Venom proteins have many diverse enzymatic activities including, but not limited to, phospholipase A<sub>2</sub>, phosphodiesterase, phosphomonoesterase, L-amino acid oxidase, acetylcholinesterase, proteolytic activity (enzymes of the serine proteinase and metalloproteinase classes), arginine esterase, 5'-nucleotidase, hyaluronidase and nicotinamide adenine dinucleotide nucleosidase as shown in Table 2. Peptides found in snake venoms may comprise of presynaptic and postsynaptic neurotoxins, potassium channel-binding neurotoxins, cytotoxins, myotoxins, cardiotoxins and platelet aggregation inhibitors (disintegrins) (40, 43). Not all of these enzymes and peptides are present in any one kind of snake venom. The proportions of different components in snake venoms vary with species. For example, the venoms of Viperidae and Crotalidae. The hydrophobic venoms are abundant in myotoxins and neurotoxins (39). However, the closer the phylogenetic relationship of snakes, the more similar venom properties and compositions (44).

**Table 2.** Enzymes found in snake venoms and composition of cobra venom (40)

<b>Venom</b>	<b>Enzyme</b>
all snake venoms	Phospholipase A <sub>2</sub> , L-amino acid oxidase, Phosphodiesterase, 5'-Nucleotidase, Phosphomonoesterase, Deoxyribonuclease, Ribonuclease, Adenosine triphosphatase, Hyaluronidase, NAD-nucleosidase, Arylamidase, Peptidase
crotalid and viperid venoms	Endopeptidase, Arginine ester hydrolase, Kininogenase, Thrombin-like enzyme, Factor X activator, Prothrombin activator
elapid venoms	Acetylcholinesterase, Phospholipase B, Glycerophosphatase
some venoms	Glutamic-pyruvic transaminase, Catalase, Amylase, B-Glucosaminidase, Lactate dehydrogenase, Heparinase-like enzyme
cobra venom	Mettalloproteinase, Serine proteinase, Acetylcholinesterase, neurotoxin, cobra venom factor

### 3.2 Pharmacology of snake venom

The specific pharmacology of snake venom has been difficult to delineate because a various venom components may have one or several receptor sites, and these are not necessary organ-specific or system-specific. When venom is dispensed subcutaneously, it is absorbed through the lymphatic system as well as the capillary bed and other cell membranes. Venom also may be injected directly into an artery or vein and distributed throughout the blood-vascular system to other tissue (27).

Basically, the venom is an adaptation to obtain food. Because the snake's prey is usually large and swallowed whole, digestion time in the snake's gut may be prolonged up to 14 days. Putrefaction may force the snake to regurgitate its meal

before digestion takes place. Injection and circulation of digestive enzymes before ingestion of the prey reduces digestive time to 2 to 5 days. The venom therefore contains a lethal protein component designed to immobilize the prey for a short period during which the second component, the digestion enzymes, may be distributed throughout the prey's tissues. Thereafter, the prey dies before it can retreat out of the snake's range of activity (45).

The lethal proteins and peptides consist of 20 to 80 amino acid chains and range in molecular weight between 4,800 and 100,000 Da. Electronmicroscopy shows that these proteins damage endothelial cells of vascular walls, causing blebs in the endothelium, dilating the perinuclear space, and breaking down the plasma membrane. Blocking neuromuscular transmission results in flaccid paralysis and impaired respiration. Plasma and erythrocytes leak into the tissues, resulting in often massive accumulation of fluid in intracellular spaces; this is manifested as edema. Plasma loss reduces the circulating blood volume and leads to hypovolemic shock, hemoconcentration, and lactic acidosis. The capillary bed of the lungs may also be affected by the proteins, which led to fluid loss into the alveoli, pulmonary edema and hemorrhage (45).

### **3.2.1 Enzymes in snake venom**

Digestive enzymes containing within snake venom cause both local and systemic damage to human tissue. At least 26 enzymes have been identified as shown in Table 2. The major enzymes and their pharmacological effects are the following (40, 44-45).

#### **3.2.1.1 Phospholipase A<sub>2</sub>**

One of the most common enzymes is found in snake venoms. All venoms of Hydrophiidae (sea snakes), Elapidae, Viperidae and Crotalidae so far investigated contain this enzyme. They catalyze the hydrolysis of the ester bond at C<sub>2</sub> position of lecithin, releasing a molecule of fatty acid and isolecithin. The enzymes thus damage the fatty molecules of all membranes. Damage to muscle fiber membrane results in local necrosis. Permeability of erythrocyte membranes is altered, allowing water to enter the cells cell, eventually resulting

in haemolysis. Precipitation of free hemoglobin and erythrocyte ghosts in kidney tubules leads to renal shutdown (7, 46).

#### 3.2.1.2 Hyaluronidase

This enzyme cleaves internal glucoside bonds of various collagens, decreasing the viscosity of connective tissue and allowing venom fractions to spread beyond the site of the bite. Although venom hyaluronidase is not toxic per se, it enhances the effect of the toxic by increasing their spread. This enzyme is also referred to as the “spreading factor”.

#### 3.2.1.3 Amino acid esterase and other thrombin-like enzymes

These enzymes promote fibrin formation by incompletely splitting either fibrinopeptide A or B from the fibrinogen molecule. Factor XII is not activated, however. Instead, an unstable fibrin clot is formed, trapping platelets. This clot is readily lysed by protein-splitting enzymes in the snake venom. The result is disseminated intravascular coagulation syndrome followed by often massive hemorrhage due to consumption of platelets and fibrinogen. This bleeding decreases the already depleted volume of blood circulation.

#### 3.2.1.4 Proteolytic enzymes and phosphomonoesterase

These enzymes include R Nase, D Nase, and 5' nucleotidase, which damage muscle fiber proteins, resulting in local necrosis if the venom is injected deeply enough to penetrate a muscle sheath. Up to five of these enzymes in this group may occur in the same type of venom.

#### 3.2.1.5 Acetylcholinesterase

Commonly, this enzyme occurs in nerves, erythrocytes, and the retina. It is also commonly present in the venom of Elapidae and Hydrophiidae but not in those of Viperidae and Crotalidae. Since acetylcholinesterase is involved in nerve transmission, it was thought at one time that venom acetylcholinesterase was responsible for the neurotoxic action of Elapidae venom.

### 3.2.1.6 Serine proteinase

Snake venom glands synthesize a variety of serine proteinases capable of affecting the hemostatic system. They act on macromolecular substrates of the coagulation, fibrinolytic, and kallikrein-kinin systems, and on platelets to cause an imbalance of the hemostatic system of the prey (47).

### 3.2.2 Toxin in snake venom

As known that, snake venom usually contains more than one toxic principle, and these tend to act in combination in actual poisoning. The overall toxicity is due to enzymes as well as to non-enzymatic proteins. However, the main lethal action, especially elapid and hydrophid venoms, can be attributed to neurotoxins. Postsynaptic neurotoxin or alpha-neurotoxin is the most lethal among the toxic components in elapid venoms. The type of toxins found in venoms are described below:

#### 3.2.2.1 Snake neurotoxin

Snake neurotoxins are peptides, which can cause skeletal muscle paralysis by inhibiting neuromuscular transmission. They are divided into two pharmacological classes based on their sites of action.

***Presynaptic neurotoxins:*** These peptide toxins have been found in the venom of Elapidae, Crotalidae and Viperidae snakes with phospholipase A<sub>2</sub> activity. These toxins interact with a target that is specifically present on the synaptic plasma membrane of motor nerve terminals. They cause blockade of neuromuscular transmission by inhibiting the release of acetylcholine from motor nerve (40, 45-48).

***Postsynaptic neurotoxins:*** These peptide toxins found predominantly in elapid venoms, are also called curare-mimetic toxins (alpha-cobratoxin or neurotoxin3) based on their mimicking action of curare on poison arrow of South American Indians. The postsynaptic neurotoxins are low molecular weight basic proteins found mostly in Elapidae or hydrophid snakes (24). Two types of postsynaptic neurotoxins can be distinguished on the basis of their sizes and disulfide linkages. These are short chain toxins containing 60-62 amino acid residues with four disulfide bonds and long chain

toxins containing 71-74 residues and four or five disulfide bonds. Both types show extensive homology in amino acid sequence and act in similar manner: blocking neuromuscular transmission by binding specifically and with high affinity to the nicotinic acetylcholine receptor. However, short chain toxin shows faster dissociate rate than that of long chain ones. They are immunochemically distinct from each other; hence antibodies produced against them do not cross-react. Moreover, they differ in circular dichroism spectra and stability including heat resistance, lyophilization and chemical modification (40, 44, 49-51).

One of the best known snake postsynaptic neurotoxins in *Naja kaouthia* (alpha-cobratoxin or neurotoxin3), which accounts for 20-30% of the venom, dried weight. This is the highest content of an individual neurotoxin found in venom of any terrestrial snakes in Thailand. It is the basic polypeptide containing 71 amino acid residues with 5 disulfide bridges. The structure was shown in Figure 4. The molecular weight of this toxin is 7821 daltons (39, 50-52). It consists of three finger-like loops: loop I, II and III. It blocks nerve transmission by binding to the nicotinic acetylcholine receptor (nAChR) on the postsynaptic membranes of skeletal muscle and/or neurons, causing paralysis by preventing acetylcholine binding to the nicotinic acetylcholine receptor (nAChR) (9). This postsynaptic neurotoxin is largely responsible for the toxicity and lethality of Thai cobra venom. nAChR mediates excitatory transmission at the neuromuscular junction and/or in the central and peripheral nervous systems. The soluble acetylcholine-binding protein (AChBP) from the freshwater snail *Lymnaea stagnalis* is a structural homolog of the extracellular ligand-binding domain of muscle-type and neuronal nAChRs (10-11). Its pentamers composed of either identical or homologous transmembrane subunits. Recently, the NMR and crystal structure of a Cbtx-AChBP complex (1YI5) was discovered. The amino acid residues from Cbtx that bind AChBP are Thr6, Pro7, Ile9 in loop I, Trp25, Cys26, Cys30, Asp27, Ala28, Phe29, Ser31, Ile32, Arg33, Gly34, Lys35, Arg36, Val37 in loop II and Phe65, Arg68 for C-terminus (12-14). Since this initial discovery, AChBP have been identified in the molluscan species, *Bolinus truncatus* (*Bt*), and the marines-species, *Aplysia californica* (*Ac*) (15-16).

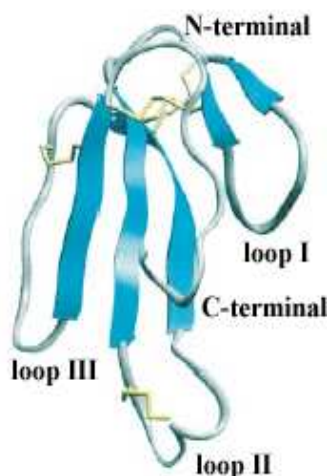


**Figure 4.** The structure of  $\alpha$ -cobratoxin. Disulfide bridges are in yellow line (8).

#### 3.2.2.2 Cardiotoxin

Cardiotoxins are other low molecular weight (around 6000-7000 kDa) basic peptide toxins found in elapid venoms. They are single-chain polypeptides chemically and structurally related to the postsynaptic neurotoxins. They contain approximately 60 amino acid residues and 4 disulfide bridges. They have lytic effect on a wide range of cells so they were named as “Direct Lytic Factor”, cytotoxins or membrane toxins. However, the name cardiotoxins were extensively used because the heart appears to be the main target of these toxins and that the toxins are much more selective in their actions than other names above.

Cardiotoxins cause death “shock” follows quickly by fastened  $K^+$  released from lysed RBC. The lethality of cardiotoxins is greatly increased in the presence of phospholipase  $A_2$ , which also has a synergistic effect on other activities displayed by this toxin.

Apart from lytic effect on erythrocytes and various cell types, they also induce depolarization resulting in blockade of axonal conduction in peripheral nerve, ventricular fibrillation, systolic arrest of heart muscle and prolonged muscular contractures with paralysis. It was shown that cardiotoxins affect the membrane and not the myofibril itself. The effect is irreversible. However, addition of  $Ca^{++}$  can prevent this effect due to inhibition of toxin binding (40, 44, 53).

### 3.2.2.3 Cobra venom factor

In addition to the hemolytic pathways, which involve the venom phospholipases and cardiotoxin, red cell lysis can be produced through an entirely different mechanism by one component in cobra venoms called “Cobra Venom Factor” (CVF). CVF is active on the alternative pathway complement system. Cobra venom factor (CVF) is the complement-activating protein from venom, causing complement consumption or complement depleting in human and mammalian serum (54). The complement system is an integral component of the immune system and plays important roles in immune response and host defense. The system is comprised of approximately 20 plasma proteins and a number of cell surface receptors. In addition to its physiological role, the complement system is also activated in many disease states and contributes importantly to the pathogenesis of many diseases and conditions of major medical importance including, rheumatoid arthritis and other immune complex diseases, certain types of glomerulonephritis, autoimmune hemolytic anemia, myasthenia gravis and other autoimmune diseases, and reperfusion injury (55). The pathway of complement activation was shown in Figure 5.

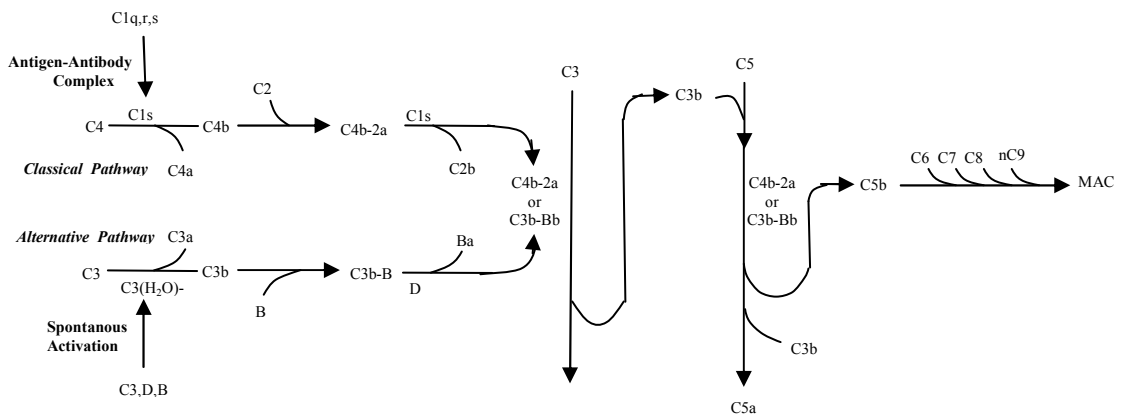


**Figure 5.** Pathways of complement activation.

The latter refers to the tissue damage that occurs after reopening of a blocked vessel after a heart attack, stroke, or reperfusion with a recipient's blood after organ transplantation. The molecular interactions of CVF with human complement were elucidated experimentally, simultaneously revealing the reaction sequence of the

alternative complement pathway and the functional analogy of CVF and C3b, the activated form of C3. The diagram of the alternative pathway was shown in Figure 6. Like C3b, CVF binds to factor B in human and mammalian serum to form the complex CVF-B (56), which is cleaved by factor D into the bimolecular enzyme CVF-Bb and Ba. The bimolecular complex CVF-Bb is a C3/C5 convertase that activates C3 and C5 analogously to the C3/C5 convertase formed with C3b (57-61).

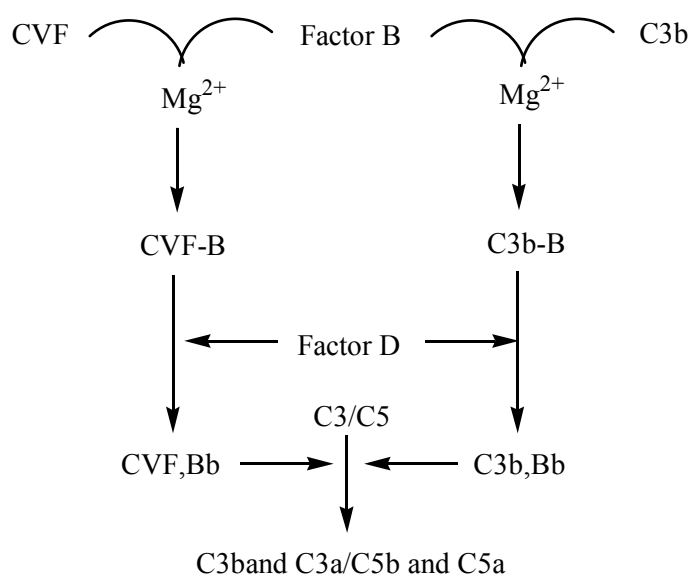


**Figure 6.** The diagram of the alternative pathway of CVF.

CVF is a three-chain 149 kDa glycoprotein (58-59). The functional similarity of CVF and C3b correlates with many structural similarities, including immunological cross reactivity, secondary structure, and N-terminal amino acid sequences (60-61). From these data, it was concluded that CVF structurally resembles C3c, a physiological degradation product of C3 which lacks an intramolecular thioester and a free sulfhydryl group. The degradation product of C3 was shown in Figure 7. There are several reasons why there is significant interest in CVF. For one, CVF can serve as a tool to investigate the multifunctionality of C3, a protein that interacts specifically with more than ten different plasma proteins or cell surface receptors. The elucidation of the structural differences between C3 and CVF, two closely related molecules that share some properties e.g., formation of a C3/C5 convertase but differ in others e.g.,

the susceptibility to regulation by factors H and I, can be expected to help identify functionally important regions of the C3 molecule. Both C3b-Bb and CVF-Bb exhibit spontaneous decay dissociation at 37 °C into the two respective subunits. However, the half-life of this decay dissociation is 7 h. for CVF-Bb and only 1.5 min for C3b-Bb. C3b-Bb is effectively disassembled by factor H and C3b is subsequently inactivated by factor I (62). In contrast, CVF-Bb and CVF are resistant to these two regulatory proteins, factor H and factor I (58, 63-64). Because of its stability and resistance to regulation, the CVF-Bb will continuously hydrolyze C3 and C5, eventually resulting in complement depletion. According to the potential of CVF in clinical relevance, CVF has been tested and shown that CVF to be safely administered to laboratory animals (65). The CVF has been used in numerous studies to deplete the plasma complement activity in order to investigate the role of complement in host defense or pathogenesis of disease. CVF is a promising therapeutic agent for complement depletion in clinical conditions where activation is involved in the pathogenesis of disease. This includes such diverse clinical conditions as reperfusion injury (66), xenograft rejection (67), rheumatoid arthritis and retroviral gene therapy. Another potential application of CVF is its use in antibody conjugates for targeted complement activation to induce tumor-cell killing (68).

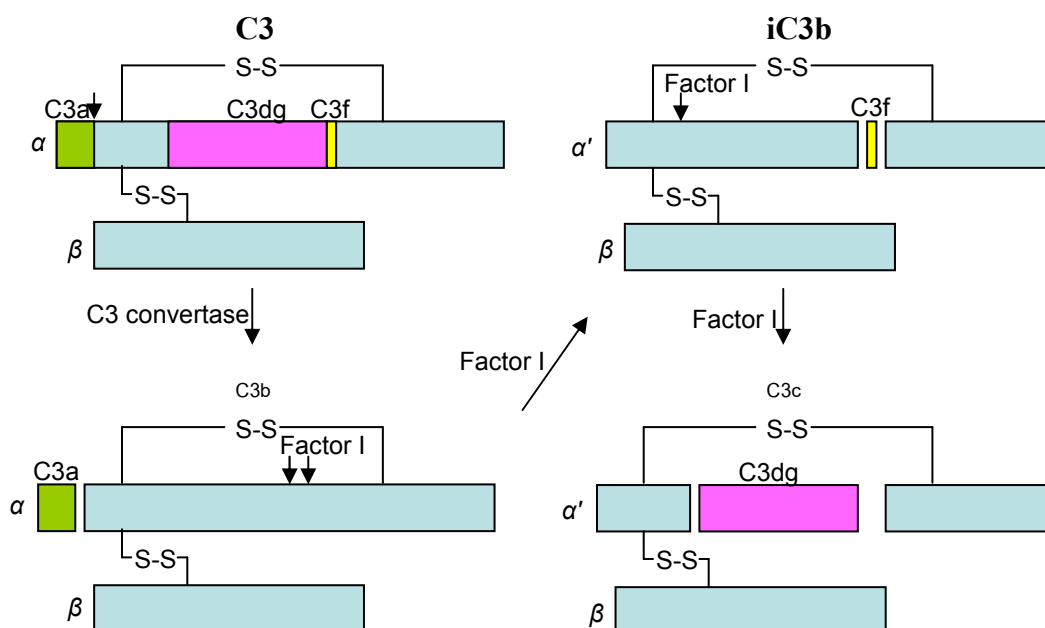


**Figure 7.** Schematic drawing of the degradation products of human C3.

The molecular cloning and derived primary structure of CVF were reported. CVF mRNA is more than 5924 nucleotides in length (69). It contains a single open reading frame of 4926 nucleotides, coding for a pre-pro-protein of 1642 amino acids. The single-chain pre-pro-CVF consists of a 22-amino acid signal sequence, a 627-amino acid  $\alpha$ -chain, and a 989-amino acid precursor chain for the CVF  $\gamma$ - and  $\beta$ -chains. The 627 amino acid  $\alpha$ -chain has three potential N-glycosylation sites at residues 131, 136, and 187. Immediately following the C terminus of the  $\alpha$ -chain, there are 4 arginine residues and a 79 amino acid peptide resembling a C3a anaphylatoxin. There is a single potential glycosylation site at position 640 in the "C3a" domain, though this site is not present in the mature protein. The  $\gamma$ -chain begins at position 711. The exact position of the C terminus of the  $\gamma$ -chain is still unknown and is apparently heterogeneous. Based on the size of the  $\gamma$ -chain on SDS/PAGE and the lack of a free sulfhydryl group, the  $\gamma$ -chain must terminate in the immediate proximity to the C terminus of what would be C3g in C3. Assuming the C terminus of the  $\gamma$ -chain to correspond to the C terminus of the C3g domain in human C3, the  $\gamma$ -chain would be 252 residues long with its C terminus being at position 962. The  $\gamma$ -chain contains no glycosylation sites. The  $\gamma$ -chain is followed by a 279-residue-long "C3d" domain that is not present in the mature CVF protein. The  $\beta$ -chain of CVF begins at position 1242 and extends for 379 residues to the end of the open reading frame. The  $\beta$ -chain contains a single glycosylation site at position 1324 (69). The post-translational proteolytic processing of pro-C3 is limited to the removal of four arginine residues, resulting in the mature two-chain C3 molecule consisting of a 115-kDa  $\alpha$ -chain and a 70-kDa  $\beta$ -chain, the proteolytic processing of pro-CVF in the venom gland is more complex. It involves in addition to the removal of four arginine residues, the proteolytic removal of the C3a-like and C3d-like domains, resulting in the mature three-chain form of CVF consisting of the 70-kDa  $\alpha$ -chain, 48-kDa  $\beta$ -chain, and the 32 kDa  $\gamma$ -chain (70). Pro-CVF contains five potential glycosylation sites, of which only three can be expected to be glycosylated in mature CVF. Like C3, pro-CVF contains 27 cysteine residues and a homologous thioester site in the C3d-like region. The amino acid sequence of pro-CVF was shown in Figure 8.

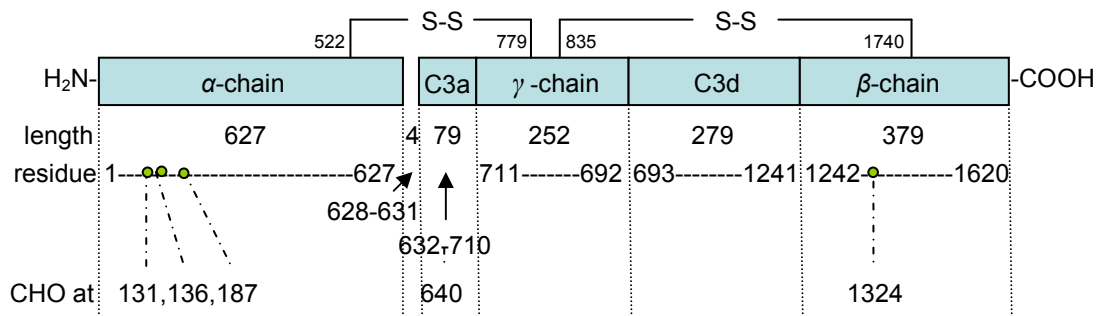


**Figure 8.** The amino acid sequence of pro-CVF.

#### 4. Symptom and pathology of cobra bite

The common symptoms and pathology of snakebite patients can be classified in three groups, neurotoxic effects, myotoxic effects and haematotoxic effects, according to the mechanism of action of the toxic substances containing in snake venoms (23). The three major families of venomous snakes, which led to cause of neurotoxic, haematotoxic and myotoxic effects, are the elapids, vipers and sea snakes, respectively. The clinical features of snakebite are summarized in Table 3 (71). Furthermore, the ultimate severity of any venomous snakebite depends on the quantity of venom injected and the comparative toxicity of the venom.

Factors that affect the amount of venom to be injected included the extent or the anger motivates the attack, the length of time the snake hold on, the site of injection, the number of bite, the bite depth, interference by clothing and the age, size, and species of the snake (72).

**Table 3.** Main clinical features of snakebite (71)

Snake	Percentage capable of poisoning	Effects of poisoning		Approximate natural mortality (%)	Average time to death (h)
		Local	Systemic		
Elapids	50	Slow swelling, then necrosis with Asian cobras, African spitting cobras, Usually no local effects with other elapids	Neurotoxic effects: ptosis, glossopharyngeal palsy, respiratory paresis, cardiac effects	10	5-20
Sea snakes	80	None	Myotoxic effects: myalgia on moving, paresis, myoglobinuria, hyperlalaemia	10	15
Vipers	30	Rapid swelling, necrosis in 5-10% (some vipers only)		1-15	48

#### 4.1 Local symptoms

Pain, then variable swelling and later necrosis, were the outstanding features of local poisoning. The pain commences in the bitten area and frequently radiate up the limb and may last from less than 1 to over 10 days depending on the extent of the necrosis. Swelling is one of the most common features of cobra bite. It commences 2-3 hours after the bite and reaches its maximum extent 24-48 hours after the bite and may persist for up to 18 days. A bite on finger may lead to swelling of the hand and forearm (73-74).

Local necrosis is now accepted as the most common sequelae to an effective cobra bite but once was classified as peculiar to cobra bite. Approximately fifty percent of the victims bitten by the cobra face the problem of local tissue necrosis, which is difficult to treat (75). After bite, a dusky discoloration around the bite marks extent in area and deepening in colour each day. After 3-4 days, a grayish black area

becomes encircled by a red raised rim and sanguineous blisters may occur. Then fluctuation was often evident: incision released red-yellow material and revealed necrosis of skin and subcutaneous tissue. Local tissue necrosis is detected between 36 hours and ten days, usually by the fifth day (76). The area of skin necrosis may be found vary from a few to 600 cm<sup>2</sup>. The extensive skin loss may take several months to heal (73).

#### **4.2 Systemic symptoms**

Before going to the stage of paralysis, many preparalytic symptoms occur. These include: vomiting, loss of consciousness, headache, vasomotor sign such as pallor, sweating, weak to absent pulse and hypotension, pain in regional lymph nodes including tenderness and enlargement. Normally, the earliest systemic poisoning is drowsiness occurs 1-5 hours after the bite. Also observed are spitting, vomiting and coughing of blood, allergic reaction and cobra venom conjunctivitis in case of spitting cobra venom gains access to the eyes (74-75).

The recognition of these preparalytic symptoms and signs of envenomation assumes great importance because, if they are recognized for what they are and antivenin is given at this stage, it may effectively prevent paralysis and necrosis developing or may limit its extent. However the paralytic latent period of cobra bite can be vary short, so these symptoms may occur in the same time of muscle paralysis.

The muscle paralysis, however, is not common sequelae to a cobra bite, but if it occurs, it tends to occur early in the course of envenomation and its progress is frequently rapid (76). The paralysis of several muscle groups are usually involved and are reported as difficulty in seeing or double vision, difficulty in opening the mouth, swallowing, speaking and breathing, difficulty in lifting limbs, eyelids and head. The muscles supplied by the cranial nerves are always affected first. The susceptibility of various muscles to neurotoxins varies considerably. The most susceptible are extrinsic eye muscles and elevator of eyelids while superficial facial muscle and diaphragm are resistant.

In some cases, neurotoxic symptoms resolve rapidly, usually within a week. Drowsiness, ptosis, facial paresis, and difficulty in swallowing ensued. Limb and neck paresis were followed by depression then loss of tendon reflexes and these

neurotoxic symptoms did not resolve completely until two weeks after the bite (72-74, 77).

## 5. Treatment of snake envenomation

The antivenom is the most recommended and the mainstay of treatment for snake venom poisoning. However, antivenom is a time proven and medically accepted standard in virtually every country. It should be given early after envenomation, because its effectiveness is both dose and time related (78). It was found that almost half of the patients receiving horse sera showed signs of hypersensitivity reactions (40, 45). It is therefore not only safe, but it is also highly desirable to wait for clear clinical evidence of systemic poisoning before giving antivenom. It should not be given routinely in all cases of snakebite. A patient with a mild envenomation can be managed without antivenom but the patient must be under close observation.

The only remedy for cobra bite is a monospecific antivenom produced by Queen Saovabha Memorial Institute, The Thai Red Cross Society. The horse antivenom against *Naja kaouthia* is very difficult to produce, expensive and in short supply. Only 20% of the horses immunized with Thai cobra venom produce adequate neutralizing activity for antivenom production. Furthermore, the neutralizing activity considered adequate is in fact quite low. Administration of antivenom to patient may cause hypersensitivity. Hypersensitivity reactions may be either type I (anaphylactic) or type III (complex mediated hypersensitivity). It was reported that approximately 25% of patients develop anaphylaxis in response to horse serum-derived antivenin and that 50% of those reactions could be life threatening. Skin testing is necessary before antivenin is administered. However, both false-positive and false-negative test results occur. Moreover, antivenin does not provide enough protection against venom, which need a long schedule, is expensive and requires ideal storage condition (39, 79).

Over the years many attempts have been made for the development of chemical antagonists which may provide protection against snakebite. These chemicals mostly receive from the medicinal plants due to the folk medicinal used of people in rural part of different countries. Not many compounds are known, even today, which is proved to be effective to counter venom action.

## **Part II. Medicinal plant against snake venom**

Plant have long been used for treatment envenomation by snakebite. Many examples could be cited of plants, whose use as snake-venom antidotes can be traced back to antiquity. Ethnobotanical reports from every corner of the world abound with such citation (80). However, from several points of view, an overview of such plants would be useful. From a scientific viewpoint, it is important to know the truth of “anti-snakebite treatments” preceding the advent of serum therapy less than 100 year ago. Another is more practically oriented: if certain substances from plants are really active against snakebite, they could be used as first-aid measures or to support any other treatment. Thirdly, industrial companies world wide are now interested in plants which have been used previously in folk medicine; quite a number of such substances have been successfully introduced into modern therapy against various diseases.

There are about thirty eight plants in Thailand reported to be effective in treating snake bites. Most of them are the mixture more than 2 types of plants for treatment and it was shown in Table 4 (17). One of the potential plants among these Thai plants was *Trigonostemon rediocides* (Kurz) Craib, which is known as *Lotthanong* in Thai and belongs to the Euphorbiaceae family. The roots, ground with water, have been used in traditional medicine as an emetic for food and shell, and also used a laxative and anti-asthmatic. The herb has also been used in the treatment of bloody and mucous sputum or stool. Topically, it was applied to reduce abscesses and to alleviate sprains, swelling and bruises. The herb is particularly effective in treating snake bites especially against snake neurotoxins (81). According to the research report, it was found that the crude extract from *Lotthanong*'s root can extend the survival time of mice after being injected by Thai cobra venom (82). The major components of *Lotthanong* were shown in Figure 9.

**Table 4.** Medicinal plants in Thailand

<i>Aloe vera</i> Linn.	<i>Gynurapseudochina</i> DC. Var.
<i>Andrographis paniculata</i> (Burm.) Wall.	<i>Lygodium flexuosum</i> Kinn. SW.
<i>Antidesma leucopodum</i> Mig.	<i>Melastomr normale</i>
<i>Typhonium trilobatum</i> Schott.	<i>Micromelum</i> sp.
<i>Barleria lupulina</i> Lindl.	<i>Mimosa pudica</i> Linn. Var. hispida Bren.
<i>Boesenbergia pandurata</i> (Roxb.) Schltr.	<i>Mitragyna speciosa</i> Korth.
<i>Brachiaria distachya</i> Linn. Stapt.	<i>Musa balbisiana colla</i>
<i>Centella asiatica</i> (Linn.) Urban.	<i>Pandanus momothecca</i> Martelli
<i>Cleome viscosa</i> Linn.	<i>Phyllanthus glollrayi</i> Beille
<i>Clinacanthus nutans</i> (Burm.f.)	<i>Phyllanthus oxyphyllus</i> Mig.
<i>Cocos nucifera</i> Linn.	<i>Plumcia Rubra</i>
<i>Curcuma longa</i> Linn. Roxb.	<i>Psidium guajava</i> Linn.
<i>Cyathostemma micranthum</i> (A.DC.) J.Sincl.	<i>Scirpus mucronatus</i> Linn. ssp. mucronatus
<i>Cyathula prostrate</i> (Linn.) Bl.	<i>Tamarindus indica</i> Linn.
<i>Cyclea</i> sp.	<i>Tetracera loureiri</i> Pierre
<i>Dischidia imbricate</i> (Blume) Steud.	<i>Thunbergia laurifolia</i> Linn.
<i>Drynaria quercifolia</i> (L.) J.Sm.	<i>Tiliacora triandra</i> Diels.
<i>Glycosmis pentaphylla</i> Corr.	<i>Tithomsnospora crispa</i> F.
<i>Grammatophyllum speciosum</i> BL.	<i>Typhonium trilobatum</i> Schott.

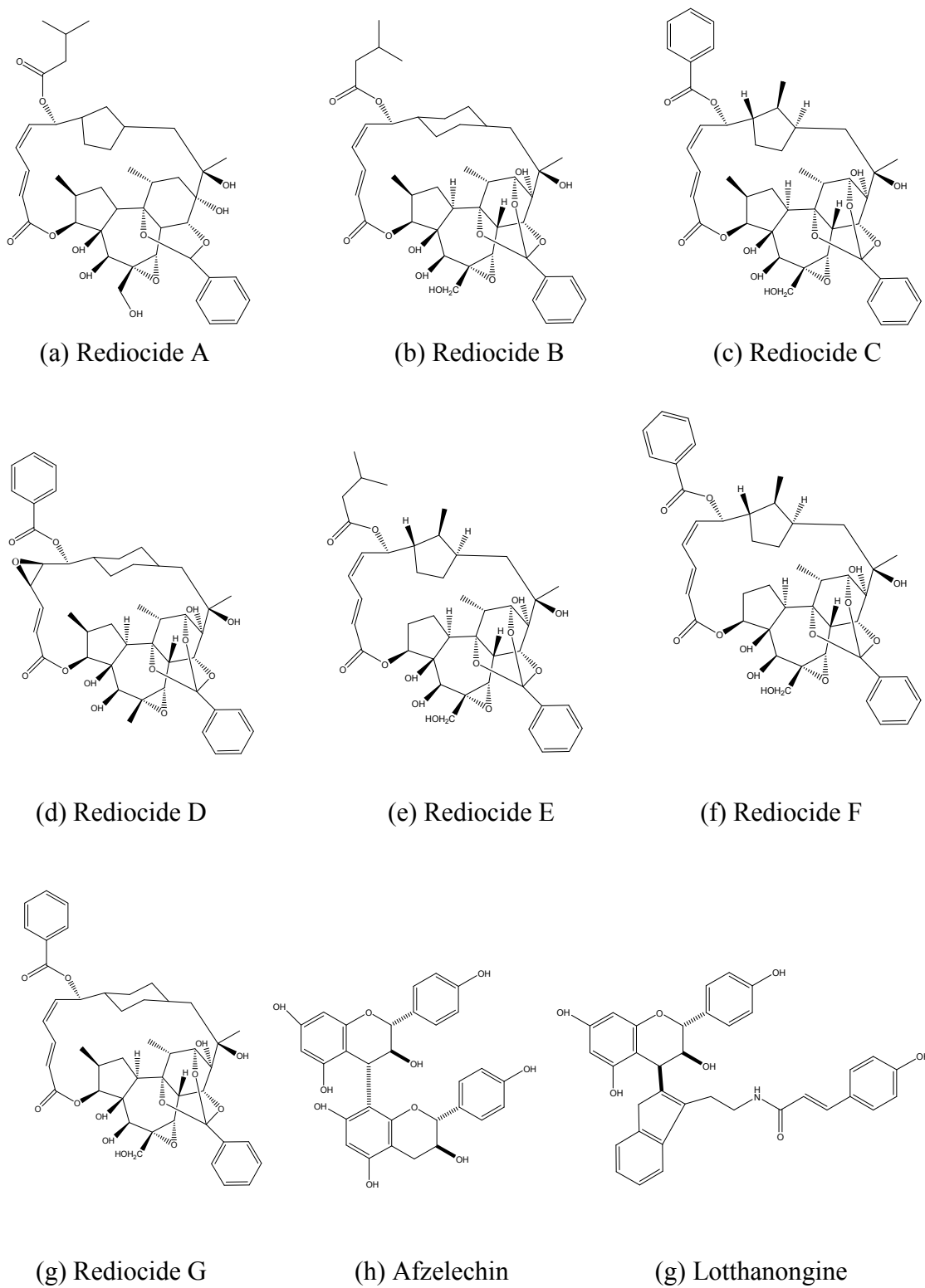
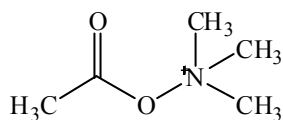


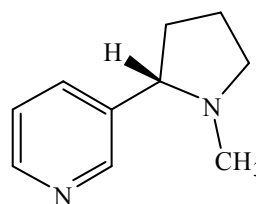
**Figure 9.** The major components of *Lotthanong*.

### Part III. Nicotinic Acetylcholine Receptor

Nicotinic acetylcholine receptors, or nAChRs, are cholinergic receptors that form ligand-gated ion channels in the plasma membrane of certain neurons. Being ionotropic (i.e. ligand-gated) receptors, nAChRs are directly linked to an ion channel and do not make use of a second messenger like metabotropic receptors do. Like the other type of acetylcholine receptors, muscarinic acetylcholine receptors (mAChRs), the opening of the ion pore of an nAChR is triggered by the binding of the neurotransmitter acetylcholine (ACh) and also by nicotine. The name "nicotinic" based on the ability of the nicotine to mimic the effects of ACh as a neurotransmitter (83). Nicotinic acetylcholine receptors are present in many tissues in the body, and are the best-studied of the ionotropic receptors. The neuronal receptors are found in the central nervous system and the peripheral nervous system. The neuromuscular receptors are found in the neuromuscular junctions of somatic muscles; stimulation of these receptors causes muscular contraction.



Acetylcholine



Nicotine

#### 1. Structure

Nicotinic receptors, with a molecular mass of 290 kDa (84), are made up of five subunits, arranged symmetrically around the central pore. They share similarities with GABA<sub>A</sub> receptors, glycine receptors, and the type 3 serotonin receptors. They are also called ionotropic receptors or the signature Cys-loop proteins (85). Twelve types of nicotinic receptor subunits,  $\alpha 2$  through  $\alpha 10$  and  $\beta 2$  through  $\beta 4$ , combine to form pentamers. The subunits are somewhat similar to one another, especially in the hydrophobic regions. At the neuromuscular junction, the two  $\alpha$  subunits of the nAChR are combined with up to four other subunits ( $\beta, \gamma, \delta, \epsilon$ ) in the ratio  $2\alpha:\beta:\epsilon:\delta$  (83, 86). The neuronal forms are much more homogeneous, and are made up of only receptor subunit types ( $\alpha$  and  $\beta$ ) present in a ratio of  $3\alpha:2\beta$ . The neuronal forms also

differ from the muscle forms in that they are not sensitive to  $\alpha$ -bungarotoxin. The acetylcholine binding site is on the outside of the  $\alpha$  subunit near the N terminus. When an agonist binds to the site, the  $\alpha$  subunits become more similar to the other subunits, the channel becomes more symmetrical (87), and a pore with a diameter of about 0.65 nm opens. Acetylcholine receptor (nicotinic) from electric torpedo rays and *Lymnaea stagnalis* were shown on Figure 10 and 11, respectively.

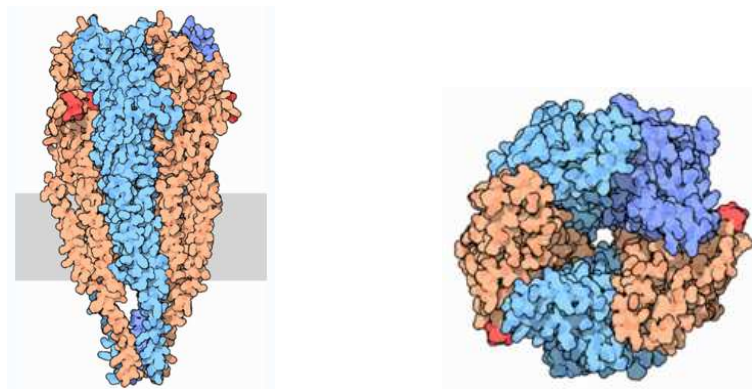


**Figure 10.** Acetylcholine receptor (nicotinic) from electric torpedo rays (very similar to human receptor) is made of 5 subunits, 2 of which (shown in orange) bind ACh (red). Structure was determined by electron crystallography at 4 Å resolution (PDB code: 2bg9).

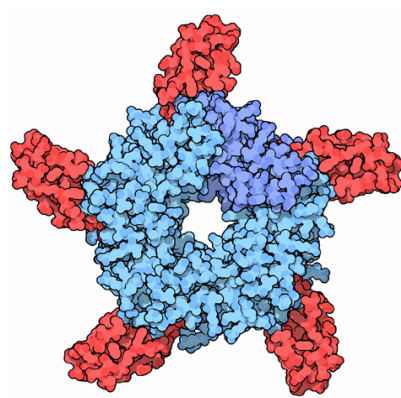


**Figure 11.** Acetylcholine receptor blocked by cobra venom (PDB code: 1YI5). A similar effect can be achieved by high doses of curare or nicotine.

## 2. Opening the Channel

Nicotinic AChRs may exist in different interconvertible conformational states. Binding of an agonist stabilizes the open and desensitized states. Opening of the channel allows positively charged ions to move across it, in particular, sodium and potassium, to enter the cell. The nAChR is a non-selective cation channel, meaning that several different positively charged ions can cross through. It is permeable to  $\text{Na}^+$  and  $\text{K}^+$ , with some subunit combinations that are also permeable to  $\text{Ca}^{2+}$ . The amount of sodium and potassium the channels allow through their pores (their conductance) varies from 50-110 pS, with the conductance depending on the specific subunit composition as well as the permeant ion (88). Interestingly, because some neuronal nAChRs are permeable to  $\text{Ca}^{2+}$ , they can affect the release of other neurotransmitters (83). The channel usually opens rapidly and tends to remain open until the agonist diffuses away, which usually takes about 1 millisecond. However, AChRs can sometimes open with only one agonist bound and in rare cases with no agonist bound, and they can close spontaneously even when ACh is bound. Therefore, ACh binding only creates a probability of pore opening, which increases as more ACh binds (87).

## 3. Effects

The activation of receptors by nicotine modifies the state of neurons through two main mechanisms. On one hand, the movements of cations cause a depolarization of the plasma membrane (which results in an excitatory postsynaptic potential in neurons), but also by the activation of other voltage-gated ion channels. On the other hand, the entry of calcium acts, either directly or indirectly, on different intracellular cascades leading, for example, to the regulation of the activity of some genes or the release of neurotransmitters.

## 4. Receptor Regulation and Roles

Ligand-bound desensitization of receptors was first characterized by Katz and Thesleff in the nicotinic acetylcholine receptor (89). Prolonged or repeat exposure to a stimulus often results in decreased responsiveness of that receptor for a stimulus. nAChR function can be modulated by phosphorylation and the activation of second messenger-dependent protein kinases (90). Phosphorylation of the nAChR by protein kinase A and protein kinase C results in its desensitization (91-92). It has been

reported that after prolonged receptor exposure to the agonist, the agonist itself causes an agonist-induced conformational change in the receptor, resulting in receptor desensitization.

The subunits of the nicotinic receptors belong to a multigene family (17 members in human) and the assembly of combinations of subunits results in a large number of different receptors. These receptors, with highly variable kinetic, electrophysiological and pharmacological properties, respond differently to nicotine, at very different effective concentrations. This functional diversity allows them to take part in two major types of neurotransmission. Classical synaptic transmission (wiring transmission) involves the release of high concentrations of neurotransmitter, acting on immediately neighbouring receptors. In contrast, paracrine transmission (volume transmission) involves neurotransmitters released by synaptic buttons, which then diffuse through the extra-cellular medium until they reach their receptors, which may be distant. Nicotinic receptors can also be found in different synaptic locations, for example the muscle nicotinic receptor always functions post-synaptically. The neuronal forms of the receptor can be found both post-synaptically (involved in classical neurotransmission) and pre-synaptically where they can influence the release of multiple neurotransmitters (93).

To date 17 nAChR subunits have been identified, these are divided into muscle-type and neuronal-type subunits (Table 5). Of these 17 subunits,  $\alpha 2$ - $\alpha 7$  and  $\beta 2$ - $\beta 4$  have been cloned in humans, the remaining genes identified in chick and rat genomes (94). The nAChR subunits have been divided into 4 subfamilies (I-IV) based on similarities in protein sequence (95). In addition, subfamily III has been further divided into 3 tribes.

Nicotinic receptors are pentamers of these subunits, i.e. each receptor contains five subunits. Thus, there is an immense potential of variation of the aforementioned subunits. However, some of them are more notable than others, specifically  $(\alpha 1)_2\beta 1\delta\epsilon$  (muscle type),  $(\alpha 3)_2(\beta 4)_3$  (ganglion type),  $(\alpha 4)_2(\beta 2)_3$  (CNS type) and  $(\alpha 7)_5$  (another CNS type) (96). A comparison was shown in Table 6.

**Table 5.** 17 nAChR subunits (95)

<b>Type</b>	<b>Subtype</b>	<b>Subunit</b>
Neuronal I		$\alpha 9, \alpha 10$
Neuronal II		$\alpha 7, \alpha 8$
Neuronal III	1	$\alpha 2, \alpha 3, \alpha 4, \alpha 6$
	2	$\beta 2, \beta 4$
	3	$\beta 3, \alpha 5$
Muscle IV		$\alpha 1, \beta 1, \gamma, \delta, \epsilon$

**Table 6.** Notable variations of nAChR (96)

<b>Receptor type (location)</b>	<b>Effect</b>	<b>Agonists</b>	<b>Antagonists</b>
Muscle type: ( $\alpha 1$ ) <sub>2</sub> ( $\beta 1$ ) $\delta \epsilon$ or $\alpha 1 \beta 1 \delta \gamma \epsilon$ (neuromuscular junction)	EPSP, mainly by increased Na <sup>+</sup> and K <sup>+</sup> permeability	acetylcholine carbachol suxamethonium	$\alpha$ -bungarotoxin $\alpha$ -conotoxin tubocurarine pancuronium
Ganglion type: ( $\alpha 3$ ) <sub>2</sub> ( $\beta 4$ ) <sub>3</sub> (autonomic ganglia)	EPSP, mainly by increased Na <sup>+</sup> and K <sup>+</sup> permeability	acetylcholine carbachol nicotine epibatidine dimethylphenylpiperaz inium varenicline	$\alpha$ -bungarotoxin mecamylamine trimetaphan hexamethonium bupropion dextromethorphan ibogaine 18-methoxycoronaridine
CNS type: ( $\alpha 4$ ) <sub>2</sub> ( $\beta 2$ ) <sub>3</sub> (brain)	Post- and presynaptic excitation, mainly by increased Na <sup>+</sup> and K <sup>+</sup> permeability	nicotine epibatidine acetylcholine cytisine	mecamylamine methylcaconitine $\alpha$ -conotoxin
(another) CNS type: ( $\alpha 7$ ) <sub>5</sub> (brain)	Post- and presynaptic excitation, mainly by increased Ca <sup>2+</sup> permeability	epibatidine dimethylphenylpiperaz inium	mecamylamine $\alpha$ -bungarotoxin $\alpha$ -cobratoxin

#### **Part IV. Automated Docking**

Molecular recognition of small molecules by enzymes is a fundamental step in most biological processes, and predicting binding conformation and affinities of small molecules is a challenge in computational chemistry. Computational techniques including rapid database searching, automated docking, molecular mechanics, free energy perturbation, and lambda dynamics have been integrated with structural information from x-ray crystallography and/or NMR in an effort to understand the physical forces that drive molecular recognition. One application of these affords has been structure-based drug design. The design of inhibitors for HIV-1 protease (97) and inhibitors of malaria cysteine protease (98) are considered major successes of structure-based drug design. The number of protein targets for structure-based drug design is rapidly increasing due to advances in crystallography, homology modeling, genomics, and proteomics. It is important to develop, evaluate, and improve computational methods in parallel with structural determination.

Automated docking is one strategy for predicting ligand-protein interactions and estimating interaction energies. Important features that distinguish automated docking methods from one another are the scoring (or energy) function and the strategy used to search for the lowest score. Ideally, one would want to computationally determine protein-ligand interactions by finding the global energy minimum within a complex energy binding landscape that contains local minima. The energy landscape would accurately account for hydrophobic packing, electrostatic interactions, hydrogen bonding, solvation / desolvation, and entropic terms. However, there is a trade-off between speed and accuracy that is inherent in any computational approach attempting to model molecular recognition.

AutoDock is an automated docking method that uses a grid-based force field to rapidly dock flexible ligands to a protein target (99). In grid-based methods, a three-dimensional lattice of regularly spaced points is created around the binding site. A grid map is computed for each atom type in the ligand that is to be docked. Most grid-based methods allow the user to define the size and placement of a grid, thereby allowing the extent of grid maps to range from a known protein active site to the entire macromolecule. Grids used during AutoDock runs are calculated prior to docking

using the AutoGrid module. Within the AutoGrid parameter file, the user specifies coordinates of the grid center, the number of points in each dimension, and the spacing between points. Ligands are treated as sets of atoms. At each grid point, the interaction energy for a probe atom of the ligand with the surrounding macromolecule is computed using the energy function. During docking, the interaction energy of each ligand atom with the protein is computed by interpolating between the energy values stored at the grid points that are closest to the docked position of that atom.

The primary advantage of grid-based force fields is that pairwise calculations are performed prior to the docking simulation. During docking, the interaction energy between the ligand and protein is calculated, essentially, by summing atomic affinities of each ligand atom at its location with the grid map. There may be additional calculations, such as penalties for restricting rotatable bonds, internal interaction energy of the ligand, and interpolation between grid points, but none of these terms depend upon the number of atoms in the protein. Therefore, in grid-based methods, the interaction energy calculation for a ligand position is function of approximately order  $O(n)$ , where  $n$  is the number of atoms in the ligand. The calculation done during docking using a grid-based method depends solely on the ligand, which generally contains significantly fewer atoms than the protein.

In AutoDock, the binding free energy is estimated as the sum of the energy of complex formation in a vacuum and the energy required to desolvate the surfaces on the ligand and the macromolecule that are buried when the complex formed. The AutoDock energy function uses a simplified molecular mechanics force field that is represented by a linear combination of van der Waals, hydrogen bonding, electrostatics, torsional restraint, and solvation energy terms:

$$\Delta G = \Delta G_{vdW} + \Delta G_{H-bond} + \Delta G_{elec} + \Delta G_{tor} + \Delta G_{solvation} \quad \text{Equation 1}$$

This equation neglects conformational changes in the protein and covalent geometric distortion, but includes estimates for desolvation ( $\Delta G_{solvation}$ ) and entropic loss due to torsional restraint in the ligand ( $\Delta G_{tor}$ ).

The first three terms in the equation 1 are typical molecular mechanics interactions: van der Waals (steric fit), hydrogen bonding, and electrostatics. Van der Waals interaction energy between two atoms,  $\Delta G_{vdW}$ , is 12-6 Leonard-Jones potential.

In this model, when the distance between the two atoms is small, the atoms repel each other. At longer distances, there is attractive force between the atoms. The Lennard-Jones energy function is at its minimum when two atoms are separated by their equilibrium internuclear separation.

Hydrogen bonding interaction energy,  $\Delta G_{H-bond}$ , is a model with a 12-10 Lennard-Jones potential. The 12-10 Lennard-Jones potential creates a deeper energy potential well for two atoms than the 12-6 potential. Thus, hydrogen bond reactions are shorter and stronger than van der Waals interactions.

Electrostatic interaction energy,  $\Delta G_{elec}$ , is modeled as a distance-dependent Coulombic potential.

The fourth term,  $\Delta G_{tor}$ , is a measure of the unfavorable entropy due to restriction of ligand conformation and is proportional to the number of rotatable bonds. These four terms,  $\Delta G_{vdW}$ ,  $\Delta G_{H-bond}$ ,  $\Delta G_{elec}$  and  $\Delta G_{tor}$ , constitute the in vacuo ligand-binding energy.

The fifth term,  $\Delta G_{solvation}$ , is the most challenging to estimate in AutoDock. Ligand binding requires at least partial desolvation of the surfaces that become buried when the ligand-macromolecule complex forms. The energy required to desolvate these surfaces makes significant contributions to the overall binding energy. In AutoDock, the desolvation energy is computed for hydrophobic atoms. It is an approximation of the energy required when hydrophobic ligand atoms (e.g. carbon and aromatic carbon) desolvate protein atoms in a binding site.

For search strategies, the most common searching strategies for grid-based automated docking are Monte Carlo simulated annealing and the genetic algorithm. Both methods have been implemented in AutoDock. For the genetic algorithm is initiated by creating a randomized population of ligand binding orientations. The binding orientations are doubled by crossover of the genes of the individuals, a process analogous to mating. Random point mutations are also introduced. The fitness, or interaction energy, of each ligand binding orientation is computed and is used as selection-criteria for survival to the next generation. Favorable binding orientations are identified through iterative generations of population doubling and survival selection.

The Lamarkian genetic algorithm, a variant of the genetic algorithm, was the most efficient method of the search methods tested in AutoDock 3.0. The Lamarkian genetic algorithm was inspired by Jean Baptiste de Lamark's theory that phenotype changes occurring during an individual's lifetime can be passed on as genetic changes to its offspring. In the Lamarkian genetic algorithm, a global genetic algorithm search is combined with adaptive local minimization searching capability, and thus an individual can improve its binding orientation through local search and minimization and then pass on the improved binding orientation information.

### **Part V. Virtual Screening**

In medicine, biotechnology and pharmacology, drug discovery is the process by which drugs are discovered and/or designed. In the past, most drugs have been discovered either by identifying the active ingredients from traditional remedies or by serendipitous discovery. A new approach has been to understand how diseases and infections are controlled at the molecular and physiological level and to target specific entities based on this knowledge. The process of drug discovery involves the identification of candidates, synthesis, characterization, screening and assays for therapeutic efficacy. Once a compound has shown its value in these tests, it will begin the process of drug development prior to clinical trials.

Virtual screening (VS) has become an integral part of the drug discovery process in recent years. Related to the more general and long pursued concept of database searching, the term "virtual screening" is relatively new. Walters, *et al.* define virtual screening as "automatically evaluating very large libraries of compounds" using computer programs (100). As this definition suggests, VS has largely been a numbers game focusing on questions like how can we filter down the enormous chemical space of over  $10^{60}$  conceivable compounds to a manageable number that can be synthesized, purchased and tested. Although filtering the entire chemical universe might be a fascinating question, more practical VS scenarios focus on designing and optimizing targeted combinatorial libraries and enriching libraries of available compounds from in-house compound repositories or vendor offerings. There are two broad categories of screening techniques: ligand-based and structure-based.

## **1. Ligand-based Drug Design**

Given a set of structurally diverse ligands that binds to a receptor, a model of the receptor can be build based on what binds to it. These are known as pharmacophore models. A candidate ligand can then be compared to the pharmacophore model to determine whether it is compatible with it and therefore likely to bind (101).

## **2. Structure-based Drug Design**

Structure-based virtual screening involves docking of candidate ligands into a protein target followed by applying a scoring function to estimate the likelihood that the ligand will bind to the protein with high affinity (102-103).

The main goal of a virtual screen is to come up with hits of novel chemical structures that yield a unique pharmacological profile. Thus, success of a virtual screen is defined in terms of finding interesting new scaffolds rather than many hits. Interpretations of VS accuracy should therefore be considered with caution. Low hit rates of interesting scaffolds are clearly preferable over high hit rates of already known scaffolds. Once the hit has been established with sufficient target potency and selectivity and favourable drug-like properties, one or two hits will then be proposed for drug development. The best of these is generally called the lead compound, while the other will be designated as the "backup".

## CHAPTER III

### EXPERIMENTAL

This chapter was separated in to 3 parts which are (i) molecular modeling (*in silico*) experiment, (ii) *in vitro* binding assay i.e. radioligand competition assay and sodium dodecyl sulfate polyacrylamide gel electrophoresis (SDS-PAGE) experiment and (iii) *in vivo* experiment.

#### A. Molecular Modeling (*In Silico*) Experiment

##### 1. Materials

- 1.1 Bluefish (computer for linux cluster at central computing resources of The Scripps Research Institute).
- 1.2 Software ChemOffice 8.0 for Windows (CambridgeSoft Corporation, USA)
- 1.3 Software AutoGrid and AutoDock 3.0.5 (The Scripps Research Institute)
- 1.4 National Cancer Institute (NCI) diversity set
- 1.5 Alpha-cobratoxin crystal structures ( $\alpha$ -cbtx) 1CTX, 2CTX, 1YI5 (Protein Data Bank) (104)

##### 2. Methods

###### 2.1 Protein Template Preparation

A crystallographic structure of  $\alpha$ -cobratoxin (PDB entry code: 1CTX (8) and 2CTX (105) and  $\alpha$ -cobratoxin bound to acetylcholine binding protein (AChBP, PDB entry code: 1YI5 (13)), a soluble homolog of the extracellular binding domain of nicotinic acetylcholine receptor, were selected to prepare  $\alpha$ -cobratoxin active binding site template for docking. It was solved by X-ray diffraction techniques with a resolution of 2.8, 2.4 and 4.2 Å for 1CTX, 2CTX and 1YI5, respectively. The  $\alpha$ -cobratoxin (1CTX and 2CTX) and  $\alpha$ -cobratoxin/AChBP complex (1YI5) were used in

the virtual screening whereas only 1YI5 was selected for studying the rediocide binding mode. Prior to docking studies,  $\alpha$ -cobratoxin was read in and repeated using SwissPDBViewer before using AutoDock (ADTools version 1.3). In order to prepare the target protein as a template, the AChBP and crystallographic water were removed. Polar hydrogen atoms were added and Kollman charges were assigned to all atoms. The grid maps representing the  $\alpha$ -cobratoxin were calculated with AutoGrid. The dimensions of the grid were 60 x 88 x 86 grid points for 1YI5 and 86 x 60 x 88 for 1CTX and 2CTX, with a spacing of 0.375 Å between the grid points. The grid box was centered on the coordinates 118.056 x 160.484 x 64.991 for 1YI5 and 29.652 x 49.388 x 4.481 for 1CTX and 2CTX. The grid maps were computed using AutoGrid 3.0 for each protein model.

### 2.1.1 Template Validation

The constructed  $\alpha$ -cobratoxin template from 1YI5 was validated. The Ser182 – Tyr 192 from AChBP, the binding site of  $\alpha$ -cobratoxin, was selected to be the control peptide. It was designed to have 9 rotatable bonds from the single bonds of the residues except amide bond. In order to validate the prepared  $\alpha$ -cobratoxin template, the Ser182 – Tyr 192 was docked back into the prepared template. If the result showed the largest cluster of docked conformations and the docked conformations were close to that of the crystal pose with root-mean-square deviation (RMSD) < 2 Å, the re-docking result indicated that the prepared  $\alpha$ -cobratoxin protein is a good model for docking studies.

## 2.2 Ligand Preparation

### 2.2.1 NCI Diversity Set

The NCI diversity set is a reduced set of 1990 compounds selected from the original NCI-3D structural database for their unique pharmacophores (106). The diversity set was derived by others from the almost 140,000 compounds available on plates. The 71,756 compounds meeting this criterion were then reduced to the final set using the program Chem-X (Oxford Molecular Group). Chem-X uses defined centers (hydrogen bond acceptor, hydrogen bond donor, positive charge, aromatic, hydrophobic, acid, base) and defined distance intervals to create a particular finite set

of pharmacophores. The 3-point pharmacophores were used with the default settings, resulting in almost 1,000,000 possible pharmacophores. The Chem-X diverse subset generating function reads through a set of structures and for every structure, determines the acceptable conformations of that structure. For each acceptable conformation, it determines all the pharmacophores for that conformation. The pharmacophores for the current structure are compared to the set of all pharmacophores found in structures already accepted into the diverse subset. If the current structure has more than a preset number of new pharmacophores, it is added to the diverse subset. The requirements were set as 5 new pharmacophores and, additionally, 5 or fewer rotatable bonds. Because the selection procedure is order dependent, the order in which the structures were considered was randomized. This procedure resulted in the selection of 1990 compounds. For ligand preparation, All hydrogen were added and Gasteiger charges were assigned for each compound (107). Then the non-polar hydrogens were merged, aromatic carbons identified, and lastly, the rigid root and rotatable bonds were assigned via AutoTors (85).

### **2.2.2 Rediocides (A & G)**

The three-dimensional structures of rediocides were generated and cleaned up by the ChemDraw Ultra version 8.0.7 program. After cleaned up structure, the structure was minimized the energy by Chem3D Ultra version 8.0.3 using the MM2 method. The molecular dynamics was performed and the run parameters used were as follows: the step interval was 1.0 fs; the frame interval was 100 fs; the termination criterion was 10,000 steps; the target temperature was 300 kelvin; the heating/cooling rate was 1.000 kcal/atom/ps; and the job type was record every iteration. Every iteration was changed to pdb file. All hydrogens were added and Gasteiger charges were assigned to each pdb file. Then the non-polar hydrogens were merged, aromatic carbons were identified, and lastly, the rigid root and rotatable bonds were assigned via AutoTors.

## **2.3 Molecular Docking**

The program AutoDock3.0.5 (85) from The Scripps Research Institute, USA that used Larmarkian genetic algorithm for docking flexible ligands into protein

binding sites to explore the full range of ligand conformational flexibility with the rigid protein was used for docking study. The AutoDock run parameters used were as follows: the number of GA runs were 100; the population size was 150; the maximum number of energy evaluations was increased to 10,000,000 per run; and the maximum number of generations was 27,000. The crossover rate was set to 80% and the mutation rate to 2% with Cauchy distribution parameters  $a=0$  and  $b=1$ . The jobs were run on Bluefish at The Scripps Research Institute. Final docked conformations were clustered using a tolerance of 2 Å root-mean-square deviation (RMSD). The final docked structure, RMSD from the bound crystal structure and docked energy were all used to analyse its interaction with the active site.

### 2.3.1 Binding Mode of Redioides (A & G)

Each conformation of redioides from the molecular dynamic was docked with  $\alpha$ -cobratoxin template prepared from 1YI5. After docking, the lowest docking energy of each conformation (101 conformations) was ranked from lowest docking energy to highest docking energy. The conformation that bound in the binding site of  $\alpha$ -cobratoxin with lowest energy in the highest cluster was selected. The amino acid residues of AChBP in the sphere radius at 5 Å from redioides were shown. The distance of hydrogen bond between redioides and interacted amino acid residues was measured.

### 2.3.2 Virtual Screening

The  $\alpha$ -cobratoxin template derived from 1CTX, 2CTX and 1YI5 were used for molecular docking against 1990 ligands in NCI diversity set. The virtual screening was performed on Bluefish by the script (a 64-bit 576 processor LINUX cluster). After docking, the lowest docking energy of each ligand binding to each  $\alpha$ -cobratoxin template (1YI5, 1CTX and 2CTX) was ranked from lowest docking energy to highest docking energy. The top 175 compounds from 1990 compounds with the best docking energies from each protein template were selected. The selected compounds (3 x 175 compounds) that matched 3 proteins were selected for the experiment.

**B. *In Vitro* Binding Assay****1. Materials****Equipment**

Analytical balance	Precisa 240A and Precisa 4000C (Oerlikon, Switzerland)
LS 6500 liquid scintillation counter	Beckman Scientific (California, USA)
Micropipettes 0.5-10 $\mu$ l	High Tech Lab (Warsaw, Poland)
Micropipettes 2-20 $\mu$ l	High Tech Lab (Warsaw, Poland)
Micropipettes 20-200 $\mu$ l	High Tech Lab (Warsaw, Poland)
Micropipettes 100-1000 $\mu$ l	Genex Beta, UK
Mildmixer SI-36	Taitec Corporation (Saitama, Japan)
MINI protein <sup>®</sup> 3	BIO-RAD (California, USA)
Power supply	BIO-RAD and e-power 100 (California, USA)
Vortex mixer	Vortex-genie (New York, USA)
Water bath	Neslab Instrument (New Hampshire, USA)

**Chemicals**

AChBP from <i>Aplysia californica</i>	University of California, San Diego, USA
AChBP from <i>Bolinus truncatus</i>	University of California, San Diego, USA
AChBP from <i>Lymnaea stagnalis</i>	University of California, San Diego, USA
Acrylamide	BIO-RAD (California, USA)
Alpha-cobratoxin (C6903)	Sigma (Missouri, USA)
Ammonium persulfate	BDH Laboratory Supplies (Poole, England)
Anti-mouse SPA	Amersham Biosciences (New Jersey, USA)
Bromophenol blue	Sigma (Missouri, USA)
Coomassie Blue R-250	USB Corporation (Ohio, USA)
Crude cobra venom	Thai Red Cross Society (Bangkok, Thailand)

Dimethyl sulfoxide (DMSO)	E. Merck (Darmstadt, Germany)
Glacial acetic acid	Lab-Scan (Bangkok, Thailand)
Glycerol	Carlo Erba Reagenti (Milan, Italy)
Glycine	Fisher Scientific (Leicestershire, UK)
[ <sup>3</sup> H] epibatidine	University of California, San Diego, USA
Hits from NCI diversity set	National Cancer Institute, USA
Hydrochloric acid (HCl)	Lab-Scan (Bangkok, Thailand)
[ <sup>125</sup> I] $\alpha$ -bungarotoxin	University of California, San Diego, USA
Low range protein standard	BIO-RAD (California, USA)
2-mercaptoethanol	BIO-RAD (California, USA)
Methanol	Lab-Scan (Bangkok, Thailand)
Methyllycaconitine (MLA)	Sigma (Missouri, USA)
Monoclonal anti-FLAG M2	Sigma (Missouri, USA)
N,N,N',N'-tetramethylene-ethylenediamine	BIO-RAD (California, USA)
N, N'-methylene-bisacrylamide	Serva (Heidelberg, Germany)
Precision plus protein standard #1610374	BIO-RAD (California, USA)
Rediocides (A & G)	Bansomdejchaopraya Rajabhat Univ. (Bangkok, Thailand)
Sodium lauryl sulfate	Scharlau (Barcelona, Spain)
Tris (hydroxymethyl)-aminomethane	Fisher Scientific (Leicestershire, UK)
Tween 80	Sigma (Missouri, USA)

## 2. Methods

### 2.1 Radioligand Competition Assay

#### 2.1.1 Screening Test

The assay was performed to determine the fraction of [<sup>3</sup>H] epibatidine. An adaptation of a scintillation proximity assay was used to determine the apparent  $K_d$  value (108). The test compound 10  $\mu$ M, methyllycaconitine 15  $\mu$ M (positive control) and phosphate buffer 0.1 M, pH 7.0 (negative control) were added to AChBP (~500 pM binding sites), polyvinyltoluene anti-mouse SPA scintillation beads (0.1 mg/ml), monoclonal anti-FLAG M2 antibody from mouse. Methyllycaconitine is a non-specific binding ligand to AChBP. The mixture was incubated at room temperature

for 2 hours. After that, agonist [ $^3\text{H}$ ] epibatidine (5 nM for *Lymnaea stagnalis* and *Bolinus truncatus*, 20 nM for *Aplysia californica*) were added and allowed to equilibrate at room temperature for a minimum of 2 h. [ $^3\text{H}$ ] epibatidine that bound on the bead was measured in a LS 6500 liquid scintillation counter. The result was calculated in the fraction of [ $^3\text{H}$ ] epibatidine between sample and the control (total binding from negative control substrates with the background from methyllycaconitine). The ligand that has the fraction of [ $^3\text{H}$ ] epibatidine lower than 0.6 was selected for the determination of  $K_d$  values in section 2.1.2.

### 2.1.2 Determination of $K_d$

#### 2.1.2.1 [ $^3\text{H}$ ] epibatidine

The test compound, methyllycaconitine 15  $\mu\text{M}$  (positive control) and phosphate buffer 0.1 M, pH 7.0 (negative control) were added to AChBP ( $\sim 500$  pM binding sites), polyvinyltoluene anti-mouse SPA scintillation beads (0.1 mg/ml), monoclonal anti-FLAG M2 antibody from mouse. The mixture was incubated at room temperature for 2 hours. After that, agonist [ $^3\text{H}$ ] epibatidine (5 nM for *Lymnaea stagnalis* and *Bolinus truncatus*, 20 nM for *Aplysia californica*) were added and allowed to equilibrate at room temperature for a minimum of 2 h and measured the [ $^3\text{H}$ ] epibatidine that bound on the bead in a LS 6500 liquid scintillation counter. The result was calculated in fraction of [ $^3\text{H}$ ] epibatidine. The result was calculated in fraction of [ $^3\text{H}$ ] epibatidine. The data obtained were normalized, fit to a sigmoidal dose-response curve (variable slope), and the  $K_d$  calculated from the observed  $\text{EC}_{50}$  value using GraphPad Prism version 4.02 for Windows (San Diego, CA).

#### 2.1.2.2 [ $^{125}\text{I}$ ] $\alpha$ -bungarotoxin

The test compound, methyllycaconitine 15  $\mu\text{M}$  (positive control) and phosphate buffer 0.1 M, pH 7.0 (negative control) were added to AChBP ( $\sim 500$  pM binding sites), polyvinyltoluene anti-mouse SPA scintillation beads (0.1 mg/ml), monoclonal anti-FLAG M2 antibody from mouse. The mixture was incubated at room temperature for 2 hours. After that, antagonist [ $^{125}\text{I}$ ]  $\alpha$ -bungarotoxin (10 nM for *Lymnaea stagnalis* and 20 nM for *Aplysia californica*) were added and allowed to equilibrate at room temperature for a minimum of 2 h and measured the [ $^{125}\text{I}$ ]  $\alpha$ -

bungarotoxin that bound on the bead in a LS 6500 liquid scintillation counter. The result was calculated in fraction of [ $^{125}\text{I}$ ]  $\alpha$ -bungarotoxin. The data obtained were normalized, fit to a sigmoidal dose-response curve (variable slope), and the  $K_d$  calculated from the observed  $\text{EC}_{50}$  value using GraphPad Prism version 4.02 for Windows (San Diego, CA). The effective concentration ( $\text{EC}_{50}$ ) is defined as the concentration of a compound which bound to AChBP halfway between the baseline and maximum.

## **2.2 Sodium Dodecyl Sulfate Polyacrylamide Gel Electrophoresis (SDS-PAGE)**

### **2.2.1 Solutions**

#### **2.2.1.1 Stock Solution**

**2 M Tris-HCl (pH 8.8).** Distilled water (50 ml) was added into 24.2 g of Tris base. Afterthat, the concentrated HCl was added slowly and adjusted to pH 8.8. The volume was adjusted with distilled water to 100 ml.

**1 M Tris-HCl (pH 6.8).** Distilled water (50 ml) was added into 12.1 g of Tris base. Afterthat, the concentrated HCl was added slowly to pH 6.8. The volume was adjusted with distilled water to 100 ml.

**10% SDS (w/v).** Distilled water was added in 10 g of SDS to make 100 ml.

**50% Glycerol.** Distilled water (50 ml) was added into 50 ml 100% glycerol.

**1% Bromophenol Blue, (w/v).** Distilled water (10 ml) was added into 100 mg of bromophenol blue. Afterthat, the mixture was stirred until dissolved and filtered to remove the aggregated dye.

**Coomassie Gel Stain.** One liter of Coomassie gel stain was prepared by adding 1g of Coomassie Blue R-250, 100 ml of glacial acetic acid and 450 ml of methanol into 450 ml of distilled water.

**Coomassie Gel Destain** One liter of Coomassie gel destain was prepared by adding 100 ml of glacial acetic acid and 100 ml of methanol into 800 ml of distilled water.

### 2.2.1.2 Working Solution

**Solution A (Acrylamide Stock Solution).** Distilled water was added in 29.2 g of acrylamide and 0.8 g of N, N'-methylene-bisacrylamide to make 100 ml. The solution was covered with parafilm and stirred under hood until acrylamide powder is completely dissolved. The solution can be stored for months in the refrigerator.

**Solution B (4x Separating Gel Buffer).** Distilled water (21 ml) and 4 ml of 10% SDS were added into 75 ml of 2 M Tris-HCl (pH 8.8). The solution can be stored for months in the refrigerator.

**Solution C (4x Stacking Gel Buffer).** Distilled water (46 ml) and 4 ml of 10% SDS were added into 50 ml of 1 M Tris-HCl (pH 6.8). The solution can be stored for months in the refrigerator.

**10% Ammonium Persulfate.** Distilled water (1 ml) was added into 0.1 g of ammonium persulfate. The solution can be stored for months in a capped tube in the refrigerator.

**Electrophoresis Buffer.** Distilled water was added in Tris (hydroxymethyl)-aminomethane (3 g), glycine (14.4 g) and SDS (1 g) to make 1 liter. The pH should be approximately 8.3 and the solution can be stored at room temperature.

**5x Sample Buffer.** Ten milliliter of 5x Sample Buffer was prepared by adding 0.6 ml of 1 M Tris-HCl (pH 6.8), 5 ml of 50% glycerol, 2 ml of 10% SDS, 0.5 ml of 2-mercaptoethanol and 1 ml of 1% bromophenol blue into 0.9 ml of distilled water. The solution can be stored for weeks in the refrigerator or for months at  $-20^{\circ}\text{C}$ .

## 2.2.2 Effect of Rediocides (A & G) on $\alpha$ -Cobratoxin and AChBP

### 2.2.2.1 Effect of Rediocides on $\alpha$ -Cobratoxin

SDS-PAGE (109) was performed with 15% acrylamide gels using MINI protein<sup>®</sup> 3 as marker. The separating gel was made by mixing acrylamide solution, 4x Separating Gel Buffer, de-ionized water, ammonium persulfate and TEMED (N,N,N',N'-tetramethylene-ethylenediamine) in the particular ratio as shown in Table 5. The separating gel was subjected to space between the sandwich glasses, overlaid with de-ionized water and allowed to polymerize. De-ionized water was removed

after the separating gel was polymerized and stacking gel was set by mixing of acrylamide solution, 4x stacking gel buffer, de-ionized water, 10% ammonium persulfate and TEMED (Table 7). Mixed stacking gel was poured on top of the separating gel and the comb was inserted. After the stacking gel was completely polymerized, the comb was removed, and the whole unit of the gel and the glass-plate sandwich were attached to the electrophoresis chamber. The tank was filled with electrophoresis buffer both top and bottom of the tank.

The redioides (A & G) samples were prepared by mixing 5x sample buffer with venom solution to bring the final concentration of sample buffer to 1x and then the samples were boiled for 5 minutes and centrifuged. The supernatant were loaded into each well and electrophoresis was performed at 150 volts until the dye front reached to the end of the gels. After electrophoresis, the gels were stained with Coomassie blue R-250 (0.001% in glacial acetic acid: methanol: water, 10:45:45, v/v) and then destained with 10% methanol and 10% glacial acetic solution until the gel was clear.

**Table 7.** The composition of separating gel and stacking gel

Ingredients	Separating gel		Stacking gel
	15% gel	20% gel	
Solution A (acrylamide stock solution)	5 ml	6.66 ml	0.67 ml
Solution B (4x separating gel buffer)	2.5 ml	2.5 ml	-
Solution C (4x stacking gel buffer)	-	-	1 ml
De-ionized water	2.5 ml	0.84 ml	2.3 ml
10% Ammonium persulfate	50 $\mu$ l	50 $\mu$ l	25 $\mu$ l
TEMED	5 $\mu$ l	5 $\mu$ l	10 $\mu$ l

### 2.2.2.2 Effect of Rediocides on $\alpha$ -Cobratoxin and AChBP

SDS-PAGE was performed again with AChBP,  $\alpha$ -cobratoxin and rediocides but the samples were dissolved in 0.1% Tween 80 and was not boiled before loading to each well. nAChBP and  $\alpha$ -cobratoxin were mixed for 10 minutes before adding the sample. The sample mixtures were loaded into each gel and electrophoresis was performed at 100 volts until the marker's dye front reached to the end of the gels. After electrophoresis, the gels were stained with Coomassie blue R-250 (0.001% in glacial acetic acid: methanol: water, 10:45:45, v/v) and then destained with 10% methanol and 10% glacial acetic solution until the gel was clear.

### 2.2.3 Effect of 3 Hits on $\alpha$ -Cobratoxin and AChBP

#### 2.2.3.1 Effect of 3 Hits on $\alpha$ -Cobratoxin

SDS-PAGE was performed with 20% acrylamide gels using MINI protein<sup>®</sup> 3 (BIO-RAD). The separating gel was made by mixing acrylamide solution, 4x Separating Gel Buffer, SDS, de-ionized (DI) water, ammonium persulfate and TEMED (N,N,N',N'-tetramethylene-ethylenediamine) in the particular ratio as shown in Table 5.

The samples were dissolved in 0.1% Tween 80, boiled for 5 minutes and centrifuged. The samples were loaded into each well and electrophoresis was performed at 100 volts until the dye front reached to the end of the gels. After electrophoresis, the gels were stained with Coomassie blue R-250 (0.001% in glacial acetic acid: methanol: water, 10:45:45, v/v) and then destained with 10% methanol and 10% glacial acetic solution until the gel was clear.

#### 2.2.3.2 Effect of 3 Hits on $\alpha$ -Cobratoxin and AChBP

SDS-PAGE was performed again with nAChBP,  $\alpha$ -cobratoxin and 3 hits but the samples were not boiled before loading to each well. The sample mixtures were loaded into each gel and electrophoresis was performed at 100 volts until the marker's dye front reached to the end of the gels. After electrophoresis, the gels were stained with Coomassie blue R-250 (0.001% in glacial acetic acid: methanol: water, 10:45:45,

v/v) and then destained with 10% methanol and 10% glacial acetic solution until the gel was clear.

### C. *In Vivo* Experiment

#### 1. Materials

##### Equipment

Analytical balance	Precisa 240A (Oerlikon, Switzerland)
Micropipettes 0.5-10 $\mu$ l	High Tech Lab (Warsaw, Poland)
Micropipettes 2-20 $\mu$ l	High Tech Lab (Warsaw, Poland)
Micropipettes 20-200 $\mu$ l	High Tech Lab (Warsaw, Poland)
Micropipettes 100-1000 $\mu$ l	Genex Beta, UK
Triple beam balance	OHAUS (Boston, USA)
Ultrasonic bath	Brason 2210 (Colorado, USA)
Vortex mixer	Vortex-genie (New York, USA)

##### Chemicals

Alpha-cobratoxin (C6903)	Sigma (Missouri, USA)
NSC 42258	National Cancer Institute, USA
NSC 121865	National Cancer Institute, USA
NSC 134754	National Cancer Institute, USA
Rediocides (A & G)	Bansomdejchaopraya Rajabhat Univ. (Bangkok, Thailand)
Tween 80	Sigma (Missouri, USA)

##### Animals

ICR mice	National Laboratory Animal Center, Mahidol University
----------	--

#### 2. Methods

##### 2.1 Determination of Median Lethal Dose

The median lethal dose (LD<sub>50</sub>) is defined as the least amount of  $\alpha$ -cobratoxin which injected intramuscularly through the leg muscle of the mice that resulted in the death of half amount of mice within 24 h. ICR mice weighing 20-30 g were kept in a

temperature-controlled room on a 12/12-h cycle. The mice were divided into 10 groups of 6 animals in each. One group served as a control group receiving vehicle (sterile water) only. The other 9 groups were injected with  $\alpha$ -cobratoxin. Nine concentrations of the  $\alpha$ -cobratoxin solutions were prepared and diluted for intramuscular injection (i.m.) at 0.01, 0.1, 0.14, 0.17, 0.18, 0.2, 0.3, 0.4 and 0.5 mg/kg in 0.1 ml of sterile water. The number of deaths occurring within 24 h were recorded, LD<sub>50</sub> was calculated from the plot between the concentration of  $\alpha$ -cobratoxin and % death.

## **2.2 Effect of Redioides and 3 Hits on Mice**

### **2.2.1 The Protection Activity**

In the protocol using redioides or hits as protecting agent, redioides or hits were injected to the mice before the injection of  $\alpha$ -cobratoxin. The sample solution, in 0.05 ml of 0.3% Tween 80, were prepared in varying concentrations. Each dose was injected to the mice intravenously (i.v.) at tail vein. The control group was injected with only the vehicle, 0.3% Tween 80. After 30 minutes,  $\alpha$ -cobratoxin at 3LD<sub>50</sub> dose in 0.1 ml of sterile water was injected (i.m.) into the mice. The survival time and number of deaths occurring within 24 hours was recorded. The results were expressed as the mean  $\pm$  SD. Statistical comparisons were calculated using Student's unpaired *t*-test, with a *p* value < 0.05 indicating significance.

### **2.2.2 The Inhibition Activity**

In the protocol using redioides or hits as antitoxin treatment, redioides or hits were injected after the injection of  $\alpha$ -cobratoxin. 3LD<sub>50</sub> of  $\alpha$ -cobratoxin in 0.1 ml of sterile water was injected (i.m) before the injection of sample in 0.05 ml of 0.3% Tween 80 (i.v). The survival time and number of deaths occurring within 24 hours was recorded. The results were expressed as the mean  $\pm$  SD. Statistical comparisons were calculated using Student's unpaired *t*-test, with a *p* value < 0.05 indicating significance.

### 2.3 Dixon's Q Test (110)

In a set of replicate measurements of a physical or chemical quantity, one or more of the obtained values may differ considerably from the majority of the rest. In this case there is always a strong motivation to eliminate those deviant values and not to include them in any subsequent calculation (e.g. of the mean value and/or of the standard deviation). This is permitted only if the suspect values can be "legitimately" characterized as outliers. Usually, an outlier is defined as an observation that is generated from a different model or a different distribution than was the main "body" of data. Although this definition implies that an outlier may be found anywhere within the range of observations, it is natural to suspect and examine as possible outliers only the extreme values. The rejection of suspect observations must be based exclusively on an objective criterion and not on subjective or intuitive grounds. This can be achieved by using statistically sound tests for "the detection of outliers".

The Dixon's Q-test is the simpler test of this type and it is usually the only one described in textbooks of Analytical Chemistry in the chapters of data treatment. This test allows us to examine if one (and only one) observation from a small set of replicate observations (typically 3 to 10) can be "legitimately" rejected or not. Q-test is based on the statistical distribution of "subrange ratios" of ordered data samples, drawn from the same normal population. Hence, a normal (Gaussian) distribution of data is assumed whenever this test is applied. In case of the detection and rejection of an outlier, Q-test cannot be reapplied on the set of the remaining observations.

The N values comprising the set of observations under examination are arranged in ascending order:  $x_1 < x_2 < \dots < x_N$ . The statistic experimental Q-value ( $Q_{\text{exp}}$ ) is calculated. This is a ratio defined as the difference of the suspect value from its nearest one divided by the range of the values (Q: rejection quotient). Thus, for testing  $x_1$  or  $x_N$  (as possible outliers), use the following  $Q_{\text{exp}}$  values:

$$Q_{\text{exp}} = \frac{X_2 - X_1}{X_n - X_{n-1}} \qquad Q_{\text{exp}} = \frac{X_n - X_{n-1}}{X_n - X_1}$$

The obtained  $Q_{\text{exp}}$  value is compared to a critical Q-value ( $Q_{\text{crit}}$ ) found in Table 8. This critical value should correspond to the confidence level (CL) we have decided

to run the test (usually: CL=95%). If  $Q_{\text{exp}} > Q_{\text{crit}}$ , then the suspect value can be characterized as an outlier and it can be rejected, if not, the suspect value must be retained and used in all subsequent calculations.

**Table 8.** Critical values of Q

N	$Q_{\text{crit}}$ (CL : 90%)	$Q_{\text{crit}}$ (CL : 95%)	$Q_{\text{crit}}$ (CL : 99%)
3	0.941	0.970	0.994
4	0.765	0.829	0.926
5	0.642	0.710	0.821
6	0.560	0.625	0.740
7	0.507	0.568	0.680
8	0.468	0.526	0.634
9	0.437	0.493	0.598
10	0.412	0.465	0.568

## CHAPTER IV

### RESULTS AND DISCUSSION

Alpha-cobratoxin ( $\alpha$ -cbtx), a member of the long  $\alpha$ -neurotoxin family, is obtained from the venom of *Naja kaouthia* (previously called *Naja naja siamensis*). Cbtx has 71 amino acid residues and 5 disulfide bridges. It consists of three finger-like loops: loop I, II and III. Alpha-cobratoxin blocks nerve transmission by binding to the nicotinic acetylcholine receptor (nAChR) on the postsynaptic membranes of skeletal muscle and/or neurons and causes paralysis by preventing acetylcholine binding to nAChR. The only remedy for cobra bite is a monospecific antivenom produced by Queen Saovabha Memorial Institute, The Thai Red Cross Society. The horse antivenom against *Naja kaouthia* is very difficult to produce, expensive and in short supply. Only 20% of the horses immunized with Thai cobra venom produce adequate neutralizing activity for antivenom production.

Application of medicinal plants with anti-snake venom activities might be useful as first aid treatment for victims of snake bite. There are about forty plants in Thailand reported to be effective in treating snake bites. One of the potential plants among these Thai plants was *Trigonostemon redioides* (Kurz) Craib belonging to the Euphorbiaceae family, which is known as “Lotthanong” in Thai. The herb is particularly effective in treating snake bites especially against snake neurotoxins. The daphnanediterpenoids (redioides A and G) have been found as the major components in the roots of this plant.

In search of an antidote of cobra venom by preventing the  $\alpha$ -cobratoxin from binding to the nicotinic acetylcholine receptor, the molecular docking was carried out to investigate the binding mode of redioides to  $\alpha$ -cobratoxin. The aim is to find the mechanism of redioides against cobra venom at the molecular level to promote the utilization of medicinal plant in clinical use. In addition to the investigation of the molecular mechanism of redioides, virtual screening was accomplished by using  $\alpha$ -

cobratoxin as template and docked with 1990 compounds in NCI diversity set. The objective of virtual screening is to discover the novel scaffold of new lead for drug design. The *in vitro* SDS-PAGE and binding assays as well as *in vivo* anti-toxin tests were performed to support the *in silico* results. The findings will be useful for patients who are bitten by snakes and will be useful for medical treatment in Thailand.

### **A. Molecular Modeling (*In Silico*) Experiment**

Molecular docking was carried out to investigate the docking energy and binding mode of redioides bound to neurotoxin or  $\alpha$ -cobratoxin ( $\alpha$ -cbtx) by using AutoDock program version 3.0.5 (22). Among three reported crystal structures of the  $\alpha$ -cobratoxin from the *Naja naja siamensis* or *Naja kaothia*, 1CTX (8) and 2CTX (92) were unbound  $\alpha$ -cobratoxin crystals and 1YI5 (13) was  $\alpha$ -cobratoxin co-crystallized with pentameric acetylcholine binding protein (AChBP) from snail (*Lymnaea stagnalis*, *Ls*). The AChBP from *Ls* mimics the binding domain of nicotinic acetylcholine receptor (nAChR) which mediates excitatory transmission at the neuromuscular junction and in the central and peripheral nervous systems. The binding mode of  $\alpha$ -cobratoxin at AChBP was displayed in Figure 12. The unbound  $\alpha$ -cobratoxin crystal structures (1CTX and 2CTX) have the structures of 71 amino acid residues while the  $\alpha$ -cobratoxin in the bound crystal structure (1YI5) has 68 amino acid residues with missing Arg68 side chain. The difference in number of amino acid residues is due to disorder of these three residues. The missing residues are at the tip of  $\alpha$ -cobratoxin loop III and was found to contribute weakly to  $\alpha$ -cobratoxin binding (13). The closest distance between the missing amino acids and AChBP was 8 Å.

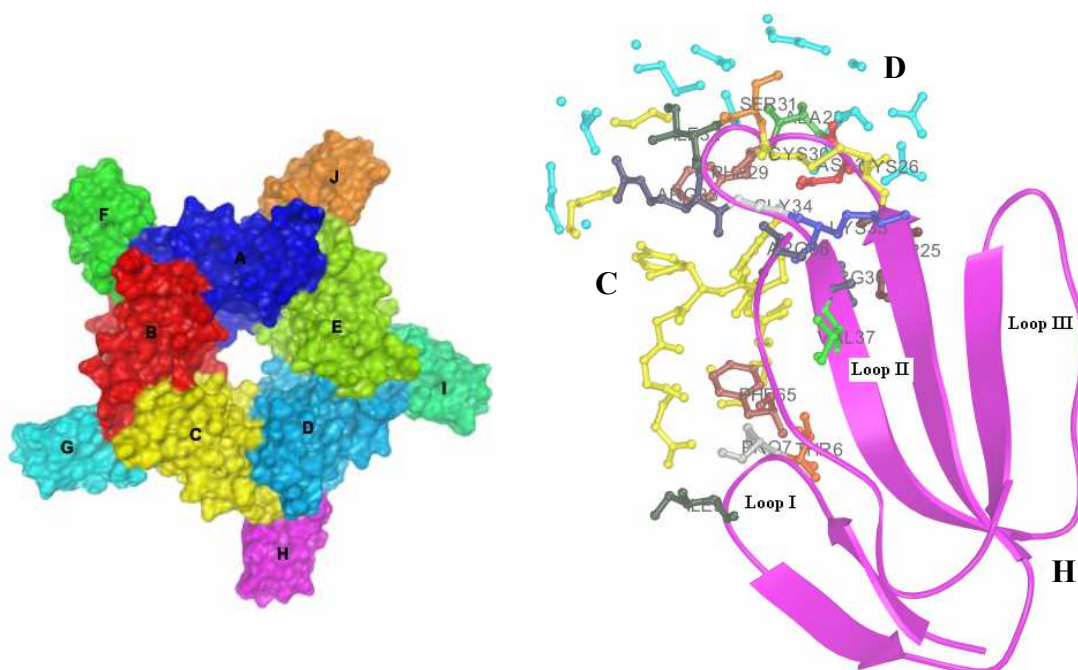


**Figure 12.** The 1YI5 bound crystal between  $\alpha$ -cobratoxin (chain F-J) and AChBP (chain A-E); (PDB: 1YI5). The binding mode of  $\alpha$ -cobratoxin at AChBP showing amino acid residues from  $\alpha$ -cobratoxin (chain H) bound the binding site of AChBP: chain C (yellow); chain D (indigo blue) (12-14).

In the experiment, 1YI5, 1CTX and 2CTX were constructed and used as templates for virtual screening. The area on AChBP that bound to  $\alpha$ -cobratoxin from 1YI5 (Figure 13) was used as a control peptide to validate the  $\alpha$ -cobratoxin template. Chain H was selected to be the  $\alpha$ -cobratoxin template, while Ser182 – Tyr 192 of chain C of AChBP was brought for the preparation of the control peptide in the validation. Nine rotatable bonds in the control peptide were allowed to rotate in the docking and these eleven residues were re-docked to validate the prepared  $\alpha$ -cobratoxin active binding site. The missing Arg68 side chain of chain H in the crystal structure of 1YI5 was reconstructed by SwissPDBViewer, the missing atoms in the side chain were a reasonable conformation. The conformation of Arg68 side chain was in the same as in the unbound crystal structures (1CTX and 2CTX). Chain H was selected from 1YI5 because it was only one chain that has complete amino acid residues comparing to other chains of  $\alpha$ -cobratoxin.

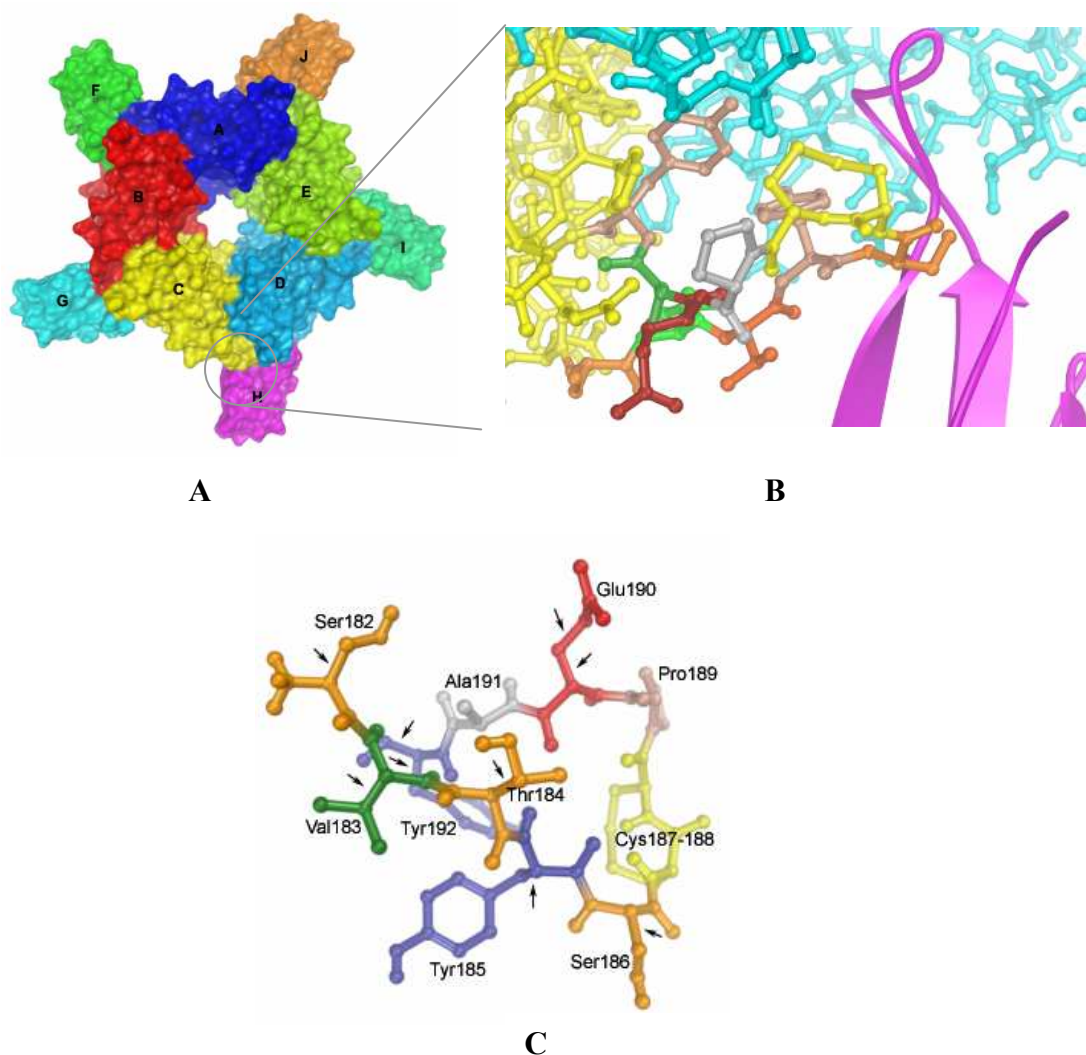


**Figure 13.** The control peptide for the  $\alpha$ -cobratoxin template validation. It composed of eleven amino acid residues from chain C of AChBP (1YI5). The arrows show 9 rotatable bonds.

The validation result of redocking the control peptide to the  $\alpha$ -cobratoxin template shows that 100% of the docked conformations grouped into a single cluster of 2.0 Å RMSD clustering tolerance (Figure 14). The docked orientation in this single cluster is close to that of the crystal pose with RMSD of 1.1020 Å. The residues interacted with the control peptide were the same amino acids in the crystal pose (Figure 15). The same interacted amino acids of the AChBP from the crystal structure and the control peptide are Ile9, Asp27, Arg33, Gly34, Lys35, Val37 and Arg68 (Table 9) (13). The validation by re-docking indicated that the prepared  $\alpha$ -cobratoxin

template is a good model for docking studies of rediocide binding modes and the diversity set.

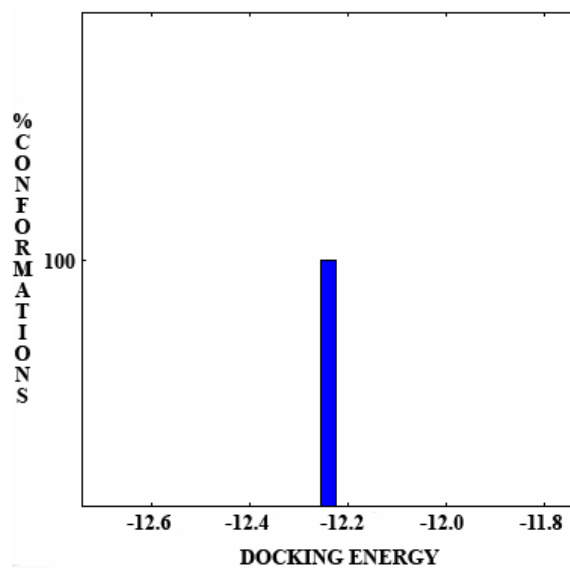


**Figure 14.** The clusters of docked control peptide in the same 3D structure (RMSD of 2 Å), docking energy is in kcal/mol.

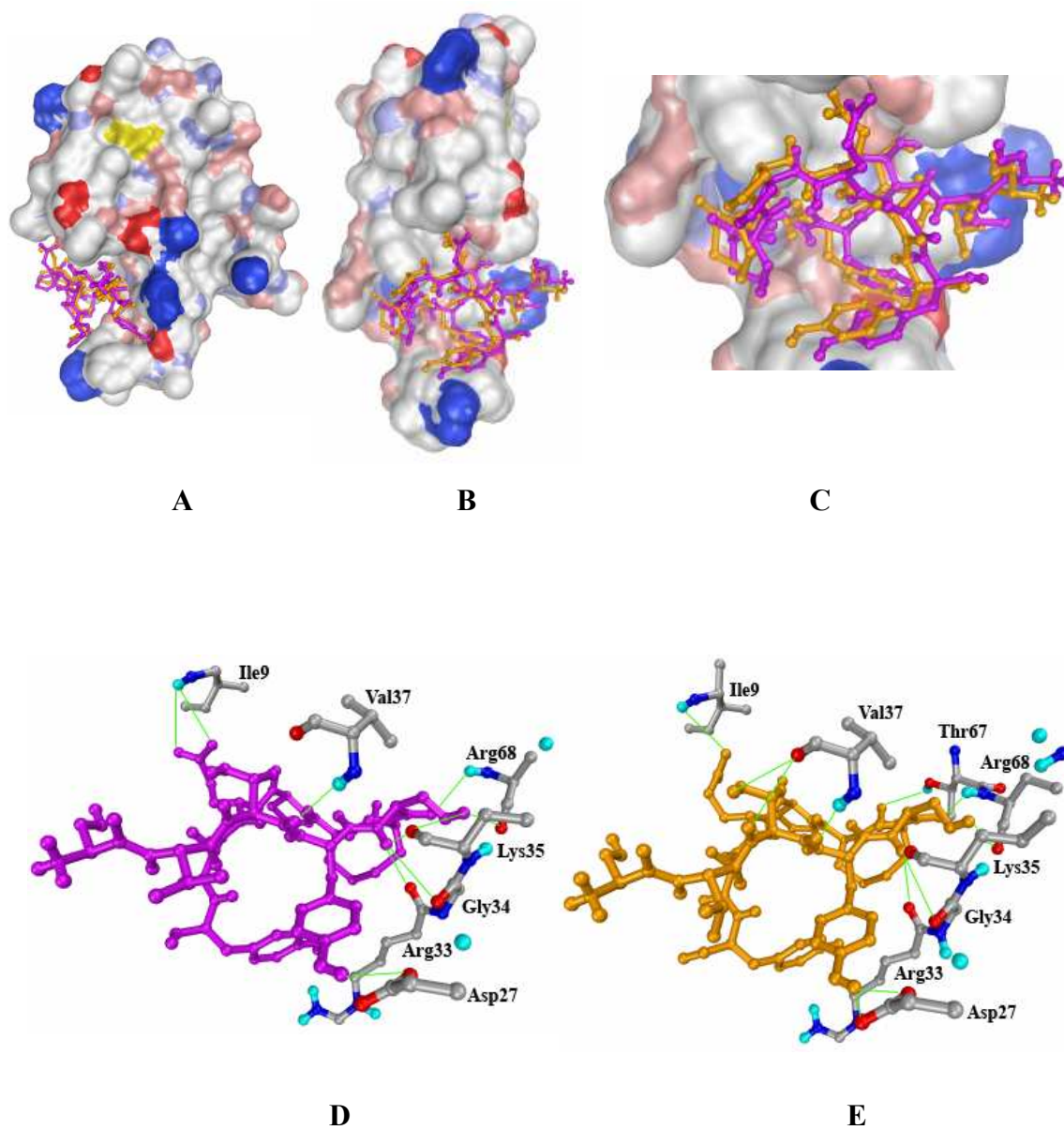


**Figure 15.** Superposition of crystallographic Ser182 – Tyr 192 of chain C from 1YI5 (purple) and docked orientation of control peptide (orange) (A-C). The amino acid residues of  $\alpha$ -cobratoxin interacted with control peptide (D) and crystal pose (E) with distance  $< 4 \text{ \AA}$ .

**Table 9.** Amino acid residues of  $\alpha$ -cobratoxin interacted with the control peptide and the AChBP in the crystal pose (1YI5)

Crystal pose (1YI5)		Control peptide (validation)	
AChBP - Cbtx	Distance (Å)	Control <sup>a</sup> - Cbtx	Distance (Å)
CO – HN (Ile9)	3.594	CO –HN (Ile9)	3.330
CO –HN (Ile9)	3.787		
OH – OC (Asp27)	1.565	OH – OC (Asp27)	1.993
OH – OC (Asp27)	2.578	OH – OC (Asp27)	2.220
NH – OC (Arg33)	3.484	NH – OC (Arg33)	3.433
NH – OC (Gly34)	3.666	NH – OC (Gly34)	3.941
NH – OC (Lys35)	2.033	NH – OC (Lys35)	2.096
OH – OC (Lys35)	2.838		
CO – HN (Val37)	2.476	CO – HN (Val37)	1.821
		OH – OC (Val37)	3.400
		NH – OC (Val37)	3.702
		CO – HO (Thr67)	3.520
CO – HN (Arg68)	3.008	CO – HN (Arg68)	1.903
OH – OC (Arg68)	3.526	OH – OC (Arg68)	3.474

<sup>a</sup>Eleven residues with 9 rotatable bonds from AChBP that bind to  $\alpha$ -cobratoxin.

### 1. Binding Mode of Redioides (A & G)

Redioides A and G are daphnanediterpenoids from *Trigonostemon redioides*. The differences between the structures of redioides A and G are (i) a 5-membered ring with a methyl side chain for redioides A and a 6-membered ring for redioides G on the backbone structure and (ii) the isobutyl ester side chain for redioides A and phenyl ring for redioides G (Figure 16). The docking study on redioides and  $\alpha$ -

cobratoxin interaction was performed to investigate the binding modes of the redioides. The docking simulation techniques have been carried out using AutoDock program. Because of the complex structures of redioides, a molecular dynamics was assigned to generate conformations. Each of the 101 conformations of redioid A and redioid G was designed to have 11 and 10 rotatable bonds respectively and docked to the  $\alpha$ -cobratoxin template with the AutoDock3 program. The 100 independent dockings were run for each ligand, the docked ligand generally converged to a small number of different positions or conformers or poses. The pose in top cluster with greatest frequency of occurrence is the most probable orientation, or conformer that bound to the active binding site with most favorable docking energy. After each of 100 docking runs, the conformations that have the lowest docked energy with the same 3D structure ( $\text{RMSD} < 2 \text{ \AA}$ ) were clustered as shown in Figure 17 and 18. There are 40 and 38 conformers in the first cluster of redioid A and redioid G, respectively (Table 10).

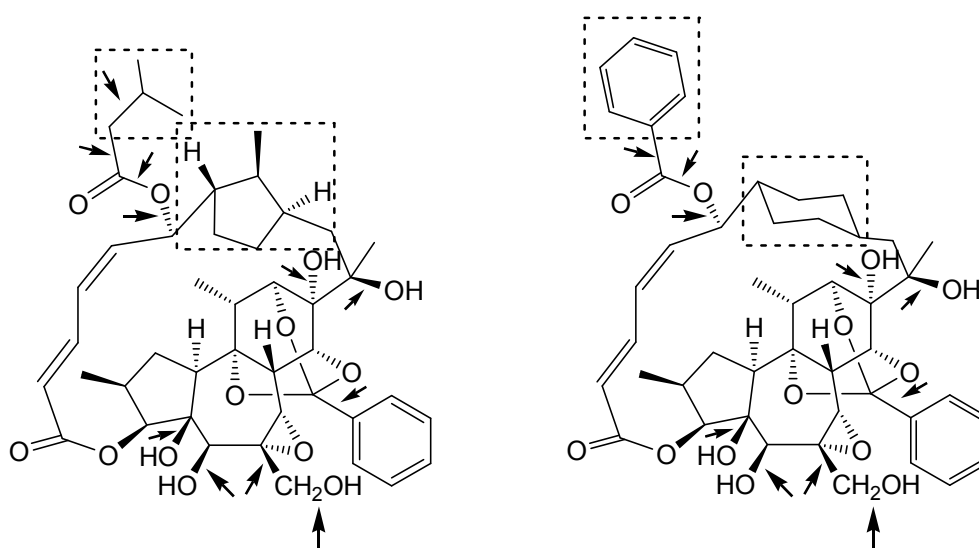


**Figure 16.** Structures of redioides A (left) and G (right). The rectangular boxes show the differences in structures between redioid A and redioid G and the arrows show the assigned rotatable bonds.

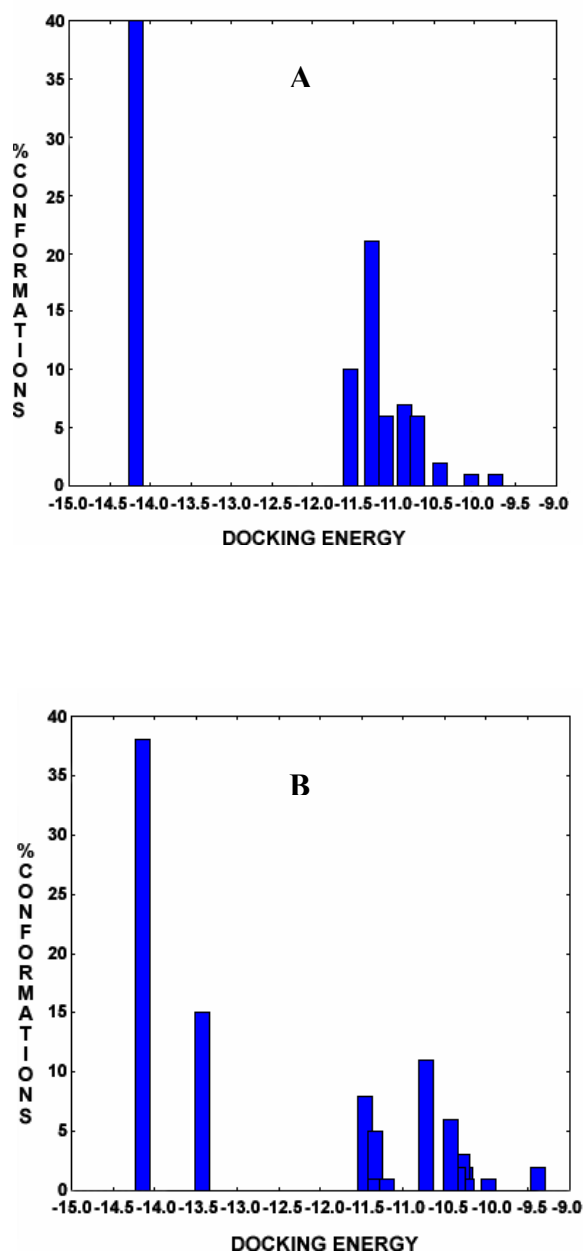


**Figure 17.** Clusters of docked rediocides in the same 3D structure (RMSD <math>< 2\text{\AA}</math>), (A) rediocide A and (B) rediocide G, docking energy is in kcal/mol.

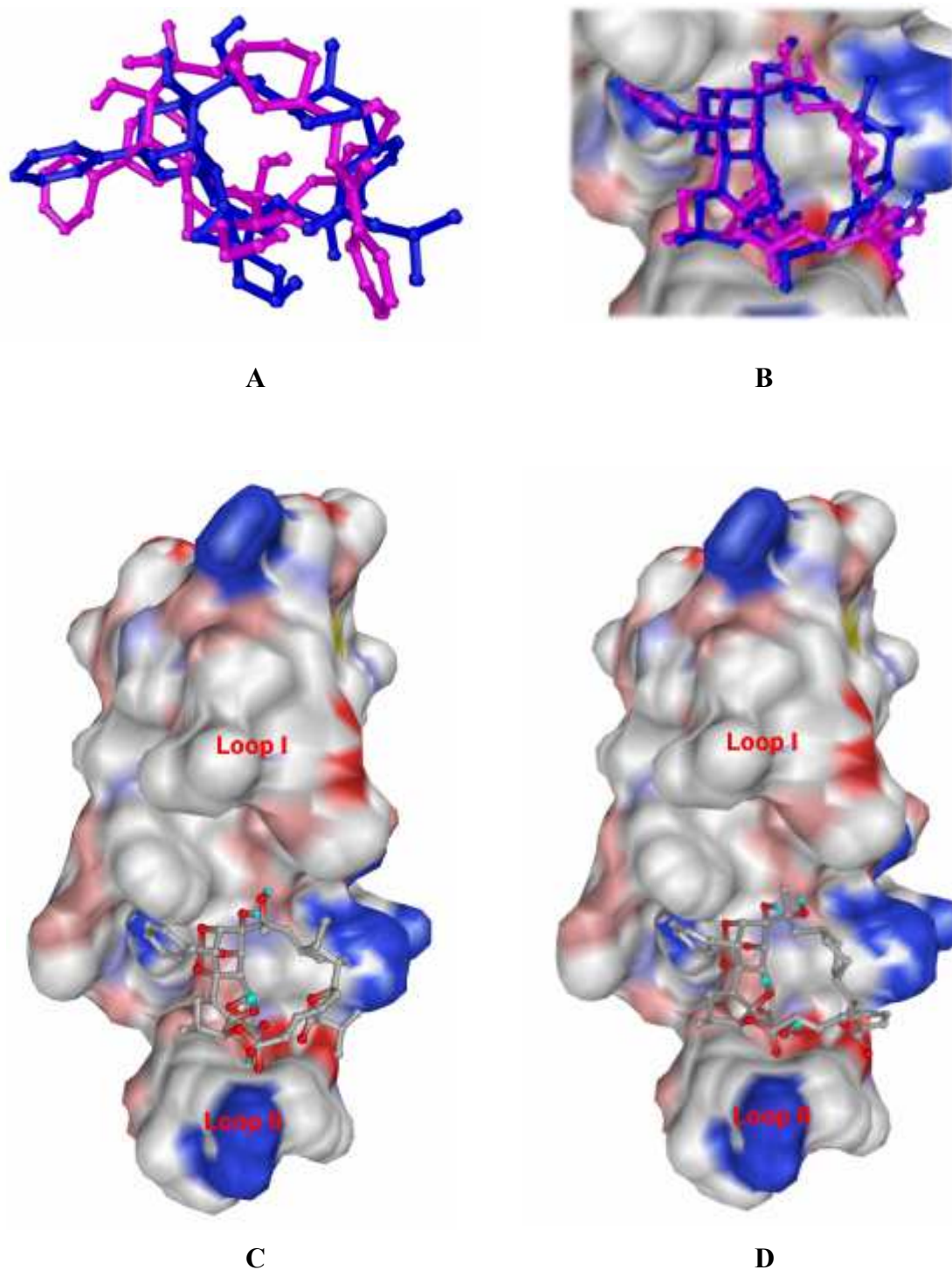


**Figure 18.** The bound conformations of redioides in the active site of  $\alpha$ -cobratoxin. The structures of redioides A (blue) and redioides G (pink) before docking (A) and after docking (B). The msms models of  $\alpha$ -cobratoxin molecule template prepared from 1YI5 bind with redioides A (C) and redioides G (D).

**Table 10.** Cluster analysis from docking  $\alpha$ -cobratoxin with redioides A and G

Ligand	Cluster number	%Member in cluster	Docking energy (Kcal/mol)
Rediocide A	1 <sup>a</sup>	40	-14.17
Rediocide G	1 <sup>a</sup>	38	-14.14
Control peptide <sup>b</sup>	1 <sup>a</sup>	100	-12.20

<sup>a</sup>The cluster with lowest docking energy of a total 100 runs.

<sup>b</sup>Alpha-cbtx binding site at AChBP (Ser182-Tyr192 from chain C of 1YI5).

The binding sites of rediocide A and rediocide G at  $\alpha$ -cobratoxin were in the same general location and preferably shifted to loop II of the  $\alpha$ -cobratoxin which provided ample space to better accommodate this larger molecule. Table 11 and Figure 19 show the interacted amino acid residues between functional groups of redioides and amino acid residues surrounding their binding sites to  $\alpha$ -cobratoxin. Hydrogen bonds were formed directly between the redioides and amino acid residues at the binding site of  $\alpha$ -cbtx. The significant positions in rediocide A were Asp27, Phe29, Arg33, Gly34, Lys35 and Val37 with the distance of 1.8-4.0 Å and those of rediocide G were Asp27, Phe29, Arg33, Lys35 and Val37 with 1.9-3.9 Å. The Phe29 and Arg33 side chains extending at the tip of  $\alpha$ -cobratoxin are well positioned for establishing hydrophobic and aromatic interactions. The amino acid residues from  $\alpha$ -cobratoxin that bind AChBP representing the acetylcholine receptor were reported to be Thr6, Pro7, Ile9 in loop I, Trp25, Cys26, Asp27, Ala28, Phe29, Cys30, Ser31, Ile32, Arg33, Gly34, Lys35, Arg36, Val37 in loop II and Phe65, Arg68 for C-terminus as shown in Figure 12 (12-14). The rediocide bound location was in the same area that the  $\alpha$ -cobratoxin bound with nicotinic acetylcholine receptor. Thus, the active binding site of  $\alpha$ -cobratoxin is occupied in the presence of redioides and consequently  $\alpha$ -cobratoxin cannot bind with the acetylcholine receptor. Therefore, the *in silico* experiment can reveal the detoxification mechanism of cobra venom at the molecular level.

**Table 11.** Amino acid residues of  $\alpha$ -cobratoxin interacted with rediocides

<b>Rediocide A - Cbtx</b>	<b>Distance (Å)</b>	<b>Rediocide G - Cbtx</b>	<b>Distance (Å)</b>
OH – OC (Asp27)	2.634	OH – OC (Asp27)	2.589
OH – OC (Phe29)	2.757	OH – OC (Phe29)	3.258
OH – OC (Phe29)	3.924	CO – HN (Arg33)	2.805
CO – HN (Arg33)	2.556	O – HN (Gly34)	3.804
OH – OC (Lys35)	3.894	OH – OC (Gly34)	2.239
O – HN (Val37)	2.730	O – HN (Val37)	2.697
OH – OC (Val37)	1.878	OH – OC (Val37)	1.946
OH – OC (Val37)	2.284	OH – OC (Val37)	1.907

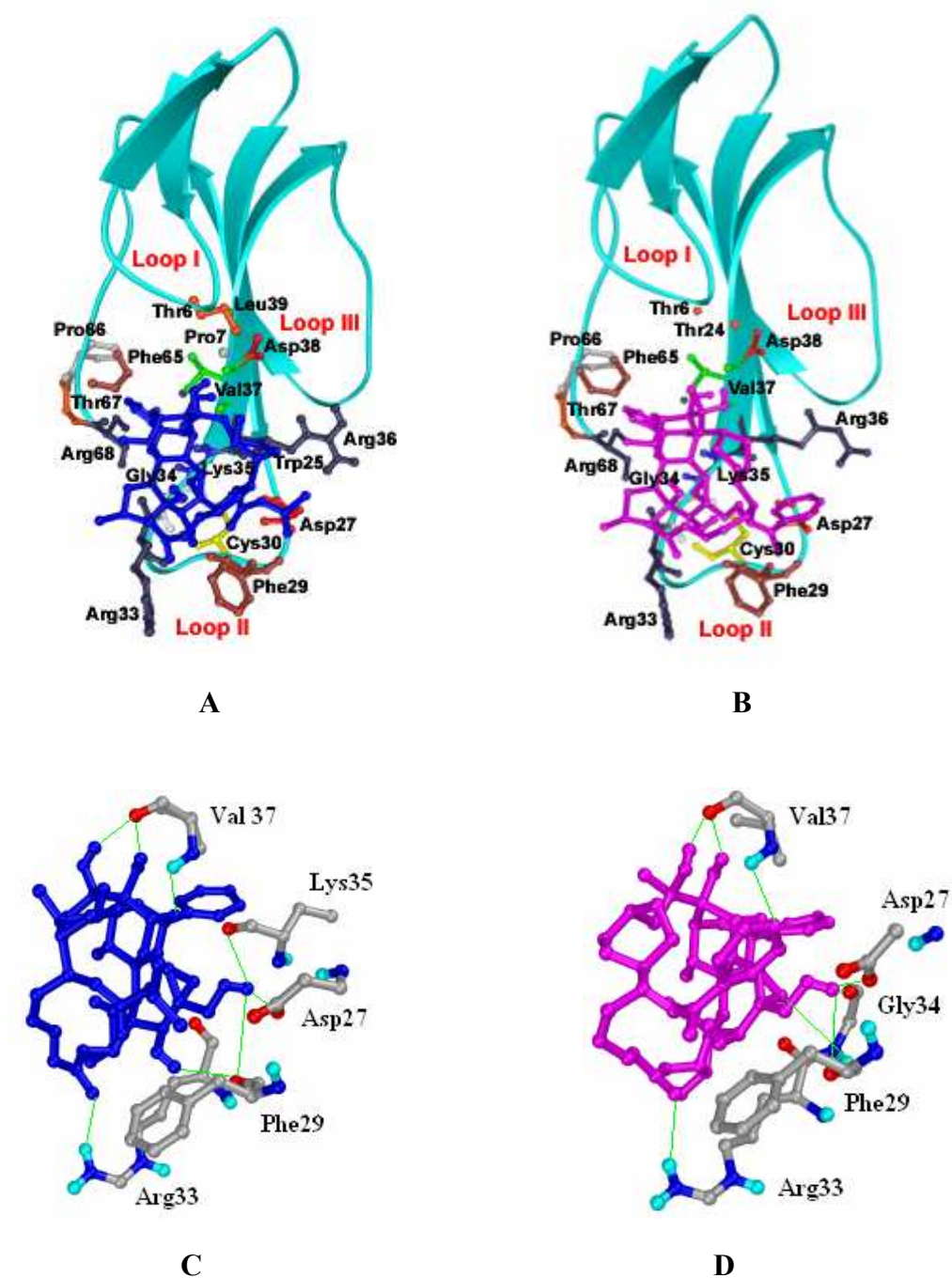


**Figure 19.** The bound conformations of redioides in the active site of  $\alpha$ -cobratoxin (A and B). The ribbon model shows the backbone of  $\alpha$ -cobratoxin catalytic domain (1YI5) with all interacting amino acid residues shown as stick and ball models, redioid A (blue), redioid G (pink). The amino acid residues of  $\alpha$ -cobratoxin interacted with redioid A (C) and redioid G (D) with distance less than 4 Å.

## 2. Virtual Screening

Virtual screening was conducted by docking the  $\alpha$ -cobratoxin template derived from 3 crystal structures (1CTX, 2CTX and 1YI5) against 1990 ligands in NCI diversity set. The virtual screening was performed on Bluefish (a 64-bit 576 processor LINUX cluster) by the unix script command for virtual screening (110). After docking, the docking energy of each ligand that bind to each  $\alpha$ -cobratoxin template (1YI5, 1CTX and 2CTX) was ranked from lowest docking energy to highest docking energy. The top 175 compounds from each  $\alpha$ -cobratoxin templates were in Table 12. The lowest docking energy for 1YI5, 1CTX and 2CTX were -13.86, -13.59 and -12.74 kcal/mol, respectively and the highest docking energy were -10.11, -10.12 and -9.52 kcal/mol for 1YI5, 1CTX and 2CTX, respectively. There are seventy seven compounds that matched 3 templates and only nineteen compounds have the “drug like” properties (molecular weight < 500, Log P < 5 and number of rotatable bonds < 5). For experimental testing, 20 more compounds were included in the *in vitro* evaluation on the basis of low docking energy and high %member in the cluster of lowest energy. The total number of compounds in the binding study was thirty nine. The docking energies from 3 templates of the 39 selected compounds were listed in Table 13.

**Table 12.** The top 175 compounds for each  $\alpha$ -cobratoxin templates

	1YI5		2CTX		1CTX	
	NCI number	Docking energy (kcal/mol)	NCI number	Docking energy (kcal/mol)	NCI number	Docking energy (kcal/mol)
↑	371884	-13.86	49487	-12.74	11241	-13.59
	49487	-13.54	11241	-11.93	371884	-13.30
	11241	-13.32	371878	-11.91	23128	-13.10
	175	371878	-13.19	372280	-11.77	134755
Cpds	.	.	.	.	.	.
↓	.	.	.	.	.	.
	105687	-10.11	136469	-9.52	14143	-10.12

**Table 13.** Selected hits from virtual screening<sup>a</sup>

Compound	NCI number	MW (Da)	Log P	Rotatable bonds	E <sub>docking</sub> in highest clustering (kcal/mol)			% member in highest cluster		
					1Y15	2CTX	1CTX	1Y15	2CTX	1CTX
1	10458	482	3.57	7	-9.64	-9.78	-10.20	28	21	57
2	12181	458	5.22	5	-10.50	-10.10	-11.41	66	16	74
<b>3</b>	<b>14410</b>	<b>444</b>	<b>0.35</b>	<b>4</b>	<b>-12.11</b>	<b>-10.81</b>	<b>-11.31</b>	<b>69</b>	<b>43</b>	<b>55</b>
4	17245	459	2.17	7	-9.74	-9.71	-10.20	26	24	11
<b>5</b>	<b>18877</b>	<b>406</b>	<b>4.62</b>	<b>4</b>	<b>-10.89</b>	<b>-9.56</b>	<b>-10.5</b>	<b>29</b>	<b>55</b>	<b>26</b>
6	23217	405	6.50	4	-11.54	-10.11	-9.64	56	26	27
7	23904	524	2.85	7	-11.00	-6.68	-10.60	28	57	18
<b>8</b>	<b>36387</b>	<b>696</b>	<b>3.18</b>	<b>4</b>	<b>-11.10</b>	<b>-9.34</b>	<b>-9.64</b>	<b>16</b>	<b>8</b>	<b>25</b>
<b>9</b>	<b>37245</b>	<b>467</b>	<b>4.33</b>	<b>4</b>	<b>-11.45</b>	<b>-9.19</b>	<b>-11.55</b>	<b>54</b>	<b>20</b>	<b>53</b>
<b>10</b>	<b>42258</b>	<b>417</b>	<b>3.27</b>	<b>4</b>	<b>-11.23</b>	<b>-8.27</b>	<b>-10.69</b>	<b>65</b>	<b>38</b>	<b>58</b>
11	45583	504	4.18	7	-10.10	-9.78	-10.5	23	35	43
12	56452	378	5.02	6	-10.80	-10.65	-11.30	13	37	25
<b>13</b>	<b>60043</b>	<b>317</b>	<b>3.56</b>	<b>4</b>	<b>-11.12</b>	<b>-9.70</b>	<b>-10.10</b>	<b>49</b>	<b>49</b>	<b>23</b>
14	74702	549	5.95	2	-11.00	-11.12	-9.80	21	17	27
<b>15</b>	<b>81509</b>	<b>352</b>	<b>1.16</b>	<b>5</b>	<b>-10.80</b>	<b>-9.20</b>	<b>-11.74</b>	<b>33</b>	<b>31</b>	<b>16</b>
16	95090	582	2.02	5	-9.85	-8.69	-1.46	13	12	64
<b>17</b>	<b>95926</b>	<b>447</b>	<b>2.71</b>	<b>5</b>	<b>-11.83</b>	<b>-10.73</b>	<b>-10.10</b>	<b>61</b>	<b>24</b>	<b>34</b>
<b>18</b>	<b>99671</b>	<b>401</b>	<b>1.06</b>	<b>4</b>	<b>-10.64</b>	<b>-9.30</b>	<b>-10.10</b>	<b>60</b>	<b>34</b>	<b>12</b>
19	105687	379	6.01	5	-9.27	-10.16	-11.29	14	36	26
<b>20</b>	<b>113491</b>	<b>470</b>	<b>-1.43</b>	<b>4</b>	<b>-12.07</b>	<b>-10.30</b>	<b>-10.00</b>	<b>74</b>	<b>34</b>	<b>21</b>
21	116654	349	2.80	6	-10.50	-9.85	-10.2	29	22	25
<b>22</b>	<b>121855</b>	<b>435</b>	<b>1.10</b>	<b>5</b>	<b>-10.50</b>	<b>-9.40</b>	<b>-8.19</b>	<b>50</b>	<b>29</b>	<b>60</b>
<b>23</b>	<b>121865</b>	<b>412</b>	<b>0.30</b>	<b>5</b>	<b>-11.09</b>	<b>-9.59</b>	<b>-9.91</b>	<b>72</b>	<b>53</b>	<b>20</b>
<b>24</b>	<b>127917</b>	<b>299</b>	<b>0.56</b>	<b>5</b>	<b>-9.71</b>	<b>-9.45</b>	<b>-10.96</b>	<b>48</b>	<b>32</b>	<b>29</b>
<b>25</b>	<b>128437</b>	<b>477</b>	<b>3.90</b>	<b>4</b>	<b>-11.83</b>	<b>-11.67</b>	<b>-10.20</b>	<b>39</b>	<b>33</b>	<b>50</b>
26	131547	476	4.19	6	-11.41	-9.43	-10.10	16	16	22
<b>27</b>	<b>134754</b>	<b>580</b>	<b>3.10</b>	<b>5</b>	<b>-10.20</b>	<b>-9.84</b>	<b>-11.00</b>	<b>44</b>	<b>71</b>	<b>22</b>
28	134755	580	3.10	5	-10.80	-9.20	-9.87	41	24	7
29	163443	394	6.26	5	-11.41	-9.51	-10.10	28	17	13
30	205511	335	3.49	6	-9.91	-10.75	-10.62	31	54	24
<b>31</b>	<b>282027</b>	<b>320</b>	<b>2.00</b>	<b>5</b>	<b>-11.01</b>	<b>-9.66</b>	<b>-10.20</b>	<b>29</b>	<b>36</b>	<b>21</b>
<b>32</b>	<b>339601</b>	<b>415</b>	<b>2.62</b>	<b>5</b>	<b>-10.75</b>	<b>-8.97</b>	<b>-9.56</b>	<b>23</b>	<b>12</b>	<b>26</b>
<b>33</b>	<b>371884</b>	<b>447</b>	<b>3.62</b>	<b>5</b>	<b>-13.20</b>	<b>-9.24</b>	<b>-12.10</b>	<b>17</b>	<b>25</b>	<b>28</b>
34	372046	493	6.89	5	-11.70	-10.70	-12.48	50	58	20
35	372280	438	5.64	5	-10.90	-11.77	-9.86	54	16	36
36	372294	454	4.54	6	-10.50	-11.51	-9.73	37	16	21
<b>37</b>	<b>600067</b>	<b>324</b>	<b>1.16</b>	<b>5</b>	<b>-11.78</b>	<b>-10.60</b>	<b>-11.84</b>	<b>77</b>	<b>78</b>	<b>40</b>
<b>38</b>	<b>659162</b>	<b>434</b>	<b>4.93</b>	<b>5</b>	<b>-10.50</b>	<b>-10.21</b>	<b>-11.31</b>	<b>46</b>	<b>25</b>	<b>28</b>
<b>39</b>	<b>659390</b>	<b>417</b>	<b>2.80</b>	<b>5</b>	<b>-8.72</b>	<b>-9.77</b>	<b>-9.62</b>	<b>28</b>	<b>42</b>	<b>18</b>

<sup>a</sup>39 compounds from NCI diversity set that match all  $\alpha$ -cbtx templates (1Y15, 1CTX and 2CTX).

## B. *In Vitro* Experiment

Thirty nine hits from virtual screening and redioides (A and G) were investigated further for their binding capability. The binding between selected hits (39 compounds) and redioides (A and G) with  $\alpha$ -cobratoxin were evaluated by (i) *in vitro* radioligand competition assay and (ii) sodium dodecyl sulfate polyacrylamide gel electrophoresis (SDS-PAGE). These experiments were carried out to substantiate the results from *in silico* experiments.

The AChBPs, a soluble extracellular binding domain of nAChR, came from snails in different species i.e. *Lymnaea stagnalis* (*Ls*), *Aplysia californica* (*Ac*) and *Bolunus truncatus* (*Bt*). They were used for the investigation of the binding capability. AChBP from *Ac* shares 33% amino acid identity with those from *Ls* and less than 33% with *Bt*. AChBPs, *Ls* and *Ac*, share 24% amino acid identity with human nAChR  $\alpha 7$  and 20% with human nAChR  $\alpha 1$  while AChBP from *Bt* shares 22% amino acid identity with  $\alpha 7$  and 17% with  $\alpha 1$  (Table 14). The amino acid sequences of AChBP from snail and human nAChR ( $\alpha 7$  and  $\alpha 1$ ) were shown in Figure 20.

**Table 14.** Percent amino acid identity of AChBPs

	<i>Ls</i> AChBP	<i>Bt</i> AChBP	Human nAChR	
			$\alpha 1$	$\alpha 7$
<i>Ac</i> AChBP	33	< 33	24	20
<i>Ls</i> AChBP			24	20
<i>Bt</i> AChBP			22	17

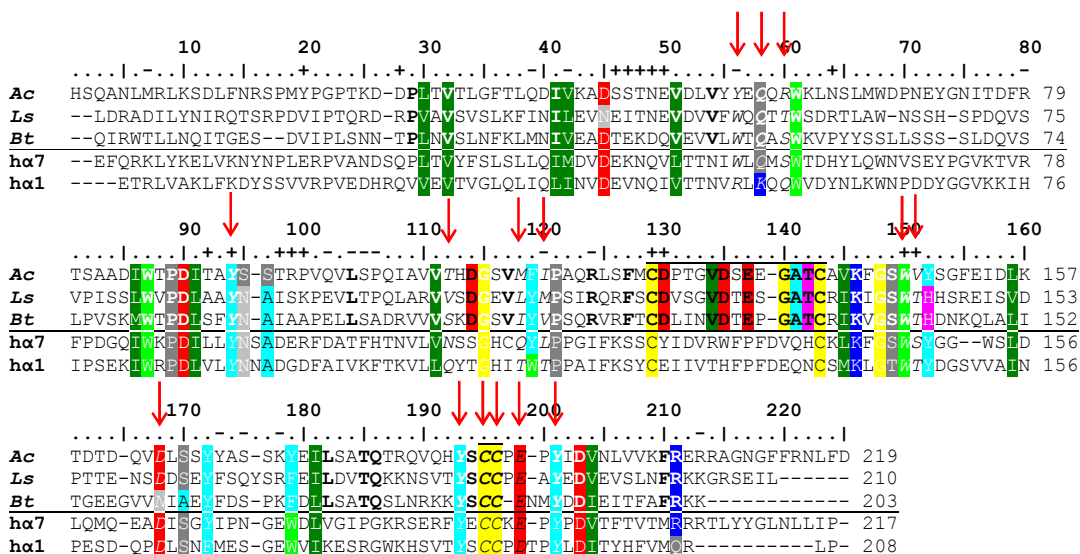


**Figure 20.** The amino acid sequences of AChBPs (*Ac*, *Ls* and *Bt*) and human nAChR ( $\alpha 7$  and  $\alpha 1$ ). Conserved residues are shown on a color background with bold denoting points of structural identity from an alignment of the crystallographic coordinates of the following complexes: AChBP from *L. stagnalis* with nicotine (PDB: 1UW6), AChBP from *A. californica* with epibatidine (PDB: 2BYQ), and AChBP from *B. truncatus* with CHAPS (3-(cyclohexylamino) propane-1-sulfonic acid, PDB: 2BJ0). The plus (+) and minus (-) denote residues within the 4.0 Å radius of interaction at the subunit interface. Residues that are within 5 Å of all three molecules (nicotine, epibatidine and CHAPS) present in the binding site are italic ( $\downarrow$ ).

### 1. Radioligand Competition Assay

In the assay, the nAChR antagonist ( $^{125}\text{I}$   $\alpha$ -bungarotoxin) and the nAChR agonist ( $^3\text{H}$  epibatidine) were the control as they completely bound with AChBP. [ $^3\text{H}$ ] epibatidine bound all three kinds of AChBPs but [ $^{125}\text{I}$ ]  $\alpha$ -bungarotoxin bound AChBP from *Ls* and *Ac* only. [ $^3\text{H}$ ] epibatidine was used for screening the hits that displaced its binding to AChBPs. AChBPs were bound to the bead with the aid of the monoclonal anti-FLAG M2 antibody from mouse (Figure 21). The bead itself is made from polyvinyltoluene which serves as a scintillant. The bead emits light when there is a

high energy emitter nearby. The amount of emitted light from the samples were measured by a scintillation counter. The amount of light emitted by each sample is proportional to the amount of radioactive epibatidine or bungarotoxin bound to the binding protein on the bead which can then be related to the ability of a compound to compete with these radioligands. The radioligand binding to AChBP bound bead was displayed in Figure 22.

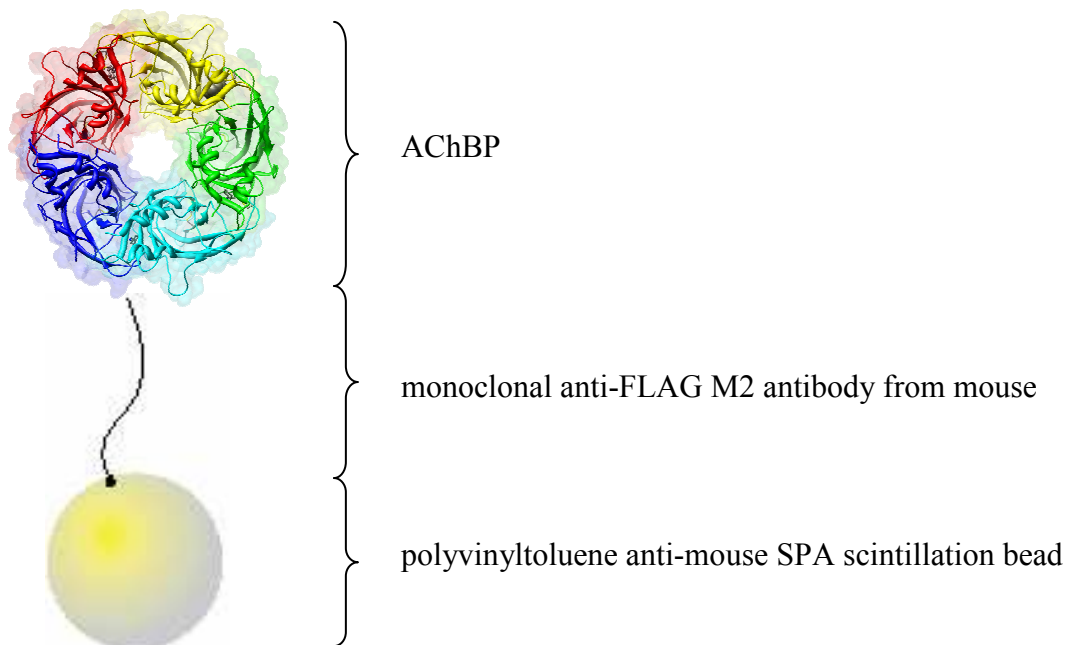


**Figure 21.** AChBPs bound to the bead by using the monoclonal anti-FLAG M2 antibody from mouse.

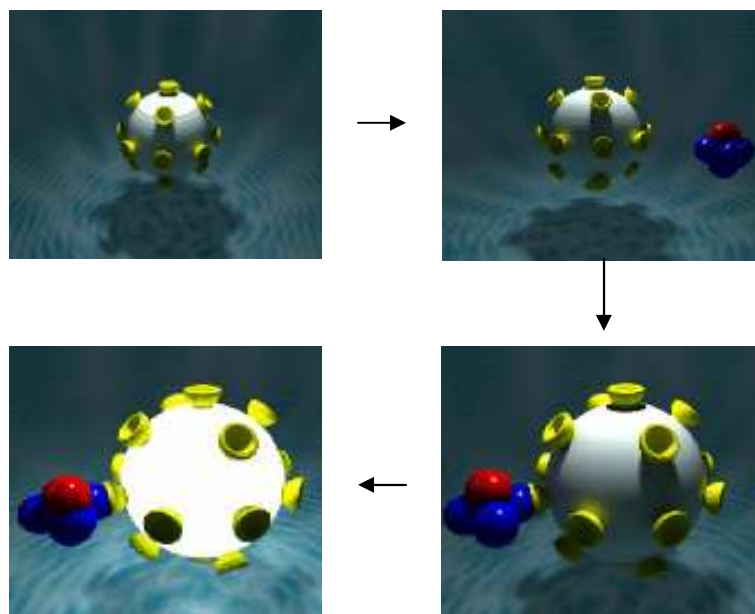


**Figure 22.** Radioactive [ $^3\text{H}$ ] epibatidine or [ $^{125}\text{I}$ ] bungarotoxin bound to the binding protein and emitted the light. Epibatidine or bungarotoxin is in blue, radioactive is in red and AChBP is in yellow. The size of each component is not to scale.

### 1.1. Screening Test

The radioligand assay was initially run to screen the 39 hits prior to the determination of  $K_d$ . Ten micromolar of each compound was screened for their ability to displace the binding of [ $^3\text{H}$ ] epibatidine to the three AChBPs (*Lymnaea stagnalis* (*Ls*), *Aplysia californica* (*Ac*) and *Bolunus truncatus* (*Bt*)) as measured by a scintillation proximity test (Figure 23). NCI36387 (compound 8), NCI42258 (compound 10), NCI121865 (compound 23) and NCI134754 (compound 27) showed the low fraction of [ $^3\text{H}$ ] epibatidine bind to AChBPs (less than 0.6). The 4 hits can bind to the agonist [ $^3\text{H}$ ] epibatidine as strong as the AChBP which led to the reduction of radioligand binding to AChBP on the bead. The results of fraction over 1.0 were possibly due to the variation in number of AChBP binding to the beads or the interferences in light emission from the hits.

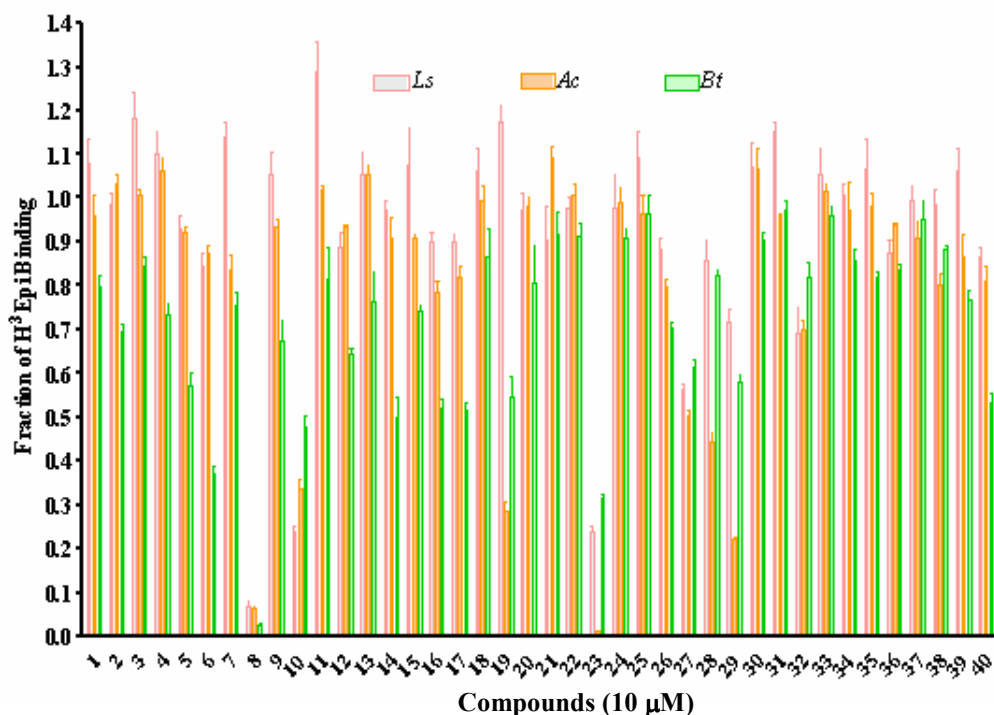
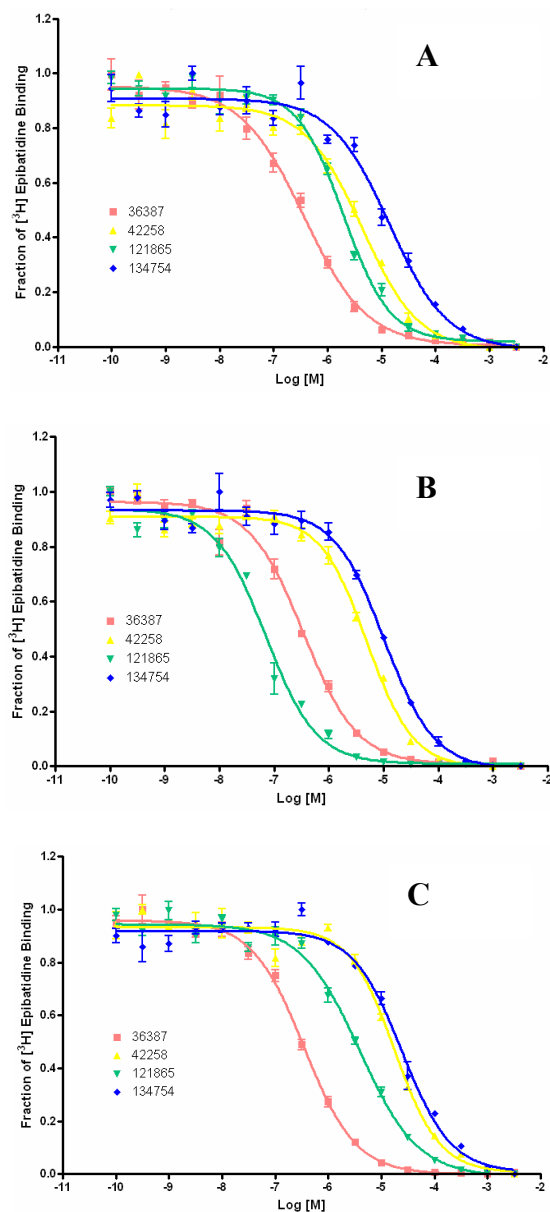


**Figure 23.** Screening test for the ability to displace the binding of [ $^3\text{H}$ ] epibatidine on AChBP from *Lymnaea stagnalis* (*Ls*), *Aplysia californica* (*Ac*) and *Bulinus truncatus* (*Bt*).

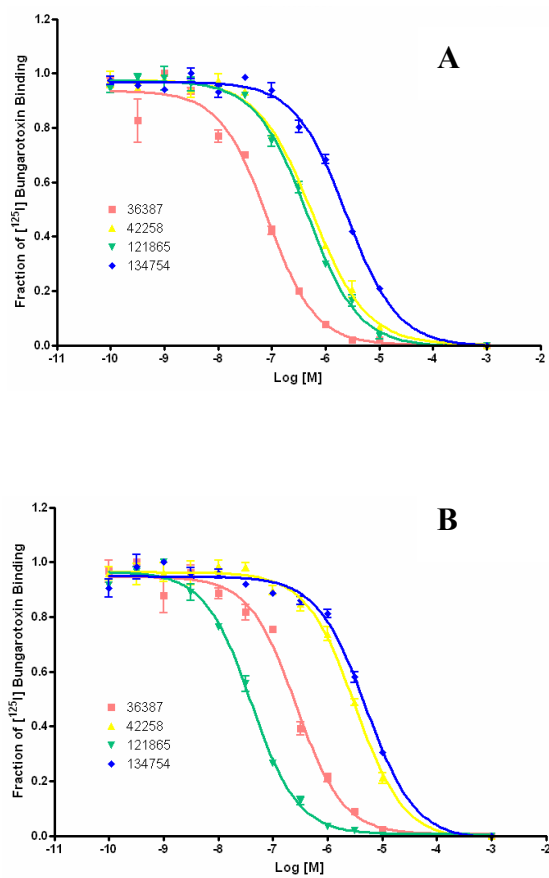
### 1.2. Determination of $K_d$

The four hits were determined for the dissociation constant ( $K_d$ ).  $K_d$  is commonly used to describe the affinity between a ligand (4 hits) and a protein (AChBPs). The smaller the dissociation constant, the more tightly bound the ligand is, or the higher the affinity between ligand and protein. Four hits (compounds 8, 10, 23 and 27) from the screening test in varied concentrations from millimolar to nanomolar were added to the fixed concentrations of AChBPs ( $\sim 500$  pM binding sites), polyvinyltoluene anti-mouse SPA scintillation beads, monoclonal anti-FLAG M2 antibody from mouse. Then, agonist [ $^3\text{H}$ ] epibatidine (5 nM for *Ls* and *Bt*, 20 nM for *Ac*) or antagonist [ $^{125}\text{I}$ ]  $\alpha$ -bungarotoxin (10 nM for *Ls* and 20 nM for *Ac*) were added and allowed to equilibrate at room temperature. The plot between fraction of [ $^3\text{H}$ ]

epibatidine or [ $^{125}$ I]  $\alpha$ -bungarotoxin and the concentration of 4 hits were shown in Figure 24 and 25, respectively.



**Figure 24.** The ability to displace the binding of [ $^3$ H] epibatidine on AChBPs ( $\sim$ 500 pM binding site) from *Lymnaea stagnalis* (A), *Aplysia californica* (B) and *Bulinus truncatus* (C). X-axis is the log concentration of the 4 hits in molar, the concentrations of [ $^3$ H] epibatidine were 5 nM for AChBPs derived from *Ls* and *Bt*, and 20 nM for *Ac*.

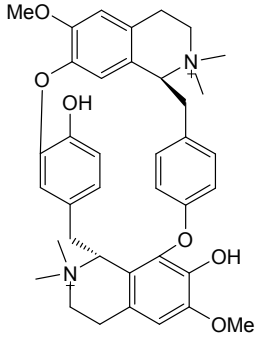
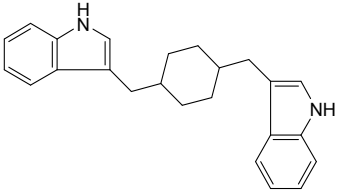
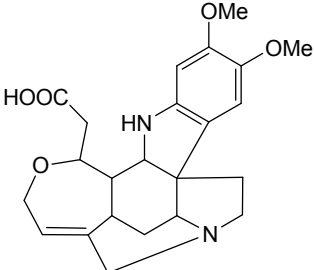
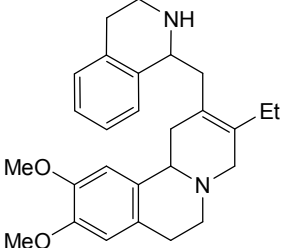


**Figure 25.** The ability to displace the binding of  $[^{125}\text{I}]$   $\alpha$ -bungarotoxin on AChBPs from *Lymnaea stagnalis* (A) and *Aplysia californica* (B). X-axis is the log concentration of the 4 hits in molar, 10 nM for AChBPs derived from *Ls* and 20 nM for *Ac*.

In the assay, four hits competitively displaced on antagonist ( $^{125}\text{I}$   $\alpha$ -bungarotoxin) and the agonist ( $^3\text{H}$  epibatidine) from their mutually exclusive binding sites on AChBPs from *Lymnaea*, *Aplysia* and *Bulinus* with the concentration from micromolar to nanomolar. Their chemical structures, NCI numbers, molecular weights,  $K_d$  values and estimated binding free energies were listed in Table 15 and 16. The hit with a better binding on AChBPs has a lower  $K_d$  value. According to [ $^3\text{H}$ ] epibatidine, NCI36387 (compound 8) was the most potent in binding with AChBPs from *Ls* and *Bt* while NCI121865 (compound 23) was most potent in binding with *Ac*. For the antagonist [ $^{125}\text{I}$ ]  $\alpha$ -bungarotoxin, NCI36387 was the most potent for binding with AChBP from *Ls* while NCI121865 most potent for binding with *Ac* AChBP. Interestingly, NCI36387 was found to be *d*-tubocurarine, the active ingredient in curare and the well known neuromuscular blocker. The results showed that the activity for competing with [ $^3\text{H}$ ] epibatidine and [ $^{125}\text{I}$ ]  $\alpha$ -bungarotoxin for NCI121865 (compound 23) was better than NCI42258 (compound 10) and NCI134754 (compound 27), respectively. The graph has shifted into in left hand side. NCI121865 was the potent lead compound and the mechanism for the anti-cobratotoxin may be competing with the toxin to bind the acetylcholine receptor. According to the virtual screening result (Table 13), the members in the lowest energy cluster of NCI42258 and NCI121865 are considerably high, 65 % and 72 %, respectively. Based on Binding Efficiency Index (BEI), the new parameter for filtering the drug like molecules, BEI value of NCI121865 is the best among the hits. BEI is calculated from  $\text{pK}_i$  and molecular weight in kDa, the ideal BEI value is 27. It is 13.32 with [ $^3\text{H}$ ] epibatidine and 32.83 with [ $^{125}\text{I}$ ]  $\alpha$ -bungarotoxin on AChBP from *Ac*.

The amino acid of  $\alpha$ -cobratotoxin interacted with 3 hits within 4 Å were shown in Figure 26-27 and Table 17. The active binding site of  $\alpha$ -cobratotoxin is occupied between loop I and II in the presence of the hits and consequently the  $\alpha$ -cobratotoxin can not bind to the acetylcholine receptor.

**Table 15.** NCI diversity set identified from virtual screening

Chemical structure	NCI number (cpd no.)	MW	Rotatable bonds	Cluster (% lowest energy clustering)	E <sub>docking</sub> (kcal/mol)	K <sub>i</sub> <sup>a</sup> (nM)
	36387 (8)	696	4	4 (16)	-11.10	224
	42258 (10)	417	4	1 (65)	-11.23	54.2
	121865 (23)	412	5	1 (72)	-11.09	68.7
	134754 (27)	580	5	7 (44)	-10.20	289

<sup>a</sup>Dissociation constant or inhibition constant ( $K_i$ ) calculated by AutoDock program from the docking between the compound (NCI) and  $\alpha$ -cobratoxin template from 1YI5 (AChBP from *Lymnaea stagnalis*).

**Table 16.**  $K_d$  of 4 hits on AChBPs

NCI number (cpd no.)	AChBP <sup>a</sup>	Radioligand			
		<sup>3</sup> H] epibatidine		<sup>125</sup> I] $\alpha$ -bungarotoxin	
		$K_d$ (nM) <sup>b</sup>	BEI <sup>c</sup>	$K_d$ (nM) <sup>b</sup>	BEI <sup>c</sup>
36387 (8)	<i>Ls</i>	20.49	18.61	13.83	12.19
	<i>Ac</i>	78.96	76.23	241.70	238.28
	<i>Bt</i>	37.45	35.19		
42258 (10)	<i>Ls</i>	245.70	239.97	93.43	88.70
	<i>Ac</i>	1147.00	1139.66	2913.00	2904.69
	<i>Bt</i>	1890.00	1882.14		
121865 (23)	<i>Ls</i>	111.50	106.53	75.90	71.34
	<i>Ac</i>	16.26	13.32	36.63	32.83
	<i>Bt</i>	415.30	408.94		
134754 (27)	<i>Ls</i>	792.60	787.60	404.40	399.91
	<i>Ac</i>	2366.00	2360.18	4620.00	4613.68
	<i>Bt</i>	2629.00	2623.10		

<sup>a</sup>Acetylcholine binding protein (AChBP) from *Lymnaea stagnalis* (*Ls*), *Aplysia californica* (*Ac*) and *Bulinus truncatus* (*Bt*), <sup>b</sup> $K_d$  calculated from the binding between hit and AChBPs, <sup>c</sup>BEI = pKi / M.W. (kDa).

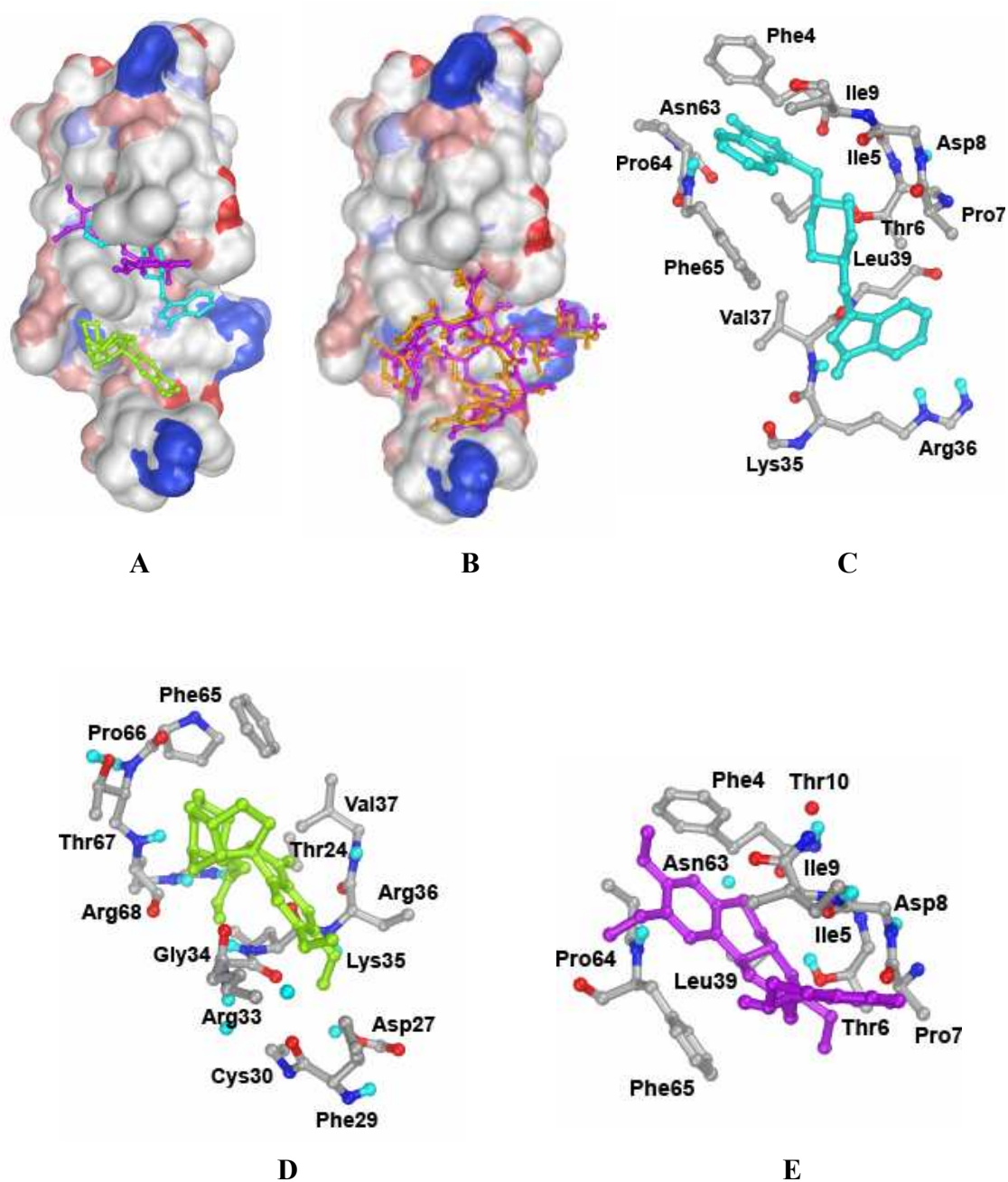


**Figure 26.** The dock orientations of NCI42258 (indigo blue), NCI121865 (light green) and NCI134754 (purple) (A) and crystallographic Ser182 – Tyr 192 of chain C from 1YI5 (purple) and control peptide (orange) (B). The amino acid residues of  $\alpha$ -cobratoxin interacted with NCI42258 (C), NCI121865 (D) and NCI134754 (E).

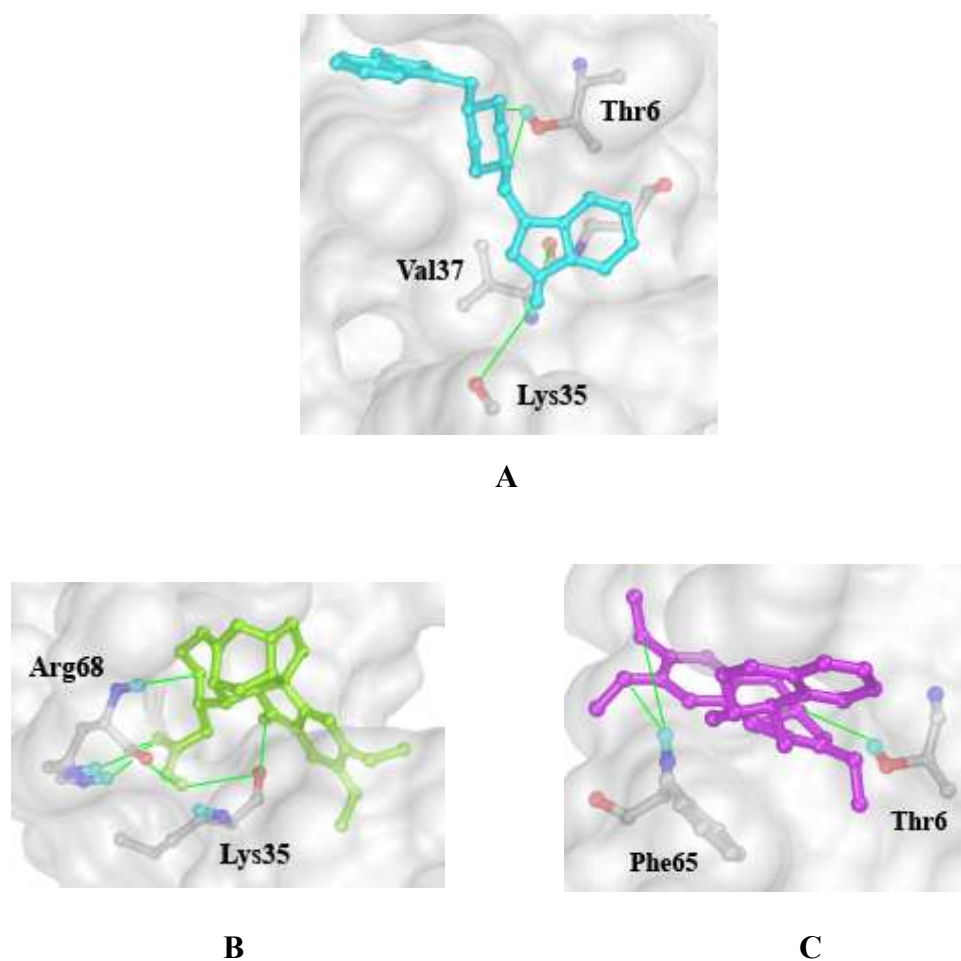


**Figure 27.** The amino acid residues of  $\alpha$ -cobratoxin interacted with NCI42258 (A), NCI121865 (B) and NCI134754 (C) with distance  $< 4 \text{ \AA}$ .

**Table 17.** Amino acid residues of  $\alpha$ -cobratoxin interacted with 3 hits

NCI42258 - Cbtx	Distance (Å)	NCI121865 - Cbtx	Distance (Å)	NCI134754 - Cbtx	Distance (Å)
N – HO (Thr6)	2.994	NH – OC (Lys35)	2.273	N – HO (Thr6)	3.474
N – HO (Thr6)	3.988	NH – OC (Lys35)	3.505	O – HN (Phe65)	3.589
NH – OC (Lys35)	3.967	O – HN (Arg68)	3.187	O – HN (Phe65)	3.743
NH – OC (Val37)	3.342	CO – HN (Arg68)	2.987		
		CO – HN (Arg68)	3.310		
		OH – OC (Arg68)	3.830		

## 2. Sodium Dodecyl Sulfate Polyacrylamide Gel Electrophoresis (SDS-PAGE)

### 2.1. Effect of Rediocides on $\alpha$ -Cobratoxin and AChBP

In order to substantiate the molecular mechanism derived from the docking experiments, SDS-PAGE was carried out to detect the binding between the  $\alpha$ -cobratoxin and rediocides. In this study, a 50:50 mixture of rediocides A and G was used as the 50:50 imitated the composition ratio of rediocides in the traditional regimen for the treatment of snake bites. The experiment was separated into 2 sections i.e. the study of interaction between rediocides and  $\alpha$ -cobratoxin as described in experimental section 2.1.1 and the binding between rediocides and  $\alpha$ -cobratoxin in the presence of AChBP as described in experimental section 2.1.2.

#### 2.1.1. Effect of Rediocides on $\alpha$ -Cobratoxin

SDS-PAGE was performed using 15% acrylamide gels and the rediocides (A & G) were dissolved in DMSO. The sample mixtures were loaded into each gel after being mixed with the sample buffer, boiled for 5 minutes and centrifuged. Electrophoresis was run at 150 volts until the marker's dye front reached to the end of the gels. Electrophoretic profiles of crude venom, a mixtures of the rediocides (A:G-50:50) and crude venom are shown in Figure 28. The protein of cobra venom (lane 2) showed two predominant bands at 10 kDa ( $\alpha$ -cobratoxin) and 14 kDa. The SDS-PAGE electrophoretograms demonstrated that the bands of  $\alpha$ -cobratoxin in crude venom decreased with the increase in concentration of the rediocides. When the crude venom was mixed with serial dilutions of rediocides (lane 3-6), the  $\alpha$ -cobratoxin band from the crude venom was neutralized by the rediocides. From the result, it can be explained that rediocides bound  $\alpha$ -cobratoxin and diminished the  $\alpha$ -cobratoxin band. However, it is also possible that venom proteins were denatured or degraded and precipitated before loading on the gel. In order to clarify this notion, the binding between rediocides and  $\alpha$ -cobratoxin in the presence of AChBP was studied in the next section.

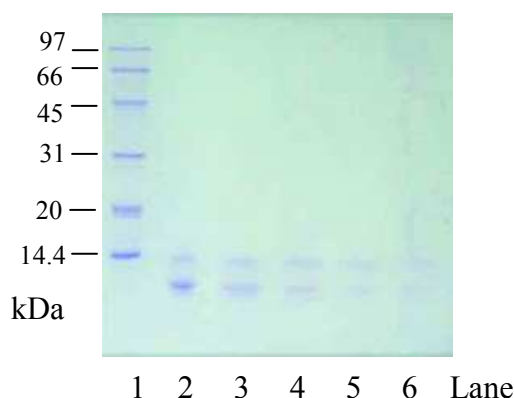


**Figure 28.** SDS-PAGE of the mixtures between crude venom and redioides (A & G). Mixture of crude venom (50  $\mu\text{g}$ ) and redioides with final concentrations of 2-fold dilution was applied to the gel, and electrophoresis was achieved with an electric current of 150 volts per gel. Lane 1: molecular weight marker, Lane 2: crude venom, Lanes 3-6: the mixtures between venom and redioides in the final concentrations of 7.5, 15, 30 and 60 mg/8  $\mu\text{l}$ , respectively.

### 2.1.2. Effect of Redioides on $\alpha$ -Cobratoxin and AChBP

In this experiment, the AChBP, a soluble extracellular binding domain of nAChRs, was added in order to study the binding between redioides and  $\alpha$ -cobratoxin. There are 3 AChBPs from snail, *Lymnaea stagnalis* (*Ls*), *Aplysia californica* (*Ac*) and *Bolunus truncatus* (*Bt*). The AChBP from *Ac* was selected in this experiment because AChBP from *Ac* was the most stable and only a small amount of monomer was degraded from the AChBP pentamer in the gel running condition. The conditions for running gel were modified to avoid the breakdown of the AChBP pentamer into monomers (25 kDa) by omitting the boiling of the sample before loading it to the gel. Electrophoresis was run at 100 volts until the marker's dye front reached to the end of the gels. Electrophoretic profiles of AChBP from *Ac*,  $\alpha$ -cobratoxin, and the redioides (A:G-50:50) are shown in Figure 29. The AChBP protein showed a single band of pentamer at 100 kDa (lane 6). In the presence of  $\alpha$ -cobratoxin (lane 5) or redioides (lane 2), the intensity of the AChBP pentamer band was increased substantially when compared with the band from AChBP alone (lane 6). The

pentamer band appeared in lane 2 is stronger in intensity than lane 6 because the redioides bound with AChBP and made AChBP more stable. The result in lane 5 was in the same manner where the  $\alpha$ -cobratoxin bound with AChBP and stabilized AChBP. In the presence of  $\alpha$ -cobratoxin and redioides (lane 4), the intensity of AChBP band (pentamer) decreased when compared with pentamer band in lane 5. It is because the redioides bound to the  $\alpha$ -cobratoxin and prevented  $\alpha$ -cobratoxin from binding with AChBP. The results from SDS-PAGE electrophoretograms demonstrated that both  $\alpha$ -cobratoxin and redioides bound with AChBP, as well as redioides bound to both  $\alpha$ -cobratoxin and AChBP.

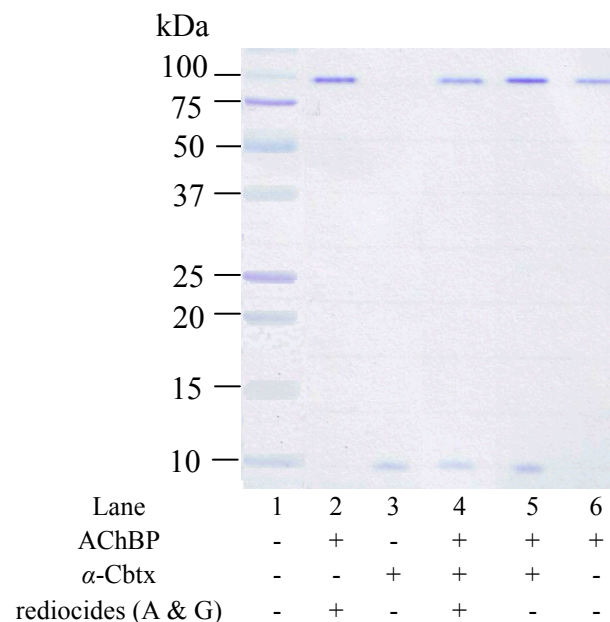


**Figure 29.** SDS-PAGE of AChBP from *Aplysia stagnalis* in the presence of  $\alpha$ -cobratoxin and redioides (A & G). Electrophoresis was achieved with an electric current of 100 volts. Lane 1: molecular weight marker, Lane 2: the mixture between AChBP and redioides (A & G), Lane 3:  $\alpha$ -cobratoxin, Lane 4: the mixture of AChBP,  $\alpha$ -cobratoxin and redioides (A & G), Lane 5: the mixture between AChBP and  $\alpha$ -cobratoxin, Lane 6: AChBP. Concentrations of AChBP,  $\alpha$ -cobratoxin and redioides (A & G) were 200  $\mu\text{g}/5 \mu\text{l}$ , 62.5  $\mu\text{g}/5 \mu\text{l}$  and 2 mg/5  $\mu\text{l}$ , respectively.

## **2.2. Effect of 3 Hits on $\alpha$ -Cobratoxin and AChBP**

### **2.2.1. Effect of 3 Hits on $\alpha$ -Cobratoxin**

SDS-PAGE was carried out to detect the binding between the 3 hits and  $\alpha$ -cobratoxin from crude venom. SDS-PAGE was performed with 20% acrylamide gels and the hits were dissolved in 0.1% Tween 80. The sample mixtures were loaded into each gel after mixed with the sample buffer, boiled for 5 minutes and centrifuged. Electrophoresis was performed at 100 volts until the marker's dye front reached to the end of the gels. Electrophoretic profiles of crude venom, 3 hits from NCI diversity set (NCI42258, NCI121865 and NCI134754) and the mixtures of hits and crude venom are shown in Figure 30. The protein of crude cobra venom showed three predominant bands at 10 kDa ( $\alpha$ -cobratoxin), 12 and 14 kDa (lane 2). This variation in the number of protein bands, 3 bands versus 2 bands in section 2.1.1 came from the different lot number of crude cobra venom. In the presence of NCI42258 or NCI134754 (lanes 3 and 5), the electrophoretic profile of  $\alpha$ -cobratoxin was different from  $\alpha$ -cobratoxin (lane 2), the bands appeared to be more diffuse and broaden. It is possible that NCI42258 and NCI134754 may alter some characteristic of the  $\alpha$ -cobratoxin. In the presence of NCI121865 (lane 4), the intensity of the  $\alpha$ -cobratoxin band significantly increased when compared with those from  $\alpha$ -cobratoxin (lane 2). From the result, it can be explained that NCI121865 bind to  $\alpha$ -cobratoxin and changed or destroyed the tertiary and quaternary structure of  $\alpha$ -cobratoxin protein leading to broaden band. For this reason, the binding of 3 hits and  $\alpha$ -cobratoxin was studied in the presence of AChBP (experimental section 2.2.2).

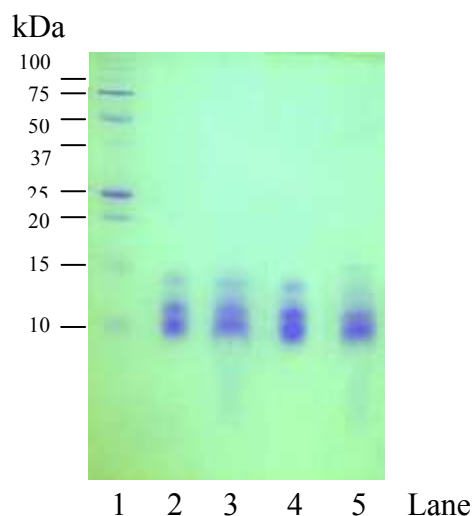


**Figure 30.** SDS-PAGE of the mixtures between crude venom and 3 hits. Electrophoresis was achieved with an electric current of 100 volts per gel. Lane 1: molecular weight marker; Lane 2: crude venom (50  $\mu\text{g}/5 \mu\text{l}$ ), Lane 3: NCI42258 (50  $\mu\text{g}/5 \mu\text{l}$ ) and venom, Lane 4: NCI121865 (50  $\mu\text{g}/5 \mu\text{l}$ ) and venom, Lane 5: NCI134754 (50  $\mu\text{g}/5 \mu\text{l}$ ) and venom.

### 2.2.2. Effect of 3 Hits on $\alpha$ -Cobratoxin and AChBP

The AChBP was included in this experiment for studying the effect of 3 hits on the binding of  $\alpha$ -cobratoxin on AChBP or the anti-venom effect. SDS-PAGE was performed using 20% acrylamide gels and the hits were dissolved in 0.1% Tween 80. The conditions for running gel were modified to avoid the breakdown of the AChBP pentamer into monomers by omitting the sample boiling before loading. Electrophoretic profiles of AChBP from *Aplysia stagnalis*,  $\alpha$ -cobratoxin, mixtures of hits and these two proteins were shown in Figure 31. The proteins of AChBP showed a predominant band at 100 kDa (pentamer) and a small band of monomer at 25 kDa. Lanes 8-10 were the bands of AChBP in the presence of hits (NCI42258 or NCI121865 or NCI134754), the AChBP pentamer bands in lanes 8-10 were not increased in the intensity but also expanded and shift up. The monomer band only in lanes 4 and 8 decreased almost completely when compared with those of AChBP in lane 2. The increase in intensity and the shift up of the pentamer bands resulted from the binding between 3 hits and AChBP which led to the reduction in monomer

breaking. The decrease in intensity of monomer band (25 kDa) in lane 8 emphasized that NCI42258 bound with AChBP and stabilized it from breaking. Lanes 4-6 were the lanes of  $\alpha$ -cobratoxin and AChBP in the presence of 3 hits, the intensity of the AChBP pentamer band in lanes 4-6 increased while AChBP monomer band in lane 4 decreased when compared with those from AChBP (lane 2). The  $\alpha$ -cobratoxin bands in lanes 4-6 shifted up when compared with  $\alpha$ -cobratoxin band (lane 7), the result confirmed that 3 hits bind the  $\alpha$ -cobratoxin and prevented the toxin to bind with the AChBP. The changes in the profile of  $\alpha$ -cobratoxin band i.e. band broadening, shifting and the increase in intensity demonstrated the interaction between hits and  $\alpha$ -cobratoxin. The stronger in the diffuse and shift of pentamer bands in lanes 4-6 comparing to the pentamer band of AChBP in lane 2 showed that both hits also bound with AChBP. The result from the pentamer band in lane 3 was in the same manner where the  $\alpha$ -cobratoxin bound with AChBP and made AChBP more stable. All 3 hits bound to the  $\alpha$ -cobratoxin and prevented  $\alpha$ -cobratoxin from binding with AChBP. It can be concluded from SDS-PAGE result that 3 hits (NCI42258, NCI121865 and NCI134754) bound both  $\alpha$ -cobratoxin and AChBP.



**Figure 31.** SDS-PAGE of  $\alpha$ -cobratoxin and AChBP from *Aplysia stagnalis* in the presence of 3 hits. Electrophoresis was achieved with an electric current of 100 volts. Lane 1: molecular weight marker, Lane 2: the mixture between AChBP and  $\alpha$ -cobratoxin, Lane 3: the mixture of AChBP,  $\alpha$ -cobratoxin and NCI42258, Lane 4: the mixture of AChBP,  $\alpha$ -cobratoxin and NCI121865, Lane 5: the mixture of AChBP,  $\alpha$ -cobratoxin and NCI134754, Lane 6: the mixture of AChBP and  $\alpha$ -cobratoxin, Lane 7:  $\alpha$ -cobratoxin, Lane 8: the mixture of AChBP and NCI42258, Lane 9: the mixture of AChBP and NCI121865, Lane 10: the mixture of AChBP and NCI134754. Concentrations for AChBP,  $\alpha$ -cobratoxin, rediocides were 200  $\mu\text{g}/5 \mu\text{l}$ , 62.5  $\mu\text{g}/5 \mu\text{l}$  and 50  $\mu\text{g}/5 \mu\text{l}$ , respectively. The blue letters are the quantity of the band in percentage using Syngene program.

### C. *In Vivo* Experiment

An *in vivo* test was carried out to investigate the effect of redioides and the three hits from NCI diversity against  $\alpha$ -cobratoxin. The median lethal dose (LD<sub>50</sub>) of  $\alpha$ -cobratoxin, the protection activity and the anti-cobratoxin were determined.

#### 1. Determination of Median Lethal Dose

LD<sub>50</sub> is defined as the least amount of  $\alpha$ -cobratoxin which injected intramuscularly through the leg muscle of the mice, resulted in the death of half amount of mice within 24 h. The plot between % death and the concentration of  $\alpha$ -cobratoxin was shown in Figure 32. A LD<sub>50</sub> of  $\alpha$ -cobratoxin was found to be 0.175 mg/kg (i.m.). Since 100% mice were death within 30 minutes at 3LD<sub>50</sub> dose (0.425 mg/kg), the dose of  $\alpha$ -cobratoxin in the experiment was 3LD<sub>50</sub> instead of 4LD<sub>50</sub>.

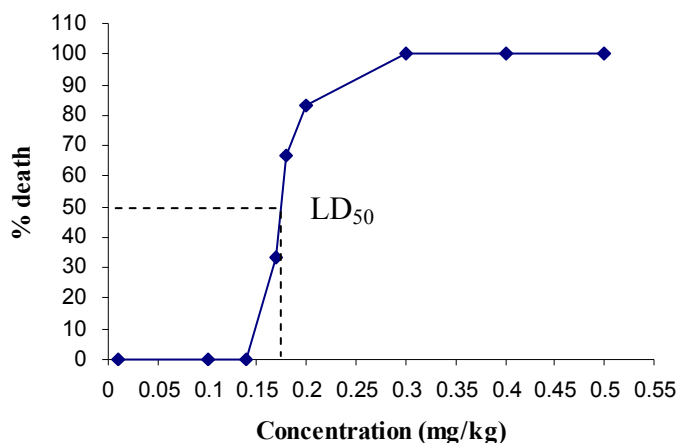


Figure 32. LD<sub>50</sub> of  $\alpha$ -cobratoxin (n=6).

#### 2. Effect of Redioides and Three Hits on Mice

##### 2.1 The Protection Activity

In this protocol, redioides or hits were tested for their protecting action. Redioides or hits were injected to the mice before the injection of  $\alpha$ -cobratoxin. The sample solution, in 0.05 ml of 0.3% Tween 80, were prepared in varying concentrations. Each dose was injected to the mice intravenously (i.v.) at tail vein. The control group was injected with only the vehicle (0.3% Tween 80). The acute toxicity test of redioides was determined prior to the test for protecting action. The

result showed that the injection of rediocides (50 mg/kg, i.v.) resulted in 100% death within 24 hours and only 50% death at 1 mg/kg dose (Table 18). The maximum concentration of rediocides without acute toxicity was 0.5 mg/kg (i.v). All mice were alive at the maximum testing dose. The survived mice treated with 1 mg/kg showed the sign of toxicity at the tail vein after 24 hours (Figure 33).

**Table 18.** Toxicity test of rediocides and 3 hits (n=6)

<b>Group</b>	<b>Dose (i.v) (mg/kg)</b>	<b>% death</b>
Rediocides	50	100
	1	50
	0.5	0
	0.15	0
42258	10	0
	5	0
	1	0
121865	10	0
	5	0
	1	0
134754	10	0
	5	0
	1	0



**Figure 33.** Toxicity of redioides (A & G). The mouse was injected with redioides (A) and NCI134754 (B).

For protection activity,  $\alpha$ -cobratoxin was injected before the injection of redioides (A & G) or 3 hits from NCI diversity (NCI42258, NCI121865 and NCI134754). The testing dose of redioides (A & G) was 0.5 mg/kg, i.v. and 1, 5 and 10 mg/kg for 3 hits. When 3LD<sub>50</sub> of  $\alpha$ -cobratoxin was injected after a redioides injection (0.5 mg/kg, i.v.), the survival time was prolonged significantly (Table 19). The survival time of the control group was  $27.1 \pm 2.8$  minutes while the survival time for redioides (A & G) was  $45.2 \pm 9.7$  minutes. The redioides was the most potent for protecting mice from the  $\alpha$ -cobratoxin.

In the same way as redioides (A & G), the hits solutions, in 0.05 ml of 0.3% Tween 80, were injected to the mice intravenously (i.v.) at tail vein. The control group was injected with only the vehicle, 0.3% Tween 80. When the hits were injected (i.v.) 30 minutes before  $\alpha$ -cobratoxin (3LD<sub>50</sub>, i.m.), the survival time increased significantly. The dixon's Q test was used to discard the outliers from the data. The  $Q_{\text{exp}}$  values of the highest numbers ( $> 24$  h and 111 minutes) at 5 mg/kg (NCI42298 and NCI121865) were higher than  $Q_{\text{crit}}$  (CL: 95%). Therefore, these two numbers were discarded as outliers. The result showed that all hits can prolong the survival time of the mice (Table 19). The survival time for control was  $27.1 \pm 2.8$  minutes while the survival time for NCI42258 and NCI121865 at 5 mg/kg dose were double,  $49.6 \pm 9.3$  minutes and  $50.6 \pm 5.0$  minutes, respectively. When the dose of hits were increased to 10 mg/kg, the survival times of the hit treated groups did not increase

further. The survival time of NCI42258, NCI121865 and NCI134754 at 10 mg/kg were  $43.2 \pm 7.6$ ,  $38.3 \pm 7.5$  and  $41.8 \pm 7.3$  minutes, respectively. The 5 mg/kg dose was the optimal dose and was chosen for the antitoxin activity.

**Table 19.** Protective effect of redioides (A & G) and 3 hits against  $\alpha$ -cobratoxin<sup>a</sup>

Group	Dose (i.v.) (mg/kg)	Survival time (min)	Average (Mean $\pm$ SD)
Control		21, 24, 25, 26, 27, 27, 28, 28, 29, 29, 30, 31	$27.1 \pm 2.8$
Redioides	0.5	33, 35, 47, 48, 49, 59	$45.2 \pm 9.7^*$
42258	10	34, 39, 40, 41, 52, 53	$43.2 \pm 7.6^*$
	5	37, 44, 50, 58, 59, >24 h <sup>b</sup>	$49.6 \pm 9.3^*$
	1	35, 37, 39, 45, 49, 50	$42.5 \pm 6.4^*$
121865	10	30, 32, 35, 40, 43, 50	$38.3 \pm 7.5^*$
	5	44, 47, 52, 54, 56, 111 <sup>b</sup>	$50.6 \pm 5.0^*$
	1	35, 36, 38, 51, 52, 54	$44.3 \pm 8.9^*$
134754	10	37, 37, 38, 40, 43, 56	$41.8 \pm 7.3^*$
	5	31, 37, 47, 48, 51, 53	$44.5 \pm 8.6^*$
	1	40, 40, 42, 44, 53, 60	$46.5 \pm 8.2^*$

<sup>a</sup>Hits was injected (i.v.) 30 minutes before injection of  $\alpha$ -cobratoxin ( $3LD_{50}$ ) (i.m.), n=6, <sup>b</sup>The outliers (Dixon's Q-test), \*p < 0.05.

## 2.2 The Antitoxin Activity

In this protocol, redioides or hits were tested for the antitoxin action by injected after the injection of  $\alpha$ -cobratoxin.  $3LD_{50}$  of  $\alpha$ -cobratoxin in 0.1 ml of sterile water was injected (i.m.) before the injection of test compounds in 0.05 ml of 0.3% Tween 80 (i.v.). The survival time and number of deaths occurring within 24 hours

was recorded. Alpha-cobratoxin was injected before the injection of redioides and resulted in the death of all the mice within 46 minutes, which was not significantly different from the control (Table 20). The result showed that the redioides at 0.5 mg/kg could not protect the mice from the  $\alpha$ -cobratoxin when they were injected after the  $\alpha$ -cobratoxin. In spite of better affinity than  $\alpha$ -cobratoxin (lower docking energy), the redioides can not prolong the survival time when injected following the  $\alpha$ -cobratoxin. It is because the better accessibility of  $\alpha$ -cobratoxin to the AChBP based on the higher of % member in the cluster than those of redioides. The docking energy between  $\alpha$ -cobratoxin and the control peptide from AChBP was  $-12.20$  kcal/mol (with 100% member in the cluster) and the docking energy between  $\alpha$ -cobratoxin and the redioides (A & G) was  $-14.17$  kcal/mol (with 40% member in the cluster) and  $-14.14$  kcal/mol (with 38% member in the cluster), respectively.

**Table 20.** Anti-cobratoxin of redioides against  $\alpha$ -cobratoxin

Group	Dose (i.v.)	Survival time (min)	Average (Mean $\pm$ SD)
Control	-	22, 23, 23, 24, 26, 32	25.0 $\pm$ 3.7
Redioides (A & G)	0.5 mg/kg	25, 26, 27, 31, 32, 46	31.2 $\pm$ 7.8

<sup>a</sup>Redioides was injected (i.v.) immediately after injection of  $\alpha$ -cobratoxin (3LD<sub>50</sub>) (i.m.), n=6.

Two hits (NCI121865 and NCI134754) at 5 mg/kg were able to protect the mice from the  $\alpha$ -cobratoxin when they were injected after the  $\alpha$ -cobratoxin (Table 21). The survival times were  $45.2 \pm 5.2$  minutes and  $53.7 \pm 15.6$  minutes for NCI121865 and NCI134754, respectively. The NCI42258 at 5 mg/kg can prolong the survival time for 5 minutes but the prolonging time was not significant in statistic. Three hits can prolong the survival time of the mice if injected 30 minutes before injection with  $\alpha$ -cobratoxin, but only NCI121865 and NCI134754 can prolong the survival time of the mice when  $\alpha$ -cobratoxin was injected before injection of hits. NCI121865 and NCI134754 are the potential candidates as they have the antitoxin activity. The results from *in vivo* experiment supported the *in vitro* and *in silico* results.

**Table 21.** Anti-cobratotoxin of 3 hits against  $\alpha$ -cobratotoxin<sup>a</sup>

Group	Survival time (min)	Average (Mean $\pm$ SD)
Control	28, 31, 37, 38, 42, 45	36.8 $\pm$ 6.4
42258	34, 34, 36, 42, 46, 56	41.3 $\pm$ 8.7
121865	38, 41, 44, 48, 48, 52	45.2 $\pm$ 5.2*
134754	40, 41, 45, 55, 60, 81	53.7 $\pm$ 5.6*

<sup>a</sup>Hits at 5 mg/kg was injected (i.v.) immediately after injection of  $\alpha$ -cobratotoxin (3LD<sub>50</sub>) (i.m.), n=6, \*p < 0.05.

#### D. Summary

Molecular docking was employed to investigate the binding mode of redioides (A & G) and 1990 compounds in NCI diversity set were screened for its binding capability against  $\alpha$ -cobratotoxin. This procedure is computationally intensive for analyzing a large database but provides the most detailed basis for determining which compounds are likely to be potent ligands. Thirty nine hits from virtual screening and redioides (A & G) were further tested for its binding. It was found that 4 hits (NCI36387, NCI42258, NCI121865 and NCI134754) showed the low fraction of [<sup>3</sup>H] epibatidine bind to AChBPs. Four hits competitively displace on antagonist (<sup>125</sup>I  $\alpha$ -bungarotoxin) and the agonist (<sup>3</sup>H epibatidine) from their mutually exclusive binding sites on *Lymnaea*, *Aplysia* and *Bulinus* AChBPs with the concentration from micromolar to nanomolar. One of the hits (NCI36387) is *d*-tubocurarine, the well known neuromuscular blocker. NCI121865 showed good competitive activity in displacing the binding of [<sup>3</sup>H] epibatidine or [<sup>125</sup>I]  $\alpha$ -bungarotoxin to all types of AChBPs. The effect of three hits (NCI42258, NCI121865 and NCI134754) and redioides (A & G) on  $\alpha$ -cobratotoxin and AChBP were also determined by SDS-PAGE. Redioides bound to  $\alpha$ -cobratotoxin in crude venom and diminished the  $\alpha$ -cobratotoxin band. NCI121865 also bound  $\alpha$ -cobratotoxin in crude venom but increased the  $\alpha$ -

cobratoin band. NCI42258 and NCI134754 changed some characteristic of the  $\alpha$ -cobratoin because the  $\alpha$ -cobratoin band appeared to be broaden.

When redioides are added to the mixture of  $\alpha$ -cobratoin and AChBP, the intensity of AChBP pentamer band decreased when compared with the pentamer band of AChBP without toxin. It is because the redioides bound to the  $\alpha$ -cobratoin and prevented  $\alpha$ -cobratoin from binding with AChBP. Both  $\alpha$ -cobratoin and redioides bound with AChBP. In the presence of 3 hits in  $\alpha$ -cobratoin and AChBP, the intensity of both AChBP pentamer band and the  $\alpha$ -cobratoin band increased. The results demonstrated that three hits (NCI42258, NCI121865 and NCI134754) bound both  $\alpha$ -cobratoin and AChBP.

Three hits (NCI42258, NCI121865 and NCI134754) and redioides (A & G) were tested in the *in vivo* experiment. All hits and redioides (A & G) can prolong the survival times of the mice if injected 30 minutes before  $\alpha$ -cobratoin injection. Only NCI121865 and NCI134754 can prolong the survival time if injected immediately after  $\alpha$ -cobratoin injection. The result from *in vitro* SDS-PAGE and binding assay as well as *in vivo* tests were in agreement with the *in silico* results. In clinical applications, NCI121865 (compound 23) and NCI134754 (compound 27) would be very useful potential leads for the treatment of snakebite victims.

## CHAPTER V

### CONCLUSION

In search of an antidote of cobra venom by preventing the  $\alpha$ -cobratoxin from binding to the nicotinic acetylcholine receptor, a comprehensive study was carried out involving *in silico* docking, virtual screening, and *in vivo* animal tests. First, molecular docking was employed to investigate the binding mode of redioides (A & G) to  $\alpha$ -cobratoxin by using the AutoDock program version 3.0.5. This study aimed to find the mechanism of action of redioides against cobra venom at the molecular level. The redioides and hits from virtual screening were investigated for anti-cobratoxin action both *in vitro* and *in vivo*. The performed studies are summarized below.

#### 1. Molecular Modeling (*In Silico*) Experiment

(i) A model of  $\alpha$ -cobratoxin was constructed and a control peptide was used to validate it by re-docking. The validation result with RMSD less than 2 Å indicated that the prepared  $\alpha$ -cobratoxin template was a good model for docking studies of redioides binding modes and the diversity set.

(ii) The docking study on redioides and  $\alpha$ -cobratoxin interaction was performed to investigate the binding modes of the redioides. The redioides were found to bind to the same location that the  $\alpha$ -cobratoxin bound to the nicotinic acetylcholine receptor. The active binding site of  $\alpha$ -cobratoxin is occupied in the presence of redioides and consequently the  $\alpha$ -cobratoxin can not bind to the acetylcholine receptor. Thus, the *in silico* experiment revealed the detoxification mechanism of cobra venom at the molecular level.

(iii) Molecular docking was used in a virtual screening to investigate the binding of over 1990 compounds to  $\alpha$ -cobratoxin. There were 77 compounds that matched the three  $\alpha$ -cobratoxin templates and only nineteen of those compounds had “drug like” properties (molecular weight < 500, Log P < 5 and number of rotatable

bonds < 5). For experimental testing, 20 more compounds were included for *in vitro* evaluation on the basis of low docking energy and high %member in the cluster of lowest energy.

## 2. Radioligand Competition Assay

(i) A radioligand assay was initially run to screen the 39 hits and redioides (A & G) prior to the determination of  $K_d$ . Four hits (NCI36387, NCI42258, NCI121865 and NCI134754) showed a low amount of fraction of [ $^3\text{H}$ ] epibatidine bind to AChBPs. The four hits either bind to the agonist [ $^3\text{H}$ ] epibatidine or the AChBP which led to the reduction of radioligand binding to AChBP on the bead.

(ii) The four hits were found to competitively displace antagonist ( $^{125}\text{I}$   $\alpha$ -bungarotoxin) and the agonist ( $^3\text{H}$  epibatidine) from their mutually exclusive binding sites on AChBPs with concentrations from micromolar to nanomolar.

## 3. Sodium Dodesyl Sulfate Gel Electrophoresis (SDS-PAGE)

SDS-PAGE was carried out to detect the binding between the  $\alpha$ -cobratoxin and redioides and hits from virtual screening.

(i) When the crude venom was mixed with serial dilutions of redioides, the  $\alpha$ -cobratoxin band from the crude venom was neutralized by the redioides. All three hits bound to the  $\alpha$ -cobratoxin and changed the profile of  $\alpha$ -cobratoxin band to be broaden.

(ii) The acetylcholine binding protein (AChBP) was included for studying the effect on the binding of  $\alpha$ -cobratoxin on AChBP or the anti-venom effect. The redioides or  $\alpha$ -cobratoxin bound with AChBP and made AChBP more stable. The redioides were found to bind both  $\alpha$ -cobratoxin and AChBP which prevent  $\alpha$ -cobratoxin from binding with AChBP. In the same way, all three hits bound to the  $\alpha$ -cobratoxin and AChBP preventing  $\alpha$ -cobratoxin from binding with AChBP.

## 4. *In Vivo* Experiment

An *in vivo* test was carried out to investigate the effect of redioides and the three hits from NCI diversity against  $\alpha$ -cobratoxin.

(i) Rediociques (A & G) and the three hits were tested for their protecting action. Rediociques or hits were injected to the mice before the injection of  $\alpha$ -cobratoxin. When 3LD<sub>50</sub> of  $\alpha$ -cobratoxin was injected in the rediociques (0.5 mg/kg, i.v.) or 3 hits treated groups (0.5 mg/kg, i.v.), the survival time was prolonged significantly. Rediociques and the three hits prolonged the survival time of the mice if injected 30 minutes before injection with  $\alpha$ -cobratoxin.

(ii) Rediociques (A & G) and the three hits were tested for antitoxin action. Rediociques or hits were injected after the injection of  $\alpha$ -cobratoxin (3LD<sub>50</sub> dose) and the survival time and number of deaths occurring within 24 hours was recorded. In spite of the better affinity for  $\alpha$ -cobratoxin than the three hits, the rediociques did not prolong the survival time significantly when injected following the  $\alpha$ -cobratoxin. Only NCI121865 and NCI134754 prolonged the survival time of the mice significantly when  $\alpha$ -cobratoxin was injected before injection of hits. NCI121865 and NCI134754 are the best potential candidates as they have both protection activity and antitoxin activity.

*In silico* screening can help to identify the most promising leads for anti-cobratoxin. The results from *in vitro* binding assay and SDS-PAGE as well as *in vivo* tests substantiate the *in silico* result. NCI121865 and NCI134754 serve as novel templates/scaffolds for development of more potent and specific anticobratoxin. In clinical applications, NCI121865 and NCI134754 would be very useful potential leads for the treatment of snakebite victims.

## REFERENCES

1. Raweerith R, Ratanabanangkoon K. Immunochemical and biochemical comparisons of equine monovalent and polyvalent snake venoms. *Toxicon* 2005; 45: 369-375.
2. Dong LV, Khoo HE, Quyen LK, Gopalakrishnakone P. Optimal immunoassay for snake venom detection. *Biosensors Bioelectron* 2004; 19: 1285-94.
3. Bernheim A, Lorenzetti E, Licht A, Markwalder K, Schneemann M. Three cases of severe neurotoxicity after cobra bite (*Naja kaouthia*). *Swiss Med Wkly* 2001; 31: 227-228.
4. Chanhome L, Wongtongkam N, Khoo O, Pakmanee N, Omari-Satoh T, Sitprija V. Genus specific neutralization of *Bungarus* snake venoms by Thai red cross banded krait antivenom. *J Nat Toxins* 1999; 8: 135-140.
5. Byeon W, Weisblum B. Affinity adsorbent based on combinatorial phage display peptides that bind  $\alpha$ -cobratoxin. *J Chromatogr B* 2004; 805: 361-363.
6. Ogay Y, Rzhnevsky DI, Murashev AN, Tsetlin VI, Utkin YN. Weak neurotoxin from *Naja kaouthia* cobra venom affects haemodynamic regulation by acting on acetylcholine receptors. *Toxicon* 2005; 45: 93-99.
7. Doley R, King GF, Mukherjee AK. Differential hydrolysis of erythrocyte and mitochondrial membrane phospholipids by two phospholipase A<sub>2</sub> isoenzymes (NK-PLA<sub>2</sub>-I and NK-PLA<sub>2</sub>-II) from the venom of the Indian monocled cobra *Naja kaouthia*. *Arch Biochem Biophys* 2004; 425: 1-13.
8. Walkinshaw MD, Saenger W, Maelicke A. Three-dimensional structure of the "long" neurotoxin from cobra venom. *Proc Natl Acad Sci USA* 1980; 77: 2400-2404.
9. TseTlin V. Snake venom  $\alpha$ -neurotoxins and other 'three-finger' proteins. *Eur J Biochem* 1999; 264: 281-286.

10. Brejc K, van Dijk WJ, Klaassen RV, Schuurmans M, van Der Oost J, Smith AB, Sixma TK. Crystal structure of an Ach-binding protein reveals the ligand binding domain of nicotinic receptors. *Nature* 2001; 411: 269-276.
11. Smit B, Syed NI, Schaap D, van Minnen J, Kits KS, Lodder H, van Der Schors RC, van Elk R, Sorgedragger B, Brejc K, Sixma TK, Geraerts WP. Acetylcholine Binding Protein (AChBP), a novel glia-derived acetylcholine-receptor-like modulator of cholinergic synaptic transmission. *Nature* 2001; 411: 261-268.
12. Zeng H, Hawrot E. NMR-based binding screen and structural analysis of the complex formed between  $\alpha$ -cobratoxin and an 18-mer cognate peptide derived from the  $\alpha 1$  subunit of the nicotinic acetylcholine receptor from *Torpedo californica*. *J Biol Chem* 2002; 277: 37439-37445.
13. Bourne Y, Talley TT, Hansen SB, Taylor P, Marchot P. Crystal structure of a Cbtx-AChBP complex reveals essential interactions between snake alpha-neurotoxin and nicotinic receptors. *EMBO J* 2005; 24: 1512-1522.
14. Atassi MZ. Postsynaptic-neurotoxin-acetylcholine receptor interaction and the binding sites on the two molecules. In AT Tu (ed). *Handbook of natural toxins* Volume 5. New York: Marcel Dekker Inc., 1991, p. 53-83.
15. Celie PH, Klassen RV, van Rossum-Fikkert SE, van Elk R, van Nierop P, Smith AB, Sixma TK. Crystal structure of acetylcholine-binding protein from *Bolinus truncatus* reveals the conserved structural scaffold and sites of variation in nicotinic acetylcholine receptors. *J Biol Chem* 2005; 280: 26457-26466.
16. Hansen SB, Talley TT, Radic Z, Taylor P. Structural and ligand recognition characteristics of an acetylcholine-binding protein from *Aplysia californica*. *J Biol Chem* 2004; 279: 24197-24202.
17. [http://samui.ac.th/herbs/snake/snake\\_herbs.htm](http://samui.ac.th/herbs/snake/snake_herbs.htm)
18. Tempeam A, Thasana N, Thavornkitcharat A, et al. *In vitro* cytotoxicity of some Thai medicinal plants and daphnane diterpenoid from *Trigonostemon redioides*. *Mahidol University Journal of Pharmaceutical Science* 2002; 29(3-4): 25-31.

19. Kanchanapoom T, Kasai R, Chumsri P, Kraisintu K, Yamasaki K. Lotthanongine, an unprecedented flavonoidal indole alkaloid from the root of Thai medicinal plant, *Trigonostemon redioides*. *Tet Lett* 2002; 43: 2941-2943.
20. Jarasuriya H, Zink DL, Borris RP, Nanakorn W, Beck HT, Balick MJ, Goetz MA, Gregory L, Shoop WL, Singh SB. Redioides B–E, potent insecticides from *Trigonostemon redioides*. *J Nat Prod* 2004; 67: 228-231.
21. Jarasuriya H, Zink DL, Singh SB, Borris RP, Nanakorn W, Beck HT, Balick MJ, Goetz MA, Slayton L, Gregory L, Zakson-Aiken M, Shoop W, Singh SB. Structure and stereochemistry of redioides A, a highly modified daphnane from *Trigonostemon redioides* exhibiting potent insecticidal activity. *J Am Chem Soc* 2000; 122: 4998-4999.
22. Waszkowycz B, Perkins TDJ, Sykes RA, Li J. Large-scale virtual screening for discovering leads in the postgenomic era. *IBM Systems J* 2001; 40: 360-376.
23. ไพบุลย์จินตกุล และลาวัลย์ จันทร์โฮม. ภูมิพืชในประเทศไทย. กรุงเทพฯ: ประชาชน, 2539.
24. Wingert WA, Wainschel J. Diagnosis and management of envenomation by poisonous snakes. *South Med J* 1975; 68: 1015-1026.
25. Lim BL. Venomous snakes of Southeast Asia. *Southeast Asian J Trop Med Pub Health* 1971; 2: 56-64.
26. <http://p30city.net/showthread.php?t=1252>
27. Wasserman GS. Wound care of spider and snake envenomations. *Ann Emerg Med* 1988; 17: 1331-1335.
28. Forks TP. Evaluation and treatment of poisonous snakebites. *Am Fam Physician* 1994; 50: 123-130.
29. Karlsson E. Chemistry of protein toxins in snake venom. In CY Lee (ed). *Snake Venoms*. Germany: Springer-Verlag Berlin Heidelberg, 1979.
30. Underwood G. Classification and distribution of venomous snakes in the world. In CY Lee (ed). *Snake Venoms*. Germany: Springer-Verlag Berlin Heidelberg, 1979.

31. บุญเยี่ยม ทูมวิภาต, รองศาสตราจารย์ และวิโรจน์ นุตพันธุ์, นาวาอากาศโท. การรักษาผู้ป่วยถูกงูกัดและงูพิษในประเทศไทย (พิมพ์ครั้งที่ 1). กรุงเทพฯ: พิมพ์แสด, 2525.
32. Ganthavorn S. Toxicities of Thailand snake venoms and neutralization capacity of antivenin. *Toxicon* 1969; 7: 239-241.
33. Viravan C, Looareesuwan S, Kosakarn W, Wuthiekanum V, McCarthy CJ, Stimson AF, et al. A national hospital-based survey of snakes responsible for bites in Thailand. *Trans R Soc Trop Med Hyg* 1992; 86: 100-106.
34. Warrell D. The clinical management of snake bites in the snake bites in Southeast Asian region. *Sup South Asian J Trop Med Pub Health* 1999; 30: 22.
35. Viravan C, Veeravat U, Warrell MJ, Theakston RDG, Warrell DA. Elisa confirmation of acute and past envenoming by the monocellate Thai cobra (*Naja kaouthia*). *Am J Trop Med Hyg* 1986; 35: 173-181.
36. Wüster W, Thorpe RS. Asiatic cobras: Systematics and snakebite. *Experientia* 1991; 47: 205-209.
37. Wüster W. Taxonomic changes and toxicology: Systematics revisions of the asiatic cobras (*Naja naja* species complex). *Toxicon* 1996; 34: 399-406.
38. Wüster W, Thorpe RS. *Naja siamensis*, a cryptic species of venomous snake revealed by mtDNA sequencing. *Experientia* 1994; 50: 75-79.
39. Smith II TA, Figge HL. Treatment of snakebite poisoning. *AJHP* 1991; 48: 2190-2196.
40. Karlsson E. Enzymes in snake venom. In CY Lee (ed). *Snake Venoms*. Germany: Springer-Verlag Berlin Heidelberg, 1979.
41. Bjaranson JB, Fox JW. Hemorrhagic metalloproteinases from snake venoms. *Pharmacology & Therapeutics* 1994; 62: 325-372.
42. Markland FS. Snake venoms and the hemostatic system. *Toxicon* 1998; 36: 1749-1800.
43. Markland FS. Snake venom. *Drugs* 1997; 54 suppl: 1-10.
44. Tu AT. *Chemistry and molecular biology*. New York: John Wiley & Sons Inc., 1977.

45. Gold GS, Wingert WA. Snake venom poisoning in the United States: A review of therapeutic practice. *South Med J* 1994; 87: 579-589.
46. Kini RM. Structure-function relationships and mechanism of anticoagulant phospholipase A<sub>2</sub> enzymes from snake venoms. *Toxicon* 2005; 45: 1147-1161.
47. Serrano SMT, Maroun RC. Snake venom serine proteinases: sequence homology vs. substrate specificity, a paradox to be solved. *Toxicon* 2005; 45: 1115-1132.
48. Hawgood B, Bon C. Snake venom presynaptic toxins. In At tu (ed.). *Handbook of natural toxins Volumn 5*. New York: Marcel Dekker Inc., 1991.
49. Atassi MZ. Postsynaptic-neurotoxin-acetylcholine receptor interaction and the binding sites on the two molecules. In AT Tu (ed.). *Handbook of natural toxins Volumn 5*. New York: Marcel Dekker Inc., 1991.
50. Meng QX, Wang WY, Lu QM, Jim Y, Wei JF, Zhu SW, Xiong YL. A novel short neurotoxin, cobrotoxin c, from monocellate cobra (*Naja kaouthia*) venom: isolation and purification, primary and secondary structure determination, and trtiary structure modeling. *Comp Biochem Physiol C Toxicol Pharmacol* 2002; 132: 113-121.
51. Cheng Y, Meng Q, Wang W, Wang J. Structure-function relationship of three neurotoxins from the venom of *Naja kaouthia*: a comparison between the NMR-derived structure of NT2 with its omologues, NT1 and NT3. *Biochim Biophys Acta* 2002; 1594: 351-363.
52. Karlsson E, Eaker D. Isolation ot the principal neurotoxins of *Naja naja* subspecies from the asian mainland. *Toxicon* 1972; 10: 217-225.
53. Harvey Al. Cardiotoxins from cobra venoms. In At Tu (ed.). *Handbook of natural toxins Volumn 5*. New York: Marcel Dekker Inc., 1991.
54. Vogel C-W. Cobra venom factor: the complement-activating protein of cobra. In At Tu (ed.). *Handbook of natural toxins and ampibian venoms Volumn 5*. New York: Marcel Dekker Inc., 1991, p. 147-188.
55. [http://www.mic.hawaii.edu/dev\\_tech/biology/CobraVenom.html](http://www.mic.hawaii.edu/dev_tech/biology/CobraVenom.html)

56. Hensley P, O'Keefe MC, Spangler CJ, et al. The effects of metal ions and temperature on the interaction of cobra venom factor and human complement factor B. *J Biol Chem* 1986; 261(24): 11038-11044.
57. DiScipio RG, Smith CA, Muller-Eberhard HJ, et al. The activation of human complement component C5 by fluid phase C5 convertase. *J Biol Chem* 1983; 258(17): 10629-10636.
58. Qian-Yun S, Qiu-Min L, Wan-Yu W, et al. A highly active anticomplement factor from the venom of *Naja kaouthia*. *Acta Biochimica et Biophysica Sinica* 2001; 33(5): 483-488.
59. Sharma S, Jabeen T, Singh RK, et al. Structural studies on the cobra venom factor: isolation, purification, crystallization and preliminary crystallographic analysis. *Acta Cryst* 2001; D57: 596-598.
60. Alper CA and Balavitch D. Cobra venom factor: evidence for its being altered cobra C3 (the third component of complement). *Science* 1976; 191: 1275-1276.
61. Vogel C-W, Smith CA and Muller-Eberhard HJ. Cobra venom factor: structural homology with the third component of human complement. *J Immunol* 1984; 133(6): 3235-3241.
62. Whaley K and Ruddy S. Modulation of the alternative complement pathway by  $\beta$ 1H globulin. *J Exp Med* 1976; 144: 1147-1163.
63. Lachmann PJ and Halbwachs L. The influence of C3b inactivator (KAF) concentration on the ability of serum to support complement activation. *Clin Exp Immunol* 1975; 21: 109-114.
64. Nagaki K, Iida K, Okubo M, et al. Reaction mechanism of  $\beta$ 1H globulin. *Int Archs Allergy Appl Immunol* 1978; 57: 221-232.
65. Cochrane CG, Muller-Eberhard HJ and Aikin BS. Depletion of plasma complement *in vivo* by a protein of cobra venom: its effect on various immunologic reactions. *J Immunol* 1970; 105(1): 55-69.
66. Figueroa E, Gordon LE, Feldhoff PW, et al. The administration of cobra venom factor reduces post-ischemic cerebral injury in adult and neonatal rats. *Neurosci Lett* 2005; 380: 48-53.

67. Chen D, Cao R, Guo H, et al. Pathogenesis and pathology of delayed xenograft rejection in pigto-rhesus monkey cardiac transplantation. *Transplant Proc* 2004; 36(8): 2480-2482.
68. Vogel C-W and Muller-Eberhard HJ. Induction of immune cytolysis: tumor-cell killing by complement is initiated by covalent complex of monoclonal antibody and stable C3/C5 convertase. *Immunol* 1981; 78(12): 7707-7711.
69. Fritzing DC, Bredehorst R and Vogel C-W. Molecular cloning and derived primary structure of cobra venom factor. *Immunol* 1994; 91: 12775-12779.
70. Kock MA, Hew BE, Bammert H, et al. Structure and function of recombinant cobra venom factor. *J Biol Chem* 2004; 279(29): 30836-30843.
71. Reid HA, Theakston RDG. The management of snake bite. *Bull WHO* 1983; 61: 885-895.
72. Russell FE. Injuries by venomous animals. *Amer J nursing* 1966; 66: 1322-6.
73. Reid HA. Cobra-bite. *Brit Med J* 1964; 8: 540-545.
74. Campbell CH. Symptomatology, pathology and treatment of the bites of elapid snakes. In CY Lee (ed.). *Snake Venoms*. Germany: Springer-Verlag Berlin Heidelberg, 1979.
75. Pakmanee N, Thammapalart W, Tampitag S, Onrat D. A study of local tissue necrotic factors in siames cobra (*Naja kaouthia*) venom. In NH Tan (ed.). *Advances in venom and toxin research*. Malaysia: the Malaysian society on toxicology, 1993.
76. Warrell DA, Greenwood BM, Davidson NM, Ormerod LD, Prentice CRM. Necrosis, haemorrhage and complement depletion following bites by the spitting cobra. *Q J Med* 1976; 177: 1-22.
77. Campbell CH. Clinical aspects of snake bite in the pacific area. *Toxicon*; 7: 25-28.
78. Dwivedi S. Time limit for anti-snake venom administration. *Lancet* 1989; 9: 622.
79. Sjostrom L, Al-Abdulla IH, Rawat S, Smith D, Landon J. A comparison of ovine and equine antivenoms. *Toxicon* 1994; 32: 427-433.

80. Houghton PJ. Plant extracts active towards snake venom enzymes. In GS Bailey (ed.). *Enzymes from snake venom*. 1998.
81. Chuakul W, Saralump P, Prathanturarug S. *Medicinal Plants in Thailand. Volume II*. 1997. Amarin Printing and Publishing Public Co., Ltd. Bangkok: 192-193.
82. สมบัติ ประภาวิชา. ผลของความเข้มข้นและช่วงเวลาได้รับน้ำยาสมุนไพรโลดทะนงแดงต่อการยืดอายุการตายของหนูที่ได้รับพิษงูเห่า. รวมบทความของงานวิจัยการแพทย์แผนไทยและทิศทางการวิจัยในอนาคต สถาบันการแพทย์แผนไทย 2543.
83. Itier V, Bertrand D, Engel A, Semenza G. Neuronal nicotinic receptors: from protein structure to function. *FEBS Letters* 2001; 504 (3): 118-125.
84. Unwin N. Refined structure of the nicotinic acetylcholine receptor at 4Å resolution. *J Mol Biol* 2005; 346 (4): 967-989.
85. Cascio M. Structure and function of the glycine receptor and related nicotinic receptors. *J Biol Chem* 2004; 279 (19): 19383-19386.
86. Giniatullin R, Nistri A, Yakel JL. Desensitization of nicotinic ACh receptors: shaping cholinergic signaling. *Trends Neurosci.* 2005; 28 (7): 371-378.
87. Colquhoun D, Sivilotti LG. Function and structure in glycine receptors and some of their relatives. *Trends Neurosci.* 2004; 27 (6): 337-344.
88. Mishina M, Takai T, Imoto K, Noda M, Takahashi T, Numa S, Methfessel C, Sakmann B. Molecular distinction between fetal and adult forms of muscle acetylcholine receptor. *Nature* 1986; 321 (6068): 406-411.
89. Pitchford S, Day JW, Gordon A, Mochly-Rosen D. Acetylcholine receptor desensitization is Regulated by activation-induced extracellular adenosine accumulation. *J Neurosci* 1992; 12 (11): 4540-4544.
90. Huganir RL, Greengard P. CAMP-dependent protein kinase phosphorylates the nicotinic acetylcholine receptor. *Proc Natl Acad Sci USA* 1983; 80: 1130-1134.
91. Safran A, Sagi-Eisenbeg R, Neumann D, Fuchs S. Phosphorylation of the acetylcholine receptor by protein kinase C and identification of the phosphorylation site within the receptor  $\delta$  subunit. *J Biol Chem* 1987; 262: 10506-10510.

92. Barrantes FJ. Agonist-mediated changes of the acetylcholine receptor in its membrane environment. *J Mol Biol* 1978; 124: 1-26.
93. Wonnacott S. Presynaptic nicotinic ACh receptors. *Trends Neuroscience* 1997; 20: 92-98.
94. Graham A, Court JA, Martin-Ruiz CM, Jaros E, Perry R, Volsen SG, Bose S, Evans N, Ince P, Kuryatov A, Lindstrom J, Gotti C, Perry EK. Immunohistochemical localisation of nicotinic acetylcholine receptor subunits in human cerebellum. *Neuroscience* 2002; 113 (3): 493-507.
95. Le Novère N, Changeux JP. Molecular evolution of the nicotinic acetylcholine receptor: an example of multigene family in excitable cells. *J Mol Evol* 1995; 40: 155-172.
96. Rang HP, Dale MM, Ritter JM, Moore P. *Pharmacology* 5th ed. Churchill: Livingstone, 2003, p. 138.
97. Wlodawer A, Vondasek J. Inhibitors of HIV-protease: A major success of structure-assisted drug design. *Annual Review of Biophysics and Biomolecular Structure* 1998; 27: 249-284.
98. Li Z, Chen X, Davidson E, *et al.* Antimalarial drug development using models of enzyme structure. *Chemistry & Biology* 1994; 1: 31-37.
99. Morris GM, Goodsell DS, Halliday RS, Huey R, Hart WE, Belew RK, Olson AJ. Automated docking using a lamarckian genetic algorithm and an empirical binding free energy function. *J Comp Chem* 1998; 19: 1639-1662.
100. Walters WP, Stahl MT, Murcko MA. Virtual screening – an overview. *Drug Discov Today* 1998; 3 (4): 160-178.
101. Sun H. Pharmacophore-based virtual screening. *Curr Med Chem* 2008; 15 (10): 1018-1024.
102. Kroemer RT. Structure-based drug design: docking and scoring. *Curr Protein Pept Sci* 2007; 8 (4): 312-328.
103. Cavasotto CN, Orry AJ. Ligand docking and structure-based virtual screening in drug discovery. *Curr Top Med Chem* 2007; 7 (10): 1006-1014.
104. <http://www.rcsb.org/pdb/home/home.do>

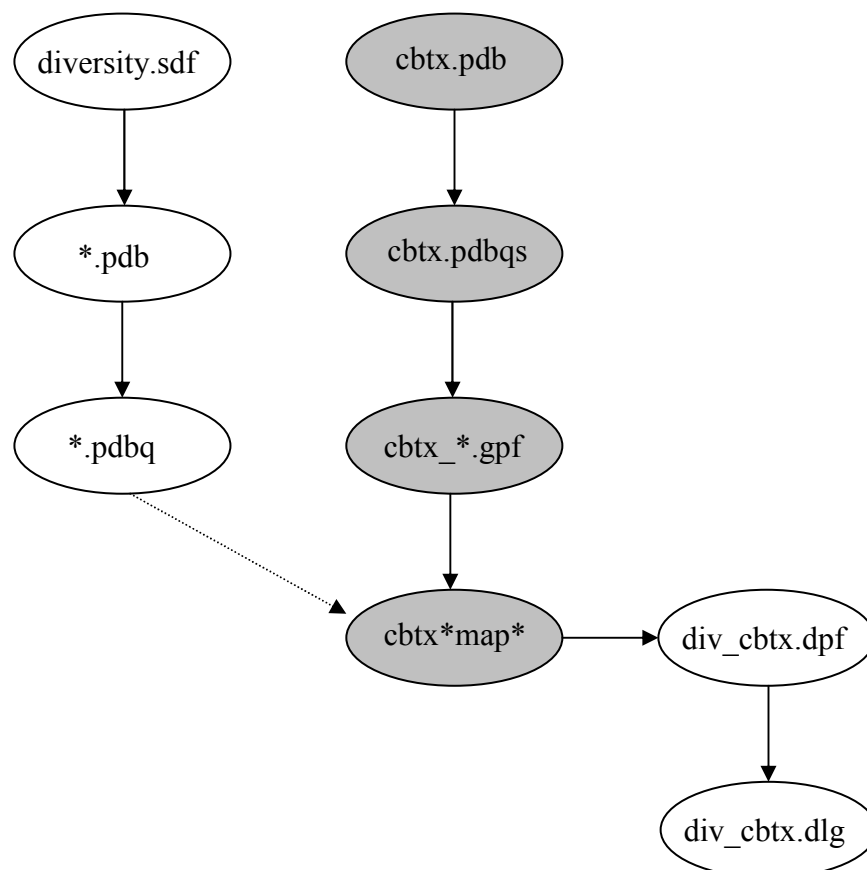
105. Betzel C, Lange G, Pal GP, Wilson KS, Maelicke A, Saenger W. The refined crystal structure of  $\alpha$ -cobrotoxin from *N.n. siamensis* at 2.4-Å resolution, *J Bio Chem* 1991; 266: 21530-21536.
106. [http://dtp.nci.nih.gov/branches/dscb/diversity\\_explanation.html](http://dtp.nci.nih.gov/branches/dscb/diversity_explanation.html)
107. Gasteiger J, Marsili M. Iterative partial equalization of orbital electronegativity—a rapid access to atomic charges. *Tetrahedron* 1980; 36: 3219-3228.
108. Hibbs RE, Talley TT, Taylor P. Acrylodan-conjugated cysteine side chains reveal conformational state and ligand site locations of the acetylcholine-binding protein. *J Biol Chem* 2004; 279: 28483-28491.
109. Laemmli UK. Cleavage of structural proteins during the assembly of the head of bacteriophage T4. *Nature* 1970; 227: 680-685.
110. [http://autodock.scripps.edu/faqs-help/tutorial/using-autodock-for-virtual-screening/UsingAutoDockforVirtualScreening\\_v7.pdf](http://autodock.scripps.edu/faqs-help/tutorial/using-autodock-for-virtual-screening/UsingAutoDockforVirtualScreening_v7.pdf)
111. [http://www.chem.uoa.gr/applets/AppletQtest/Text\\_Qtest2.htm](http://www.chem.uoa.gr/applets/AppletQtest/Text_Qtest2.htm)

## **APPENDIX**

## Appendix A

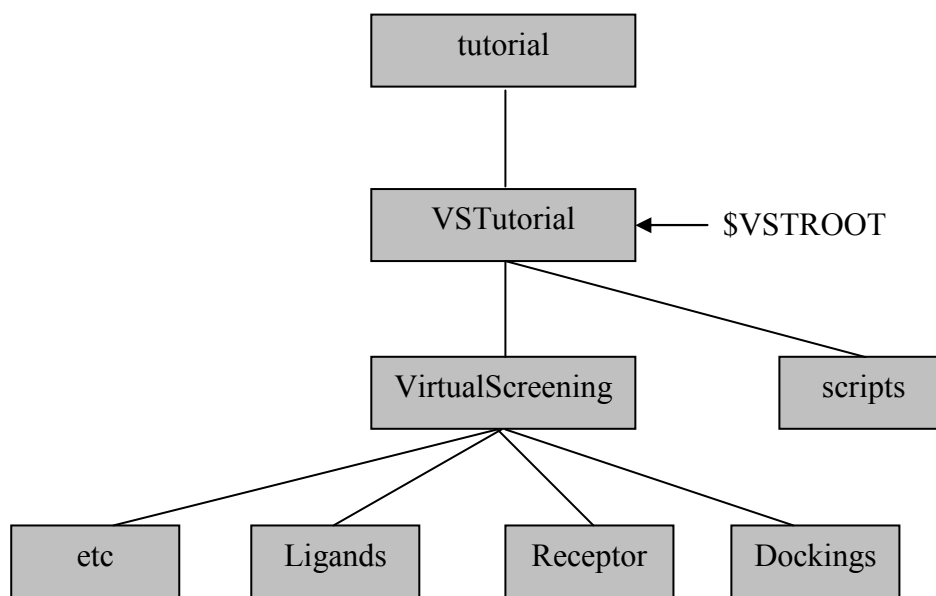
### Using AutoDock for Virtual Screening

Using AutoDock for virtual screening was written by William Lindstrom, Garrett M. Moris, Christoph Weber and Ruth Huey (109). The paper will introduce you to the process of virtual screening using UNIX shell commands and python scripts in the AutoDock suite of program. There are nine steps to prepare a library of ligand files and corresponding AutoGrid and AutoDock parameter files for the library, use AutoGrid to calculate maps, launch AutoDock calculations for each ligand followed by analysis steps (Scheme A1).



**Scheme A1.** Virtual screening map.

The directories were created as shaded boxed with line to illustrate the data structure on the local computer (Scheme A2). The diversity in pdb file is available at TSRI. The diversity set and control peptide were put into Ligands directory.



**Scheme A2.** Virtual Screening data.

First, \$VSTROOT was set up. \$VSTROOT is a short cut to the directory in which the virtual screening activities will take place. Open the terminal and then type this at the UNIX or Linux prompt:

```

Type this: ⇒ cd /usr/tmp/tutorial/VSTutorial
           source scripts/ex00.csh
           echo $VSTROOT
           cd $VSTROOT
    
```

The detail in scripts/ex00.csh

```
#!/bin/csh
# $Id: ex00.csh, v 1.3 2005/01/31 18:11:28 lindy Exp $
#
# Because this script uses "pwd" to set VSROOT it matters where (which directory
# you run it from. This script should be run as "source ./scripts/ex00.csh" So, after you
# did your "cvs co VSTutorial" a "VSTutorial" directory was created and that's the
# one that should be your working directory when you source this script.
#
# set up the root directory of the Virtual Screening Tutorial
#
setenv VSROOT `pwd`
```

The pdbq files were created by prepare\_ligand.py, a python script in the AutoDockTools module, and how to use it in a Unix foreach loop.

Type this:  $\Longrightarrow$  source scripts/ex00.csh

The detail in scripts/ex02.csh

```
#!/bin/csh
#
# $Id: ex02.csh, v 1.2 2005/01/31 00:48:01 lindy Exp $
#
# use the prepare_ligand.py script to creat pdbq files
cd $VSROOT/VirtualScreening/Ligands
foreach f (`ls *.pdb`)
    echo $f
    ../../prepareligand.py -l $f -o "$f"q -d ../etc/ligand_dict.py
end
```

The cbtx pdbqs files and grid parameter files were prepared using ADT, a graphical user interface. Each AutoGrid calculation can create up to 6 atom maps plus the electrostatics map. At this point, cbtx\_1.gpf (ACHNOS map types) and cbtx\_2.gpf (cbFIP map types) were created.

Type this:  $\Longrightarrow$  autogrid3 -p cbtx\_1.gpf -l cbtx\_1.glg  
autogrid3 -p cbtx\_2.gpf -l cbtx\_2.glg

Docking directories and the parameter files for each ligand in a library and control peptide were prepared and the dpf files were created by prepare\_dpf.py and the virtual screening data after prepared the dpf files was shown in Scheme A3.

Type this:  $\Rightarrow$  source scripts/ex08.csh

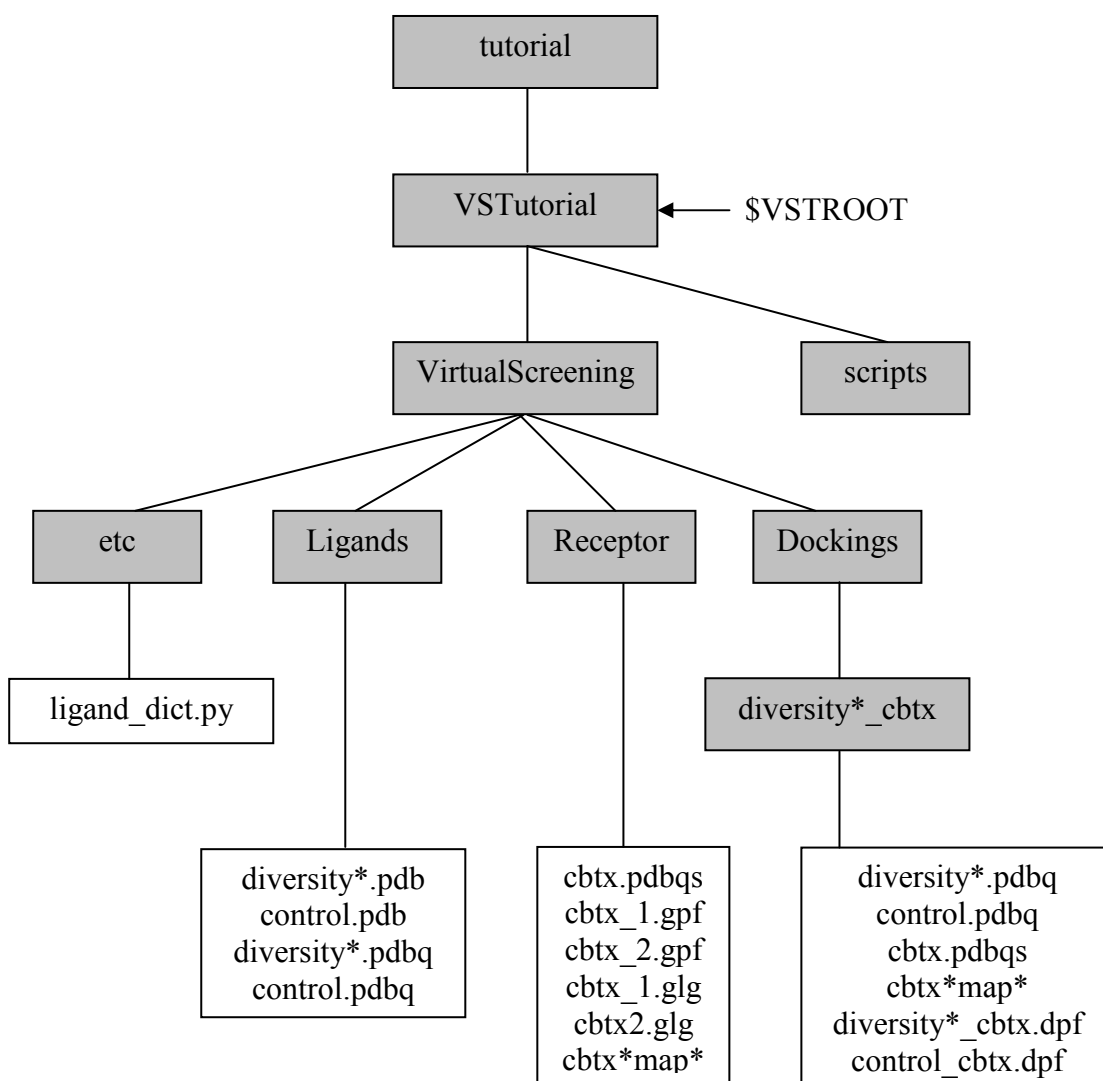
The detail in scripts/ex08.csh

```
#!/bin/csh
# $Id: ex02.csh, v 1.4 2005/01/31 16:33:49 lindy Exp $

cd Dockings

# Creat a subdirectory named <ligand>_cbtx and populate it with the docking input
# files: a) the pdbq from the Ligands directory will be copied directory; and b) the
# maps will be linked to the Receptor directory; and , c) the dpf file will be created
# using prepare_dpf.py:

foreach f (`ls ../Ligands/*.pdbq`)
set name = `basename $f .pdbq`
echo $name
mkdir "$name"_cbtx
cd "$name"_cbtx
ln -s ../../Receptor/cbtx.pdbqs .
ln -s ../../Receptor/cbtx*map* .
../../prepare_dpf.py -l `basename $f` -r cbtx.pdbqs \
    -p ga_num_evals=10000000 \
    -p ga_pop_size=150 \
    -p ga_run=1 \
    -p rmstol=2.0
cd ..
end
```



**Scheem A3.** The virtual screening data to prepare the dpf files.

### Using the TSRI Cluster: Bluefish

All input file preparation have done on the local computer. The interactive head node on the bluefish cluster is used to transfer the files from the computer to the cluster where the calculations will be carried out. A tar file of VSTutorial directory tree was created on the local computer and then transferred to bluefish using SSH Secure Shell Client.

Type this:  $\Rightarrow$  `cd /usr/tmp/tutorial`  
`tar -czvf VSTutorial.tar.gz VSTutorial`

The environment on the bluefish cluster must be set so that autodock3 executable and the python script.py are in the path. Next uncompress the VSTutorial tree and then launch the jobs by using submit.py script.

Type this:  $\Rightarrow$  set path = (\$path /bluefish/people-b/applications/autodock)

```
tar -xzf VSTutorial.tar.gz
```

```
foreach f (`/bin/ls $VSTROOT/VirtualScreening/Ligands/*.pdbq`)
```

```
    set name = `basename $f .pdbq`
```

```
    echo $name
```

```
    cd $VSTROOT/VirtualScreening/Dockings/"$name"_cbtx
```

```
    submit.py "$name"_cbtx 1
```

```
end
```

The first step of analyzing the results is to build a list sorted by energy of the lowest energy docking for each ligand. To do this, first collect all the lig\_rec.NNN.dlg to get lig\_rec.energies and then sort the lig\_rec.energies to create the file lig\_rec.energies.sort

Type this:  $\Rightarrow$  source scripts/ex10.csh

The detail in scripts/ex10.csh

```
#!/bin/csh
# $Id: ex10.csh, v 1.3 2005/01/31 02:27:03 lindy Exp $
# Extract the Free Energy and Docked Energy from the dlg files. From the docking
# log files, use grep to extract the lines containing the binding energy and docked
# energy of each complex. Use sed and awk to process these lines into the final
# output:

cd $VSTROOT/VirtualScreening/Dockings
foreach d ( `bin/ls` )
    echo $d
    egrep “^USER Estimated Free Energy of Binding |
^USER Final Docked Energy” $d/sd.dlg | sed “N;s/ \n//” |
awk -v n=$d ‘BEGIN {N=n} { print N” “$8” “$15}’ > $d/$d.energies
    end

# Save the best energy fro each docking in a single file in the pwd directory called
# all_energies.list:

touch ../etc/all_energies.list
foreach d ( `bin/ls` )
    echo $d
    head -l $d/$d.energies >> ../etc/all_energies.list
    end

# Sort the all_energies.list file to find your best docking:

cd ../etc
sort -k3n all_energies.list > all_energies.sort
```

**Appendix B****Table B1. The top 175 compounds for each  $\alpha$ -cobratoxin**

1YI5		2CTX		1CTX	
NCI number	Docking energy (kcal/mol)	NCI number	Docking energy (kcal/mol)	NCI number	Docking energy (kcal/mol)
140032 <sup>a</sup>	-24.65	1940 <sup>b</sup>	-24.62	140032 <sup>a</sup>	-24.62
86374 <sup>a</sup>	-21.40	140032 <sup>a</sup>	-24.19	86374 <sup>a</sup>	-22.68
625324 <sup>b</sup>	-20.20	625324 <sup>a</sup>	-23.54	625324 <sup>b</sup>	-22.65
274547 <sup>c</sup>	-14.87	274547 <sup>c</sup>	-13.46	274547 <sup>c</sup>	-14.39
371884	-13.86	49487	-12.74	11241	-13.59
49487	-13.54	11241	-11.93	371884	-13.30
11241	-13.32	371878	-11.91	23128	-13.10
371878	-13.19	372280	-11.77	134755	-12.95
371876	-12.72	128437	-11.67	371876	-12.52
3354	-12.36	23904	-11.66	3354	-12.49
23128	-12.23	371884	-11.60	372046	-12.48
128437	-12.19	372294	-11.51	64111	-12.44
14410	-12.11	64111	-11.39	49487	-12.28
113491	-12.07	140936	-11.35	134754	-12.08
95926	-11.83	15520	-11.27	56452	-12.04
23904	-11.82	36387	-11.26	43628 <sup>d</sup>	-11.94
26645	-11.82	87877	-11.19	166366	-11.84
53396	-11.82	113491	-11.19	600067	-11.84
211736	-11.82	74702	-11.12	89166	-11.77
343040	-11.82	303812	-11.09	211736	-11.84
600067	-11.78	131547	-10.95	81509	-11.74
43628 <sup>d</sup>	-11.70	16168	-10.89	100857	-11.72
64111	-11.69	600067	-10.87	371878	-11.61
372280	-11.67	60043	-10.83	37245	-11.55
13728	-11.59	48630	-10.83	26645	-11.52
79050	-11.59	43628 <sup>d</sup>	-10.82	131547	-11.52
234766	-11.58	14410	-10.81	13831	-11.49
36387	-11.57	116654	-10.76	95090	-11.46
95090	-11.57	150412	-10.76	128437	-11.43
12181	-11.56	205511	-10.75	12181	-11.41
23217	-11.54	95926	-10.73	36387	-11.39
659162	-11.54	131615	-10.73	63875	-11.37
322921	-11.53	106505	-10.71	172614	-11.37
93354	-11.49	372046	-10.71	402959	-11.35
63875	-11.48	3354	-10.70	101825	-11.33
119847	-11.48	5069	-10.68	106221	-11.32
172614	-11.47	680517	-10.68	350625	-11.32
93674	-11.46	56452	-10.65	14410	-11.31
37245	-11.45	134754	-10.64	659162	-11.31
131547	-11.41	282027	-10.60	105687	-11.29
163443	-11.41	371876	-10.57	18877	-11.28
409664	-11.36	120288	-10.52	633406	-11.28
361815	-11.35	255980	-10.54	106505	-11.25
227147 <sup>e</sup>	-11.33	26273	-10.53	26273	-11.21

**Table B1. The top 175 compounds for each  $\alpha$ -cobratoxin (Continued)**

1YI5		2CTX		1CTX	
NCI number	Docking energy (kcal/mol)	NCI number	Docking energy (kcal/mol)	NCI number	Docking energy (kcal/mol)
106218	-11.32	134755	-10.52	106218	-11.20
134755	-11.30	23128	-10.51	34238	-11.17
93241	-11.30	93241	-10.46	150412	-11.17
106221	-11.28	4895	-10.44	23922	-11.15
45583	-11.24	159228	-10.44	116654	-11.13
42258	-11.23	44585	-10.43	339601	-11.13
81509	-11.21	45583	-10.43	48693	-11.10
348401	-11.21	99550	-10.43	93241	-11.09
95916	-11.19	310669	-10.40	99550	-11.09
61806	-11.18	127917	-10.39	11237	-11.07
96021	-11.18	299137	-10.38	17474	-11.07
361814	-11.16	13728	-10.37	115448	-11.04
56452	-11.12	12181	-10.35	163443	-11.04
60043	-11.12	101825	-10.34	18891	-11.00
371880	-11.12	119847	-10.34	95926	-10.98
76026	-11.10	227147 <sup>e</sup>	-10.34	113491	-10.96
121865	-11.09	241993	-10.34	127917	-10.96
324065	-11.09	683770	-10.34	39863	-10.93
372046	-11.07	43413	-10.31	43413	-10.93
88915	-11.06	172614	-10.31	45208	-10.92
17245	-11.05	95090	-10.30	372060	-10.91
16168	-11.03	116702	-10.28	372280	-10.90
150412	-11.02	62598	-10.27	348401	-10.89
303812	-11.02	45582	-10.25	82147	-10.82
282027	-11.01	147758	-10.25	101824	-10.81
74702	-11.00	343040	-10.24	17245	-10.81
77037	-10.97	45208	-10.23	45583	-10.80
119886	-10.96	10458	-10.21	371872	-10.79
120688	-10.96	106221	-10.21	186066	-10.78
659390	-10.96	659162	-10.21	42384	-10.76
326203	-10.95	69540	-10.20	186057	-10.75
371684	-10.94	105687	-10.16	303812	-10.75
134754	-10.94	37245	-10.15	306698 <sup>e</sup>	-10.74
4292	-10.92	62594	-10.14	116490	-10.73
136469	-10.92	81509	-10.13	23217	-10.72
372294	-10.92	101824	-10.13	73109	-10.72
18877	-10.89	100857	-10.12	73254	-10.72
166366	-10.89	211736	-10.12	93674	-10.72
13726	-10.87	23217	-10.11	87877	-10.71
371872	-10.87	85372	-10.11	23904	-10.70
41274	-10.86	668394	-10.10	42258	-10.69
106505	-10.86	41309	-10.09	88915	-10.69
25485	-10.84	117949	-10.09	112796	-10.69
133488	-10.84	306698 <sup>e</sup>	-10.09	121855	-10.68
5069	-10.77	9746	-10.07	136563	-10.63

**Table B1. The top 175 compounds for each  $\alpha$ -cobratoxin (Continued)**

1YI5		2CTX		1CTX	
NCI number	Docking energy (kcal/mol)	NCI number	Docking energy (kcal/mol)	NCI number	Docking energy (kcal/mol)
295272	-10.77	47704	-10.05	227147 <sup>e</sup>	-10.63
10458	-10.76	73109	-10.04	205511	-10.62
402959	-10.76	163443	-10.04	295272	-10.62
339601	-10.75	43131	-10.02	351814	-10.62
69573	-10.72	638156	-10.02	99543	-10.59
299137	-10.71	646824	-10.02	119847	-10.59
101825	-10.66	154829	-10.01	36369	-10.55
371682	-10.66	115448	-9.99	99671	-10.54
39863	-10.65	327704	-9.99	99804	-10.54
350625	-10.65	294149	-9.98	169453	-10.54
99671	-10.64	26645	-9.97	190382	-10.54
116654	-10.63	148354	-9.96	372294	-10.54
14711	-10.62	402959	-9.96	62594	-10.52
117614	-10.61	119886	-9.95	119886	-10.52
18451	-10.60	13975	-9.91	159628	-10.51
641691	-10.60	82147	-9.91	656202	-10.51
116702	-10.59	86008	-9.90	53396	-10.50
159228	-10.55	94914	-9.90	112675	-10.50
7520	-10.54	120688	-9.90	34352	-10.49
169534	-10.54	659390	-9.90	306711	-10.47
48693	-10.53	53396	-9.88	13480	-10.46
43413	-10.51	327702	-9.88	69540	-10.46
109836	-10.50	18877	-9.87	121865	-10.45
121855	-10.50	65828	-9.87	170008	-10.45
13987	-10.49	120634	-9.87	97845	-10.43
373058	-10.48	18451	-9.83	114442	-10.42
24859	-10.47	88915	-9.83	147758	-10.42
109509	-10.47	41274	-9.82	372045	-10.41
37173	-10.45	92828	-9.82	10424	-10.39
162404	-10.43	42384	-9.81	74702	-10.39
205511	-10.43	88135	-9.80	371684	-10.39
14119	-10.42	326381	-9.79	639174	-10.39
319434	-10.42	8797	-9.78	35489	-10.38
17474	-10.41	23922	-9.77	47704	-10.38
633406	-10.41	133488	-9.77	28136	-10.37
85372	-10.40	211340	-9.77	44585	-10.37
7524	-10.39	140905	-9.76	5069	-10.35
147758	-10.39	176328	-9.75	154572	-10.35
65828	-10.37	41663	-9.73	18883	-10.33
327704	-10.36	639174	-9.73	52445	-10.33
136472	-10.34	131453	-9.72	154829	-10.32
176328	-10.34	170008	-9.72	350363	-10.32
84130 <sup>f</sup>	-10.33	17245	-9.71	76026	-10.31
42384	-10.32	112675	-9.71	45582	-10.30
326381	-10.33	81620	-9.70	84130 <sup>f</sup>	-10.30
87877	-10.31	95916	-9.70	65828	-10.29

**Table B1. The top 175 compounds for each  $\alpha$ -cobratoxin (Continued)**

1YI5		2CTX		1CTX	
NCI number	Docking energy (kcal/mol)	NCI number	Docking energy (kcal/mol)	NCI number	Docking energy (kcal/mol)
48223	-10.30	117614	-9.68	351351	-10.29
59620	-10.30	166366	-9.68	116491	-10.28
143491	-10.30	372127	-9.68	294149	-10.28
148354	-10.30	42258	-9.67	13987	-10.27
357756	-10.30	321598	-9.67	41663	-10.27
610930	-10.30	13987	-9.65	88135	-10.27
52445	-10.27	23173	-9.65	98905	-10.27
127917	-10.27	179703	-9.65	162404	-10.27
31076	-10.26	51132	-9.64	282027	-10.26
69540	-10.26	84130 <sup>f</sup>	-9.64	288391	-10.26
5113	-10.25	109834	-9.64	343040	-10.26
15909	-10.25	121847	-9.64	401366	-10.25
23583	-10.25	372074	-9.64	186063	-10.24
74860	-10.25	59620	-9.63	293161	-10.24
43513	-10.23	13726	-9.61	372037	-10.24
190382	-10.23	190382	-9.61	659390	-10.24
18883	-10.22	48388	-9.60	35582	-10.22
306698 <sup>c</sup>	-10.22	75749	-9.60	60043	-10.22
310669	-10.22	106218	-9.60	79050	-10.22
62349	-10.21	332429	-9.60	131815	-10.22
176327	-10.21	361815	-9.60	176327	-10.22
26273	-10.19	659694	-9.60	299137	-10.22
82802	-10.19	99671	-9.59	45554	-10.21
683770	-10.19	121865	-9.59	130830	-10.21
90616	-10.18	45554	-9.58	10458	-10.20
319095	-10.18	52445	-9.58	37881	-10.20
407628	-10.18	326203	-9.57	150117	-10.20
9608	-10.17	162404	-9.56	641691	-10.20
82147	-10.17	31076	-9.55	74472	-10.19
121137	-10.17	121855	-9.55	86467	-10.18
668394	-10.17	333003	-9.55	99676	-10.18
45208	-10.16	92601	-9.54	373058	-10.18
99543	-10.16	409664	-9.54	631160	-10.18
94820	-10.15	631160	-9.54	657704	-10.17
34238	-10.14	11237	-9.53	88903	-10.16
134244	-10.14	339601	-9.53	45236	-10.15
306711	-10.14	641691	-9.53	201579	-10.15
89166	-10.13	76064	-9.52	59486	-10.13
3364	-10.11	89166	-9.52	140936	-10.13
105687	-10.11	136469	-9.52	14143	-10.12

<sup>a</sup>The structure has Se atom<sup>b</sup>The structure has Ag atom<sup>c</sup>The structure has Au atom<sup>d</sup>The structure has Cu atom<sup>e</sup>The structure has Ni atom<sup>f</sup>The structure has As atom

## Appendix C

Table C1. The screening test data from radioligand competition assay

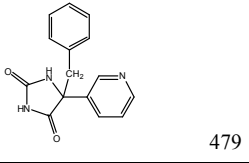
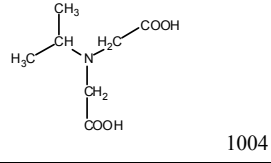
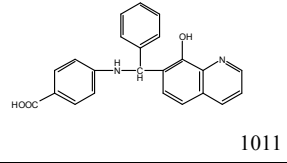
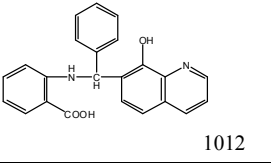
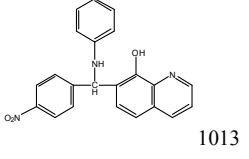
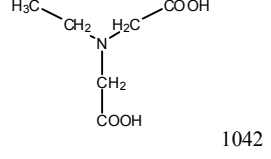
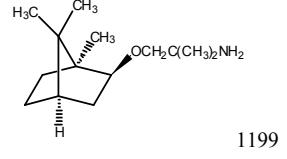
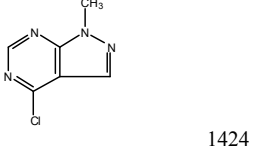
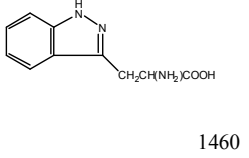
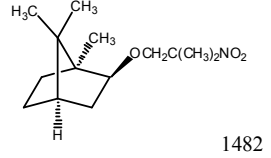
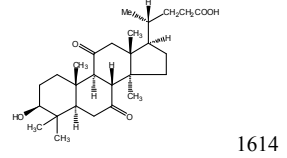
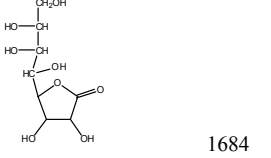
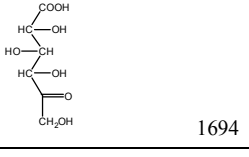
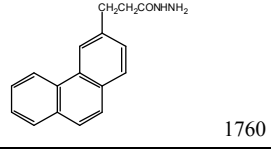
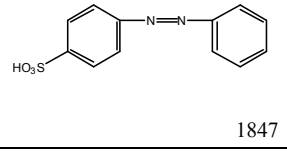
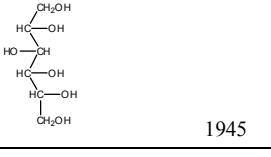
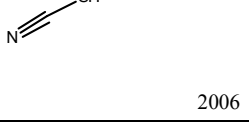
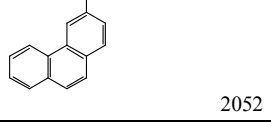
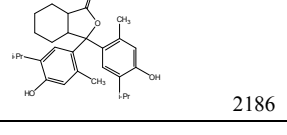
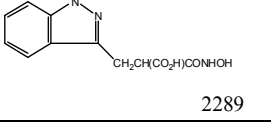
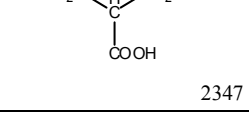
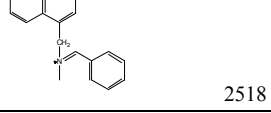
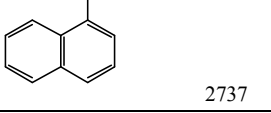
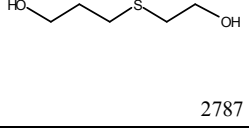
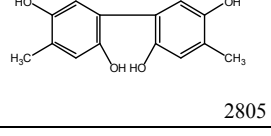
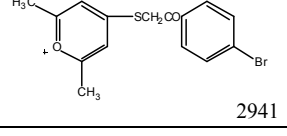
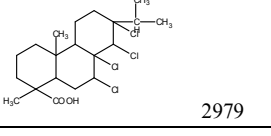
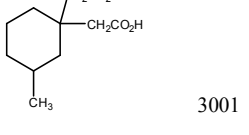
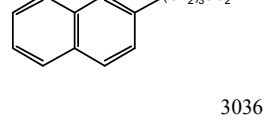
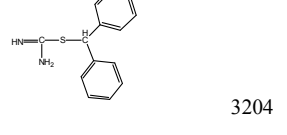
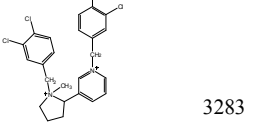
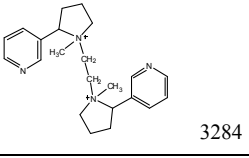
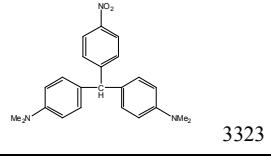
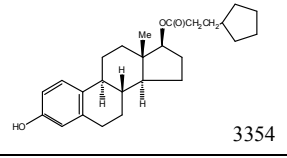
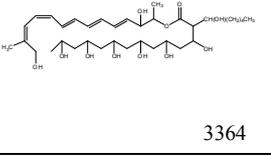
Compound	<i>Ls</i>				<i>Ac</i>				<i>Bt</i>			
	T1	T2	T1	T2	T1	T2	T1	T2	T1	T2	T1	T2
1	471	421	460	423	849	775	788	645	573	526	608	582
2	423	449	400	359	809	857	789	819	517	470	489	527
3	467	526	442	506	842	866	754	741	572	607	623	623
4	501	430	462	417	953	820	804	789	552	490	561	510
5	391	409	359	383	776	732	717	705	379	438	395	454
6	381	348	345	331	762	743	653	641	240	295	277	288
7	523	460	446	446	719	617	678	654	527	572	495	577
8	55	40	36	31	80	62	76	60	42	31	3	29
9	424	500	383	438	767	790	687	735	461	503	415	569
10	120	105	101	108	244	307	285	285	312	381	324	378
11	483	597	509	522	845	86	775	766	511	616	495	716
12	389	364	372	346	781	786	698	707	476	445	473	469
13	432	466	388	454	890	848	838	769	456	645	491	612
14	404	433	375	391	686	817	640	755	298	429	317	417
15	501	394	482	392	762	739	711	679	51	548	535	539
16	374	404	350	362	700	602	626	579	364	394	344	413
17	416	395	355	328	662	740	593	622	363	362	414	365
18	419	463	408	454	779	901	746	743	543	702	556	686
19	475	550	462	447	246	293	211	227	352	436	334	466
20	445	38	388	390	840	785	766	738	492	684	467	675
21	345	436	299	416	845	899	853	859	747	595	683	597
22	414	420	398	382	818	883	781	727	700	621	673	618
23	115	113	88	112	29	38	28	25	227	246	223	245
24	458	344	433	371	794	812	828	704	622	683	621	670
25	433	453	468	435	716	804	771	778	697	606	734	714
26	362	399	345	358	645	659	602	643	486	498	529	513
27	258	252	212	231	448	432	392	370	440	452	471	421
28	423	344	357	304	367	351	386	353	614	583	581	586
29	294	342	270	295	215	186	186	175	452	397	421	417
30	404	485	436	437	804	950	769	865	625	675	655	638
31	534	493	444	430	792	790	738	737	652	700	701	726
32	354	258	305	245	632	542	548	528	590	653	538	570
33	485	403	451	396	816	880	745	780	705	651	717	673
34	425	443	408	387	937	724	778	656	631	640	625	562
35	419	517	368	456	830	771	798	729	606	565	573	601
36	408	357	355	332	789	777	717	707	627	580	595	592
37	418	432	418	373	694	826	655	721	643	722	616	739
38	422	415	378	412	705	619	645	594	644	647	615	620
39	434	478	385	456	804	667	711	588	562	545	584	518
40	368	399	326	347	609	710	592	675	416	374	405	356

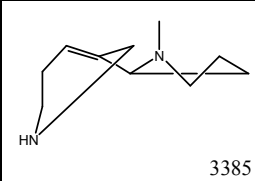
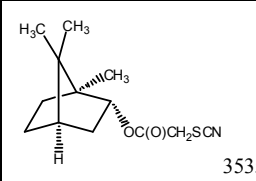
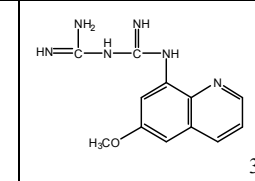
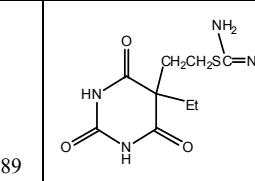
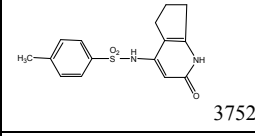
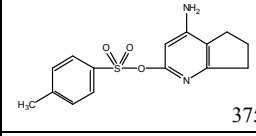
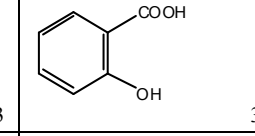
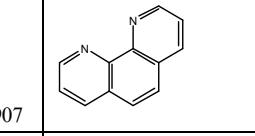
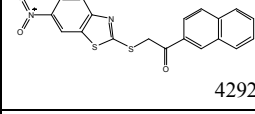
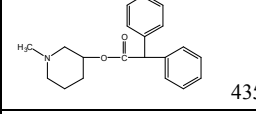
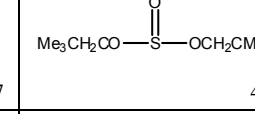
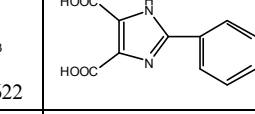
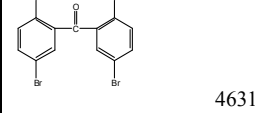
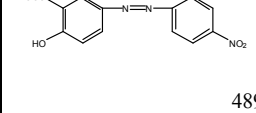
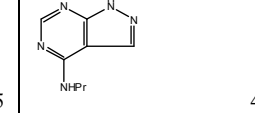
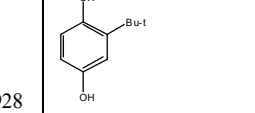
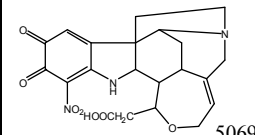
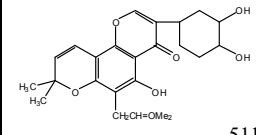
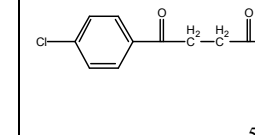
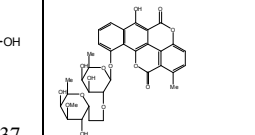
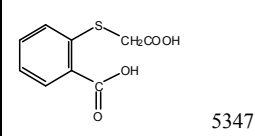
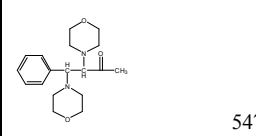
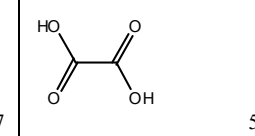
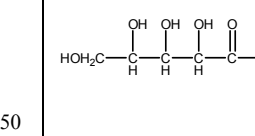
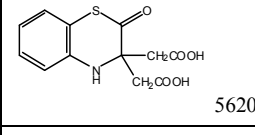
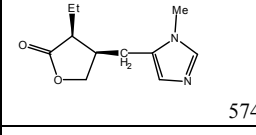
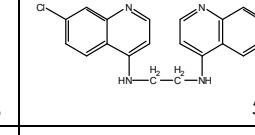
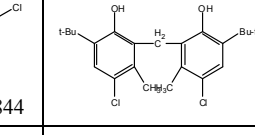
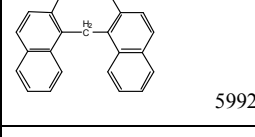
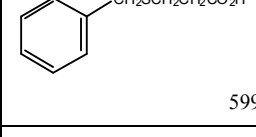
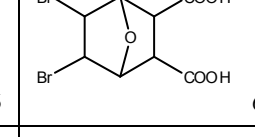
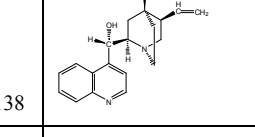
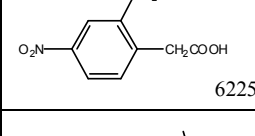
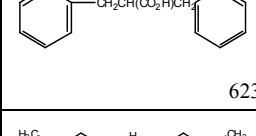
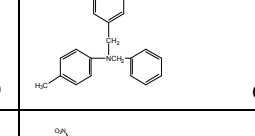
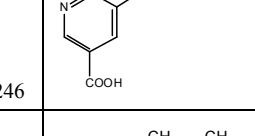
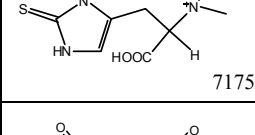
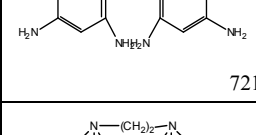
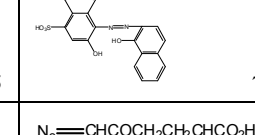
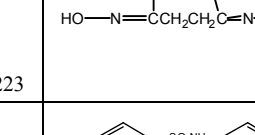
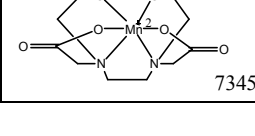
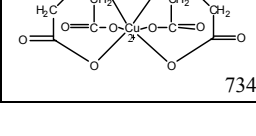
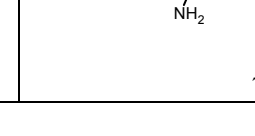
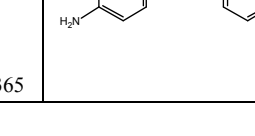
**Table C1.** The screening test data from radioligand competition assay (Continued)

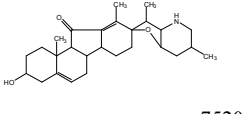
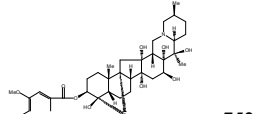
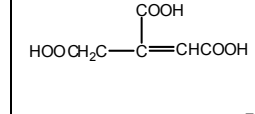
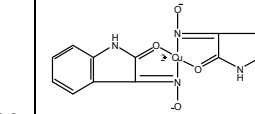
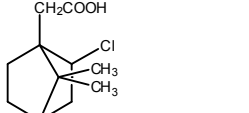
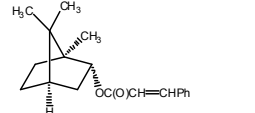
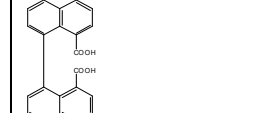
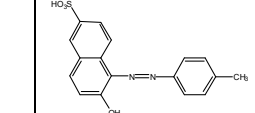
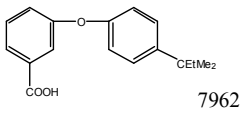
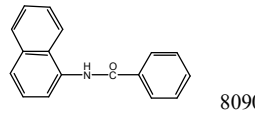
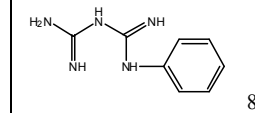
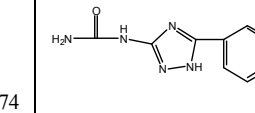
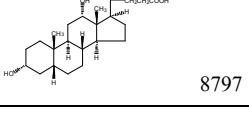
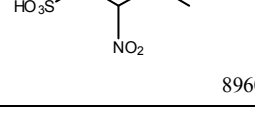
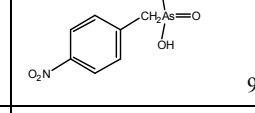
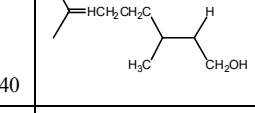
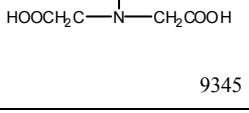
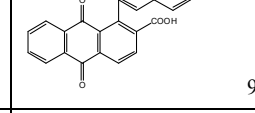
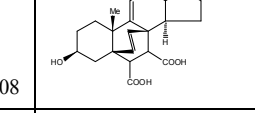
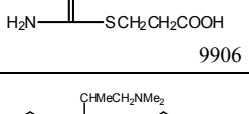
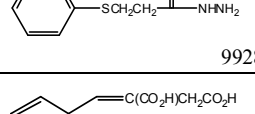
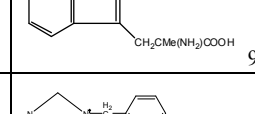
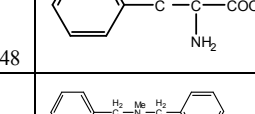
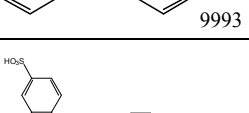
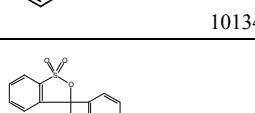
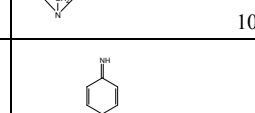
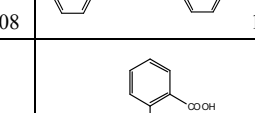
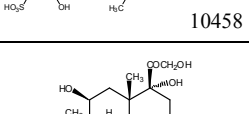
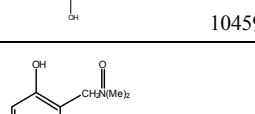
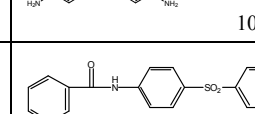
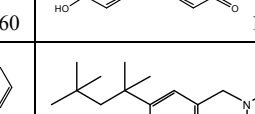
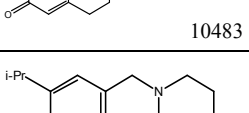
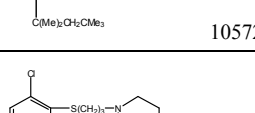
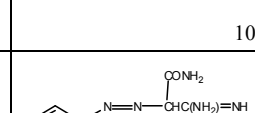
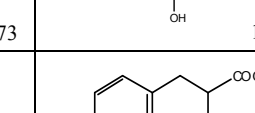
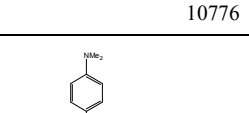
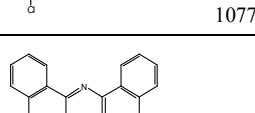
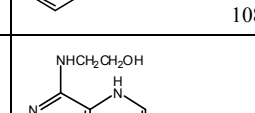
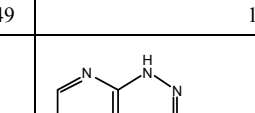
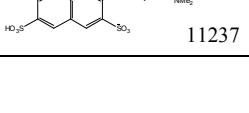
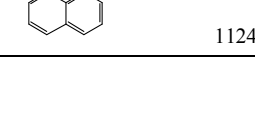
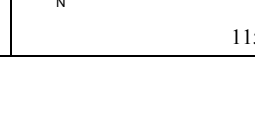
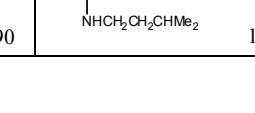
Compound	<i>Ls</i>				<i>Ac</i>				<i>Bt</i>			
	T1	T2	T1	T2	T1	T2	T1	T2	T1	T2	T1	T2
Negative control	428	403	295	337	837	838	770	795	700	736	671	750
(PBS)	478	473	440	404	790	747	778	669	701	761	684	808
	466	417	401	395	805	805	724	783	720	741	694	707
	442	456	421	363	840	972	690	860	694	673	709	664
Positive control	12	14	13	13	21	16	14	13	16	11	8	13
(MLA)	12	14	9	11	20	27	26	27	19	20	18	18
	16	11	13	9	16	15	17	21	15	19	20	19
	22	9	12	13	29	30	24	24	20	17	19	18

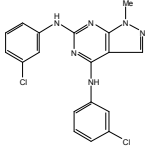
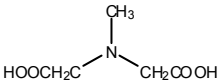
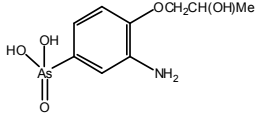
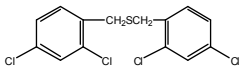
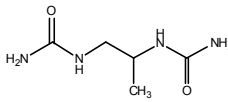
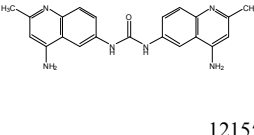
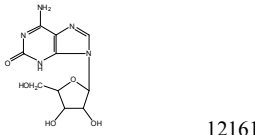
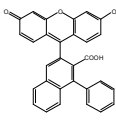
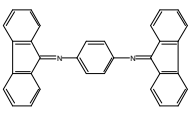
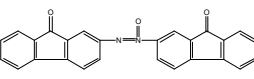
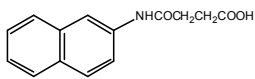
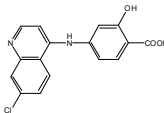
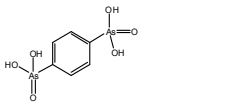
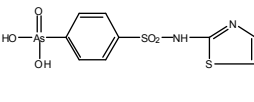
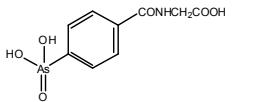
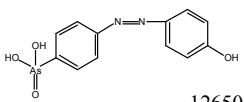
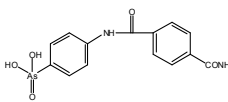
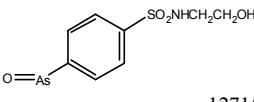
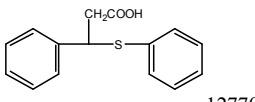
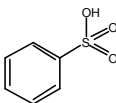
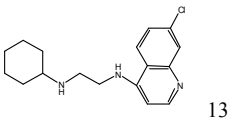
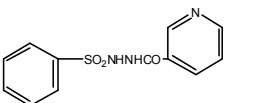
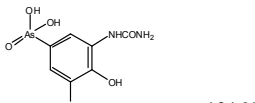
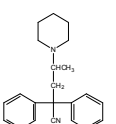
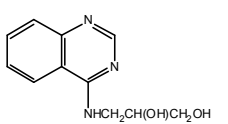
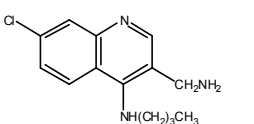
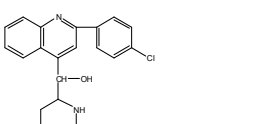
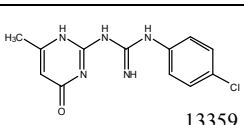
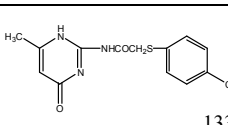
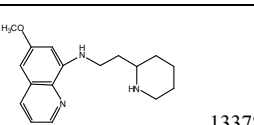
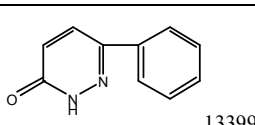
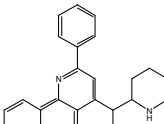
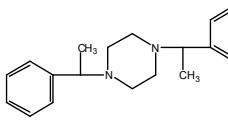
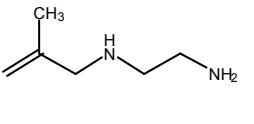
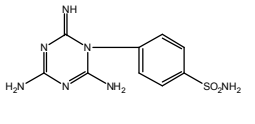
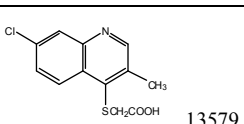
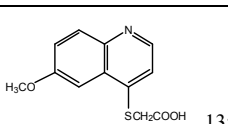
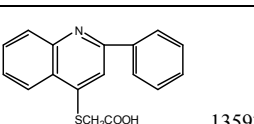
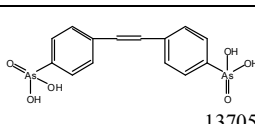
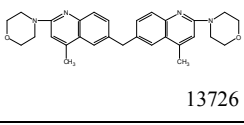
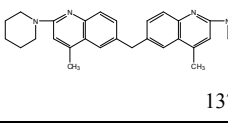
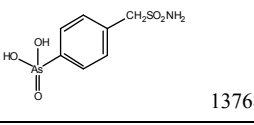
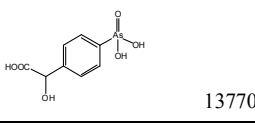
**Appendix D**

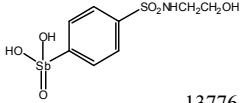
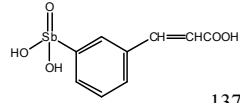
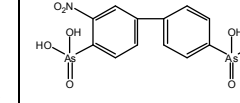
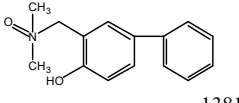
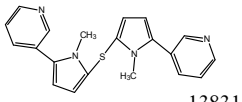
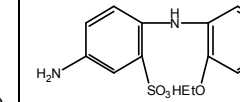
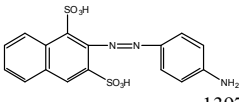
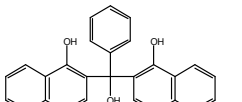
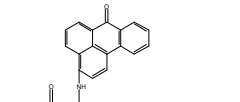
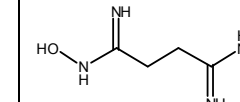
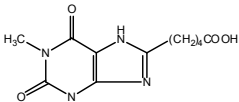
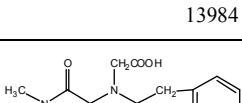
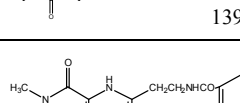
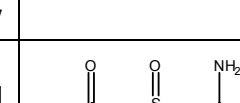
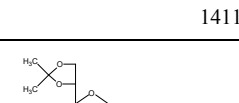
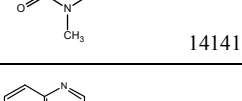
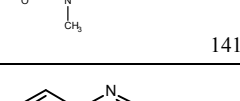
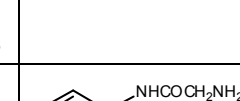
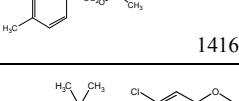
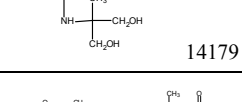
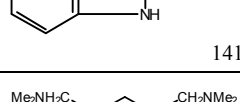
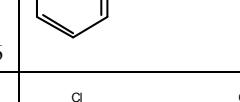
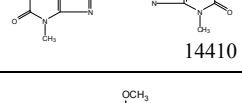
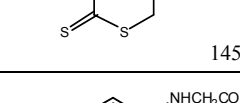
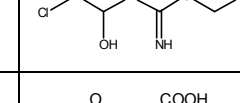
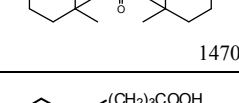
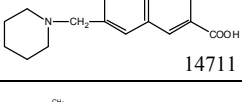
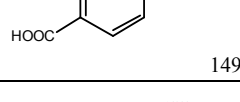
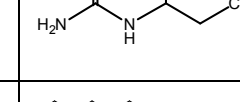
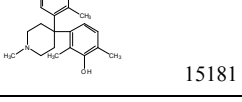
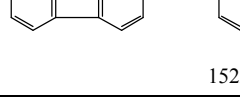
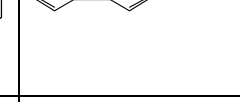
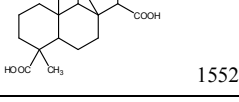
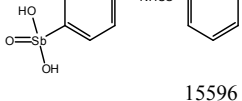
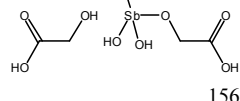
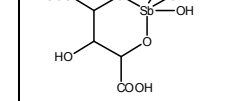
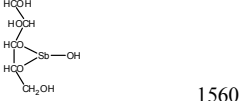
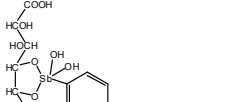
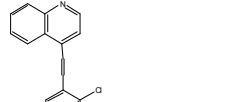
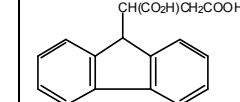
**NCI Diversity Set**

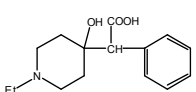
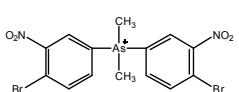
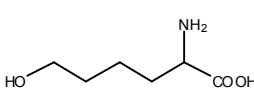
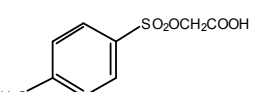
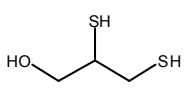
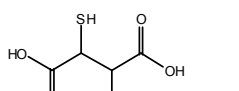
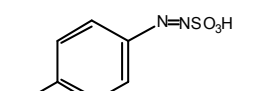
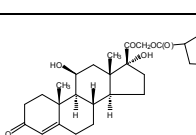
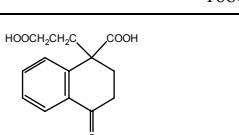
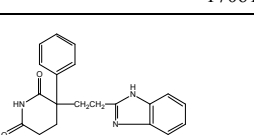
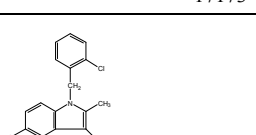
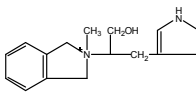
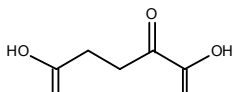
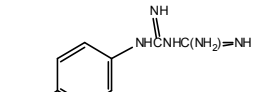
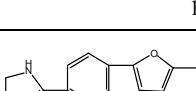
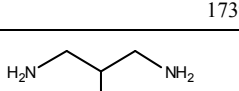
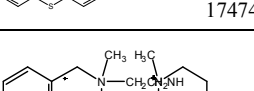
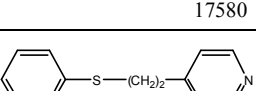
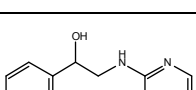
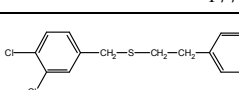
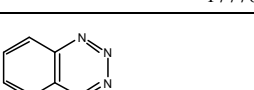
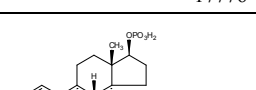
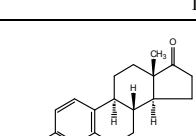
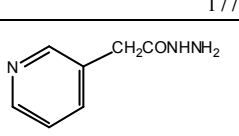
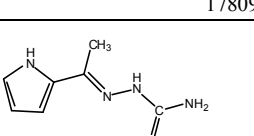
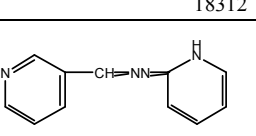
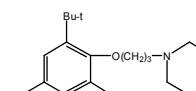
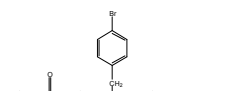
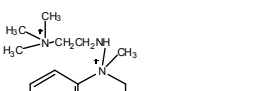
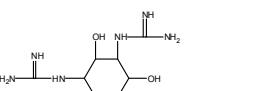
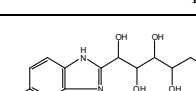
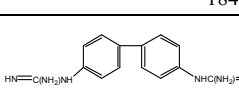
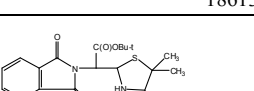
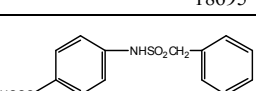
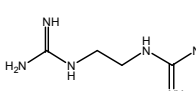
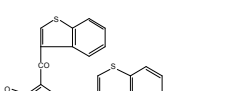
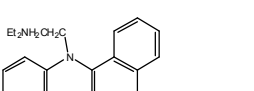
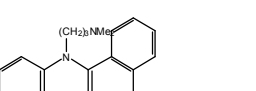
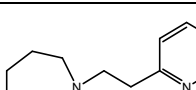
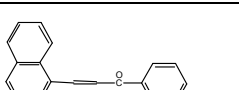
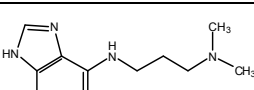
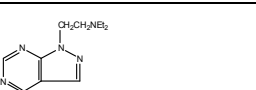
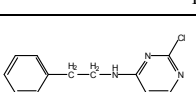
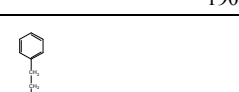
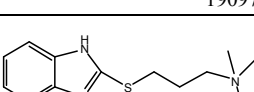
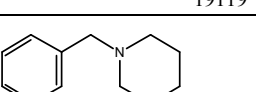
 479	 1004	 1011	 1012
 1013	 1042	 1199	 1424
 1460	 1482	 1614	 1684
 1694	 1760	 1847	 1945
 2006	 2052	 2186	 2289
 2347	 2518	 2561	 2737
 2787	 2805	 2941	 2979
 3001	 3036	 3204	 3283
 3284	 3323	 3354	 3364

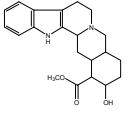
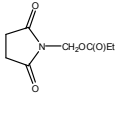
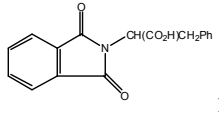
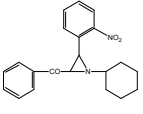
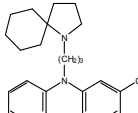
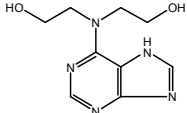
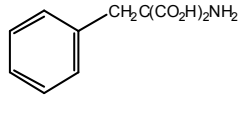
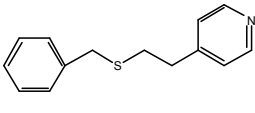
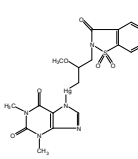
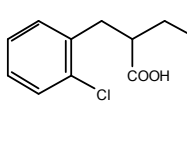
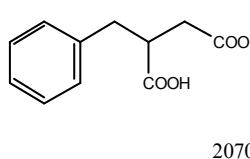
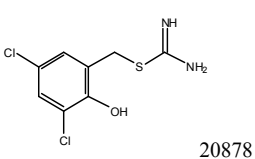
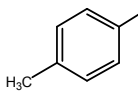
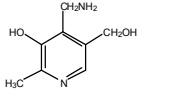
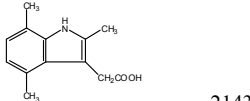
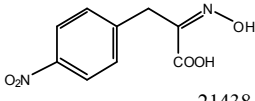
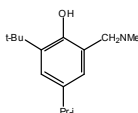
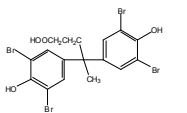
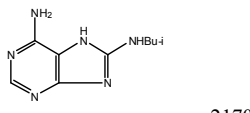
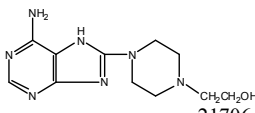
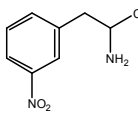
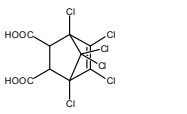
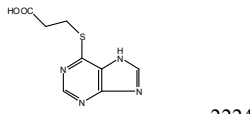
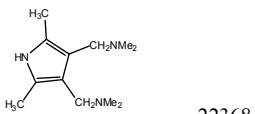
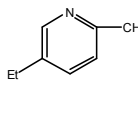
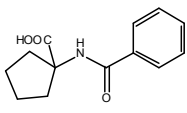
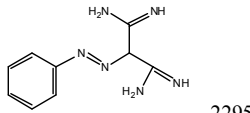
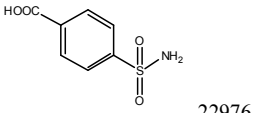
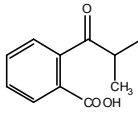
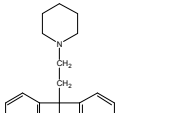
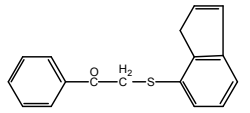
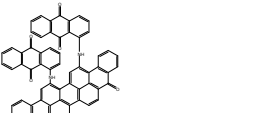
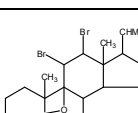
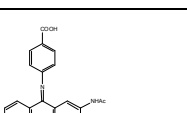
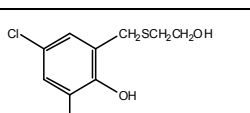
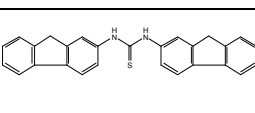
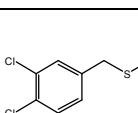
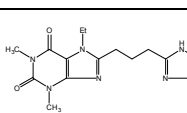
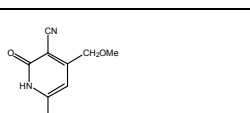
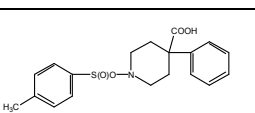
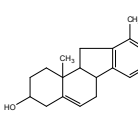
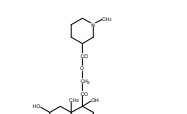
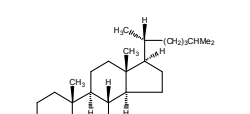
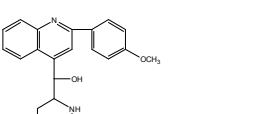
 3385	 3535	 3589	 3737
 3752	 3753	 3907	 4265
 4292	 4357	 4622	 4623
 4631	 4895	 4928	 4972
 5069	 5113	 5137	 5159
 5347	 5477	 5550	 5554
 5620	 5746	 5844	 5857
 5992	 5996	 6138	 6176
 6225	 6239	 6246	 6497
 7175	 7215	 7223	 7307
 7345	 7346	 7365	 7436

 7520	 7524	 7616	 7711
 7734	 7757	 7810	 7814
 7962	 8090	 8174	 8179
 8797	 8960	 9040	 9279
 9345	 9600	 9608	 9746
 9906	 9928	 9948	 9959
 9993	 10134	 10408	 10424
 10458	 10459	 10460	 10470
 10483	 10572	 10573	 10580
 10776	 10777	 10849	 10853
 11237	 11241	 11590	 11607

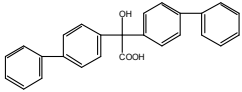
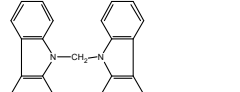
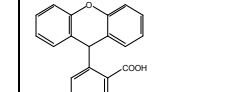
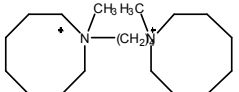
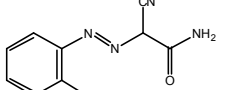
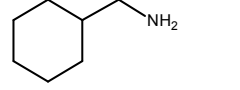
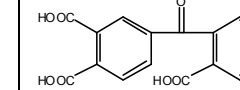
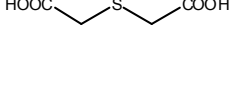
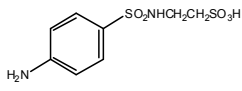
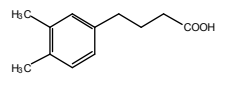
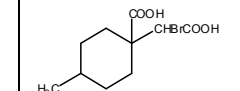
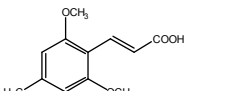
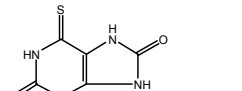
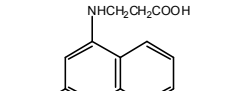
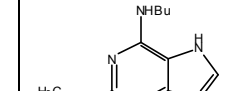
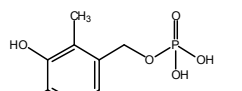
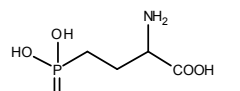
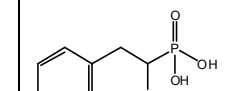
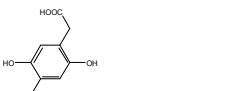
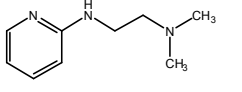
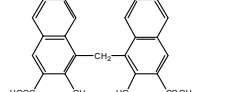
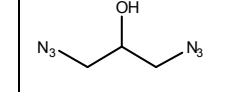
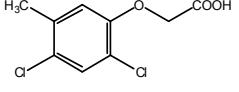
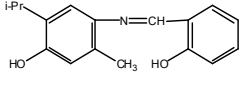
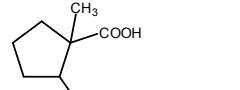
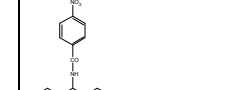
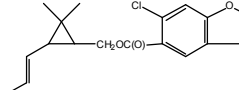
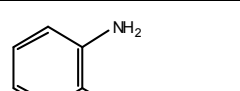
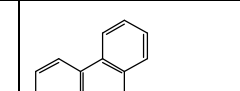
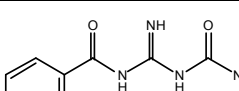
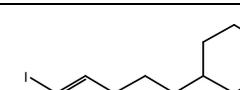
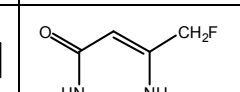
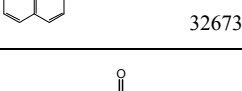
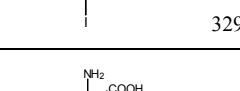
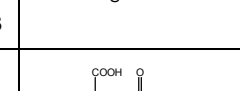
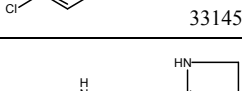
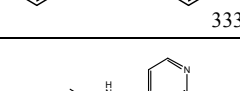
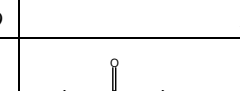
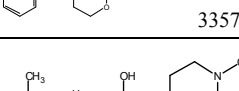
 11656	 11668	 11773	 11825
 11850	 12155	 12161	 12181
 12181	 12363	 12418	 12363
 12492	 12636	 12639	 12650
 12650	 12715	 12770	 12955
 12955	 13028	 13150	 13161
 13176	 13220	 13239	 13316
 13359	 13364	 13378	 13399
 13480	 13512	 13545	 13572
 13579	 13581	 13597	 13705
 13726	 13728	 13768	 13770

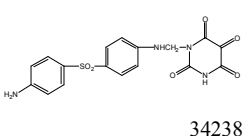
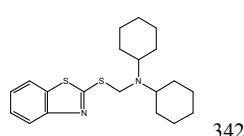
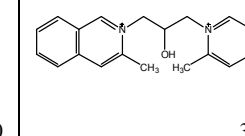
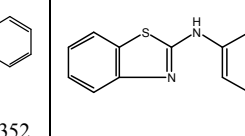
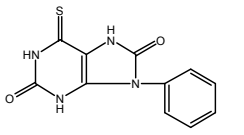
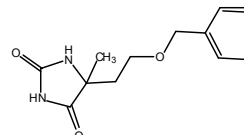
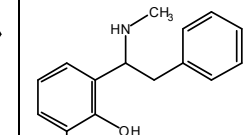
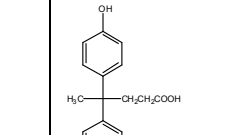
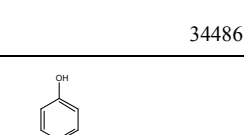
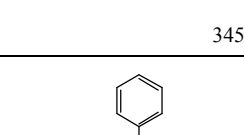
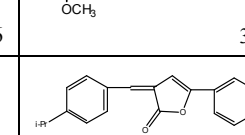
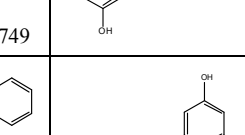
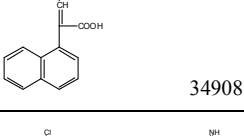
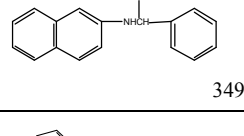
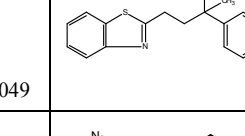
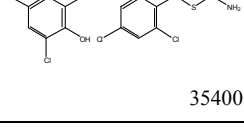
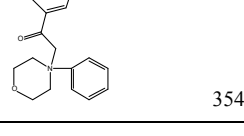
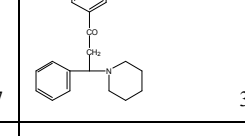
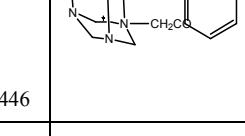
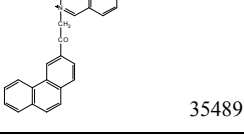
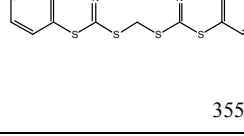
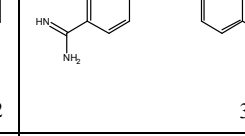
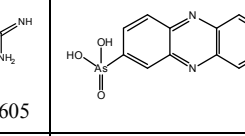
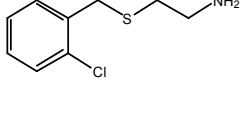
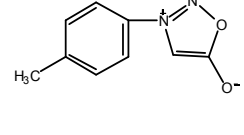
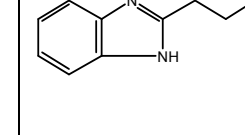
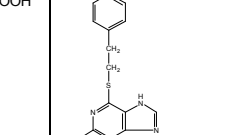
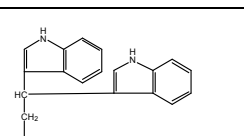
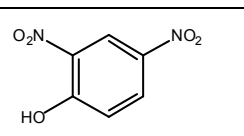
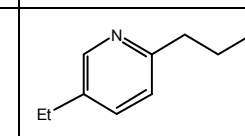
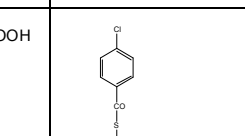
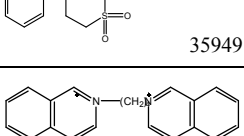
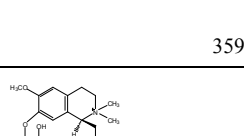
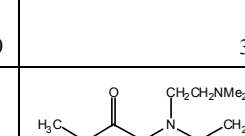
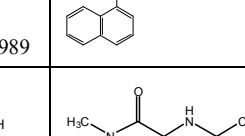
 13776	 13778	 13791	 13816
 13831	 13950	 13970	 13975
 13984	 13987	 13996	 14119
 14141	 14143	 14161	 14163
 14179	 14186	 14288	 14343
 14410	 14543	 14555	 14703
 14711	 14973	 14983	 15135
 15181	 15226	 15234	 15520
 15596	 15602	 15603	 15608
 15623	 15784	 15889	 16087
 16116	 16163	 16168	 16211

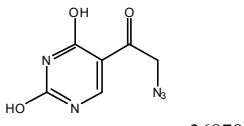
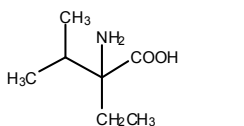
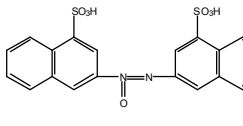
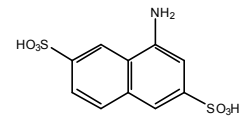
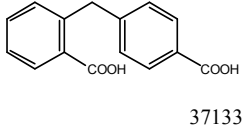
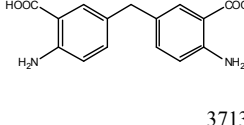
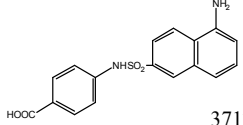
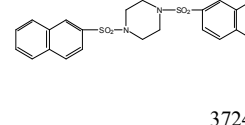
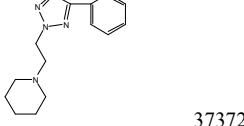
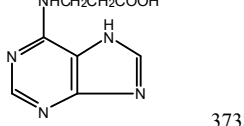
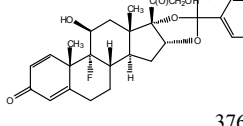
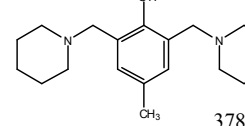
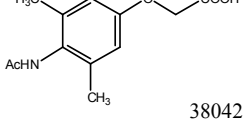
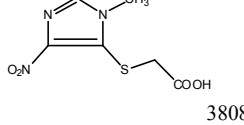
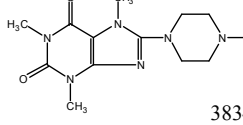
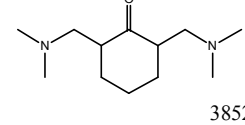
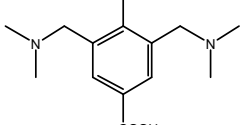
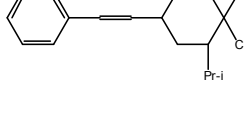
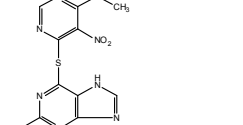
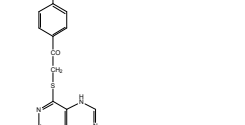
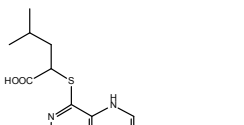
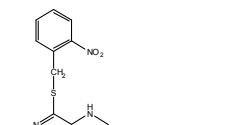
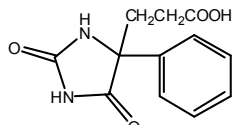
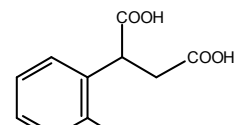
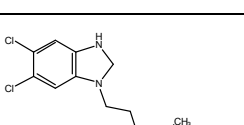
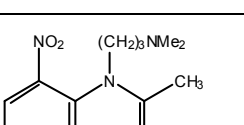
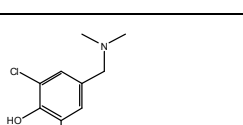
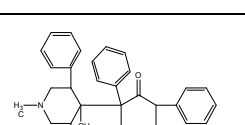
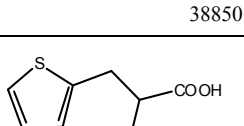
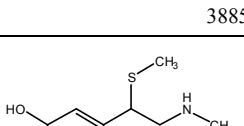
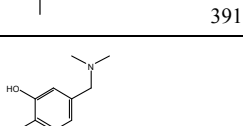
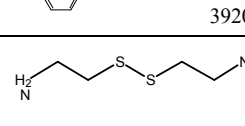
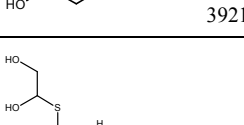
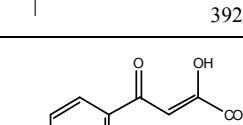
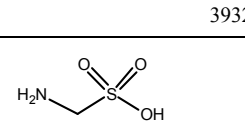
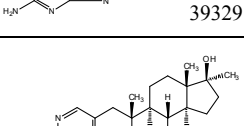
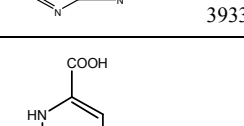
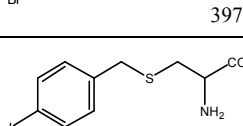
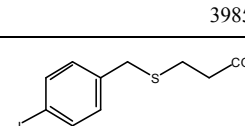
 16311	 16414	 16535	 16555
 16865	 16866	 17061	 17173
 17245	 17338	 17354	 17383
 17387	 17391	 17474	 17580
 17600	 17719	 17770	 17776
 17777	 17779	 17809	 18312
 18320	 18355	 18360	 18368
 18430	 18451	 18613	 18695
 18719	 18758	 18773	 18778
 18807	 18877	 18883	 18891
 18997	 19039	 19097	 19119
 19139	 19147	 19480	 19496

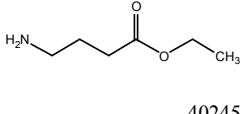
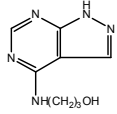
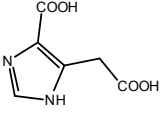
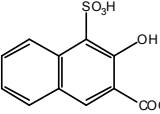
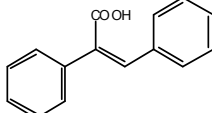
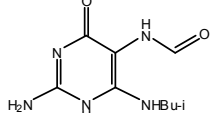
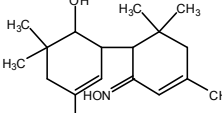
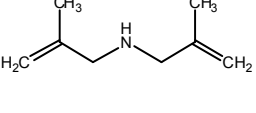
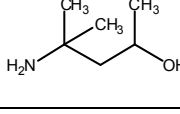
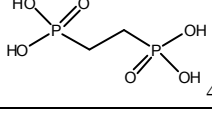
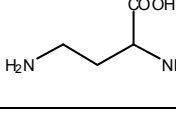
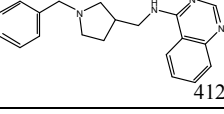
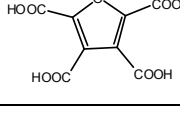
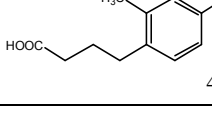
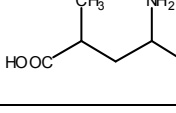
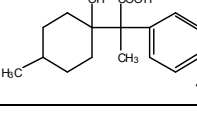
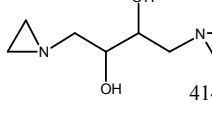
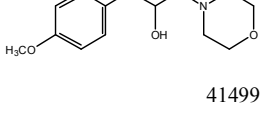
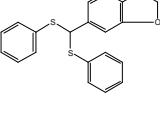
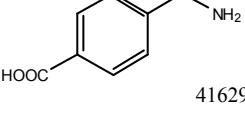
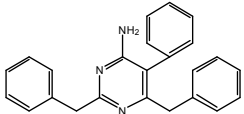
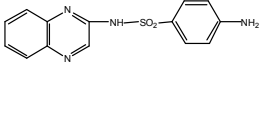
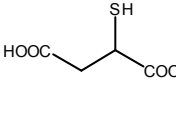
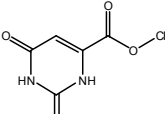
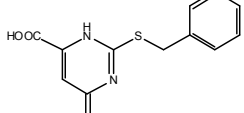
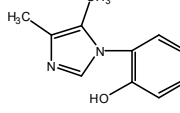
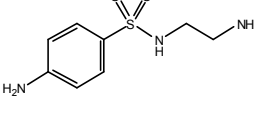
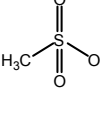
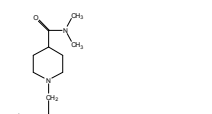
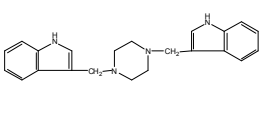
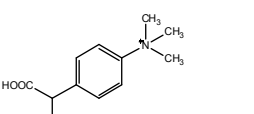
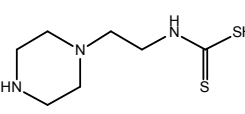
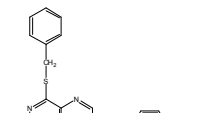
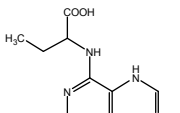
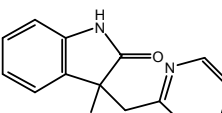
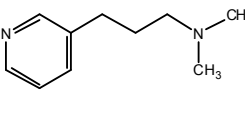
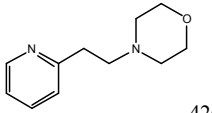
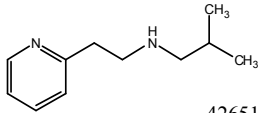
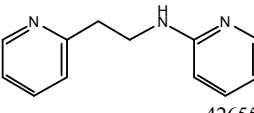
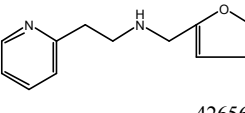
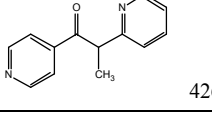
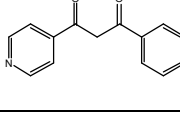
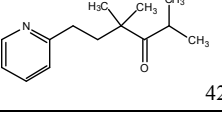
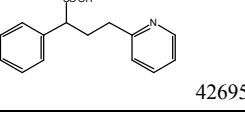
 19509	 19630	 19760	 19832
 19976	 19995	 20138	 20207
 20410	 20707	 20708	 20878
 21061	 21278	 21434	 21438
 21518	 21588	 21702	 21706
 21948	 22225	 22242	 22368
 22819	 22854	 22959	 22976
 22992	 23016	 23082	 23128
 23159	 23173	 23183	 23217
 23478	 23583	 23807	 23833
 23880	 23904	 23922	 23925

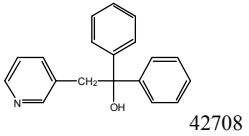
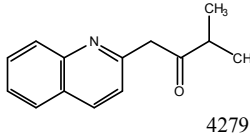
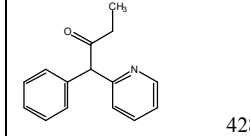
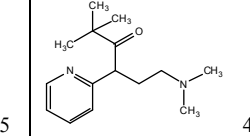
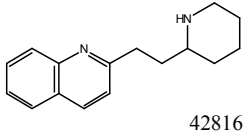
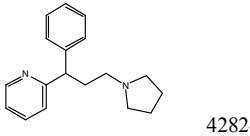
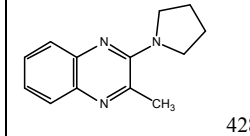
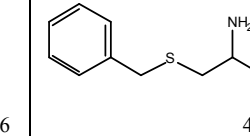
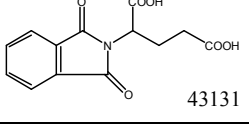
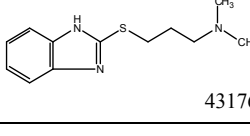
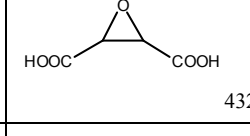
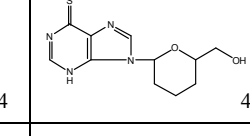
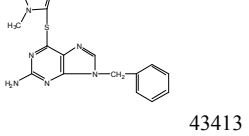
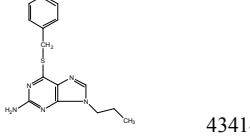
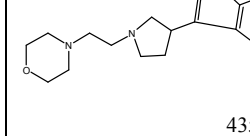
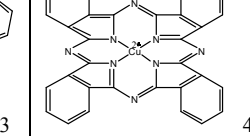
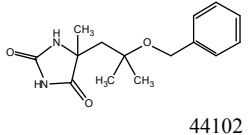
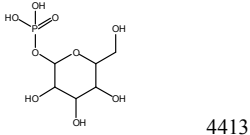
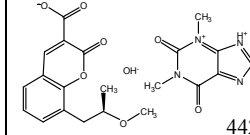
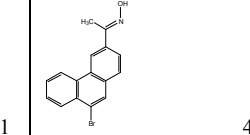
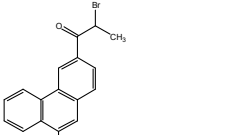
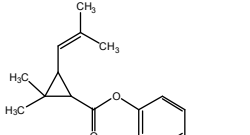
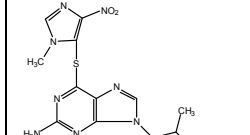
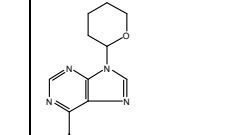
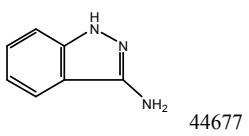
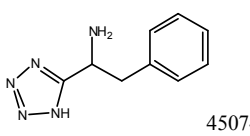
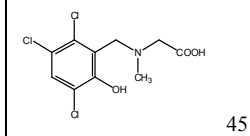
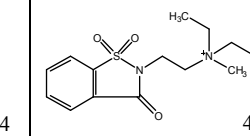
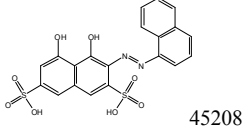
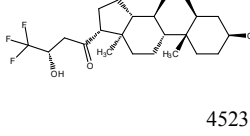
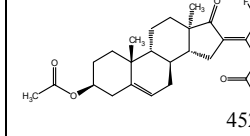
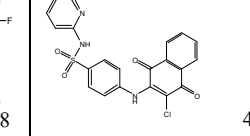
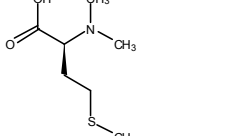
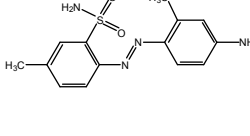
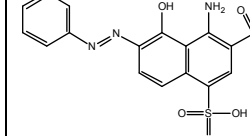
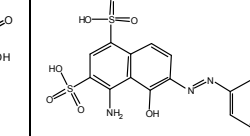
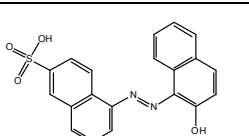
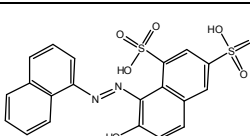
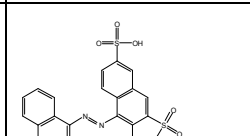
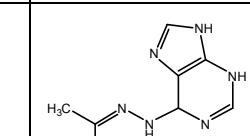


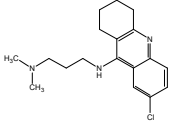
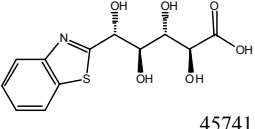
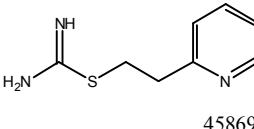
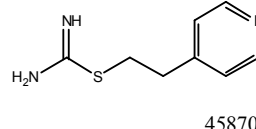
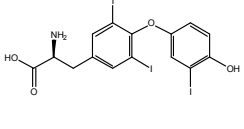
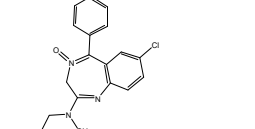
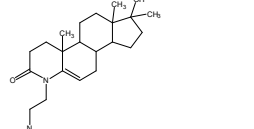
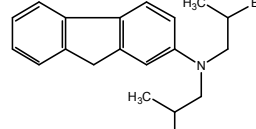
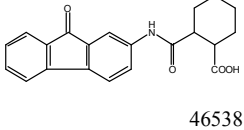
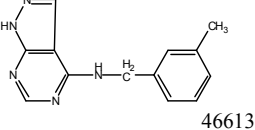
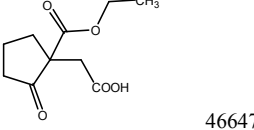
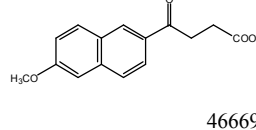
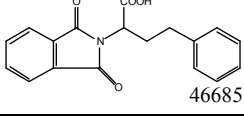
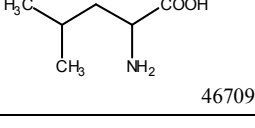
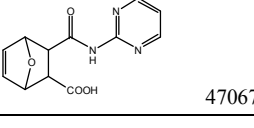
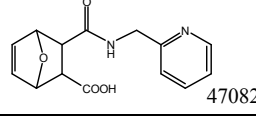
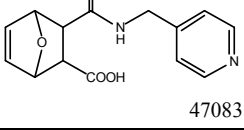
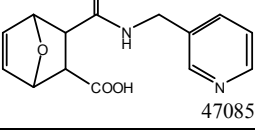
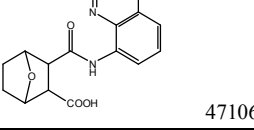
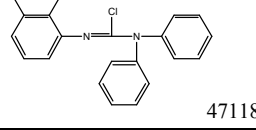
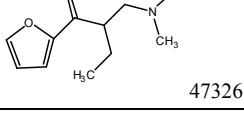
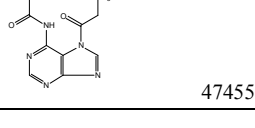
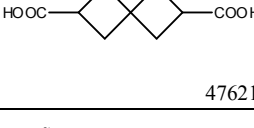
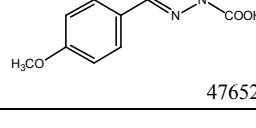
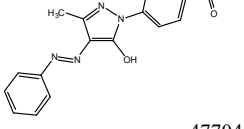
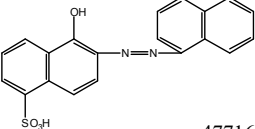
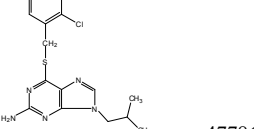
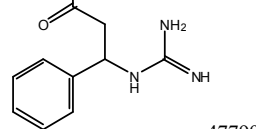
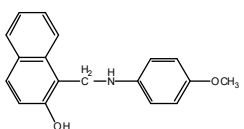
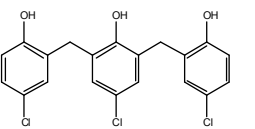
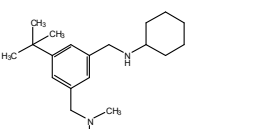
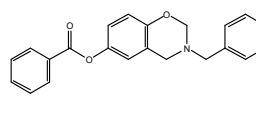
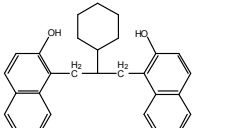
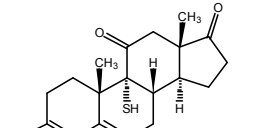
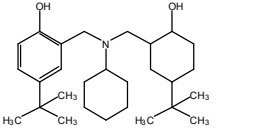
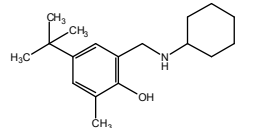
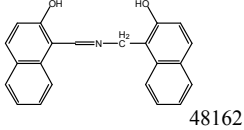
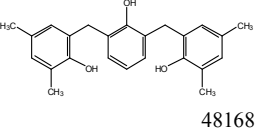
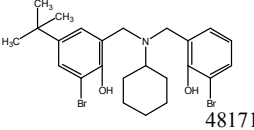
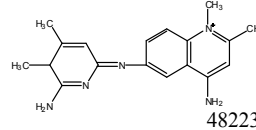
 28086	 28136	 28311	 28408
 28427	 28527	 28620	 28743
 28977	 28992	 29096	 29101
 29192	 29209	 29424	 29448
 29870	 30079	 30080	 30144
 30154	 30188	 30408	 30534
 30712	 30799	 31076	 31303
 31321	 31660	 31698	 32656
 32673	 32963	 33035	 33052
 33145	 33389	 33495	 33571
 33719	 33761	 34003	 34008

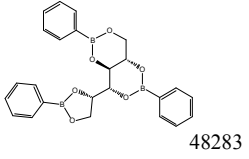
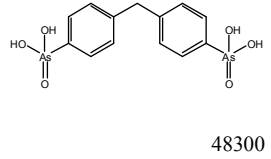
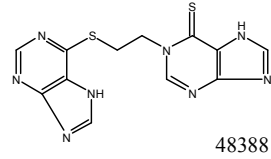
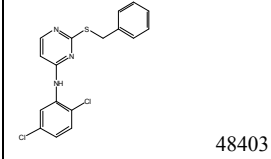
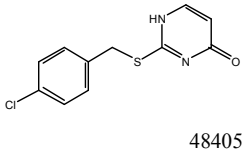
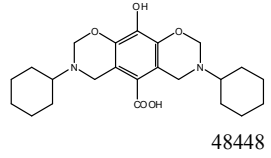
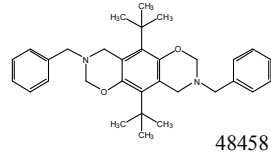
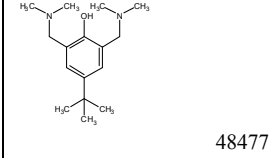
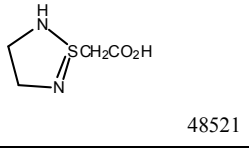
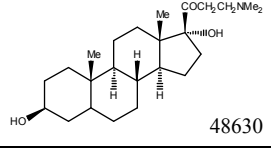
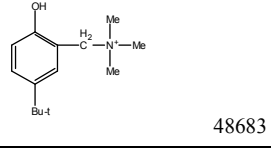
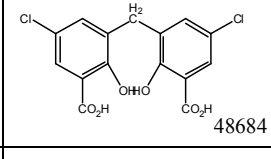
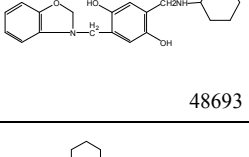
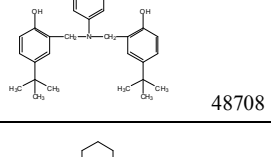
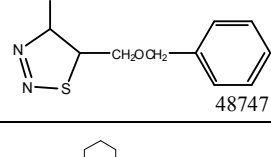
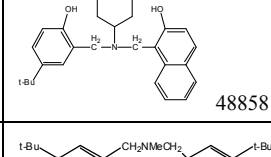
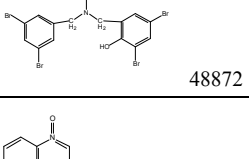
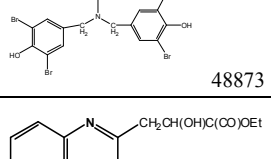
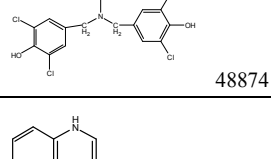
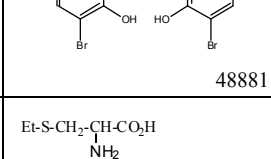
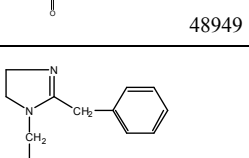
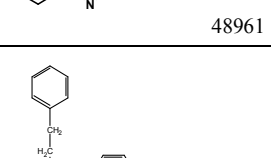
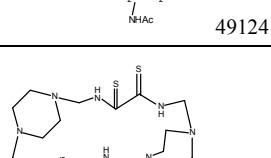
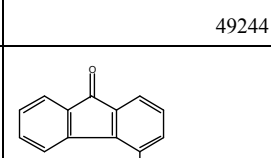
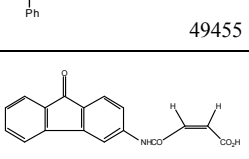
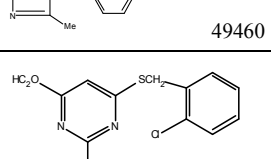
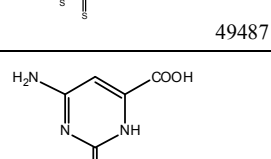
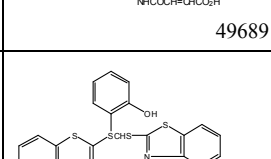
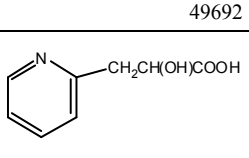
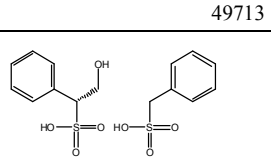
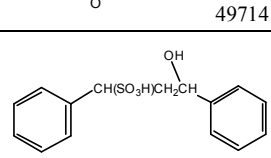
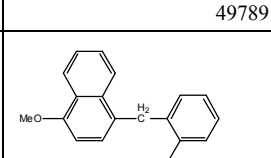
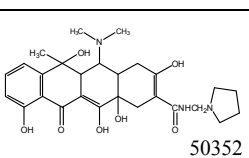
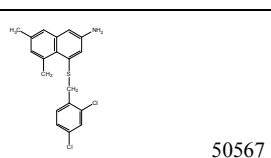
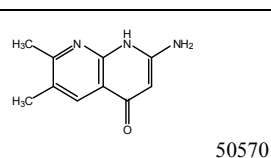
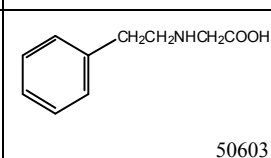
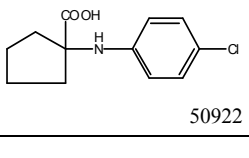
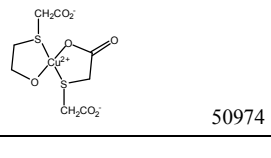
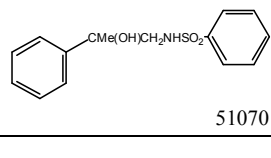
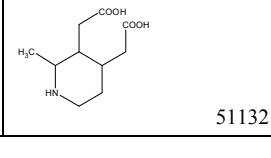
 34238	 34240	 34352	 34444
 34486	 34506	 34749	 34824
 34908	 34924	 35049	 35334
 35400	 35427	 35446	 35450
 35489	 35582	 35605	 35682
 35755	 35761	 35790	 35866
 35949	 35950	 35989	 35991
 36369	 36387	 36533	 36534
 36738	 36806	 36819	 36824

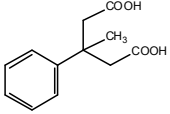
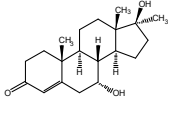
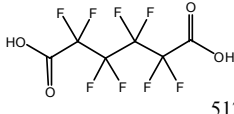
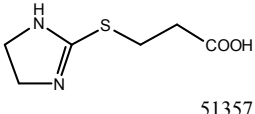
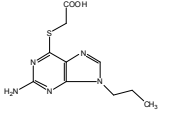
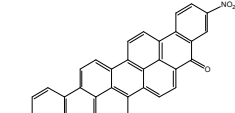
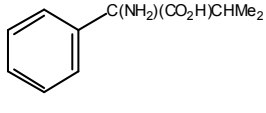
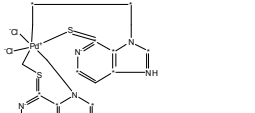
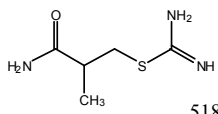
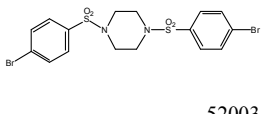
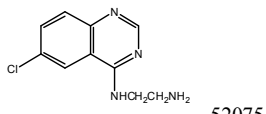
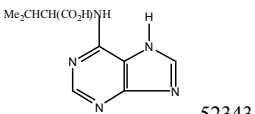
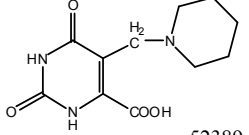
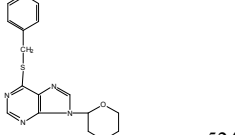
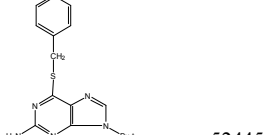
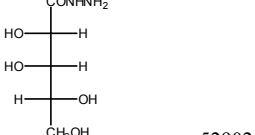
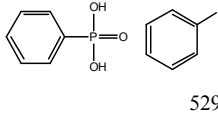
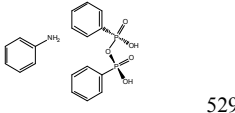
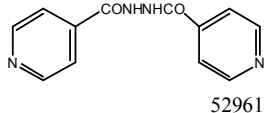
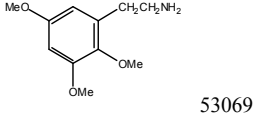
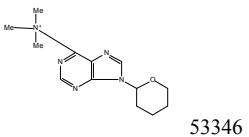
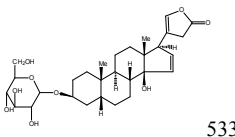
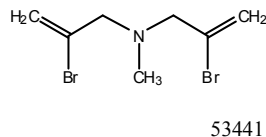
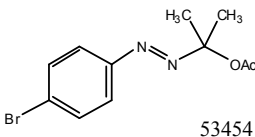
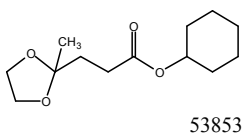
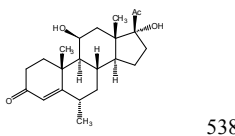
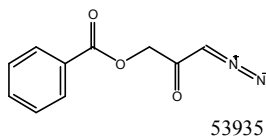
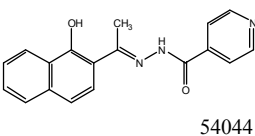
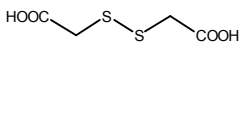
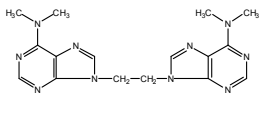
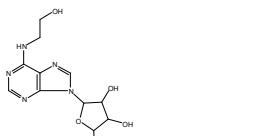
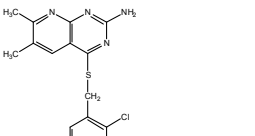
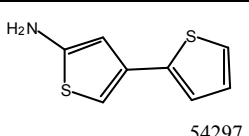
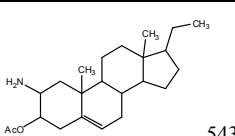
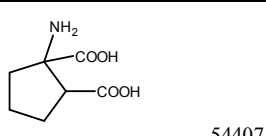
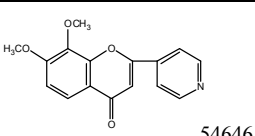
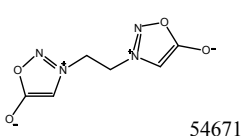
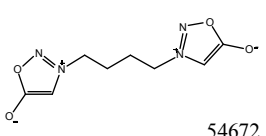
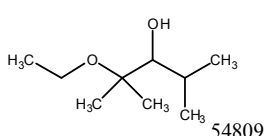
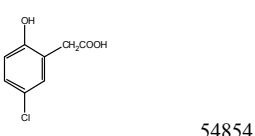
 36878	 37018	 37031	 37049
 37133	 37136	 37173	 37245
 37372	 37388	 37641	 37881
 38042	 38081	 38347	 38525
 38528	 38684	 38732	 38733
 38735	 38737	 38743	 38777
 38850	 38852	 39187	 39207
 39209	 39215	 39225	 39322
 39329	 39332	 39779	 39851
 39863	 39961	 40016	 40019

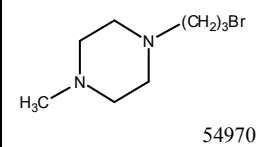
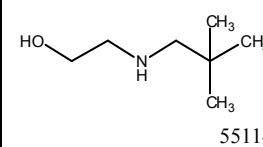
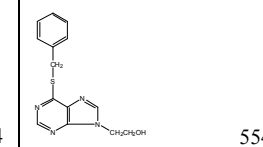
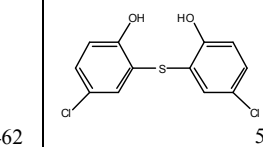
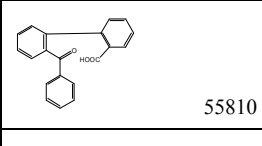
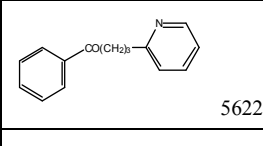
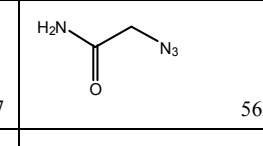
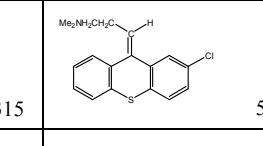
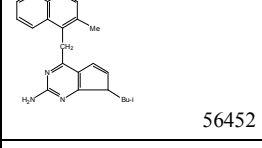
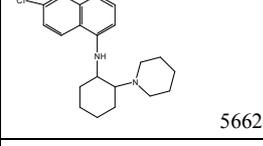
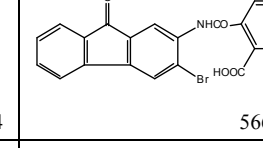
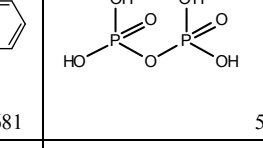
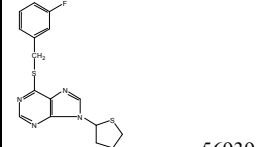
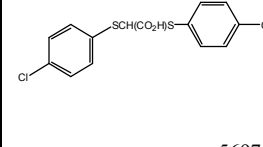
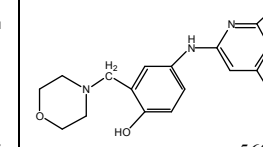
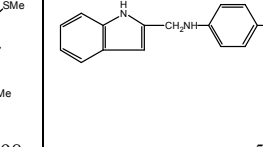
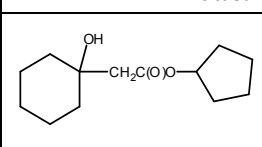
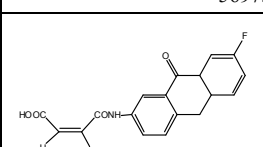
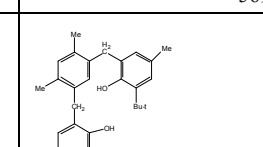
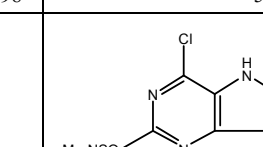
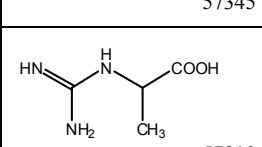
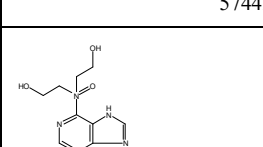
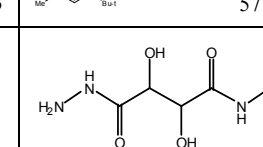
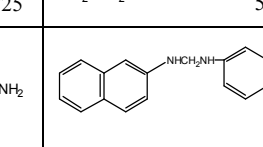
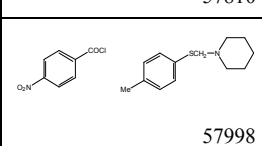
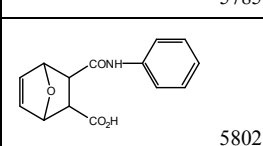
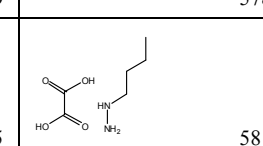
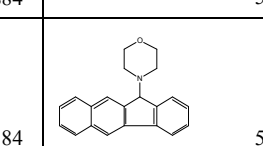
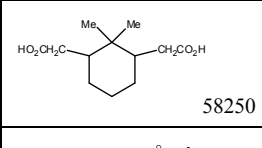
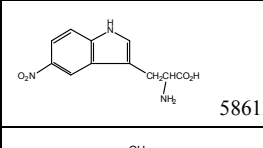
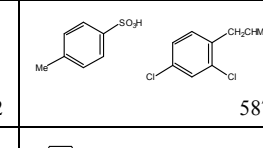
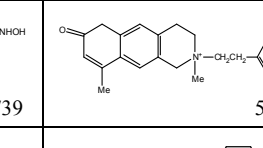
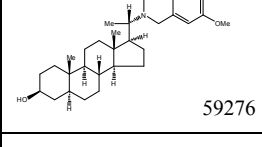
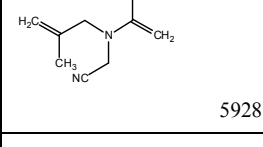
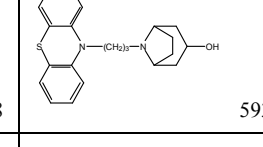
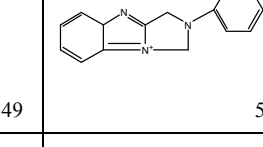
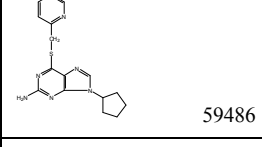
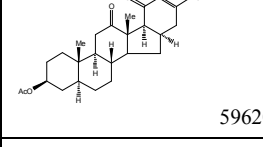
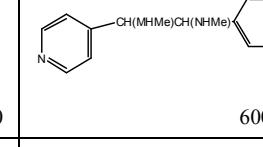
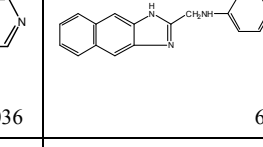
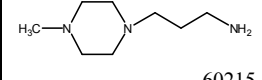
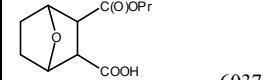
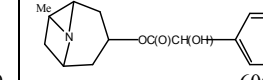
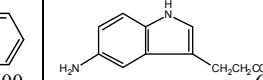
 40245	 40380	 40384	 40596
 40614	 40663	 40781	 40787
 40792	 40837	 41117	 41274
 41309	 41313	 41355	 41431
 41458	 41499	 41550	 41629
 41663	 41805	 41809	 42009
 42010	 42069	 42167	 42199
 42255	 42258	 42325	 42352
 42384	 42414	 42448	 42636
 42645	 42651	 42655	 42656
 42665	 42679	 42688	 42695

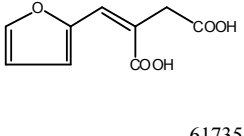
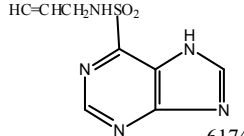
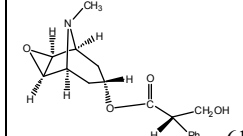
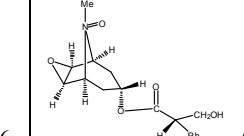
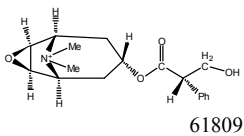
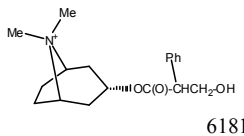
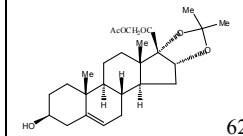
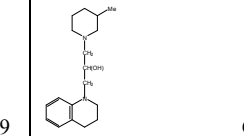
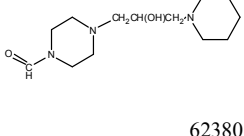
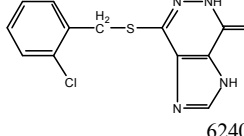
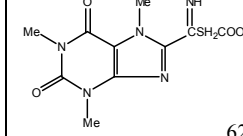
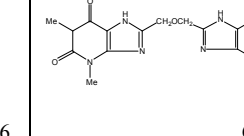
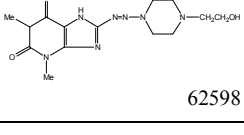
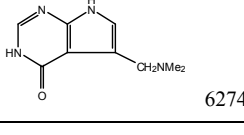
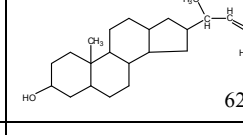
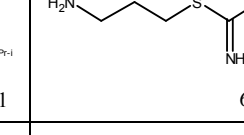
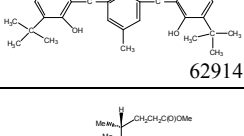
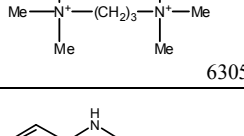
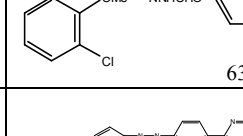
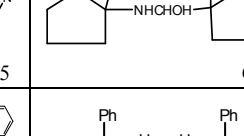
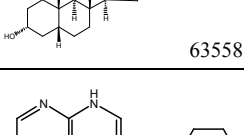
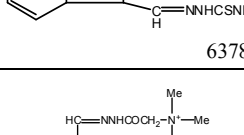
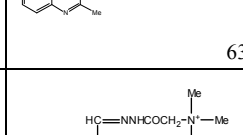
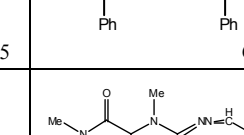
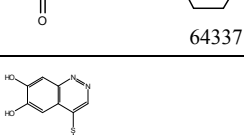
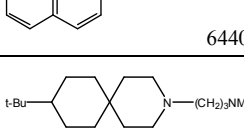
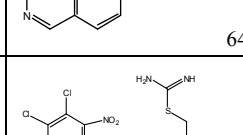
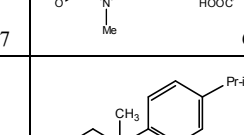
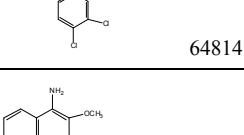
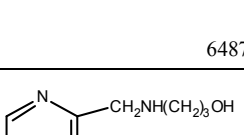
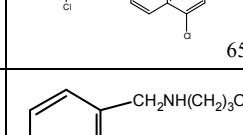
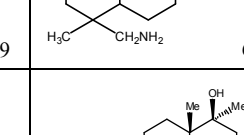
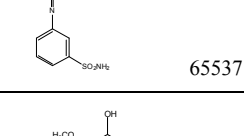
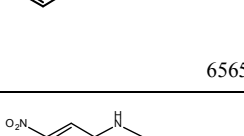
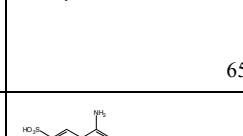
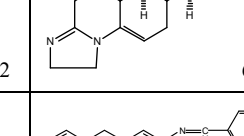
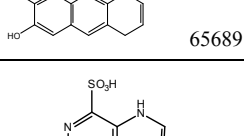
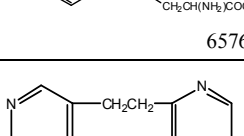
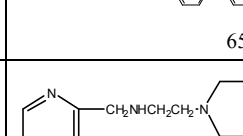
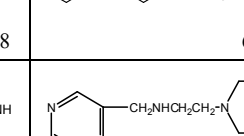
 42708	 42797	 42805	 42808
 42816	 42824	 42846	 43125
 43131	 43176	 43234	 43409
 43413	 43414	 43513	 43628
 44102	 44138	 44251	 44477
 44480	 44547	 44585	 44596
 44677	 45074	 45114	 45126
 45208	 45236	 45238	 45382
 45514	 45527	 45554	 45572
 45576	 45582	 45583	 45641

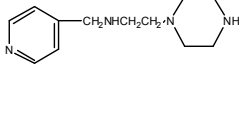
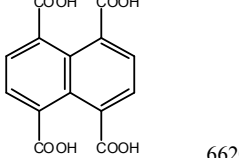
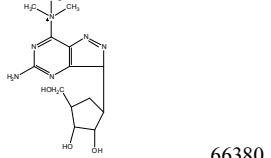
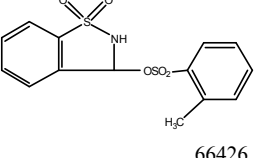
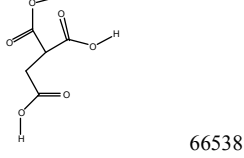
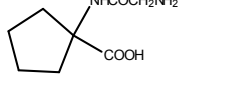
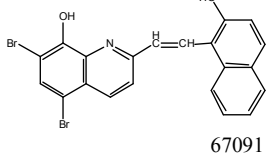
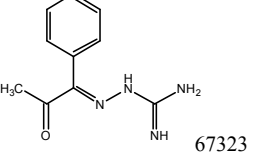
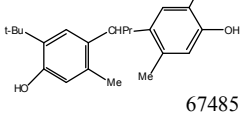
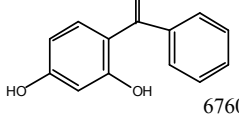
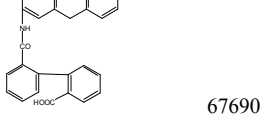
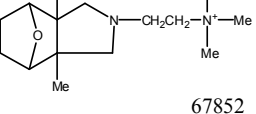
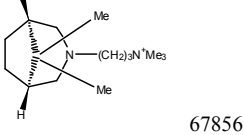
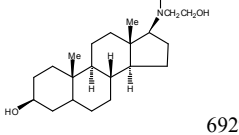
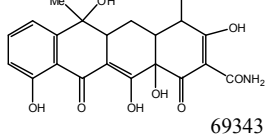
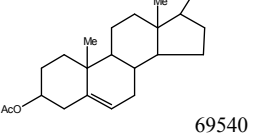
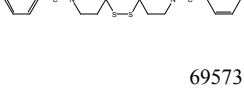
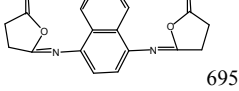
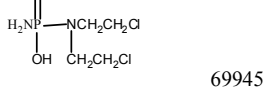
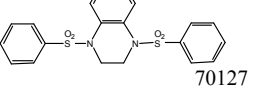
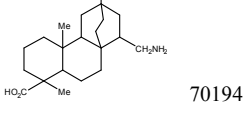
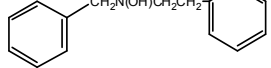
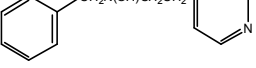
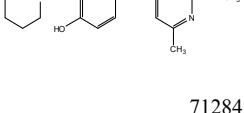
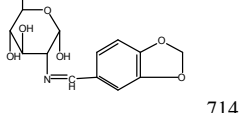
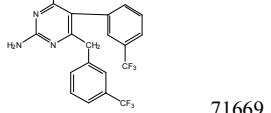
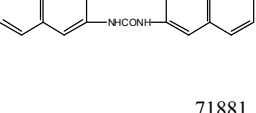
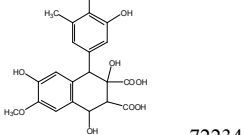
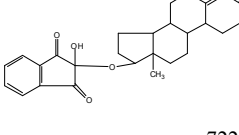
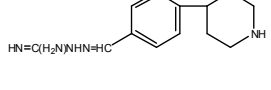
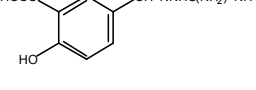
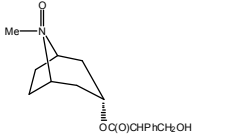
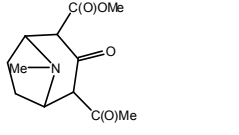
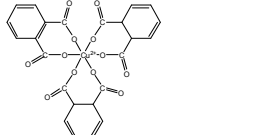
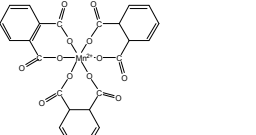
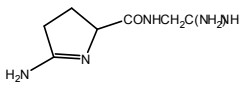
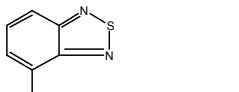
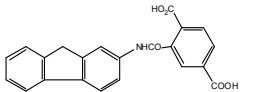
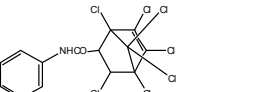
 45730	 45741	 45869	 45870
 46046	 46080	 46480	 46529
 46538	 46613	 46647	 46669
 46685	 46709	 47067	 47082
 47083	 47085	 47106	 47118
 47326	 47455	 47621	 47652
 47704	 47716	 47786	 47799
 47924	 47932	 47935	 47938
 47949	 48010	 48151	 48160
 48162	 48168	 48171	 48223

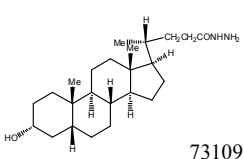
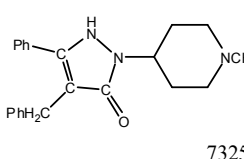
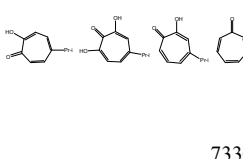
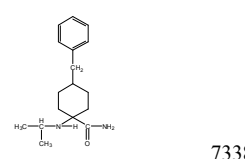
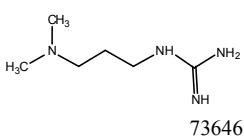
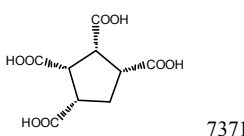
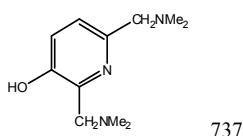
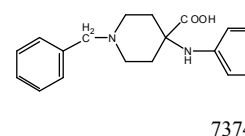
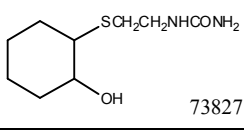
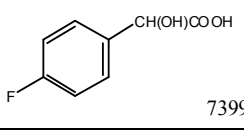
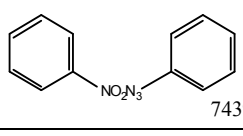
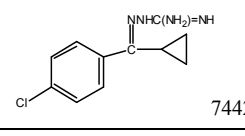
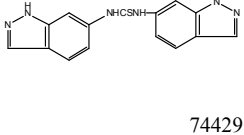
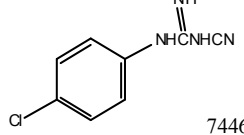
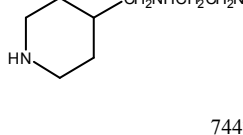
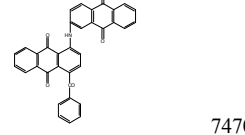
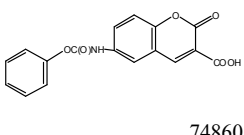
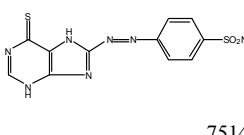
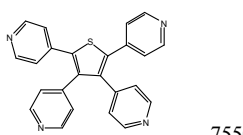
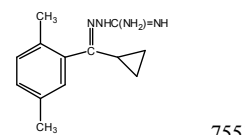
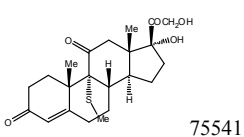
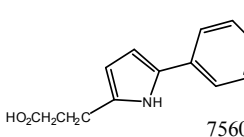
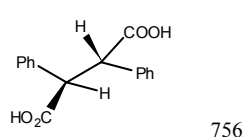
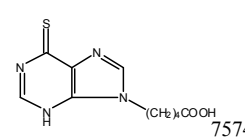
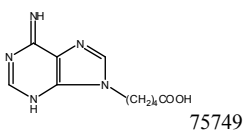
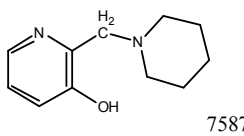
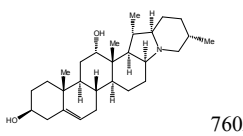
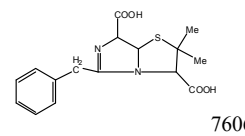
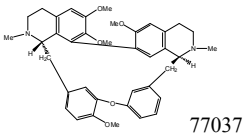
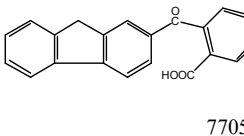
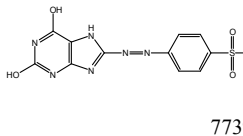
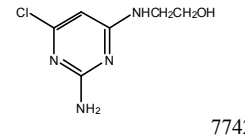
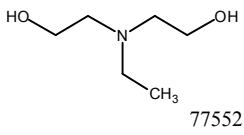
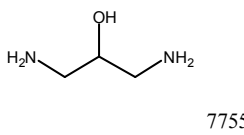
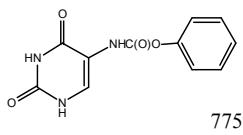
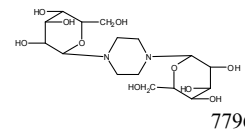
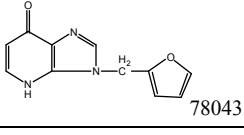
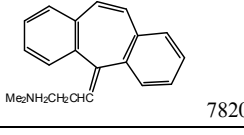
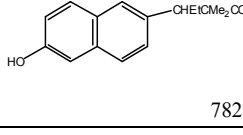
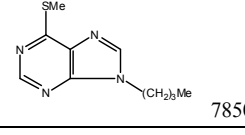
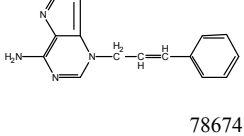
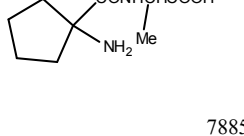
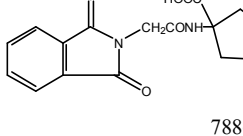
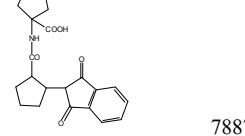
 48283	 48300	 48388	 48403
 48405	 48448	 48458	 48477
 48521	 48630	 48683	 48684
 48693	 48708	 48747	 48858
 48872	 48873	 48874	 48881
 48949	 48961	 49124	 49244
 49455	 49460	 49487	 49689
 49692	 49713	 49714	 49789
 49848	 50137	 50145	 50155
 50352	 50567	 50570	 50603
 50922	 50974	 51070	 51132

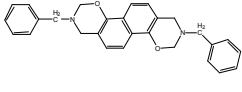
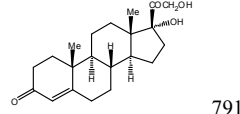
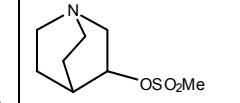
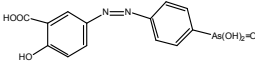
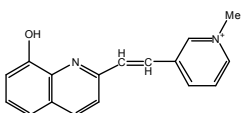
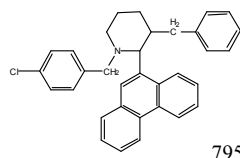
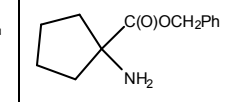
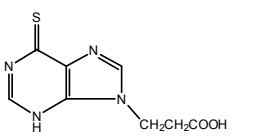
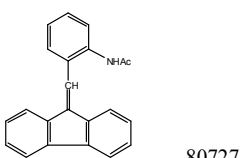
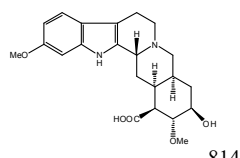
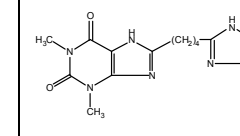
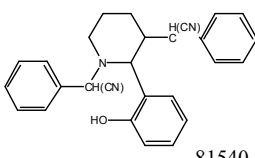
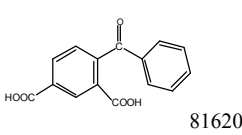
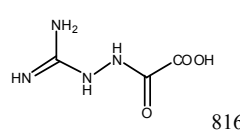
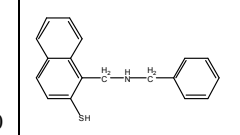
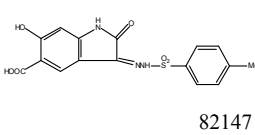
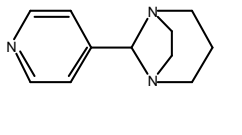
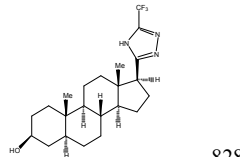
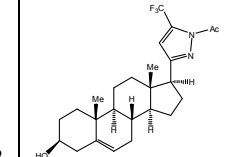
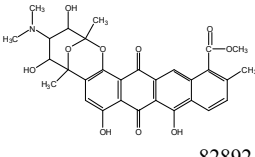
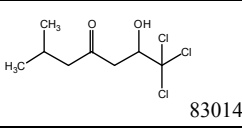
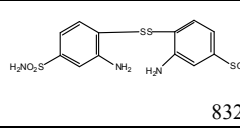
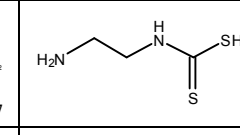
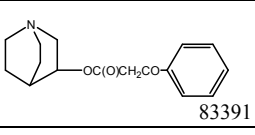
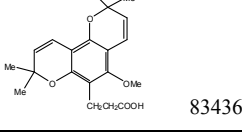
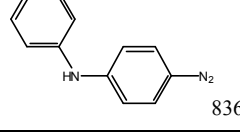
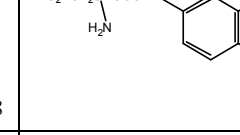
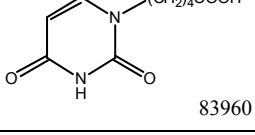
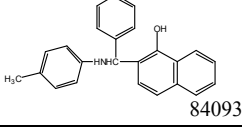
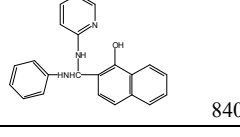
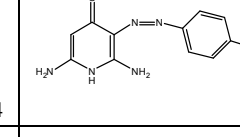
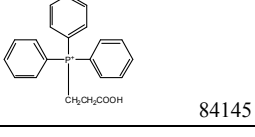
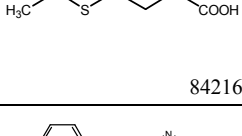
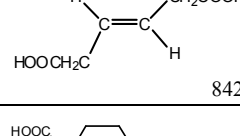
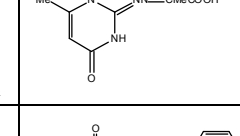
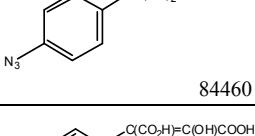
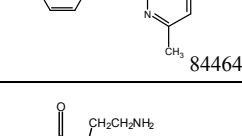
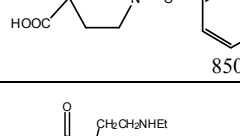
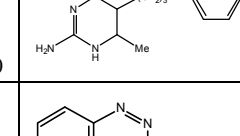
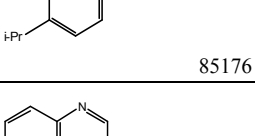
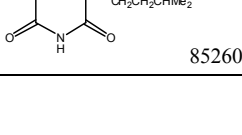
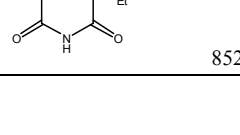
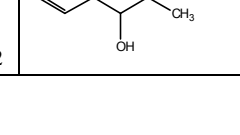
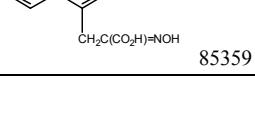
 51135	 51182	 51277	 51357
 51470	 51535	 51810	 51857
 51867	 52003	 52075	 52343
 52389	 52440	 52445	 52902
 52927	 52929	 52961	 53069
 53346	 53396	 53441	 53454
 53853	 53892	 53935	 54044
 54088	 54101	 54251	 54278
 54297	 54340	 54407	 54646
 54671	 54672	 54809	 54854

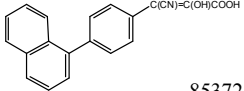
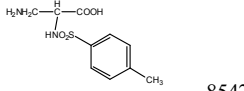
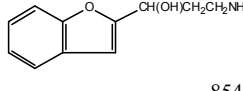
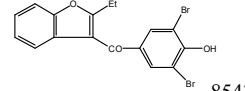
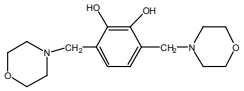
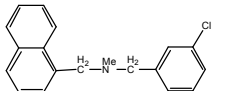
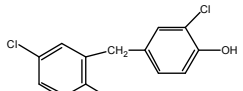
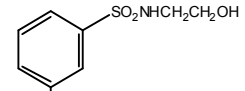
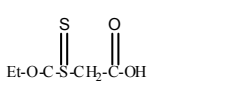
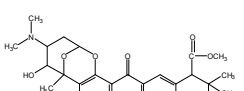
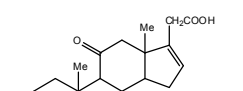
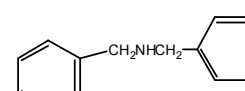
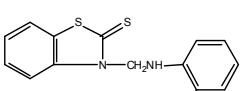
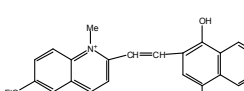
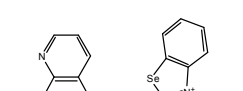
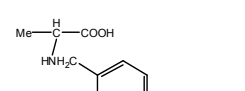
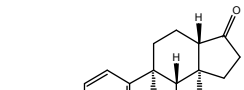
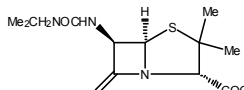
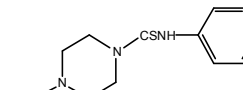
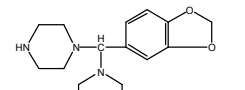
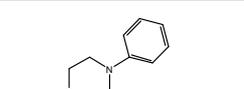
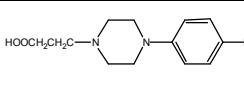
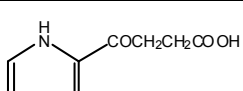
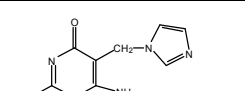
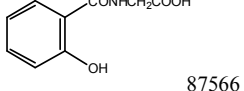
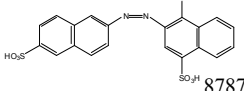
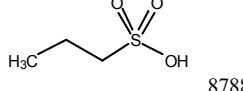
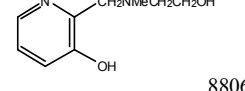
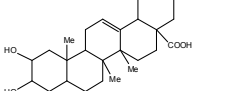
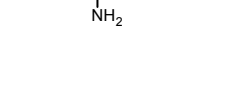
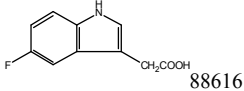
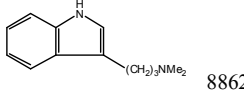
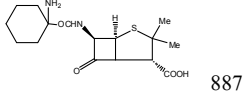
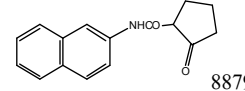
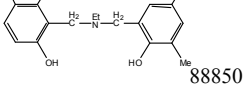
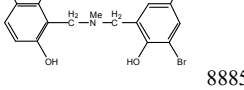
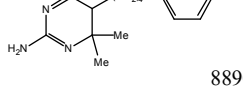
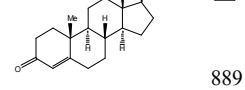
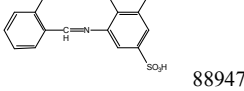
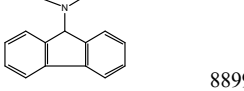
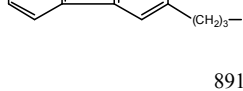
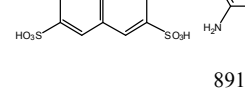
 54970	 55114	 55462	 55636
 55810	 56227	 56315	 56378
 56452	 56624	 56681	 56751
 56939	 56975	 56998	 57050
 57345	 57443	 57725	 57788
 57810	 57850	 57884	 57975
 57998	 58025	 58184	 58255
 58250	 58612	 58739	 59275
 59276	 59288	 59349	 59413
 59486	 59620	 60036	 60043
 60215	 60379	 60600	 61297

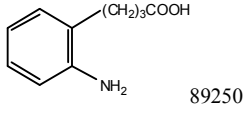
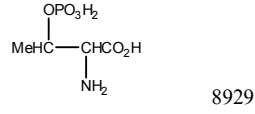
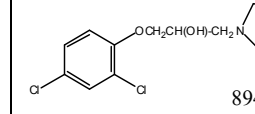
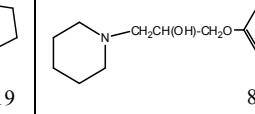
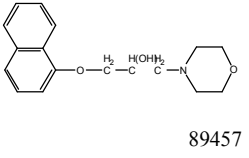
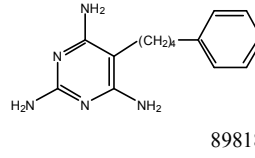
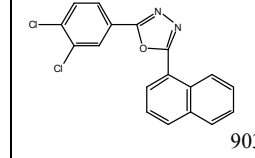
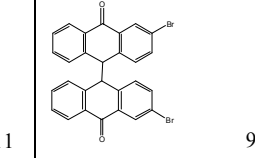
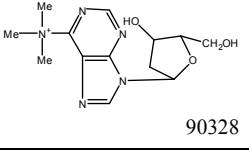
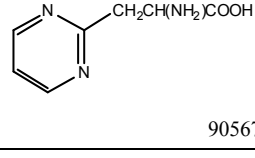
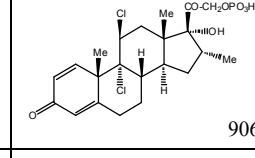
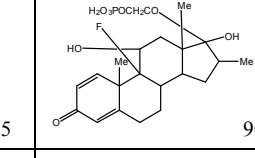
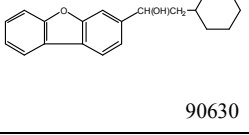
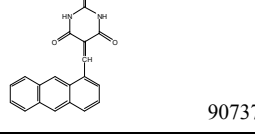
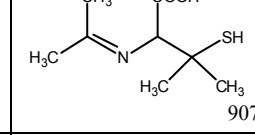
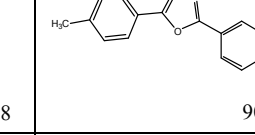
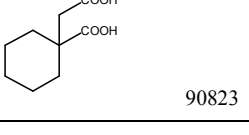
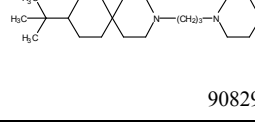
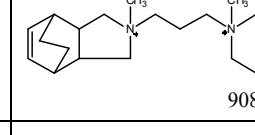
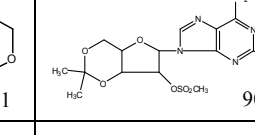
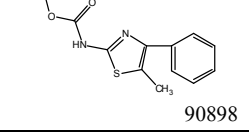
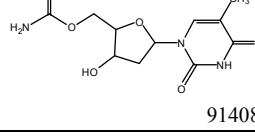
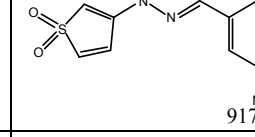
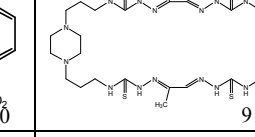
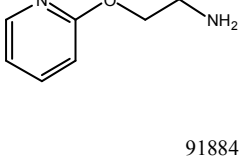
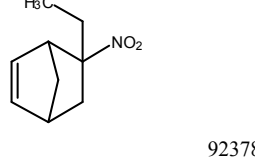
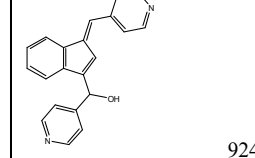
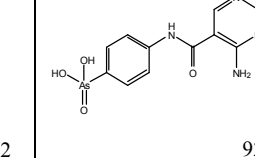
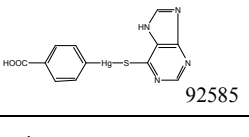
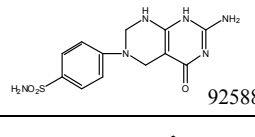
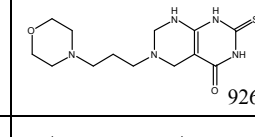
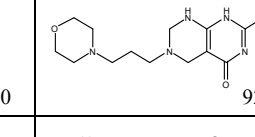
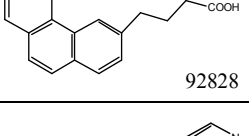
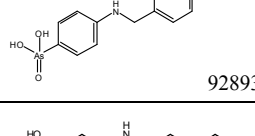
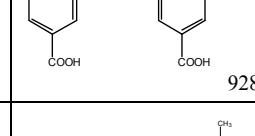
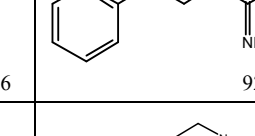
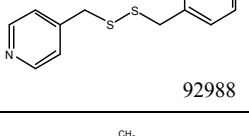
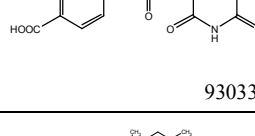
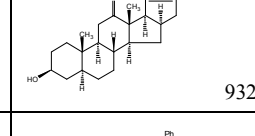
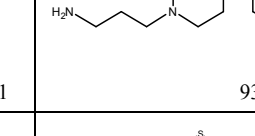
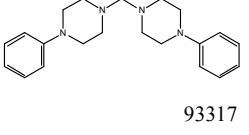
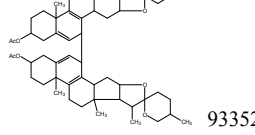
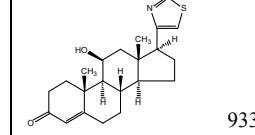
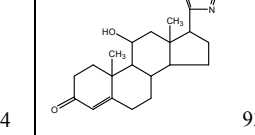
 61735	$\text{HC}=\text{CHCH}_2\text{NHSO}_2$  61747	 61806	 61807
 61809	 61810	 62349	 62378
 62380	 62406	 62586	 62594
 62598	 62749	 62791	 62857
 62914	 63052	 63135	 63331
 63558	 63786	 63875	 64111
 64337	 64408	 64617	 64678
 64814	 64875	 65219	 65238
 65537	 65650	 65652	 65683
 65689	 65763	 65828	 65933
 65990	 66162	 66183	 66184

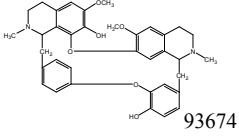
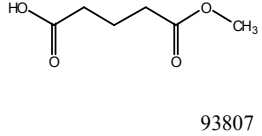
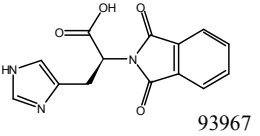
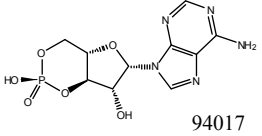
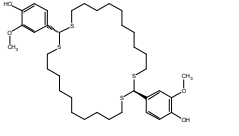
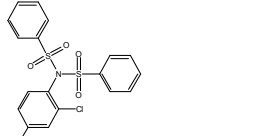
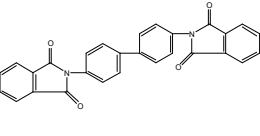
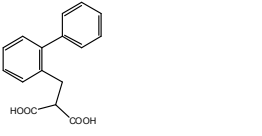
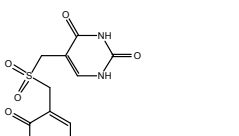
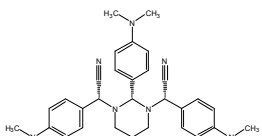
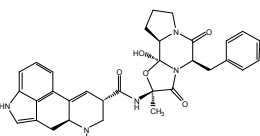
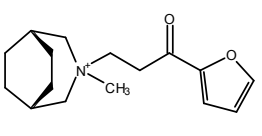
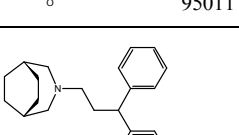
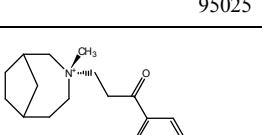
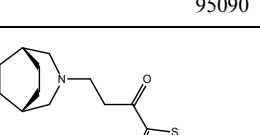
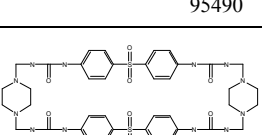
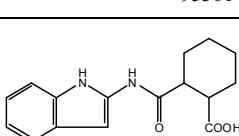
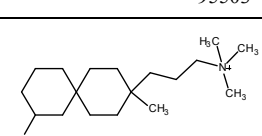
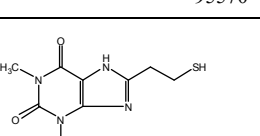
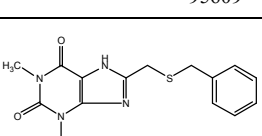
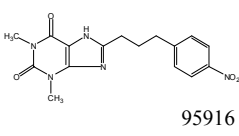
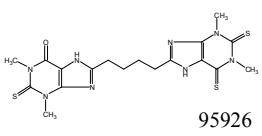
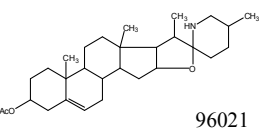
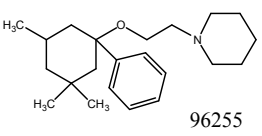
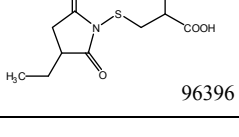
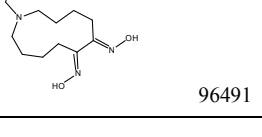
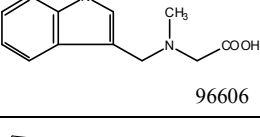
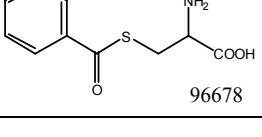
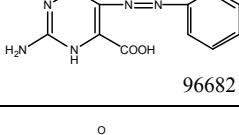
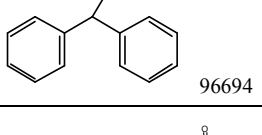
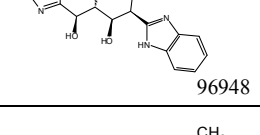
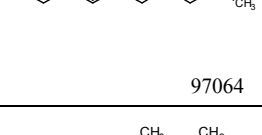
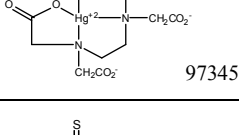
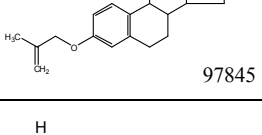
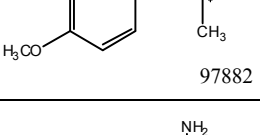
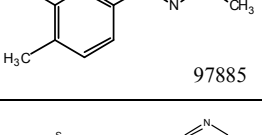
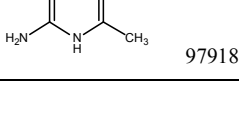
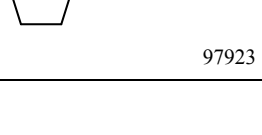
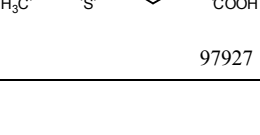
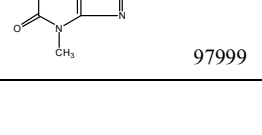
			
66185	66207	66380	66426
			
66538	66796	67091	67323
			
67485	67608	67690	67852
			
67856	69298	69343	69540
			
69573	69575	69945	70127
			
70194	70769	70817	70818
			
71284	71426	71669	71881
			
72234	72254	72528	72533
			
72861	72914	72938	72939
			
72942	73013	73100	73101

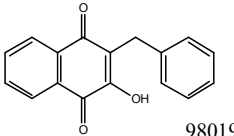
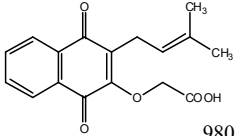
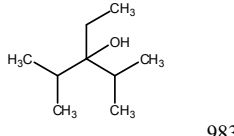
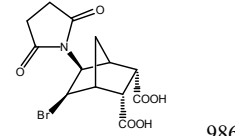
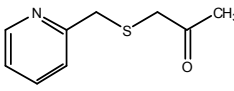
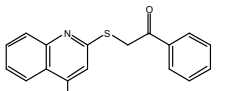
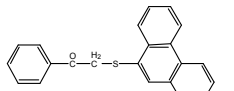
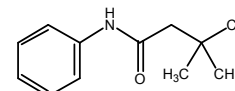
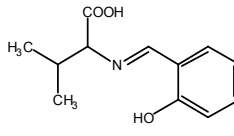
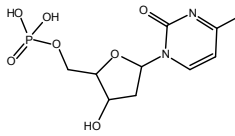
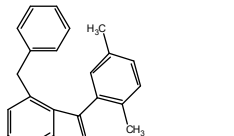
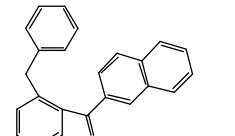
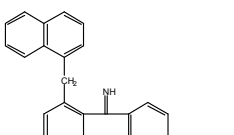
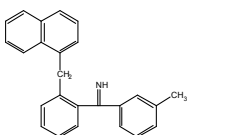
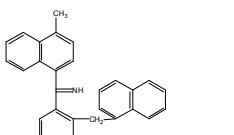
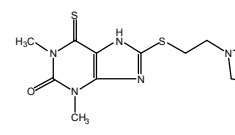
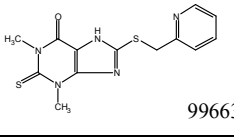
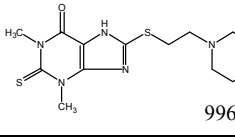
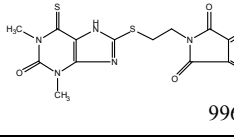
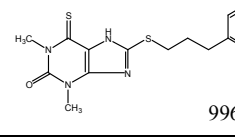
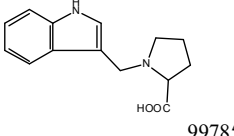
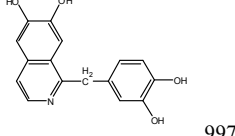
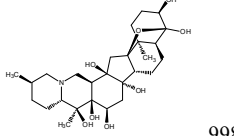
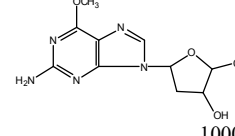
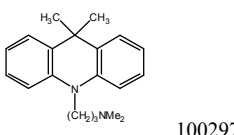
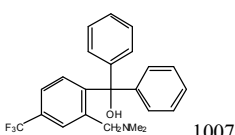
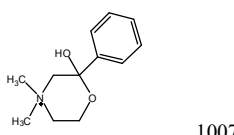
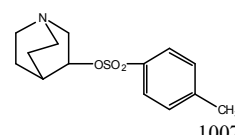
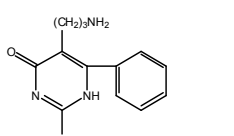
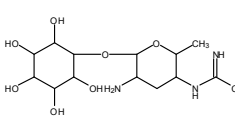
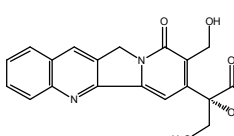
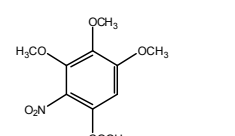
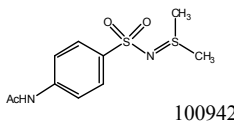
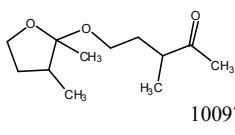
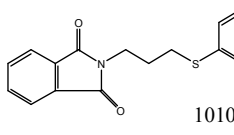
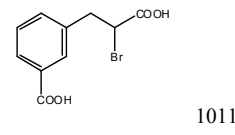
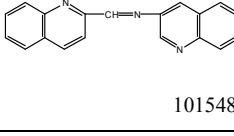
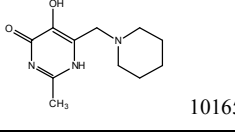
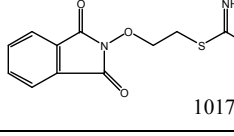
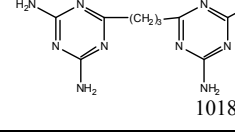
 73109	 73254	 73300	 73389
 73646	 73712	 73721	 73748
 73827	 73990	 74390	 74420
 74429	 74463	 74472	 74702
 74860	 75140	 75503	 75513
 75541	 75600	 75627	 75747
 75749	 75877	 76026	 76064
 77037	 77053	 77393	 77427
 77552	 77554	 77597	 77963
 78043	 78206	 78296	 78508
 78674	 78857	 78864	 78871

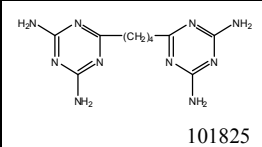
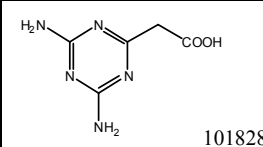
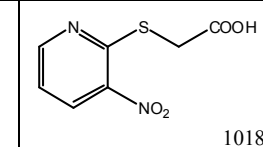
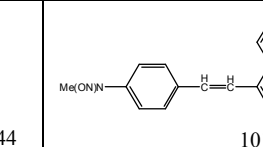
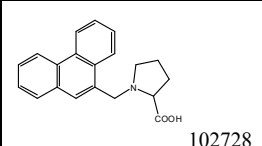
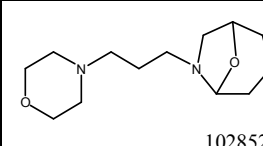
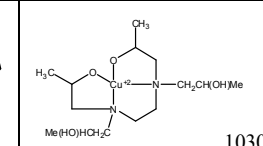
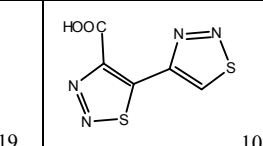
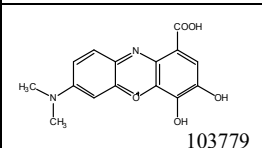
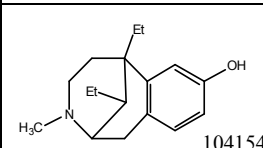
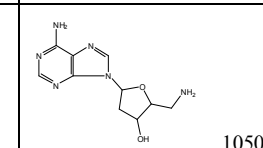
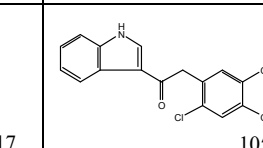
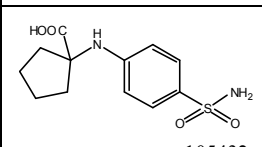
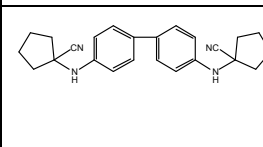
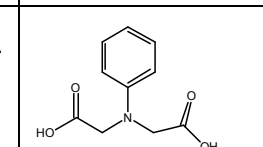
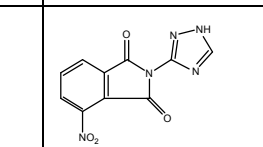
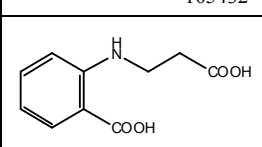
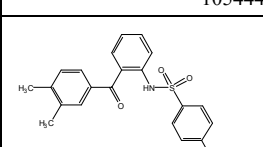
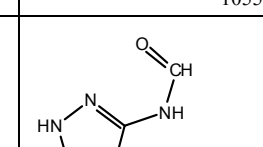
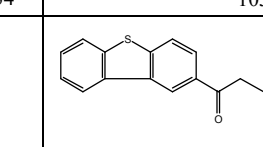
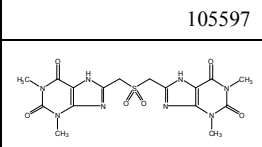
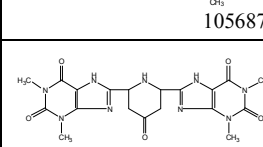
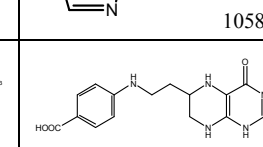
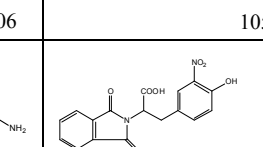
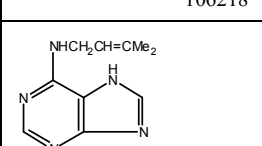
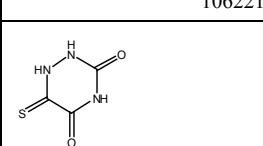
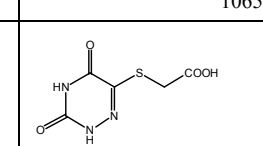
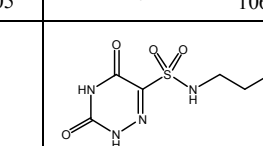
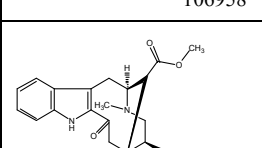
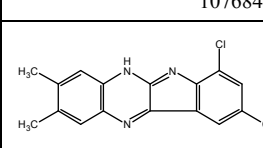
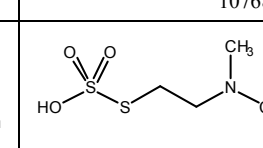
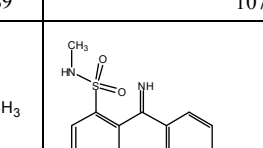
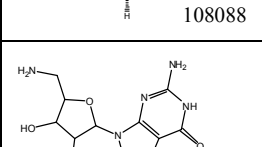
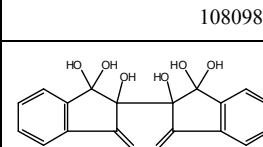
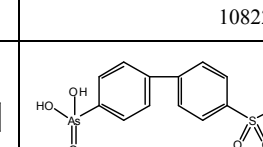
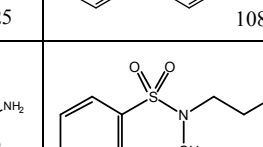
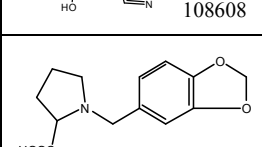
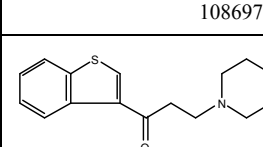
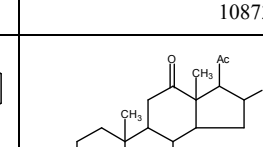
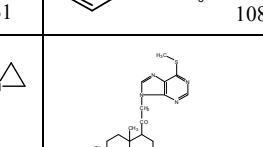
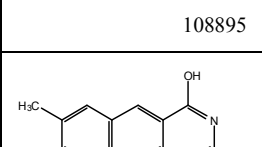
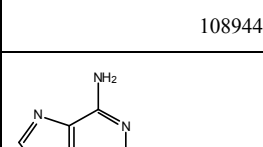
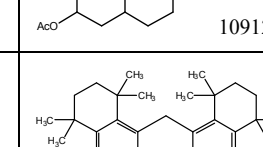
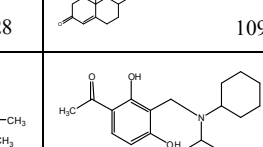
 79050	 79103	 79422	 79529
 79547	 79563	 80126	 80177
 80727	 81463	 81509	 81540
 81620	 81670	 81747	 82147
 82339	 82802	 82803	 82892
 83014	 83217	 83224	 83391
 83436	 83628	 83633	 83960
 84093	 84094	 84130	 84145
 84216	 84221	 84251	 84460
 84464	 85010	 85069	 85176
 85260	 85262	 85323	 85359

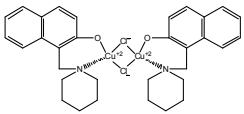
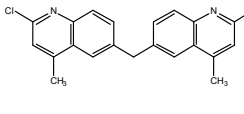
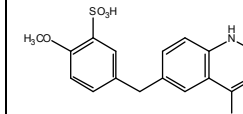
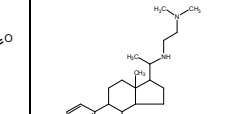
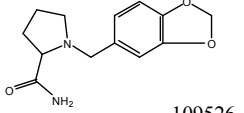
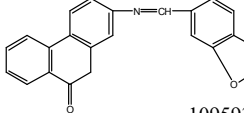
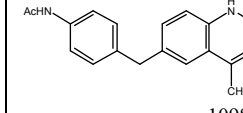
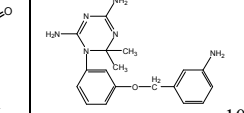
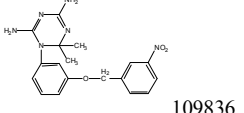
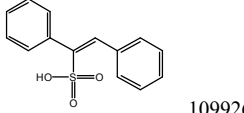
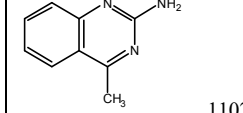
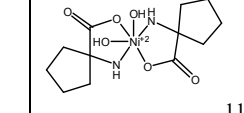
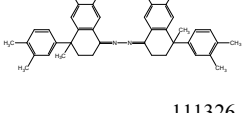
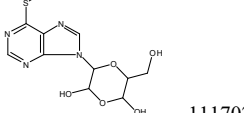
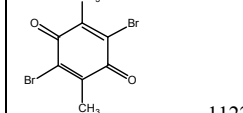
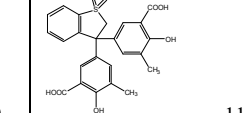
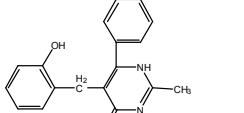
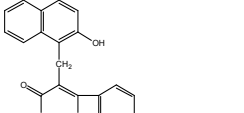
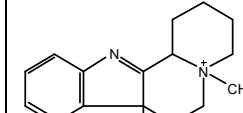
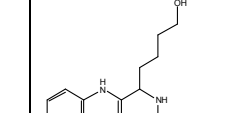
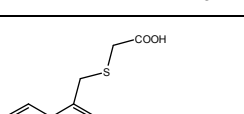
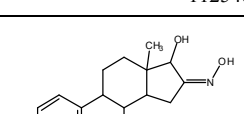
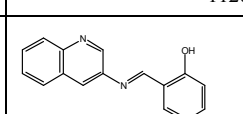
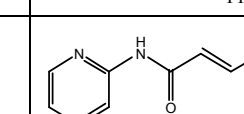
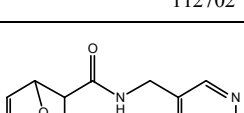
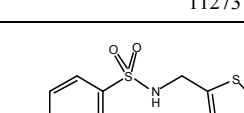
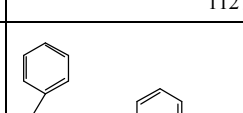
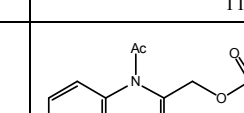
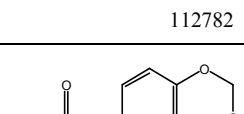
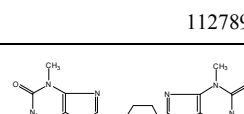
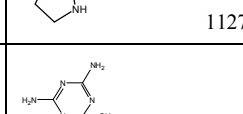
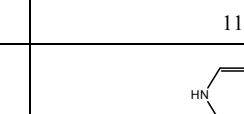
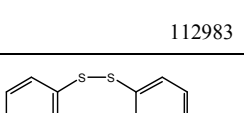
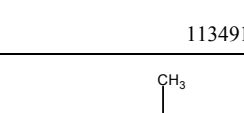
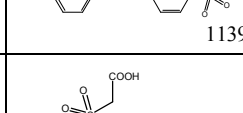
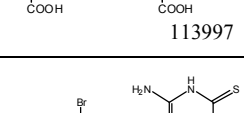
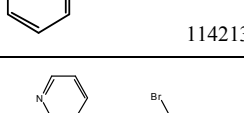
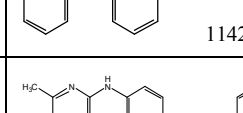
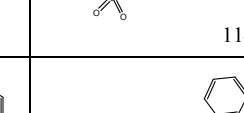
 85372	 85420	 85431	 85433
 85459	 85479	 85485	 85512
 85743	 86005	 86008	 86140
 86153	 86372	 86374	 86380
 86467	 86714	 87008	 87015
 87112	 87119	 87229	 87450
 87566	 87877	 87882	 88065
 88135	 88416	 88418	 88482
 88616	 88622	 88789	 88795
 88850	 88852	 88903	 88915
 88947	 88999	 89110	 89166

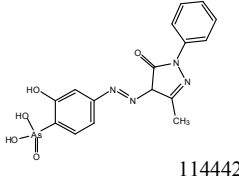
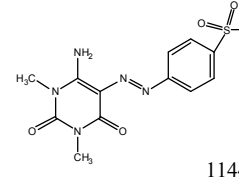
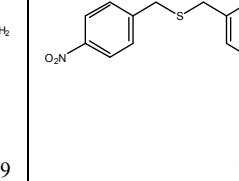
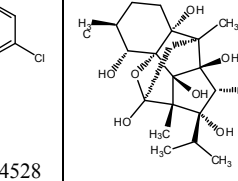
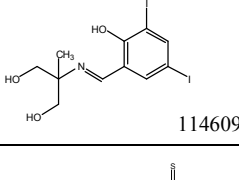
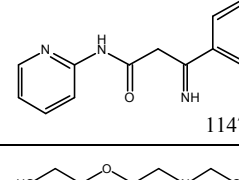
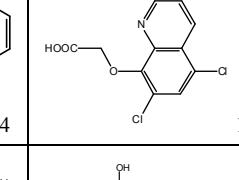
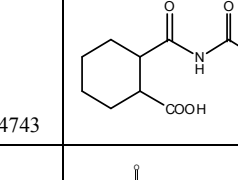
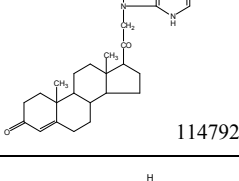
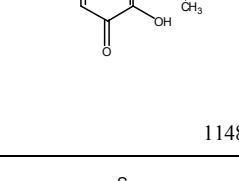
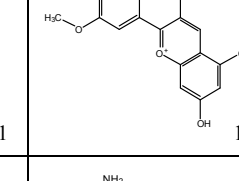
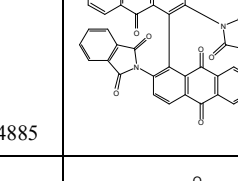
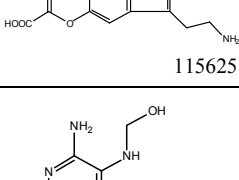
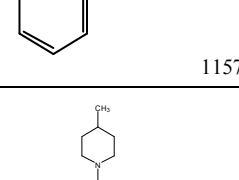
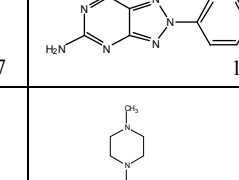
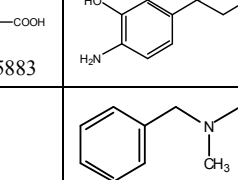
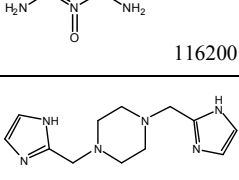
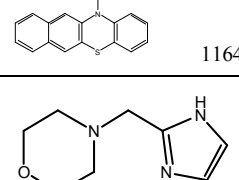
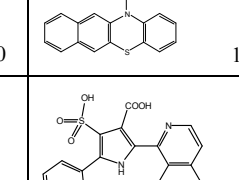
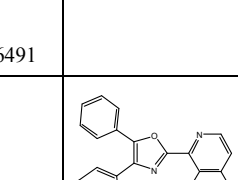
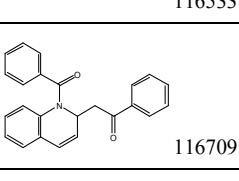
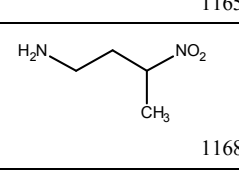
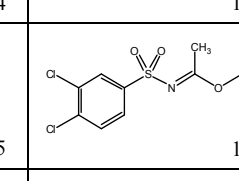
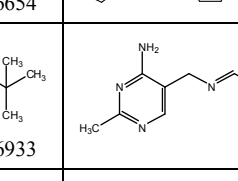
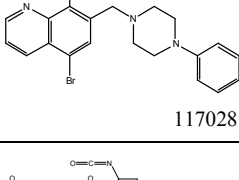
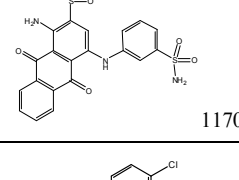
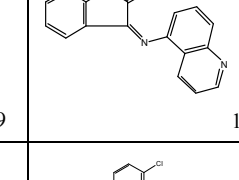
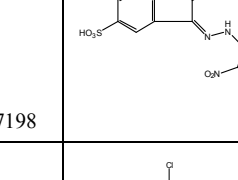
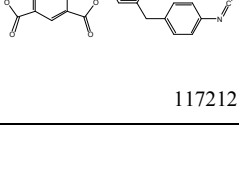
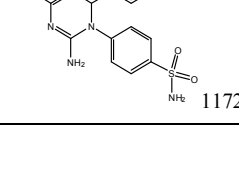
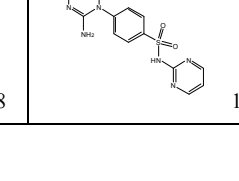
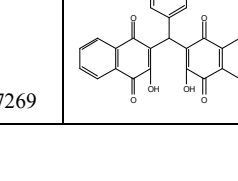
 89250	 89296	 89419	 89435
 89457	 89818	 90311	 90318
 90328	 90567	 90615	 90616
 90630	 90737	 90798	 90810
 90823	 90829	 90831	 90841
 90898	 91408	 91750	 91767
 91884	 92378	 92412	 92577
 92585	 92588	 92600	 92601
 92828	 92893	 92896	 92987
 92988	 93033	 93241	 93277
 93317	 93352	 93354	 93355

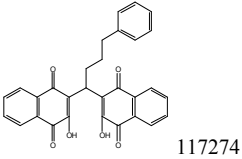
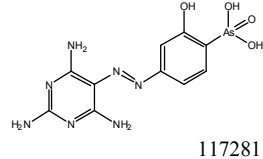
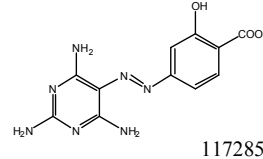
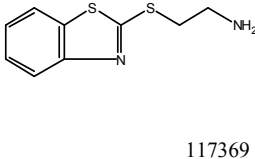
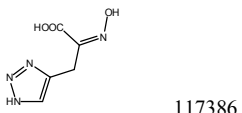
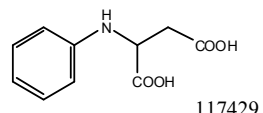
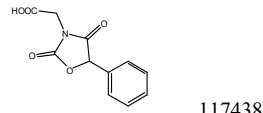
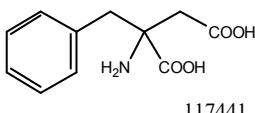
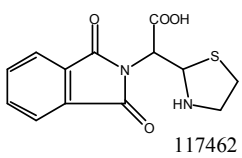
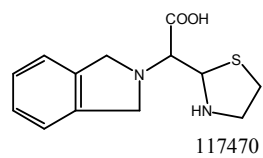
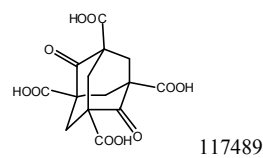
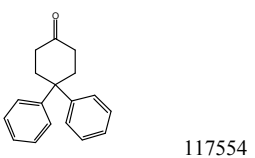
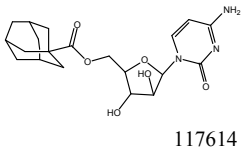
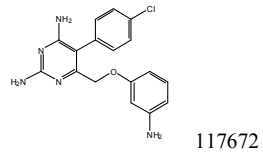
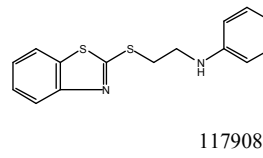
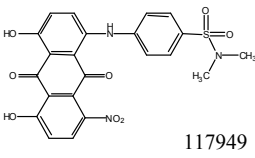
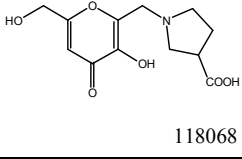
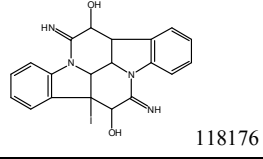
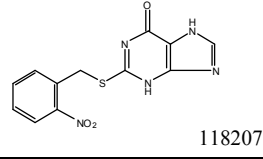
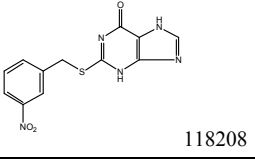
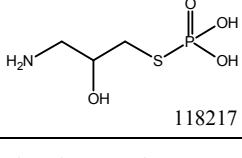
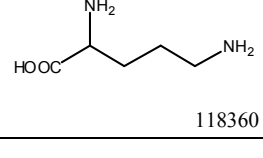
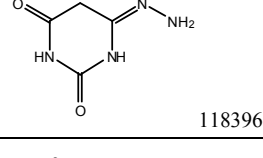
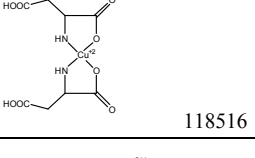
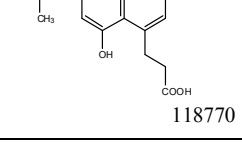
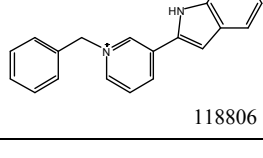
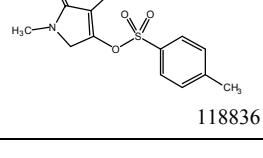
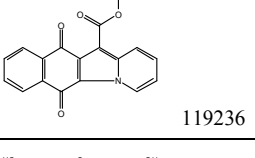
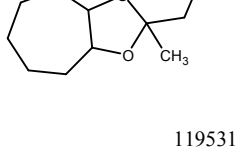
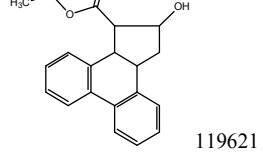
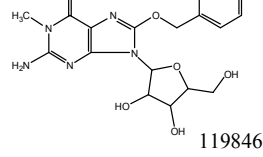
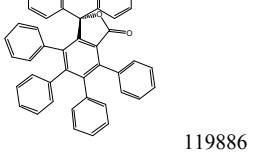
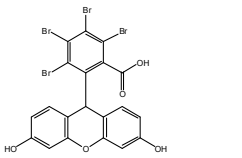
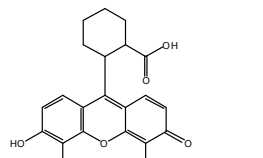
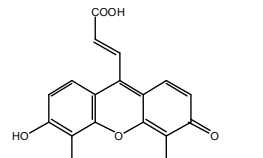
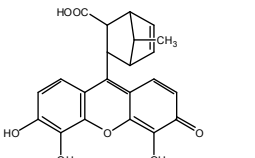
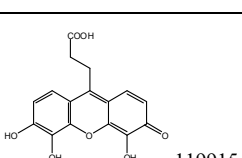
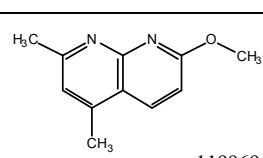
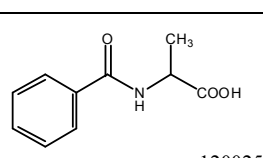
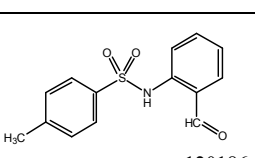
 93674	 93807	 93967	 94017
 94783	 94810	 94820	 94914
 95011	 95025	 95090	 95490
 95501	 95503	 95570	 95609
 95666	 95676	 95865	 95910
 95916	 95926	 96021	 96255
 96396	 96491	 96606	 96678
 96682	 96694	 96948	 97064
 97345	 97845	 97882	 97885
 97918	 97923	 97927	 97999

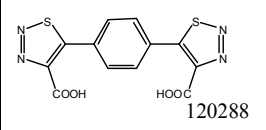
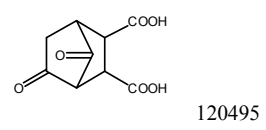
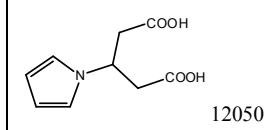
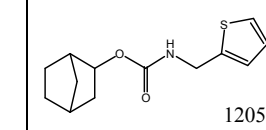
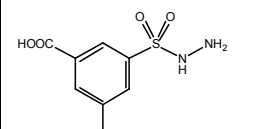
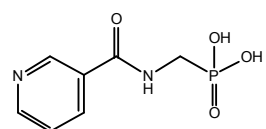
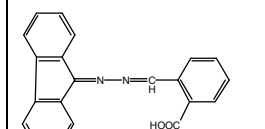
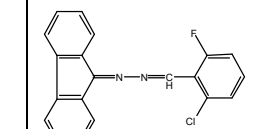
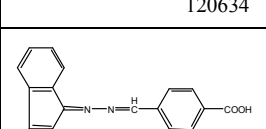
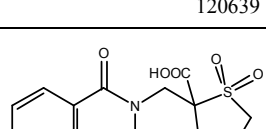
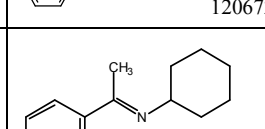
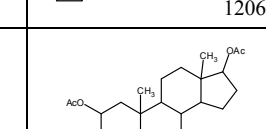
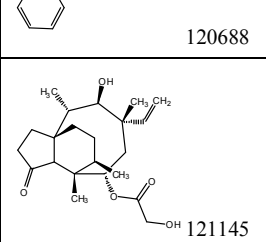
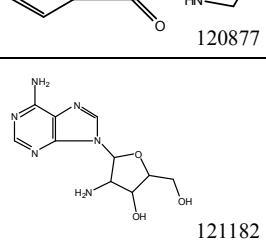
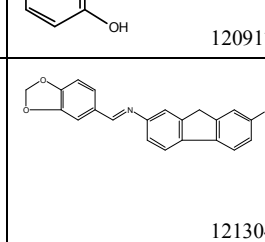
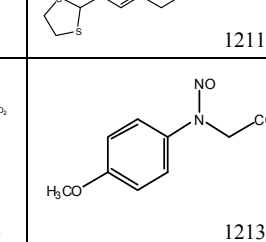
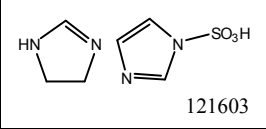
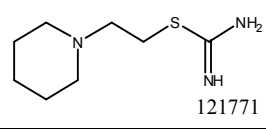
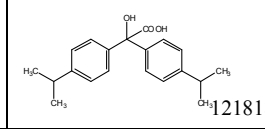
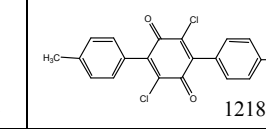
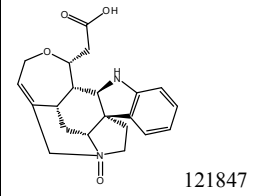
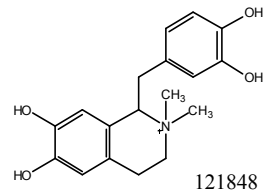
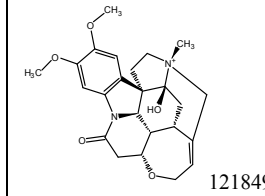
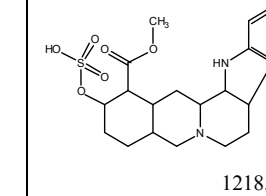
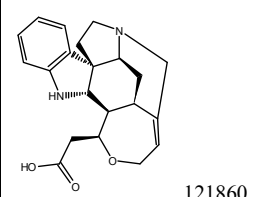
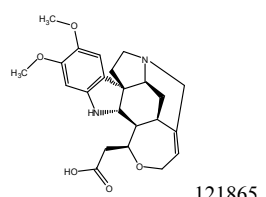
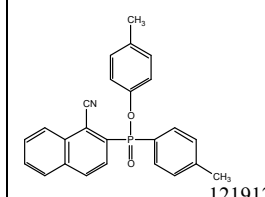
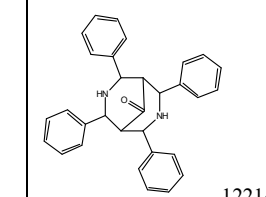
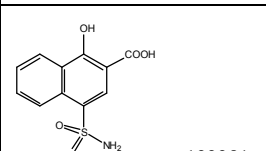
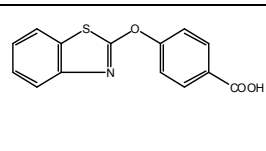
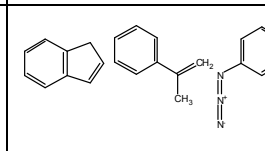
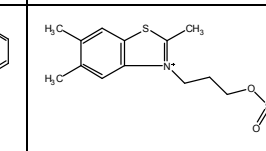
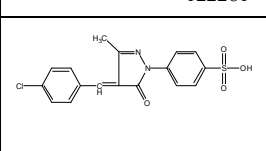
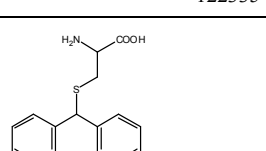
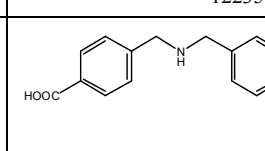
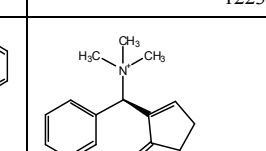
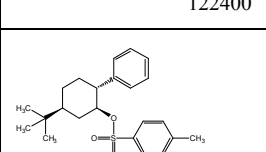
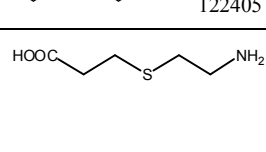
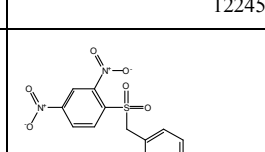
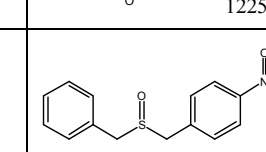
 98019	 98026	 98332	 98601
 98828	 98892	 98905	 99241
 99419	 99445	 99504	 99515
 99526	 99543	 99550	 99657
 99663	 99667	 99671	 99676
 99785	 99799	 99804	 100044
 100297	 100708	 100754	 100762
 100857	 100858	 100880	 100936
 100942	 100972	 101023	 101127
 101548	 101652	 101751	 101824

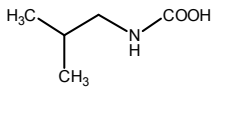
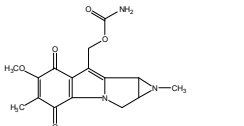
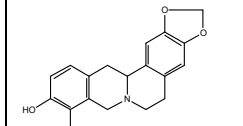
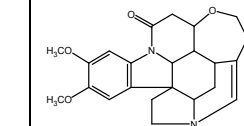
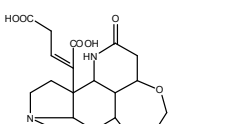
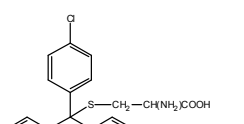
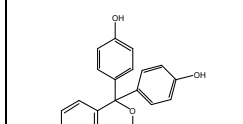
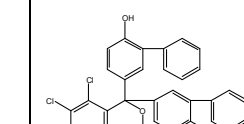
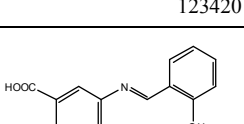
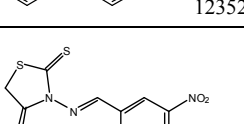
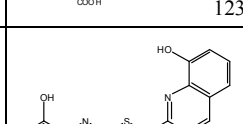
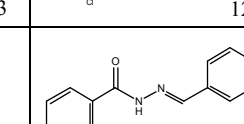
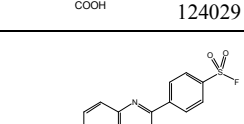
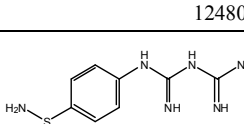
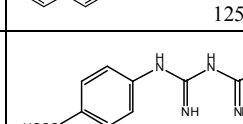
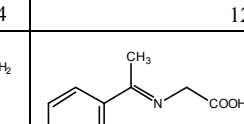
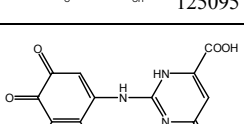
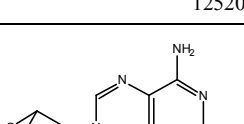
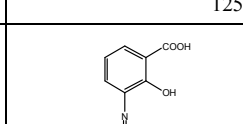
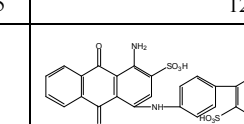
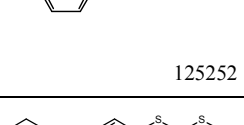
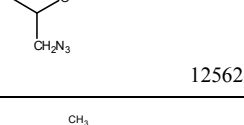
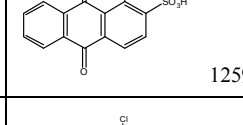
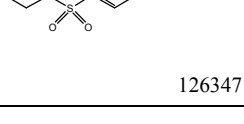
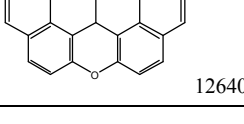
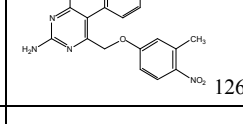
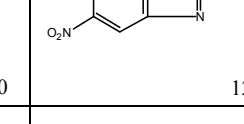
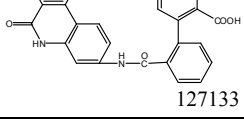
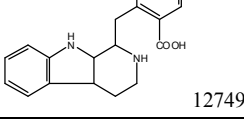
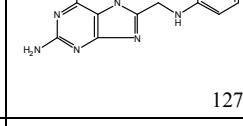
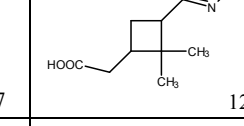
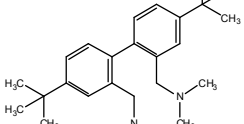
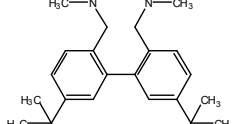
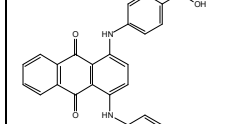
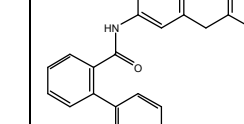
 101825	 101828	 101844	 101984
 102728	 102852	 103019	 103773
 103779	 104154	 105017	 105348
 105432	 105444	 105534	 105550
 105597	 105687	 105806	 105900
 106218	 106221	 106505	 106920
 106958	 107684	 107689	 107696
 108088	 108098	 108225	 108399
 108608	 108697	 108731	 108802
 108895	 108944	 109128	 109131
 109174	 109188	 109197	 109248

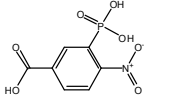
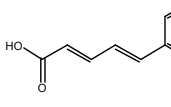
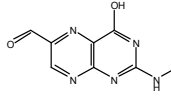
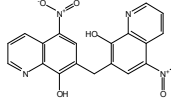
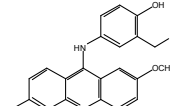
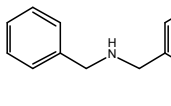
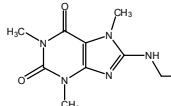
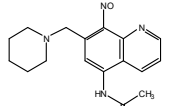
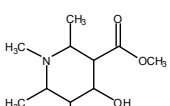
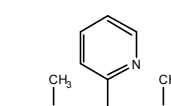
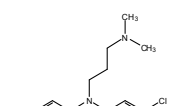
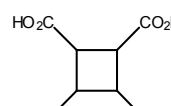
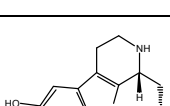
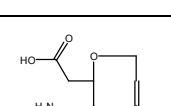
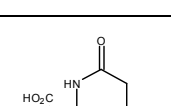
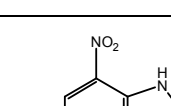
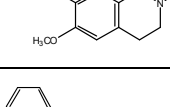
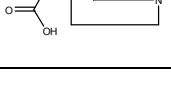
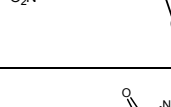
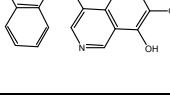
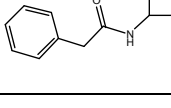
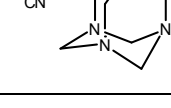
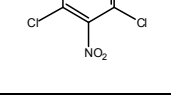
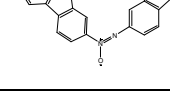
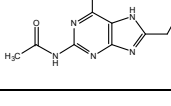
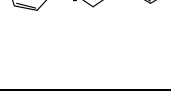
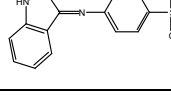
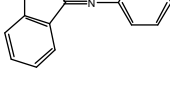
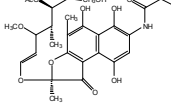
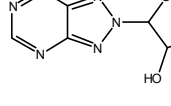
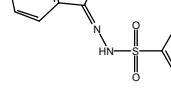
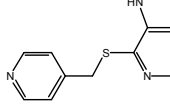
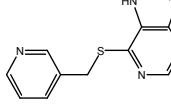
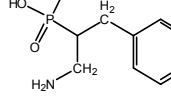
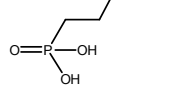
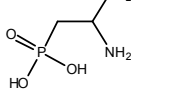
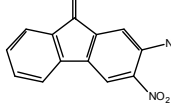
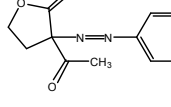
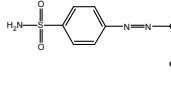
 109268	 109451	 109483	 109509
 109526	 109593	 109816	 109834
 109836	 109926	 110275	 110380
 111326	 111702	 112200	 112257
 112541	 112546	 112671	 112675
 112702	 112737	 112751	 112778
 112782	 112789	 112796	 112898
 112983	 113491	 113909	 113989
 113997	 114213	 114215	 114355
 114359	 114381	 114382	 114414

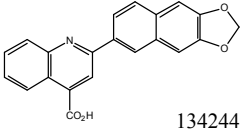
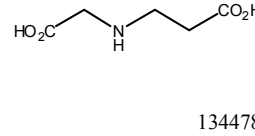
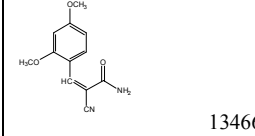
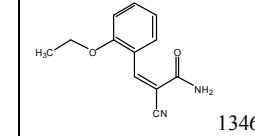
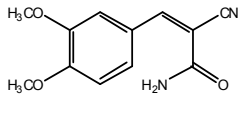
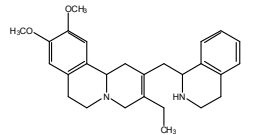
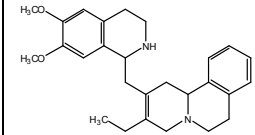
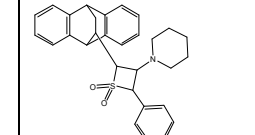
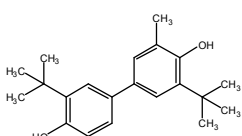
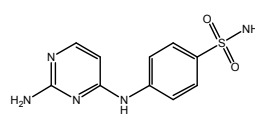
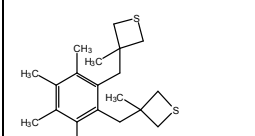
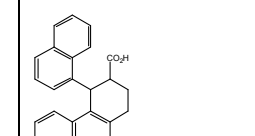
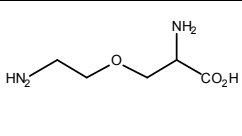
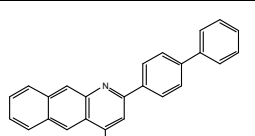
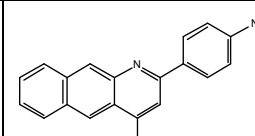
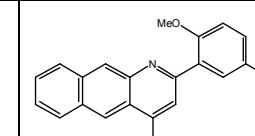
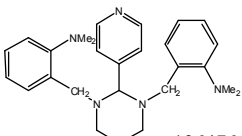
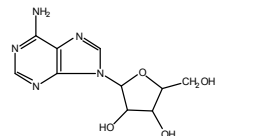
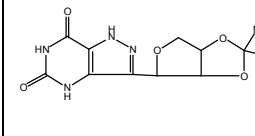
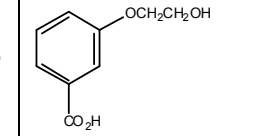
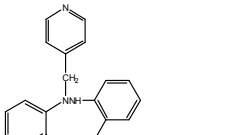
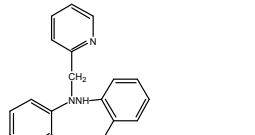
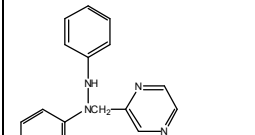
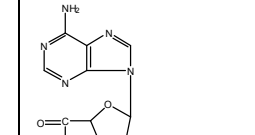
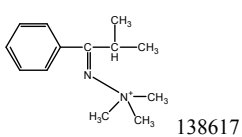
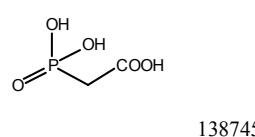
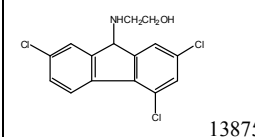
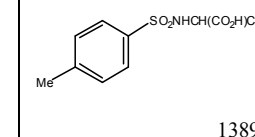
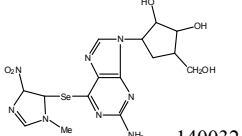
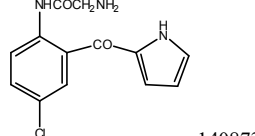
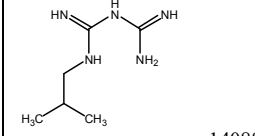
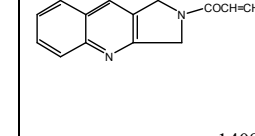
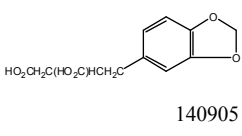
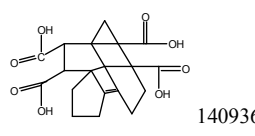
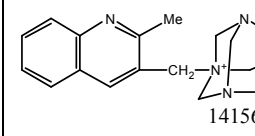
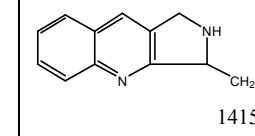
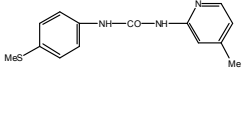
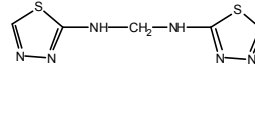
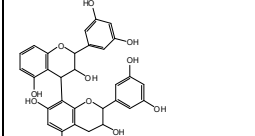
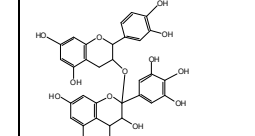
 114442	 114449	 114528	 114572
 114609	 114724	 114743	 114766
 114792	 114831	 114885	 115448
 115625	 115787	 115883	 116064
 116200	 116490	 116491	 116532
 116533	 116534	 116654	 116702
 116709	 116805	 116933	 116977
 117028	 117079	 117198	 117199
 117212	 117268	 117269	 117271

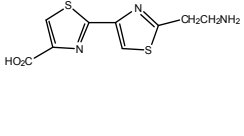
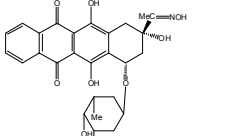
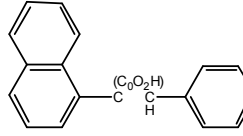
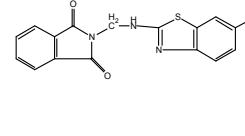
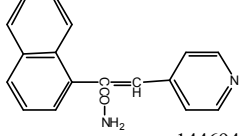
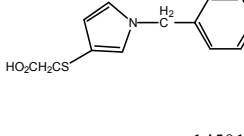
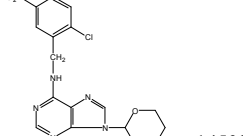
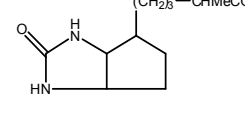
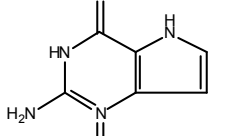
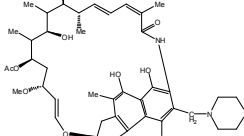
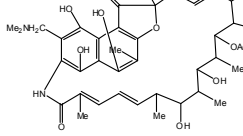
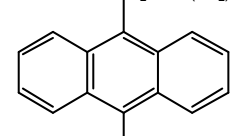
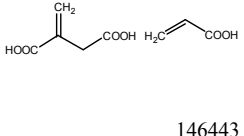
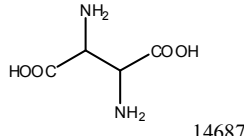
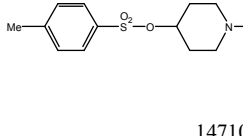
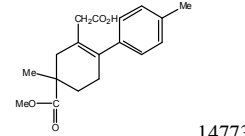
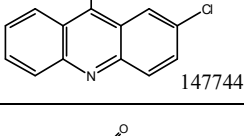
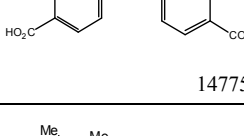
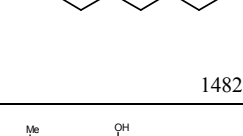
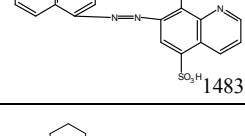
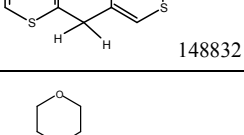
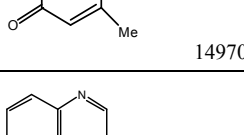
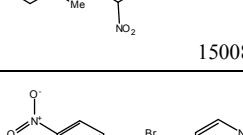
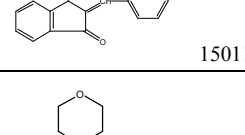
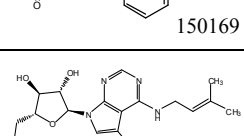
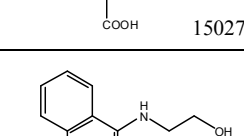
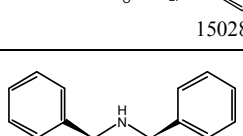
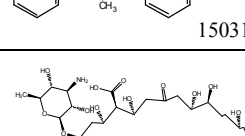
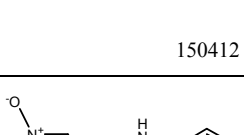
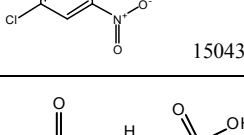
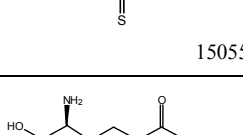
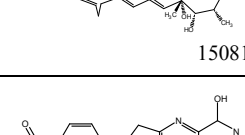
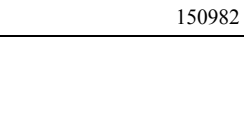
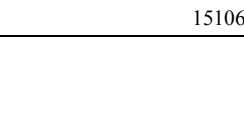
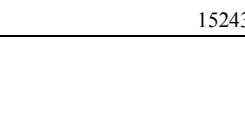
 117274	 117281	 117285	 117369
 117386	 117429	 117438	 117441
 117462	 117470	 117489	 117554
 117614	 117672	 117908	 117949
 118068	 118176	 118207	 118208
 118217	 118360	 118396	 118516
 118770	 118806	 118836	 119236
 119531	 119621	 119846	 119886
 119889	 119910	 119911	 119913
 119915	 119969	 120025	 120186

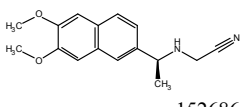
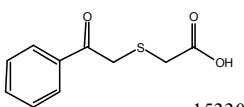
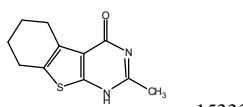
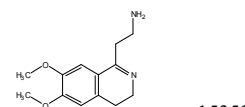
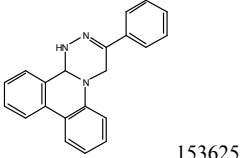
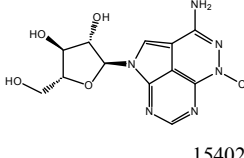
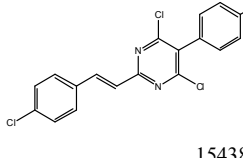
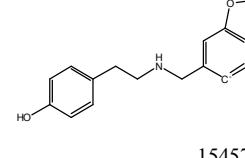
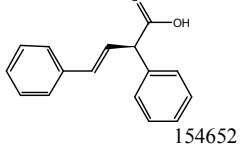
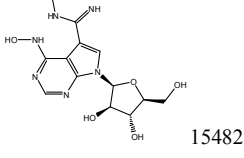
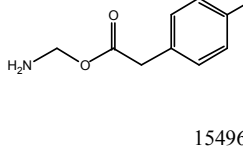
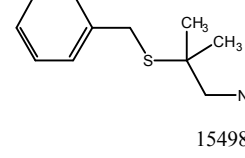
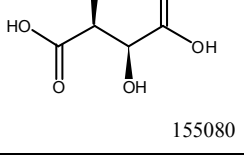
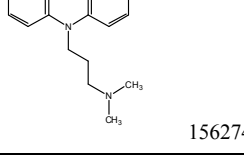
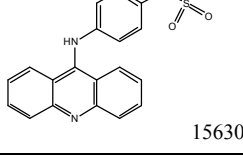
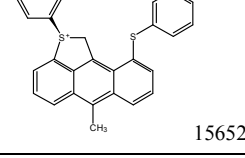
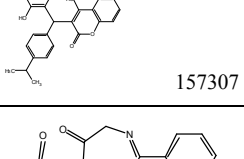
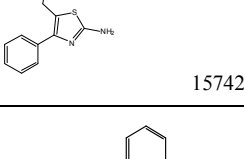
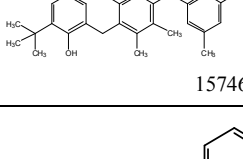
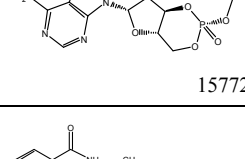
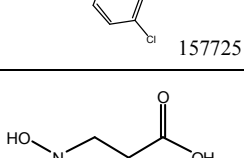
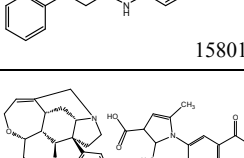
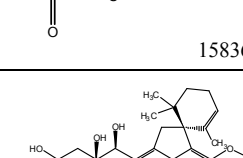
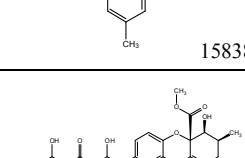
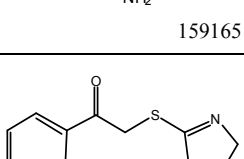
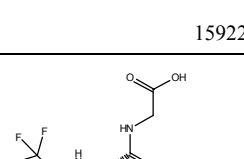
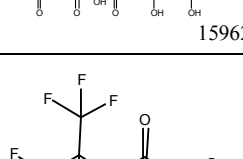
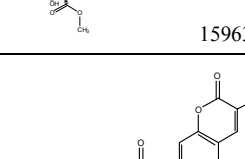
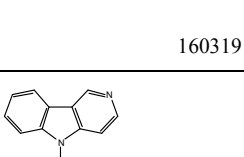
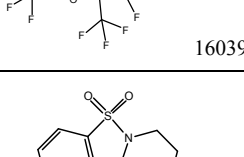
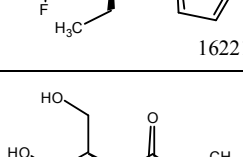
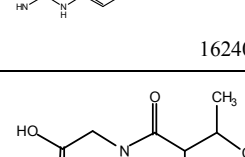
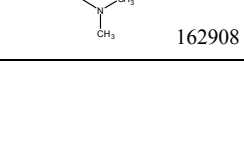
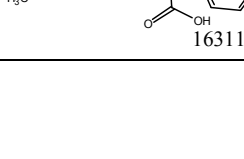
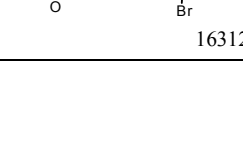
 120288	 120495	 120501	 120571
 120634	 120639	 120672	 120686
 120688	 120877	 120917	 121137
 121145	 121182	 121304	 121384
 121603	 121771	 121818	 121838
 121847	 121848	 121849	 121855
 121860	 121865	 121912	 122140
 122281	 122335	 122351	 122370
 122400	 122405	 122451	 122592
 122608	 122621	 122657	 122662

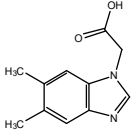
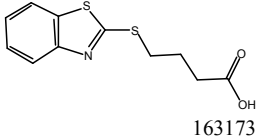
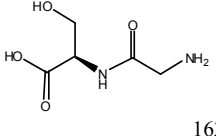
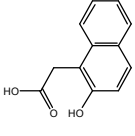
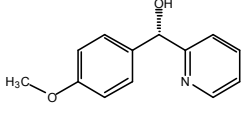
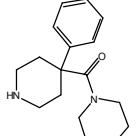
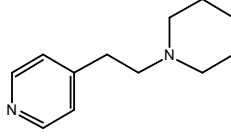
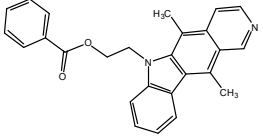
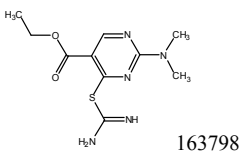
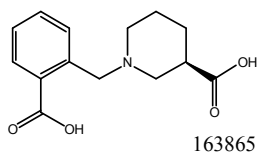
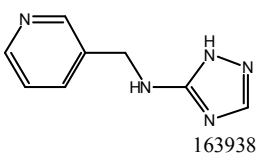
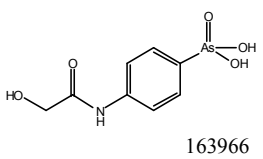
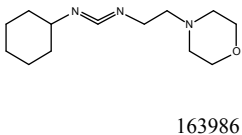
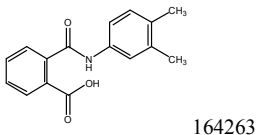
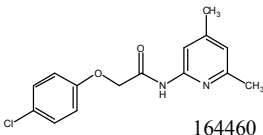
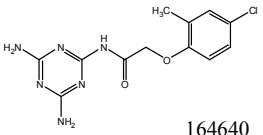
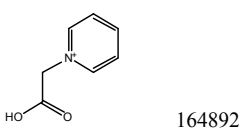
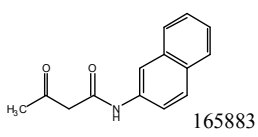
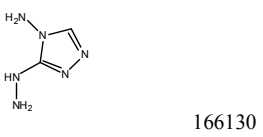
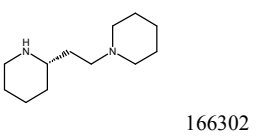
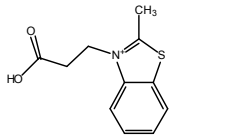
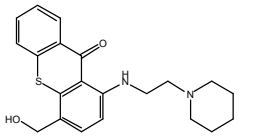
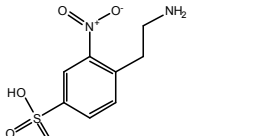
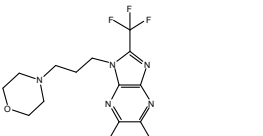
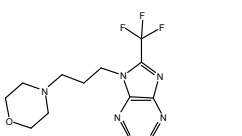
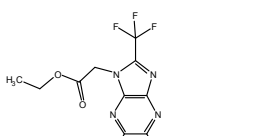
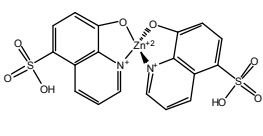
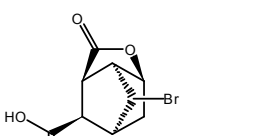
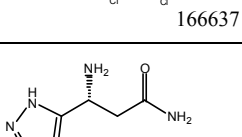
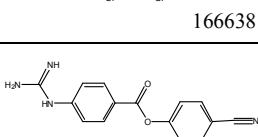
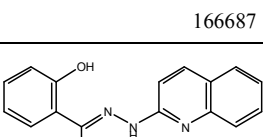
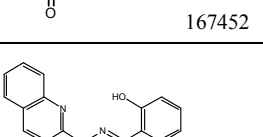
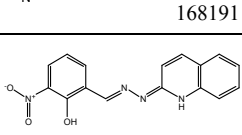
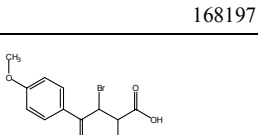
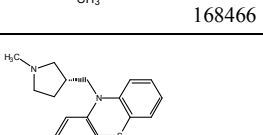
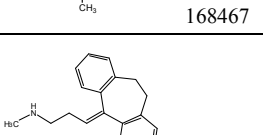
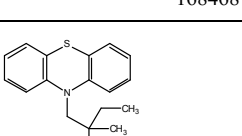
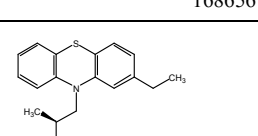
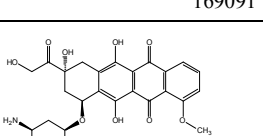
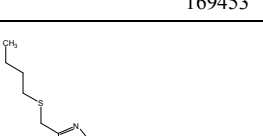
 122674	 123111	 123389	 123394
 123420	 123526	 123993	 123994
 124029	 124808	 125034	 125044
 125095	 125201	 125205	 125214
 125252	 125626	 125908	 125910
 126347	 126401	 126710	 126757
 127133	 127494	 127917	 127947
 128164	 128166	 128437	 128598
 128609	 128684	 128884	 128911

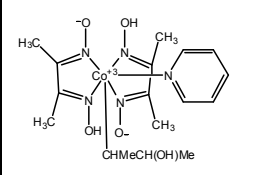
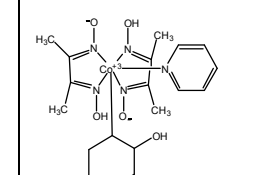
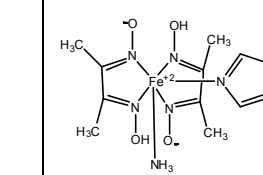
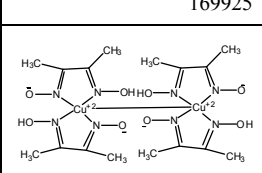
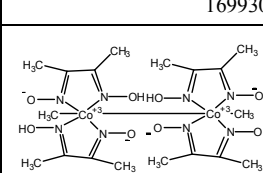
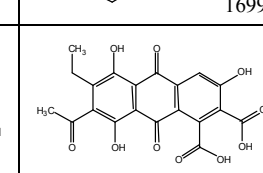
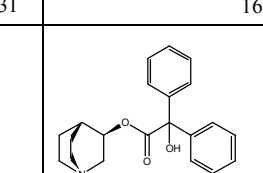
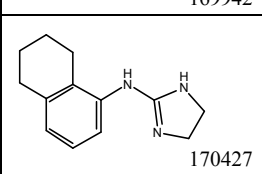
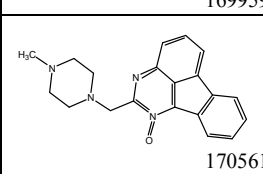
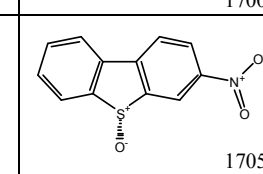
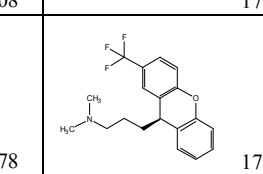
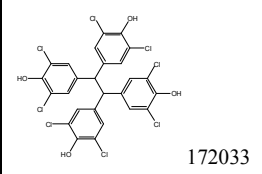
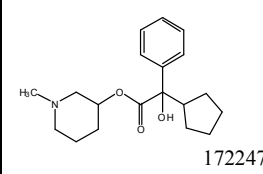
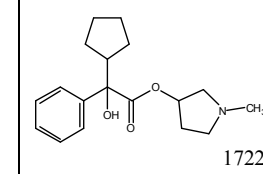
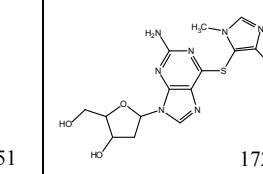
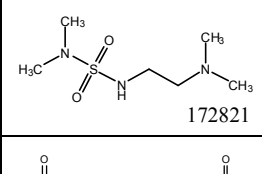
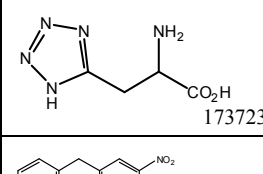
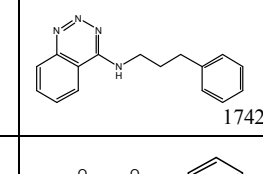
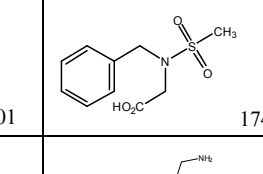
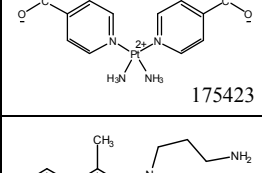
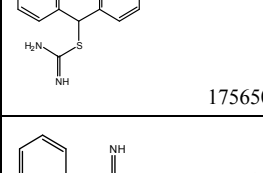
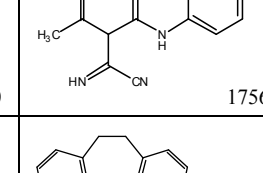
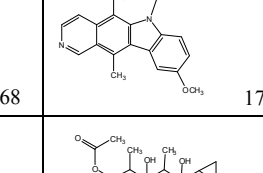
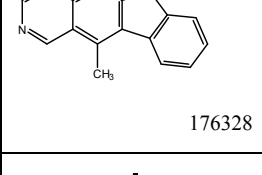
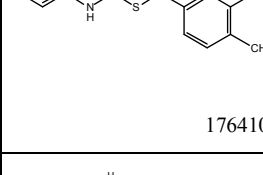
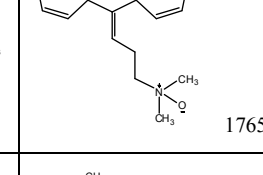
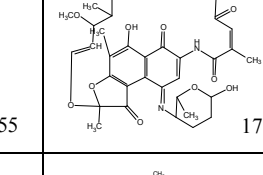
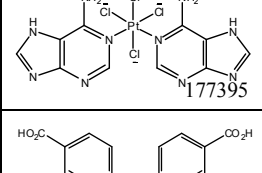
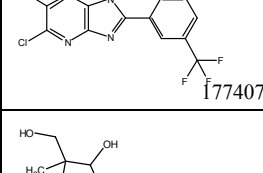
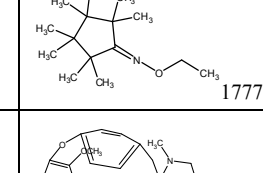
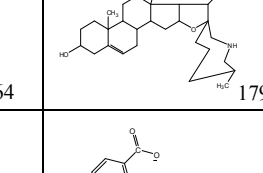
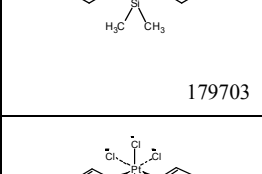
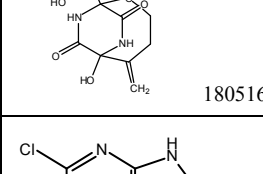
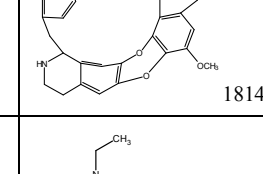
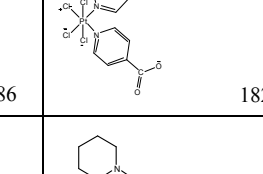
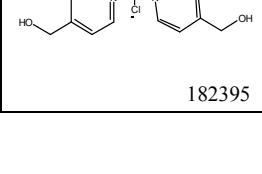
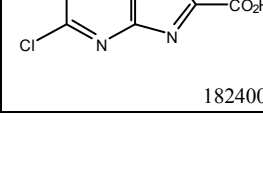
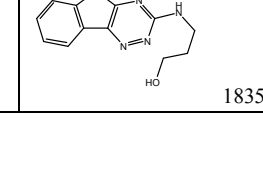
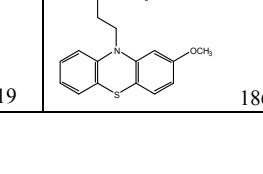
 129478	 129538	 129965	 130796
 130813	 130830	 130843	 130876
 130891	 130915	 131053	 131453
 131547	 131612	 131614	 131615
 131734	 131815	 131869	 132073
 132230	 132498	 132693	 133073
 133074	 133100	 133118	 133488
 133593	 133594	 133811	 133837
 133887	 133896	 134120	 134137
 134148	 134149	 134159	 134196

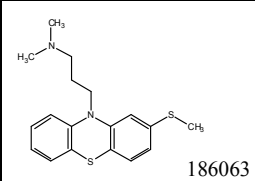
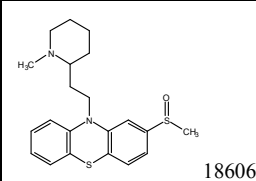
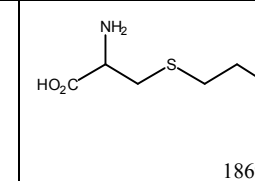
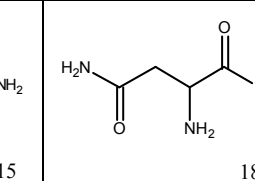
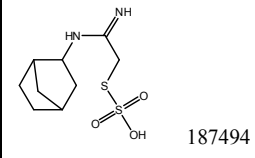
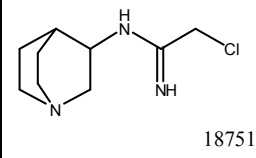
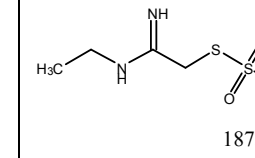
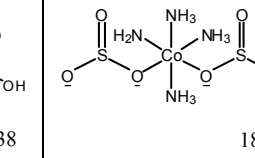
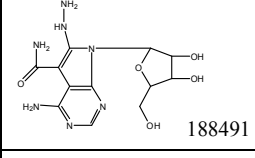
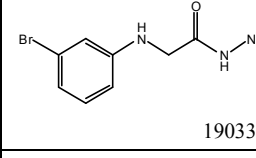
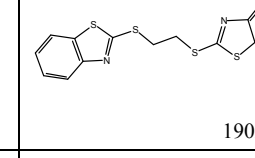
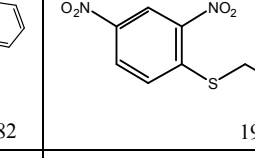
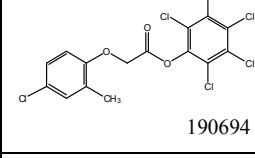
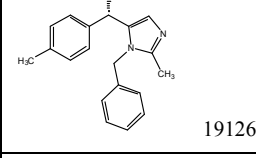
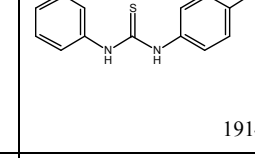
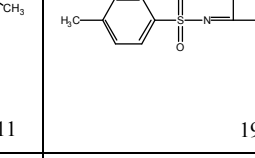
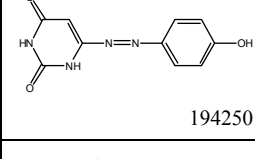
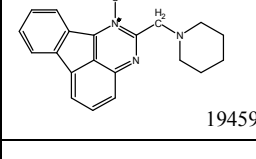
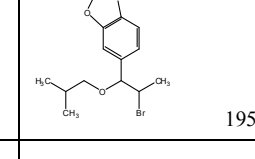
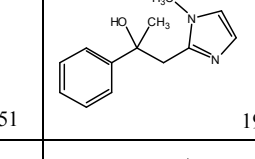
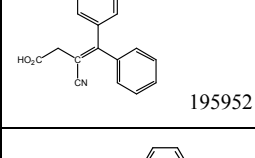
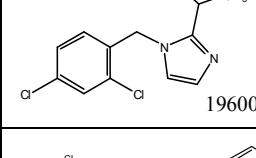
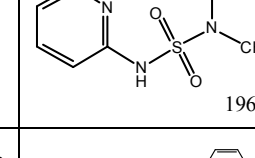
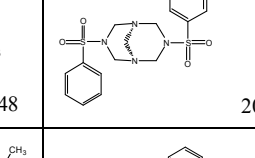
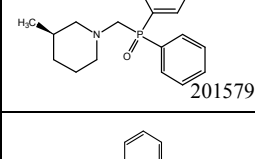
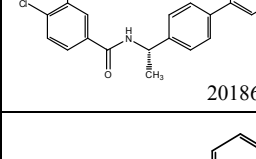
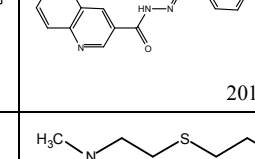
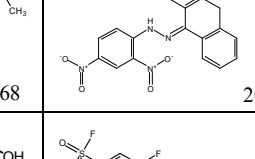
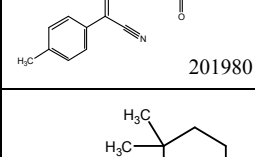
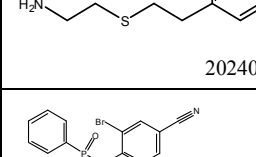
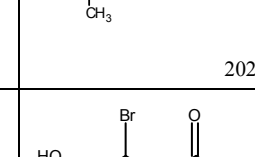
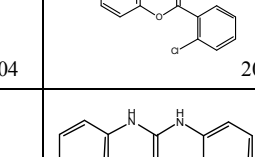
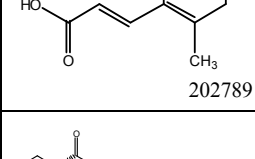
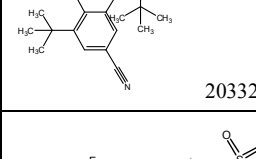
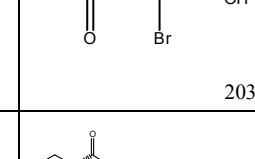
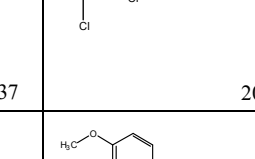
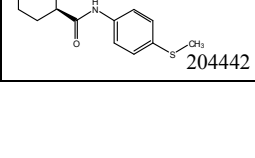
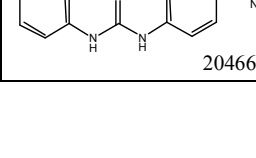
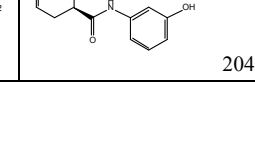
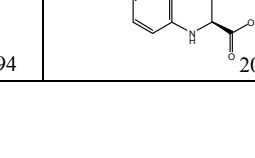
 134244	 134478	 134664	 134666
 134667	 134754	 134755	 135371
 135463	 135784	 135882	 135900
 136035	 136469	 136472	 136473
 136476	 136563	 136727	 137280
 137578	 137579	 137580	 137784
 138617	 138745	 138756	 138971
 140032	 140873	 140880	 140899
 140905	 140936	 141562	 141566
 142269	 143019	 143099	 143101

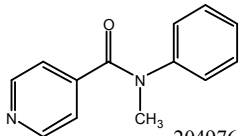
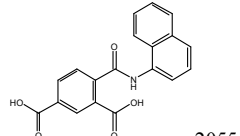
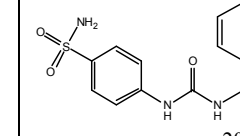
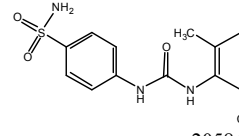
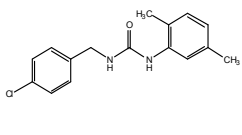
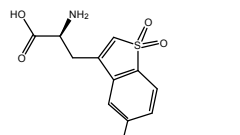
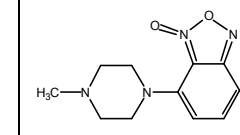
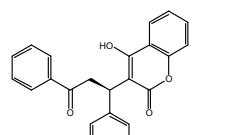
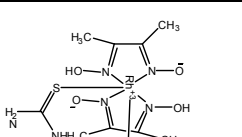
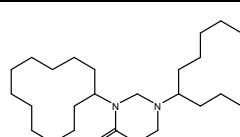
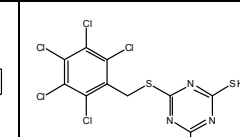
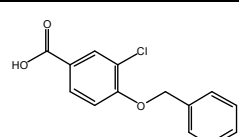
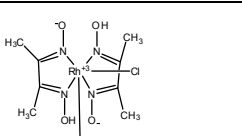
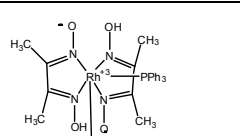
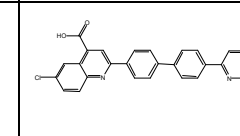
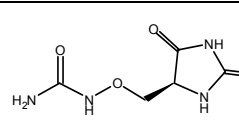
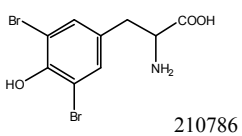
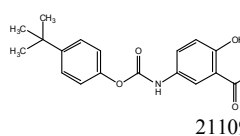
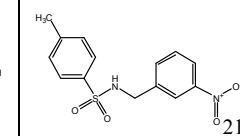
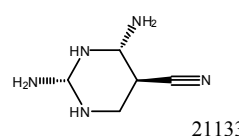
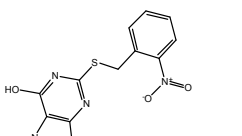
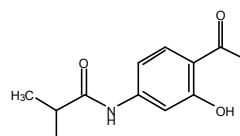
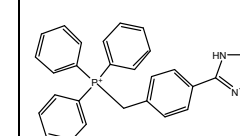
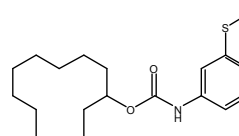
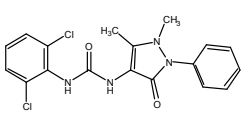
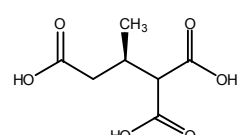
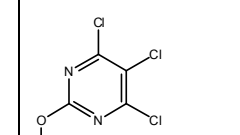
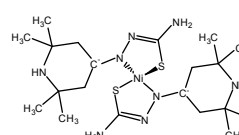
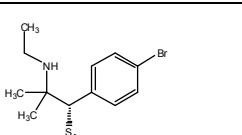
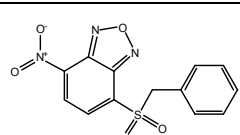
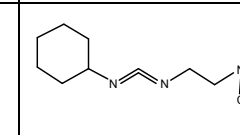
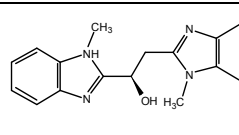
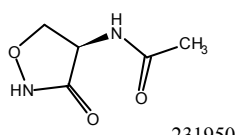
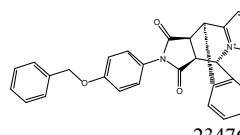
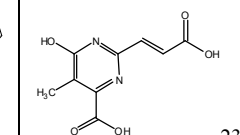
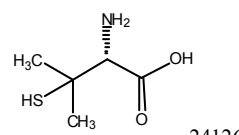
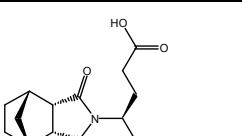
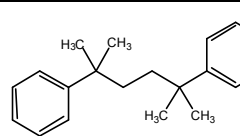
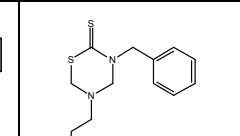
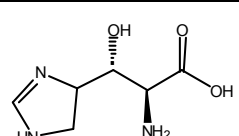
 143125	 143491	 143677	 143722
 144694	 145014	 145031	 145151
 145425	 145611	 145612	 146109
 146443	 146878	 147109	 147737
 147744	 147758	 148230	 148354
 148832	 149707	 150080	 150117
 150169	 150277	 150289	 150316
 150412	 150432	 150554	 150817
 150982	 151063	 151831	 152432

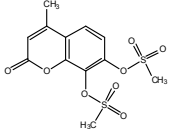
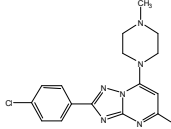
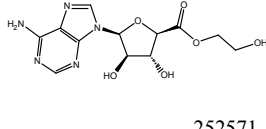
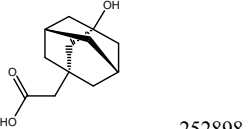
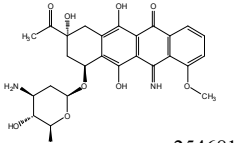
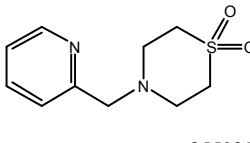
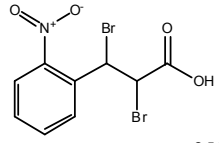
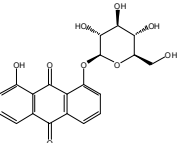
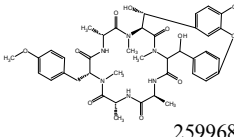
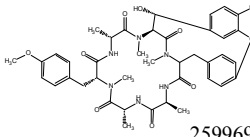
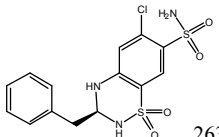
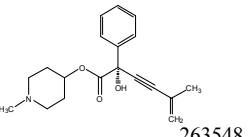
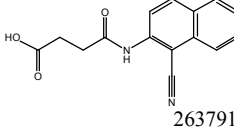
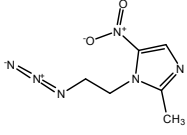
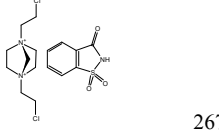
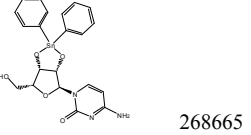
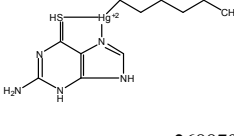
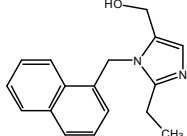
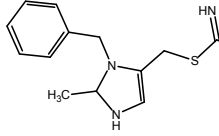
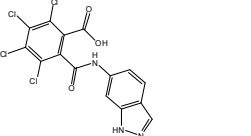
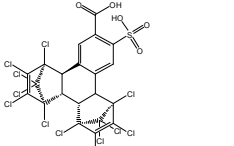
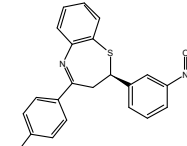
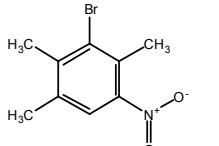
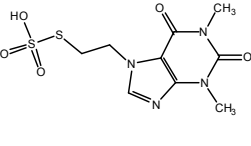
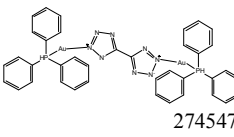
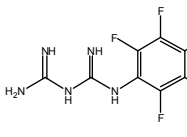
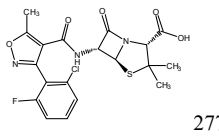
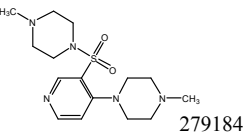
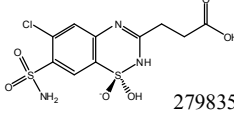
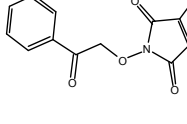
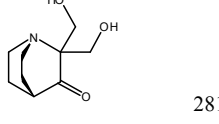
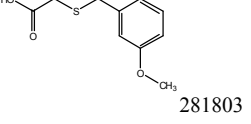
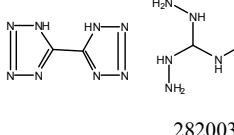
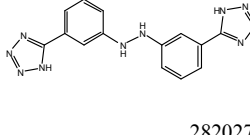
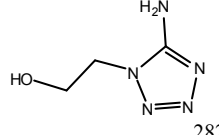
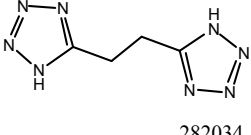
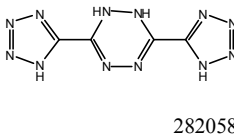
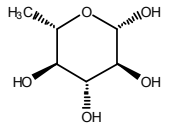
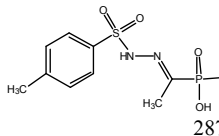
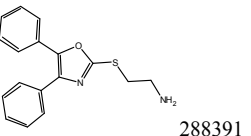
 152686	 153308	 153330	 153533
 153625	 154020	 154389	 154572
 154652	 154829	 154966	 154983
 155080	 156274	 156305	 156529
 157307	 157421	 157469	 157722
 157725	 158011	 158362	 158383
 159165	 159228	 159628	 159631
 160319	 160391	 162215	 162404
 162908	 163116	 163122	 163138

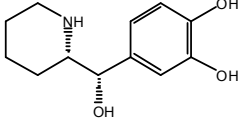
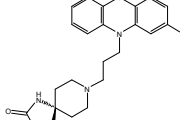
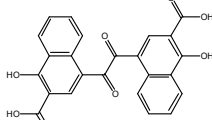
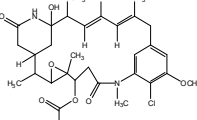
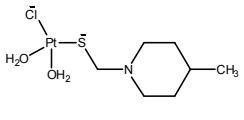
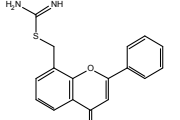
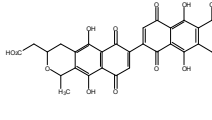
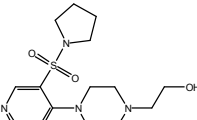
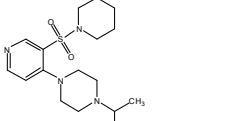
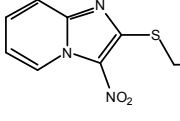
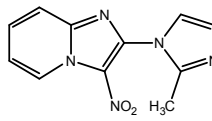
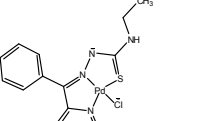
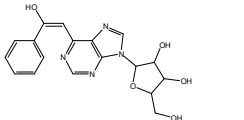
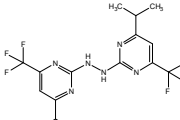
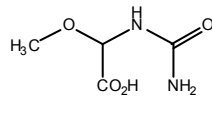
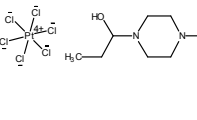
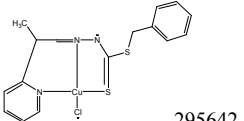
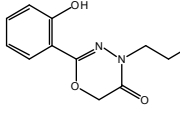
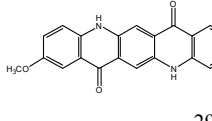
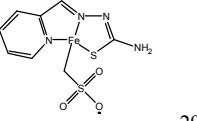
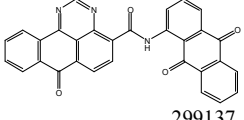
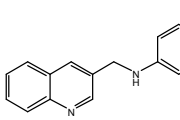
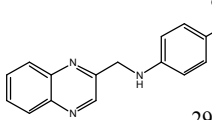
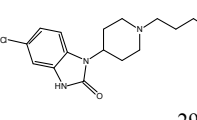
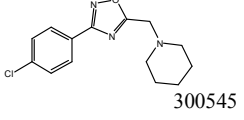
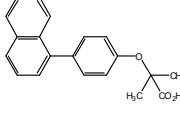
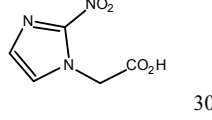
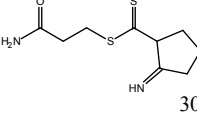
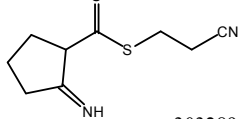
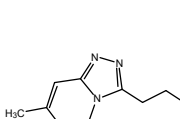
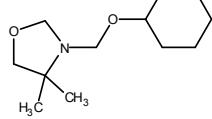
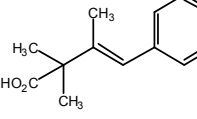
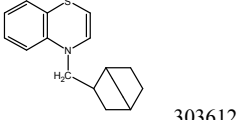
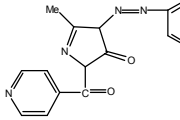
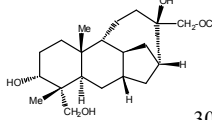
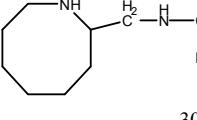
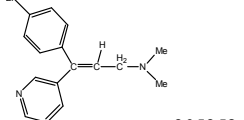
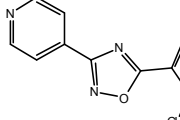
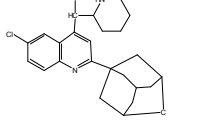
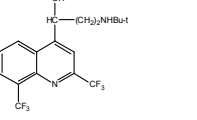
 163160	 163173	 163326	 163339
 163361	 163376	 163398	 163443
 163798	 163865	 163938	 163966
 163986	 164263	 164460	 164640
 164892	 165883	 166130	 166302
 166363	 166366	 166395	 166598
 166637	 166638	 166687	 167452
 168191	 168197	 168466	 168467
 168468	 168656	 169091	 169453
 169466	 169471	 169534	 169804

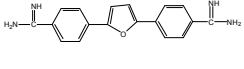
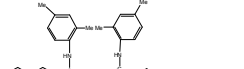
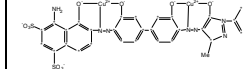
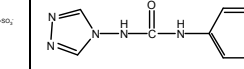
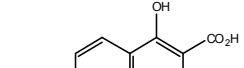
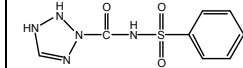
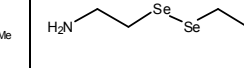
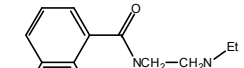
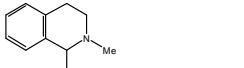
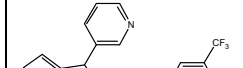
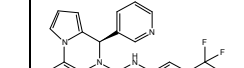
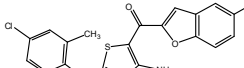
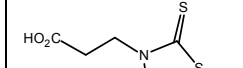
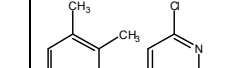
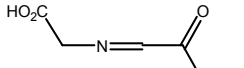
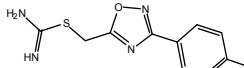
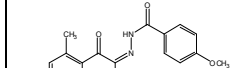
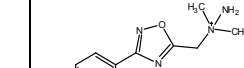
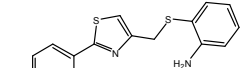
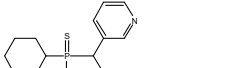
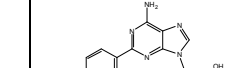
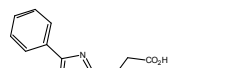
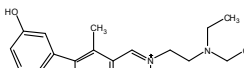
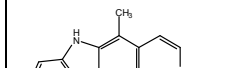
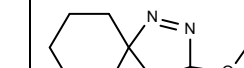
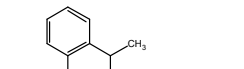
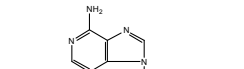
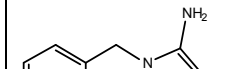
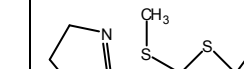
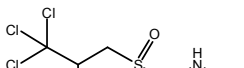
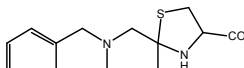
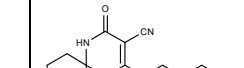
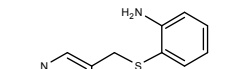
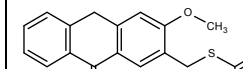
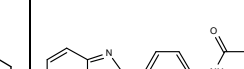
 169925	 169930	 169931	 169936
 169942	 169959	 170008	 170423
 170427	 170561	 170578	 170992
 172033	 172247	 172251	 172614
 172821	 173723	 174201	 174267
 175423	 175650	 175668	 176327
 176328	 176410	 176555	 177383
 177395	 177407	 177764	 179187
 179703	 180516	 181486	 182035
 182395	 182400	 183519	 186057

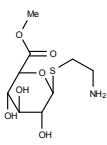
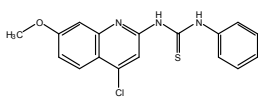
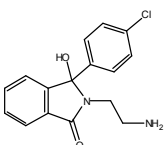
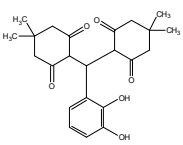
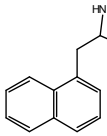
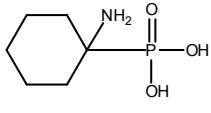
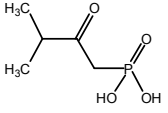
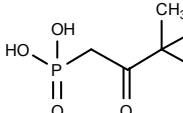
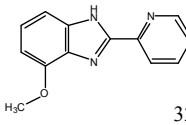
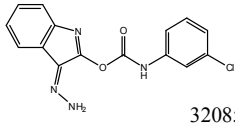
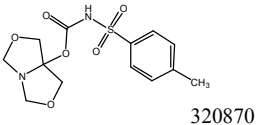
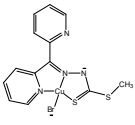
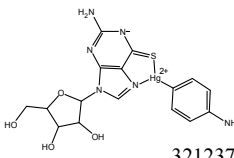
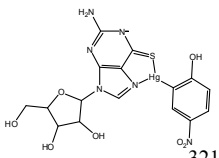
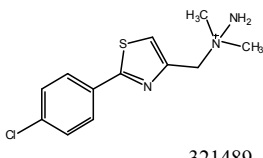
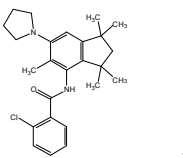
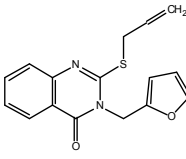
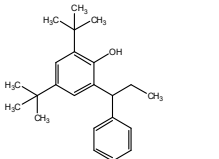
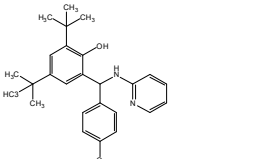
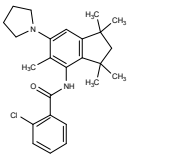
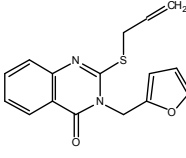
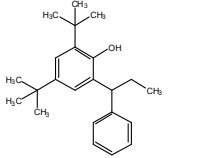
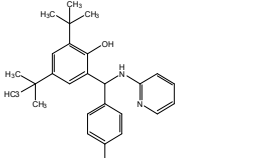
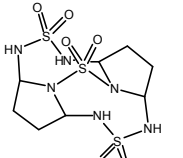
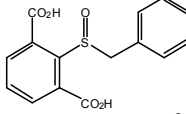
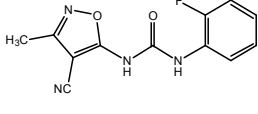
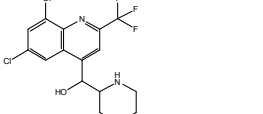
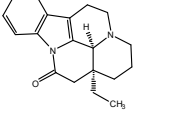
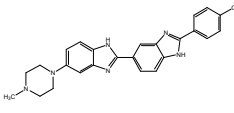
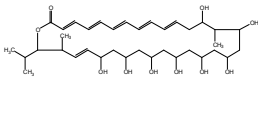
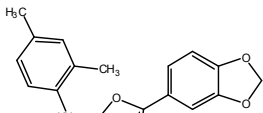
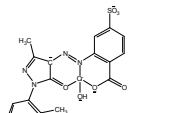
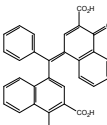
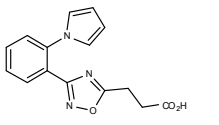
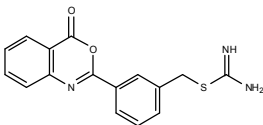
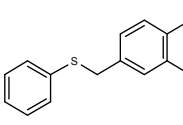
 186063	 186066	 186915	 186919
 187494	 187510	 187538	 187613
 188491	 190336	 190382	 190577
 190694	 191260	 191411	 193457
 194250	 194598	 195151	 195950
 195952	 196002	 196148	 201430
 201579	 201863	 201868	 201873
 201980	 202409	 202604	 202695
 202789	 203328	 203337	 204103
 204442	 204667	 204794	 204936

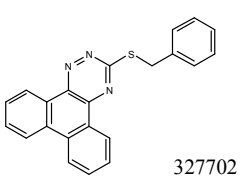
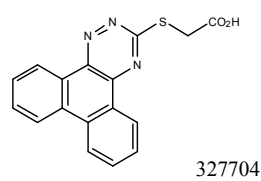
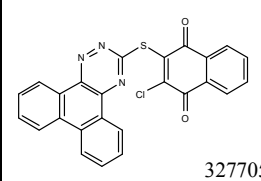
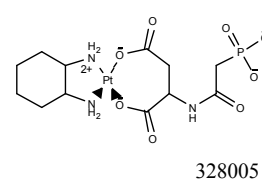
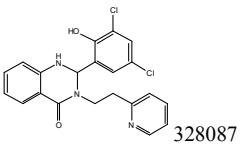
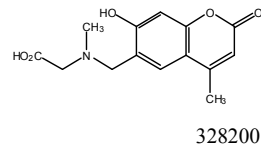
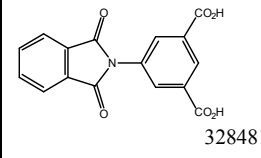
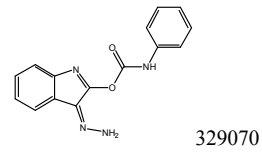
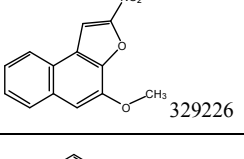
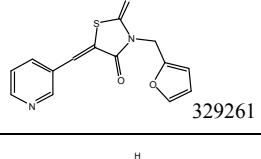
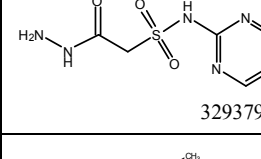
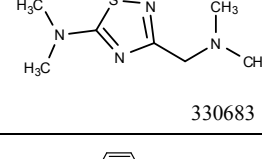
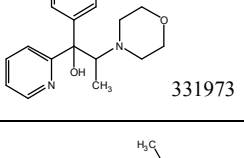
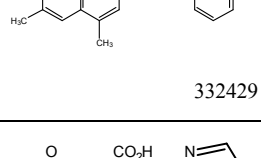
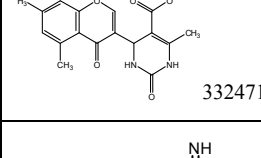
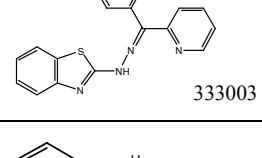
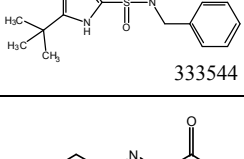
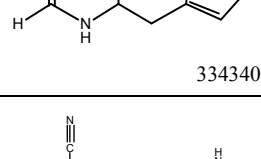
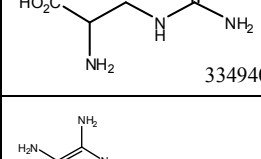
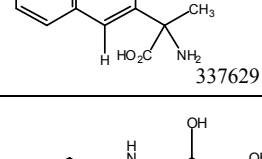
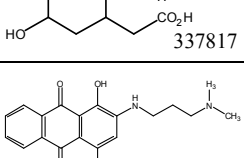
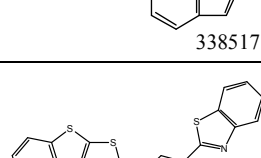
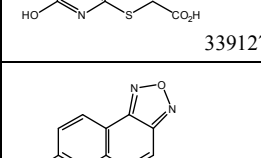
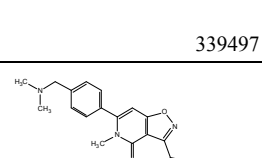
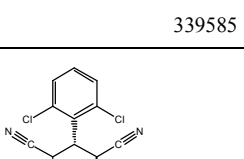
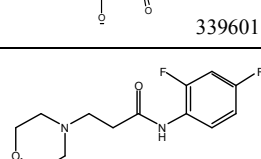
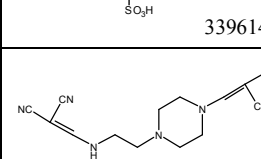
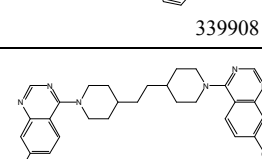
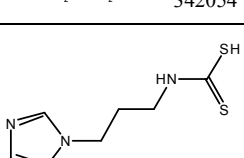
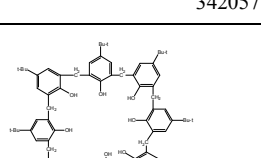
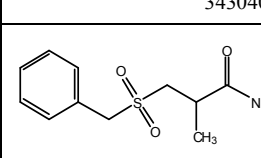
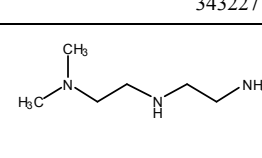
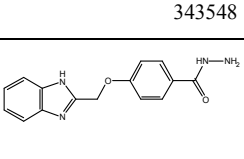
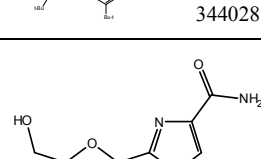
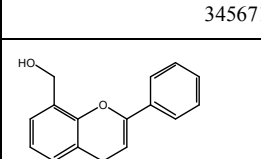
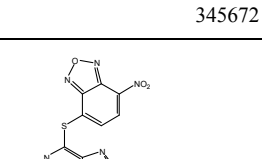
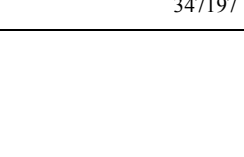
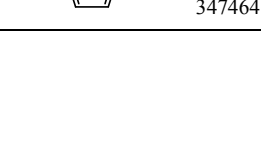
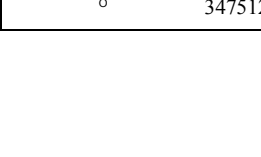
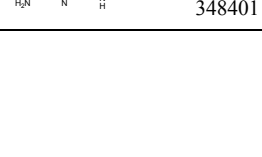
 204976	 205511	 205628	 205842
 205862	 206601	 207895	 208758
 208823	 209910	 209931	 210282
 210595	 210599	 210627	 210739
 210786	 211094	 211193	 211332
 211340	 211685	 211736	 216621
 216633	 220204	 226798	 227147
 227265	 228148	 231596	 231643
 231950	 234766	 236671	 241261
 241993	 245053	 246981	 247535

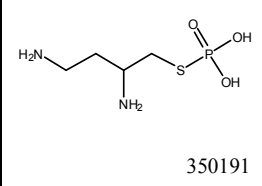
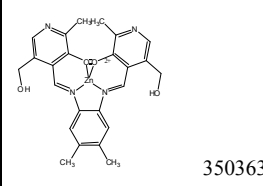
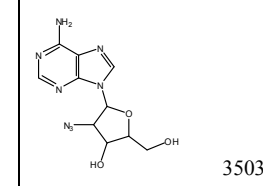
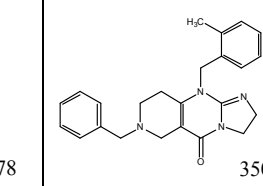
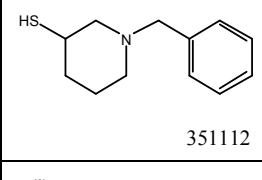
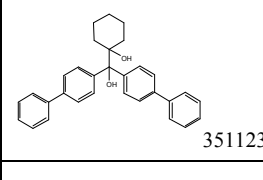
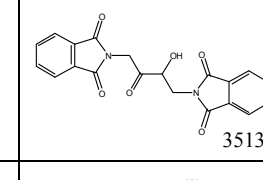
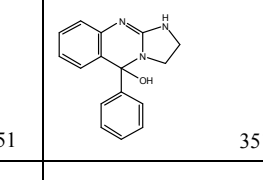
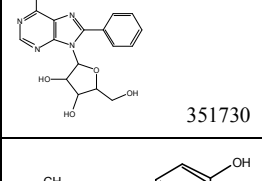
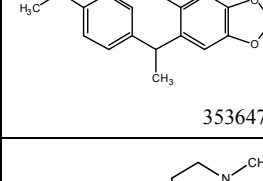
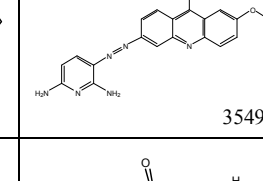
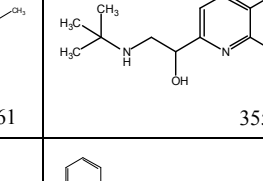
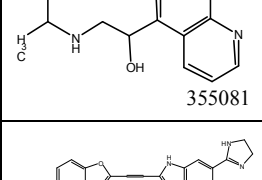
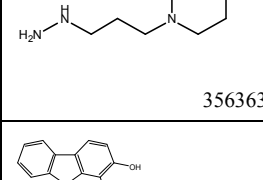
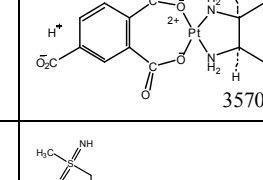
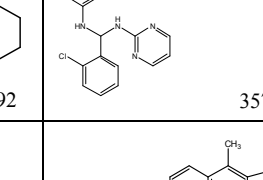
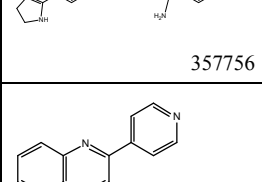
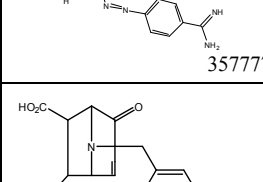
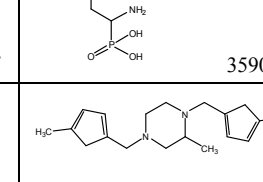
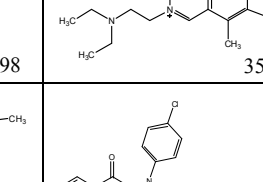
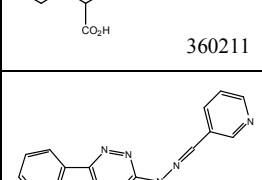
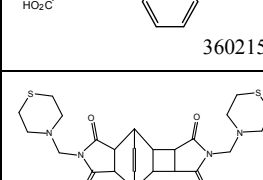
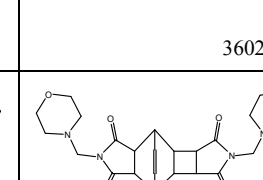
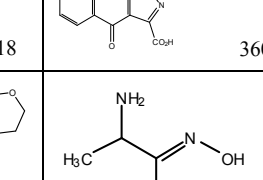
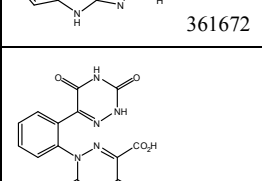
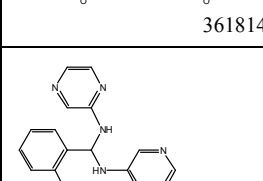
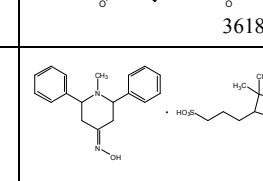
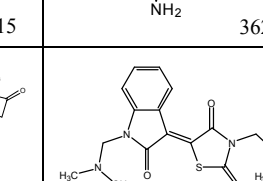
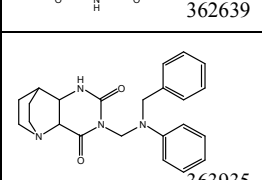
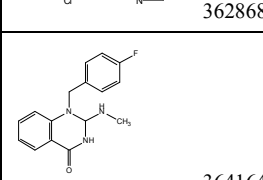
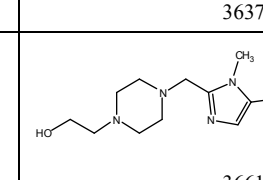
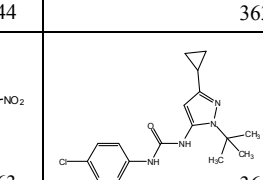
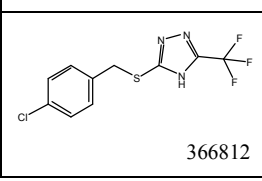
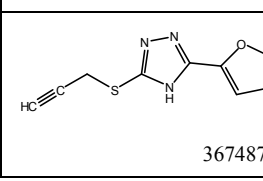
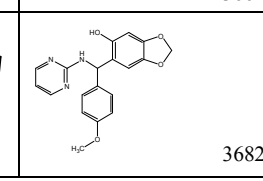
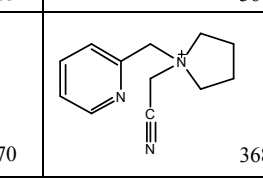
 240826	 252359	 252571	 252898
 254681	 255025	 255088	 255980
 259968	 259969	 263320	 263548
 263791	 262563	 267235	 268665
 268879	 269903	 269911	 270156
 270718	 270737	 271928	 273907
 274547	 274902	 277175	 279184
 279835	 280997	 281668	 281803
 282003	 282027	 282032	 282034
 282058	 287050	 287499	 288391

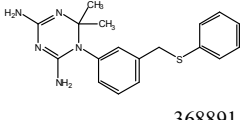
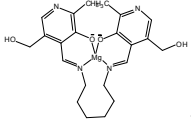
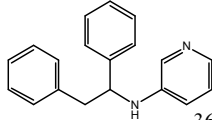
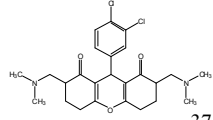
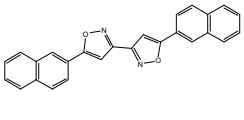
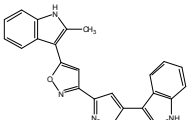
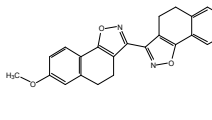
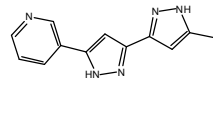
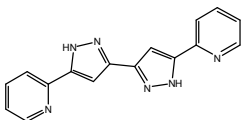
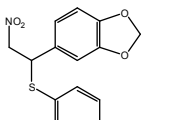
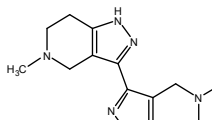
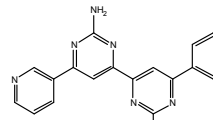
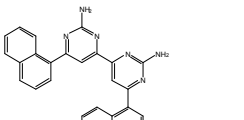
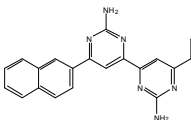
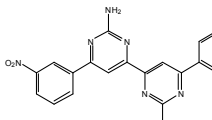
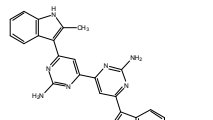
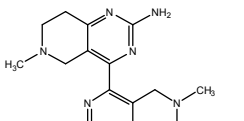
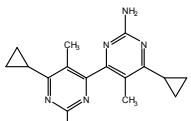
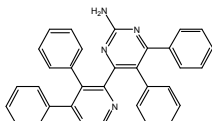
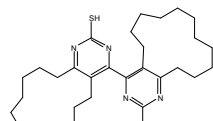
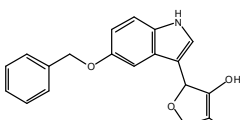
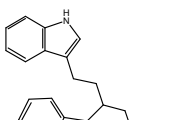
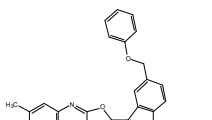
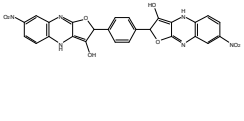
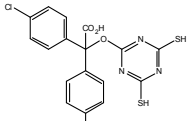
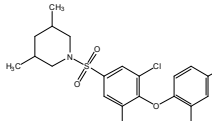
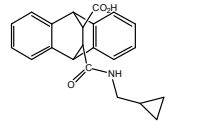
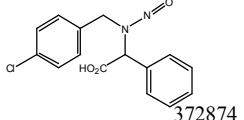
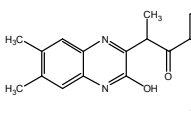
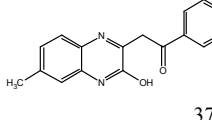
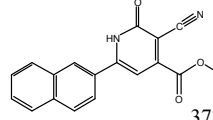
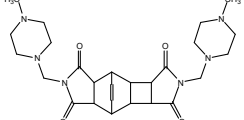
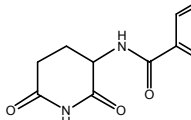
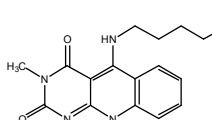
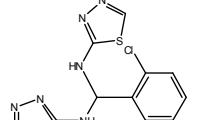
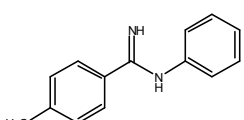
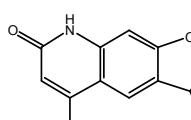
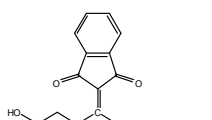
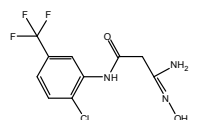
 289336	 290956	 292213	 292222
 292596	 293046	 293161	 293957
 293958	 294149	 294153	 294526
 295272	 295358	 295473	 295558
 295642	 296568	 297813	 299130
 299137	 299209	 299210	 299589
 300545	 302042	 302988	 303288
 303289	 303530	 303534	 303607
 303612	 303769	 303812	 303851
 305352	 305743	 305787	 305819

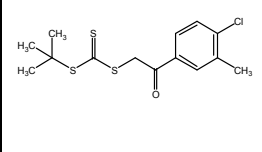
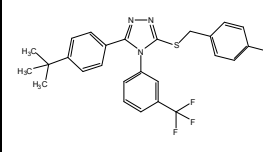
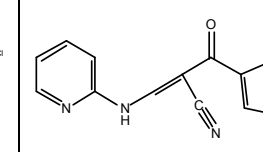
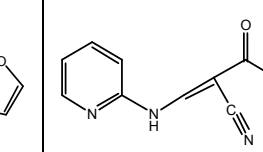
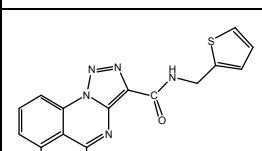
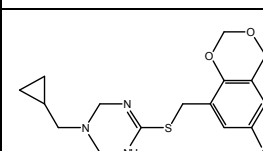
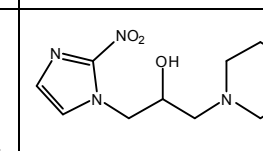
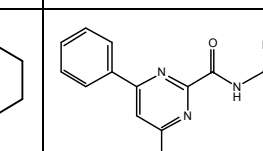
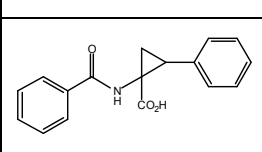
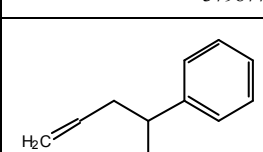
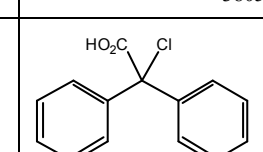
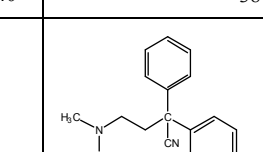
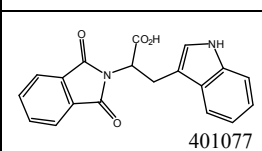
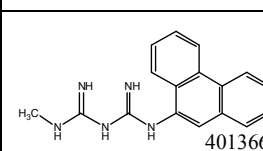
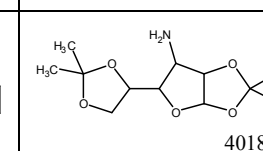
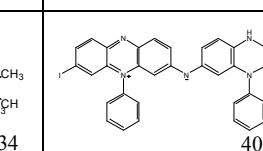
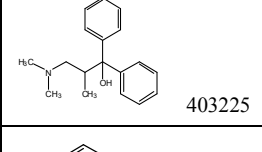
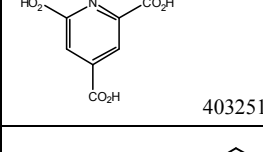
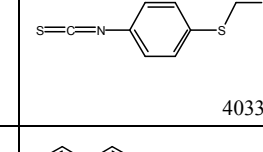
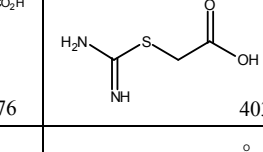
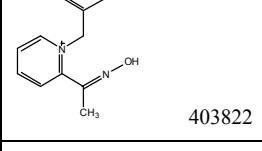
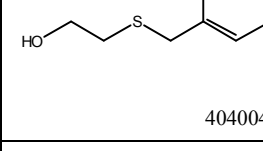
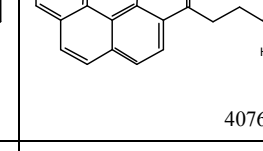
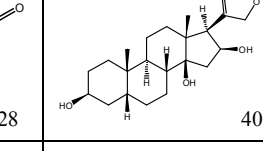
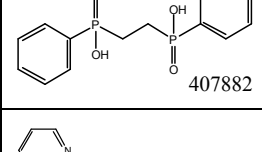
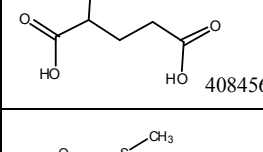
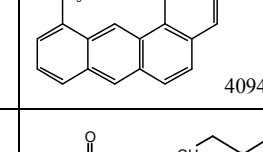
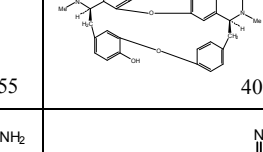
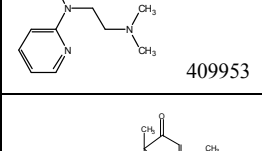
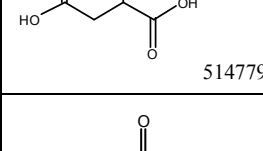
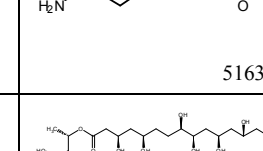
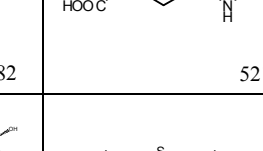
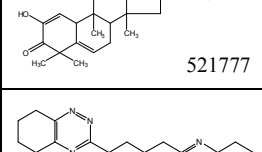
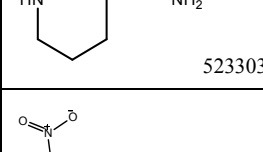
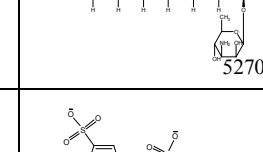
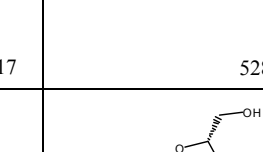
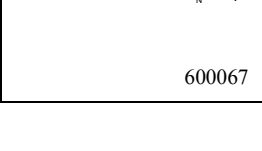
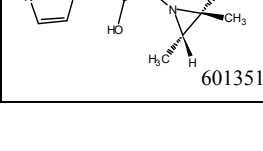
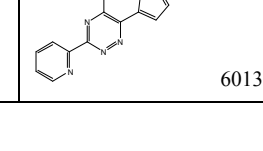
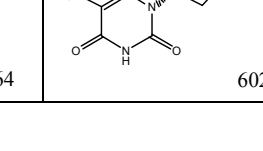
 305821	 305831	 306698	 306711
 306752	 306960	 307241	 307711
 308820	 308848	 309874	 309881
 309883	 309895	 309939	 310038
 310099	 310342	 310343	 310352
 310365	 310366	 310551	 310669
 310839	 311152	 311153	 311166
 312816	 313172	 314885	 318538
 318824	 319095	 319112	 319434
 319440	 319443	 319447	 319464

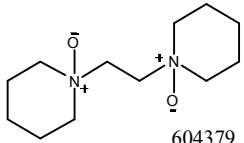
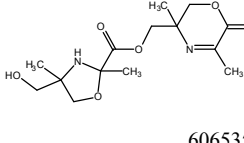
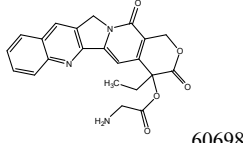
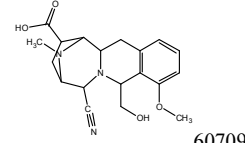
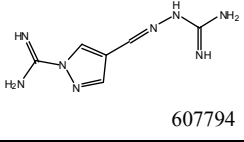
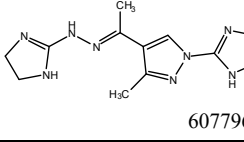
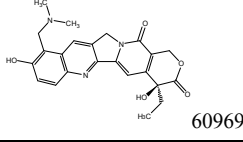
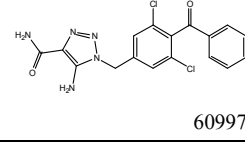
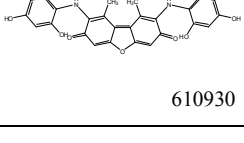
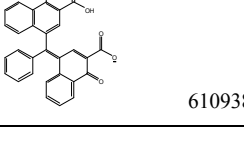
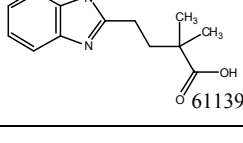
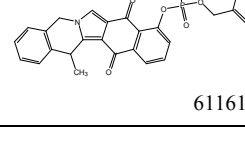
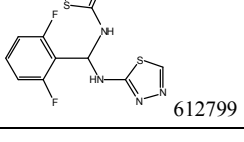
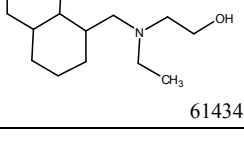
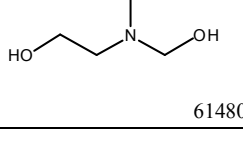
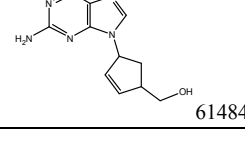
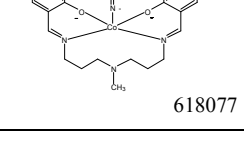
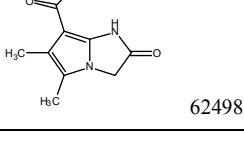
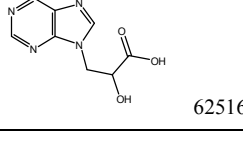
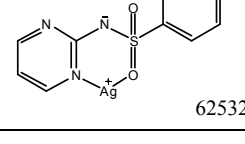
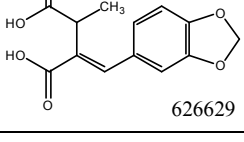
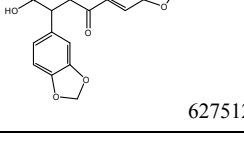
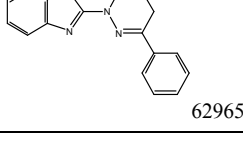
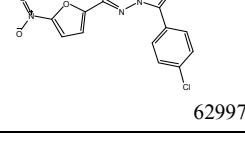
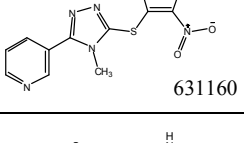
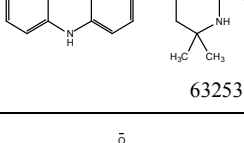
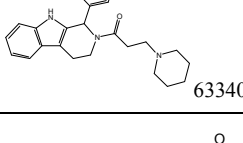
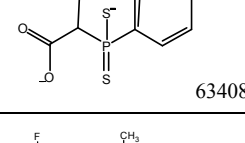
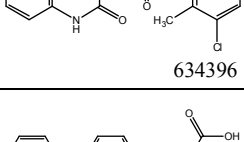
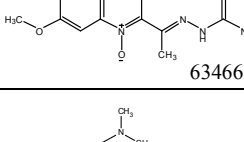
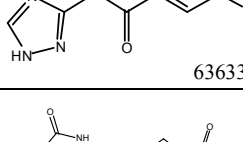
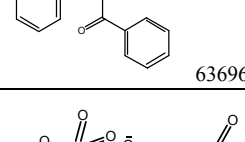
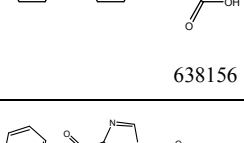
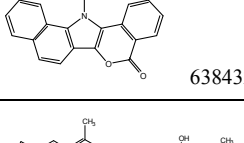
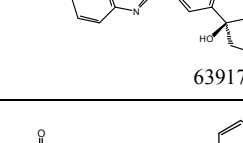
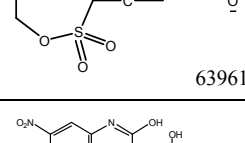
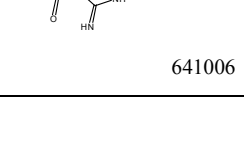
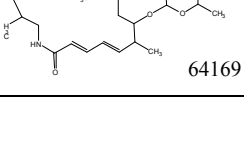
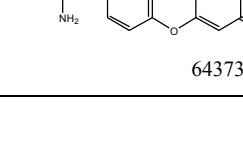
 319758	 319995	 320000	 320209
 320217	 320308	 320310	 320514
 320656	 320852	 320870	 321206
 321237	 321239	 321489	 321496
 321237	 321239	 321489	 321496
 321518	 321568	 321578	 321596
 321598	 321785	 322661	 322920
 322921	 324065	 326182	 326203
 326211	 326374	 326381	 327447

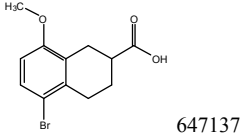
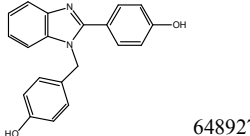
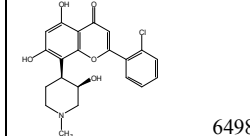
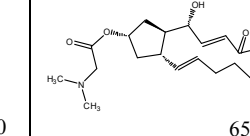
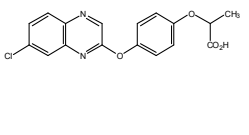
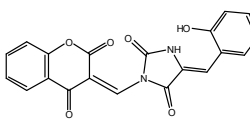
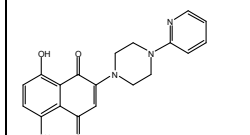
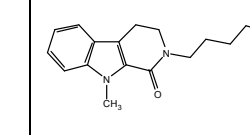
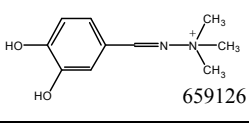
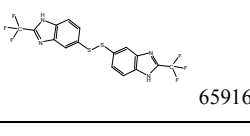
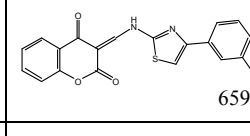
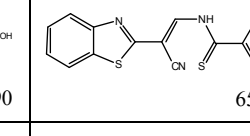
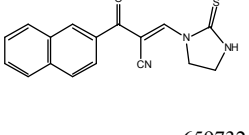
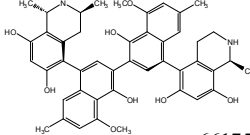
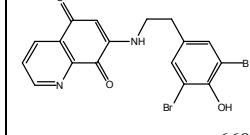
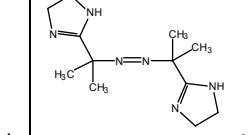
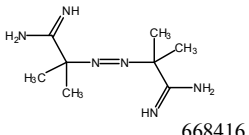
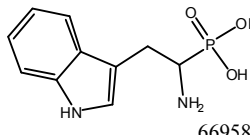
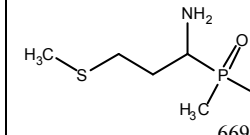
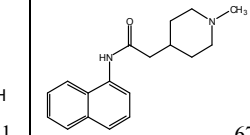
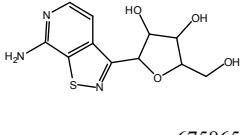
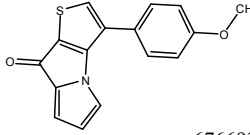
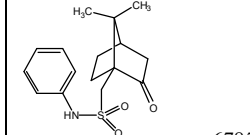
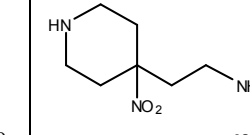
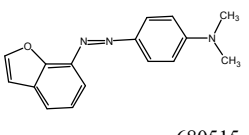
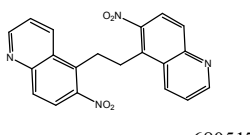
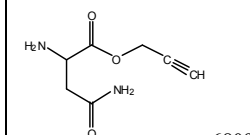
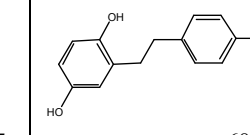
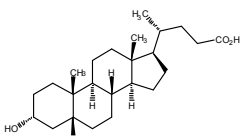
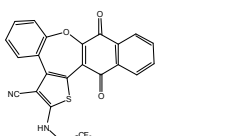
 327702	 327704	 327705	 328005
 328087	 328200	 328481	 329070
 329226	 329261	 329379	 330683
 331973	 332429	 332471	 333003
 333544	 334340	 334940	 337629
 337817	 338517	 339127	 339497
 339585	 339601	 339614	 339908
 342054	 342057	 343040	 343227
 343548	 344028	 345671	 345672
 347197	 347464	 347512	 348401

 350191	 350363	 350378	 350625
 351112	 351123	 351351	 351520
 351730	 353647	 354961	 355078
 355081	 356363	 357092	 357650
 357756	 357777	 359098	 359449
 360211	 360215	 360218	 360494
 361672	 361814	 361815	 362121
 362639	 362868	 363744	 363916
 363935	 364164	 366163	 366801
 366812	 367487	 368270	 368733

 368891	 369205	 369294	 371488
 371682	 371684	 371688	 371705
 371706	 371777	 371847	 371872
 371876	 371878	 371880	 371884
 372037	 372045	 372046	 372060
 372074	 372127	 372280	 372294
 372295	 372618	 372768	 372770
 372874	 373054	 373058	 373070
 373529	 373535	 373989	 375086
 375392	 375985	 379390	 379536

 379543	 379546	 379552	 379553
 379640	 379877	 380540	 381469
 382098	 400159	 400464	 400492
 401077	 401366	 401834	 402959
 403225	 403251	 403376	 403734
 403822	 404004	 407628	 407807
 407882	 408456	 409455	 409664
 409953	 514779	 516382	 521717
 521777	 523303	 527017	 528168
 600067	 601351	 601364	 602670

 604379	 606535	 606985	 607097
 607794	 607796	 609699	 609974
 610930	 610938	 611399	 611615
 612799	 614343	 614808	 614846
 618077	 624983	 625169	 625324
 626629	 627512	 629659	 629974
 631160	 632536	 633406	 634089
 634396	 634663	 636338	 636961
 638156	 638432	 639174	 639616
 641006	 641691	 643735	 646824

 647137	 648927	 649890	 656202
 656889	 657704	 658142	 658388
 659126	 659162	 659390	 659694
 659732	 661755	 668394	 668414
 668416	 669581	 669681	 674348
 675865	 676693	 678509	 680484
 680515	 680517	 680927	 681152
 683770	 686365		

**BIOGRAPHY**

<b>NAME</b>	Ms. Maleeruk Utsintong
<b>DATE OF BIRTH</b>	November 22, 1976
<b>PLACE OF BIRTH</b>	Kanchanaburi, Thailand
<b>INSTITUTION ATTEND</b>	Huachiew Chalermprakiat University, 1994-1999: Bachelor of Science in Pharmacy Mahidol University, 1999-2003: Master of Science in Pharmacy (Pharmaceutical Chemistry) The Scripps Research Institute, San Diego, USA, 2006: Research visit University of California, San Diego, USA, 2006: Research visit Mahidol University, 2003-2008: Doctor of Philosophy (Pharmaceutical Chemistry and Phytochemistry)
<b>POSITION &amp; OFFICE</b>	Student Department of Pharmaceutical Chemistry, Faculty of Pharmacy, Mahidol University, Bangkok, Thailand Tel. 0-2644-8678-91 ext. 1410
<b>FUND</b>	The Royal Golden Jubilee Ph.D. Program Commission on Higher Education